# Monitoring of Plant Chlorophyll and Nitrogen Status Using the Airborne Imaging Spectrometer AVIS

Dissertation

der Fakultät für Geowissenschaften

der Ludwig-Maximilians-Universität München

Vorgelegt von:

Natascha Oppelt

Eingereicht: April 2002

1. Gutachter: Prof. Dr. W. Mauser

2. Gutachter: Prof. Dr. F. Wieneke

Tag der mündlichen Prüfung: 12.07.2002

*„Don't panic"*
(Douglas Adams)

# Table of Contents

# List of Figures

# List of Tables

# List of Abbreviations

| | |
|---|---|
| AIS | Airborne Imaging Spectrometer |
| asl | above sea level |
| AVIRIS | Airborne Visible/InfraRed Imaging Spectrometer |
| AVIS | Airborne Visible/near Infrared imaging Spectrometer |
| | |
| BAHC | Biological Aspects of the Hydrological Cycle |
| BITÖK | Bayreuther Institut für Terrestrische ÖKosystemforschung (Bayreuth's institute for terrestrial ecosystem research) |
| BRDF | Bidirectional Reflectance Distribution Function |
| | |
| C | Carbon |
| CAI | Chlorophyll Absorption Integral |
| CASI | Compact Airborne Spectrographic Imager |
| CCD | Charge-Coupled Device |
| CET | Central European Time |
| Chl | Chlorophyll |
| CHRIS | Compact High Resolution Imaging Spectrometer |
| | |
| DAIS | Digital Airborne Imaging Spectrometer |
| DAS | Days After Sowing |
| DC | Dark Current |
| DFD | Deutsches Fernerkundungs-Datenzentrum (Germany's remote sensing data centre) |
| DFG | Deutsche Forschungsgemeinschaft (German research community) |
| dGPS | differential Geographical Positioning System |
| DLR | Deutsches Zentrum für Luft- und Raumfahrt (German aerospace centre) |
| DM | Dry Matter |
| DN | Digital Number |
| DOY | Day Of Year |
| DWD | Deutscher Wetter Dienst (German weather service) |
| | |
| EC | Eucarpia Code |
| EO-1 | Earth Observation 1 |
| | |
| FOV | Field of View |
| FWHM | Full Width Half Maximum |
| | |
| GIS | Geographical Information System |
| GPS | Geographical Positioning System |

GSF         Forschungszentrum für Umwelt und Gesundheit (research centre for environment and health)

H           Hydrogen
hNDVI       hyperspectral NDVI
HYMAP       HYperspectral MAPping
IFOV        Instantaneous Field of View
IR          InfraRed

LAI         Leaf Area Index

Mg          Manganese
MIR         Mid InfraRed
MLA         Mean Leaf Angle

N           Nitrogen
NBoS        National Bureau of Standards
NASA        National Aeronautics and Space Administration, USA
NDVI        Normalised Difference Vegetation Index
NIR         Near InfraRed
nm          nanometer
NN          Normal Null

O           Oxygen
OSAVI       Optimised Soil Adjusted Vegetation Index

p           statistical significance level
Pixel       Picture element
Proba       Project for on-board autonomy
PULREF      Procedure to Use Lowtran for REFlectance calibration

rmse        root mean square error
ROSIS       Reflectance Optics System Imaging Spectrometer

SNR         Signal to Noise Ratio
SPECTRA     Surface Processes and Ecosystems Changes Through Response Analysis
SWIR        Short Wave InfraRed

TM          Thematic Mapper

VIS         VISible

µm          micrometer

# Acknowledgements

Usually geographers are on the user's end of imaging spectrometers. Concerning oneself with the technical side of spectrometry, namely the construction and calibration of a new system, is not commonplace for a geographer and presented a particular challenge for me. Special thanks are therefore due to Professor Dr. Wolfram Mauser, who made it possible for me to become acquainted with the technology and as the sponsor of this thesis had a significant stake in its progress and success. In many mutual working hours and conversations, he gave me an insight into the fundamental aspects of not only the technical development and execution but also the practical application of AVIS. In the course of this doctoral thesis I constructed my first computer and "got my hands dirty" working on a sensor for the first time; things that I previously would not have considered possible. He also undertook the programming of the flight software as well as the software for the processing of the AVIS data. I would like to thank him cordially for the trust he placed in me, the favourable appraisement of my ideas and the freedom afforded to me in the implementation of the project.

This thesis originated at the Chair of Geography and Geographical Remote Sensing of the Ludwig Maximilians University Munich in connection with a project "Derivation of Plant Chlorophyll and Nitrogen Status with Hyperspectral Remote Sensing Techniques" sponsored by the Deutsche Forschungsgemeinschaft (DFG), who also partly provided financial support for building AVIS. I would like to thank DFG for providing the financial support for this thesis.

The success of this thesis is also closely associated with great teamwork within the Chair of Geography and Geographical Remote Sensing. Special thanks therefore go to all members of this working group, not only for the excellent cooperation and spontaneous support in the solution of problems, but also for the very good and friendly atmosphere. Thanks to Dr. Ingo Keding for his help in technical matters and the seemingly infinite field of statistics. I would like to thank Dr. Roswitha Stolz and Dr. Karl Schneider for letting me profit from their scientific knowledge, especially for questions regarding plant physiology. Cordial thanks to Dr. Heike Bach for her help concerning the radiometric processing of the data. Thanks to Dr. Dieter Rieger for his energetic support in creating the geographic information system of the test areas. I would especially like to thank Dr. Gertrud Strasser in whom I found a friend whose professional and friendly advice I could not have gone without.

I would like to thank Vera Erfurth, Vera Falck and Christian Michelbach for their constant obliging undertaking of design and cartographical tasks.

Not to be forgotten is the support of the many students who assisted in the extensive data collection on site. My thanks go especially to Messrs. Matthias Bernhardt and Tobias Hank,

# 1    Introduction

Man has been monitoring plants for thousands of years, especially since he started to cultivate several species. Ever since these early beginnings, the aim has been to ensure and increase the yield to guarantee the basic food supply. The development of crop rotation in the $1^{st}$ century A.D. and later on the application of organic fertilisers are examples for the progressive knowledge about plants and their dependence on environmental factors such as soil, temperature, water availability or nutrition. Nowadays, in many countries agriculture is a highly commercialised branch, which is characterised by the calculated use of fertiliser, herbicides, fungicides and machines for attaining the maximum yield.

Remote sensing is increasingly used for crop monitoring and the support of crop management. Satellite based sensors, especially the Landsat series, played and still play an important role in this task. In the last few decades, the impact of vegetation on the water budget or the carbon cycle on regional and global scales has been recognised. Remote sensing data is used to observe changes in vegetation cover and couple the results with models of the water budget and carbon cycle (ESA, 1999).

The development of spectrometers enables not only the investigation of the vegetation cover but also the derivation of individual constituents and furthermore the condition of plants. Ground-based spectrometers are used to derive plant parameters such as leaf area, water content, pigment content and biomass as well as the influence of stress or disease at leaf scale.

With the existence of airborne spectrometers, investigations and existing approaches at leaf scale were continued at canopy level. The first application of an Airborne Imaging Spectrometer (AIS) was described in 1983 (Vane & Goetz). AIS was a proof-of-concept instrument that led to the development of the AVIRIS (Airborne Visible/Infrared Imaging Spectrometer) – the first airborne spectrometer to contiguously cover the solar range from 400 to 2500nm with narrow bands which has been operational since 1989 (Vane & Goetz, 1993). Today, several airborne imaging spectrometers are available such as AVIRIS (Airborne Visible InfraRed Imaging Spectrometer, since 1987), CASI (Compact Airborne Spectrographic Imager, since 1989), ROSIS (Reflective Optics System Imaging Spectrometer, since 1990), DAIS (Digital Airborne Imaging Spectrometer, since 1991) or HYMAP (HYperspectral MAPping, since 1997).

Early research with hyperspectral data was difficult due to the lack of adequate calibration and knowledge of atmospheric effects in order to transform data to surface reflectances as well as the lack of tools to enable the scientists to analyse the data (Vane & Goetz, 1993). These issues have been overcome to a large extent, and several methods are now available for calibration, image processing and analysis of the hyperspectral data.

The first satellite-based imaging spectrometer was launched by NASA in December 2000: HYPERION, an imaging spectrometer with 220 bands in the wavelength region 400-2400nm, a geometric resolution of 30m and a spectral resolution of 5-6nm on board of EO-1 (Earth Observation 1). The first HYPERION data are now available. Examples for European sensors launched or planned are the CHRIS (Compact High Resolution Imaging Spectrometer) on board of Proba or SPECTRA (Surface Processes and Ecosystems Changes Through Response Analysis), both with similar specifications compared to HYPERION.

Airborne data acquisition benefits over satellite-based missions from being operational in the sense that the user can influence the mission in terms of flight line, position, calibration measurements, spectral resolution, ground resolution, acceptable weather conditions and time schedule (Wilson, 1994). Although airborne hyperspectral remote sensing becomes increasingly accessible due to the increasing number of commercial companies operating hyperspectral sensors, the data are often very expensive on account of the limited spatial coverage of an image scene and the fact that multitemporal approaches are often necessary. Furthermore, data processing and georeferencing is complex (Wilson, 1994). Thus the application of airborne imaging spectrometers nowadays is mainly restricted either to investigation on a local scale or to implication studies for forthcoming space-borne hyperspectral data.

At the Institute of Geography and Geographical Remote Sensing of the University of Munich, the above facts combined with the limited availability of airborne imaging spectrometers for multitemporal applications led to the development of an institute-owned system on a low-cost basis, especially for vegetation monitoring applications. The construction of the Airborne Visible / near Infrared imaging Spectrometer (AVIS) was carried out by Prof. W. Mauser with collaboration of Dr. I. Keding in 1998 and laid the foundations for this thesis (Mauser & Oppelt, 2000; Oppelt & Mauser, 2000; Mauser & Oppelt, 2001). The vegetation parameters to be investigated were determined within the scope of the project funded by the German Research Community (DFG) "Derivation of plant chlorophyll and nitrogen status with hyperspectral remote sensing techniques" (DFG MA 875-6). Therefore this thesis focuses on the following areas:

1.   Calibration and validation of AVIS,

2.   Multitemporal application in the years 1999 and 2000,

3.   Processing of the remote sensing data,

4.   Derivation of the chlorophyll and nitrogen content of vegetation applying a new approach with existing indices as references,

5.   Investigation of the temporal coverage on the one side and the spectral coverage and resolution necessary for this task.

Three different land use types were investigated, namely wheat, maize and grassland, using an empirical approach. As part of this investigation, ground measurements (Ground Truth) were carried out regularly in different test sites in both 1999 and 2000, during which AVIS measurements were also conducted.

The investigation deals with several research questions:

1.      Is hyperspectral remote sensing more accurate than multispectral sensors for the derivation of vegetation parameters?

2.      What dependency exists between the chlorophyll and nitrogen content of plants using measurements conducted during the ground truth campaigns?

3.      What measurements are necessary to derive vegetation parameters chlorophyll and nitrogen on a mean field basis?

4.      Can the chlorophyll and nitrogen content of plants be derived applying species optimised as well as species independent vegetation indices?

5.      Is it possible to derive the spatial distribution of chlorophyll and nitrogen content within a field?

This results in the following structure of the thesis, which is also presented in Figure 1-1.
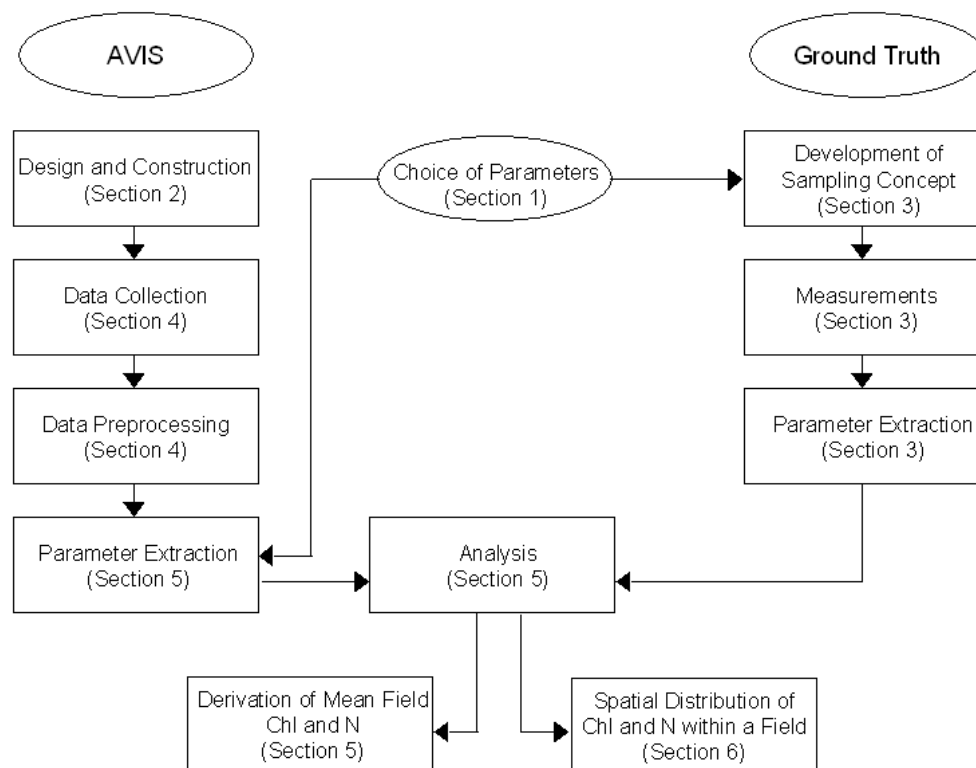


*Figure 1-1:        Structure of the thesis*

An introduction to hyperspectral remote sensing and the importance of the vegetation parameters chosen, namely chlorophyll and nitrogen, follows in section 1. Section 2 describes the most important system parameters of AVIS and the system calibration. Sections 3 and 4 include the ground based and airborne measurements, which were conducted during the vegetation periods 1999 and 2000. In section 3 follows the analysis of the ground truth data, while in section 4 the processing steps for the remote sensing data are described. The measurements of section 3 and 4 form the basics for the analysis of the data regarding the derivation of the chlorophyll and nitrogen content for the investigated land use types, which is focused in section 5. This analysis is based on mean field values derived from either ground or airborne measurements. Finally, the application of the AVIS data for the derivation of the spatial distribution of chlorophyll and nitrogen within a field is described for a field, which is distinguished by an extensive data basis regarding ground based measurements as well as GPS-based yield measurements. This enables a detailed discussion of the derived parameter distribution. The last section includes a summary and an outlook on the further development of the system AVIS as well as the potentialities of the investigated approaches.

## *1.1 Hyperspectral Remote Sensing and Imaging Spectrometry*

Remote sensing is practised by the examination of features as observed in several regions of the electromagnetic spectrum (Figure 1-2).
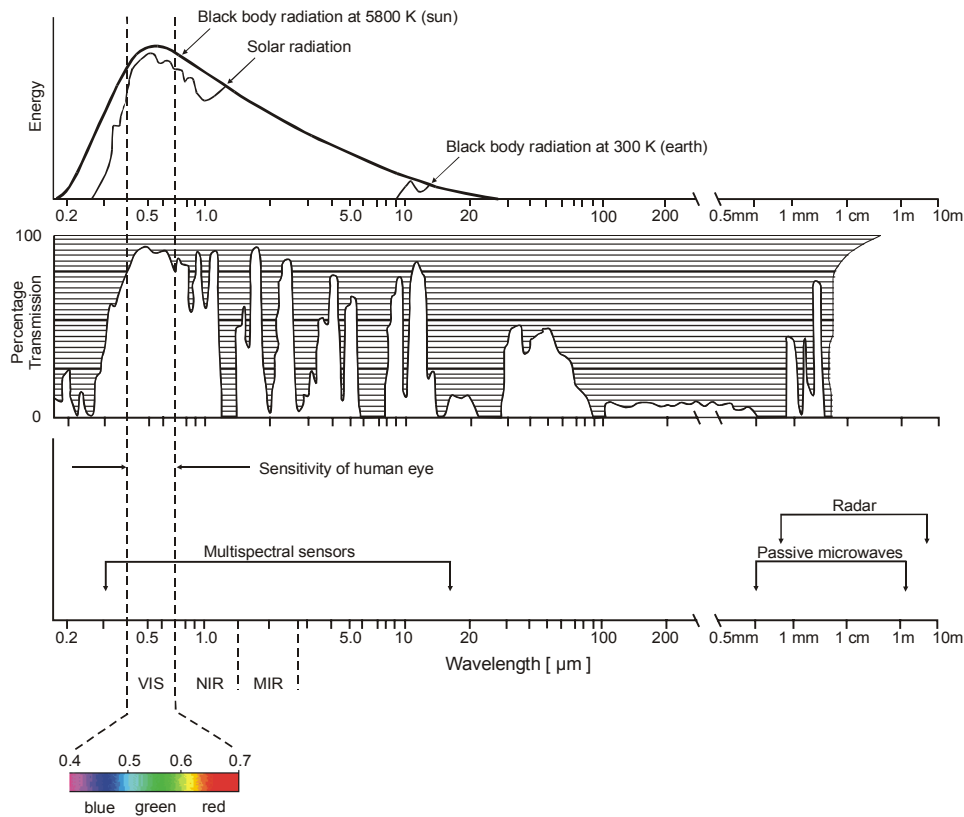


*Figure 1-2:    Electromagnetic spectrum (Kappas, 1994, modified; cartography: V. Falck)*

Conventional remote sensing is based on the use of several rather broadly defined spectral bands, while hyperspectral remote sensing is based on the examination of many narrowly defined spectral bands over a broad range of the electromagnetic spectrum, which enables the recording of a continuous reflectance spectrum. Thus, hyperspectral data have detail and accuracy that permit investigation of phenomena and concepts that greatly extend the scope of traditional remote sensing. Such capabilities present opportunities for much more precise identification of features than is possible with broadband sensors, for use of spectral libraries, for detailed investigation of biologic and geologic phenomena. Due to the measurement that mainly includes the uppermost vegetation or soil layer the obtained spectra are top-of-canopy reflectance spectra (Campbell, 1996; Vane & Goetz, 1993).

Imaging spectrometry is the application of hyperspectral remote sensing for the recording of precise, accurate and detailed spectral measurements of the radiation, which is

reflected or emitted from the earth's surface. This part of the electromagnetic spectrum can be divided into several domains (Campbell, 1996; Wolfe, 1997):

- o the visible spectrum (VIS) ranges from 400nm to 700nm and is limited by the sensitivity of the human eye. The visible light can be divided into three primary additives, defined approximately from 400-500nm (blue), 500-600nm (green) and 600-700nm (red), which is also illustrated in Figure 1-2.

- o Wavelengths longer than the red portion of the visible spectrum are designated as the infrared region (IR). This segment of the spectrum is large relative to the visible region and extends from 700nm to 15µm. The reflected portion of the IR ranges from 700nm to 3µm and can be divided into the near infrared (NIR) ranging from 700nm to 1.3µm and the mid wave infrared (MIR, 1.3-3µm).

  Radiation in the NIR and MIR behaves, in respect to the optical systems, in a manner analogous to radiation in the visible spectrum. Whereas near and short wave infrared radiation is essentially solar radiation reflected from the earth's surface, the thermal infrared (TIR) beyond 3µm is emitted by the earth.

Hyperspectral sensors necessarily employ designs different from those of usual sensor systems. An objective lens collects radiation reflected or emitted from the earth's surface, a collimating lens projects the radiation as a beam of parallel rays through a diffraction grating or prism, whereby the radiation is dispersed into discrete spectral wavelengths
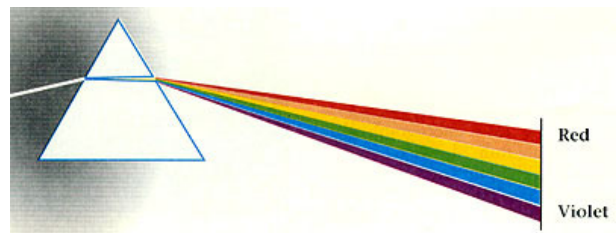


Figure 1-3: Dispersion of light by a prism

(Figure 1-3). The energy in each spectral band is then detected by one ore several arrays as image line. The superimposition of the same surface, observed at different wavelengths lead to an image cube (Figure 1-4). The two dimensions formed by the x and y axes of the usual map or image display is formed by the movement of the sensor over the ground, while the third (z) is formed by the accumulation of spectral data as bands. The top of the cube is an image composed of data collected at the shortest wavelength, and the spectral band of the longest wavelength of the sensor forms the bottom. Intermediate wavelengths are found as slices through the cube at intermediate positions. Values for an individual pixel observed along the edge of the cube form a spectral trace describing the spectra of the surface presented by the pixel (Campbell, 1996; Wolfe, 1997).
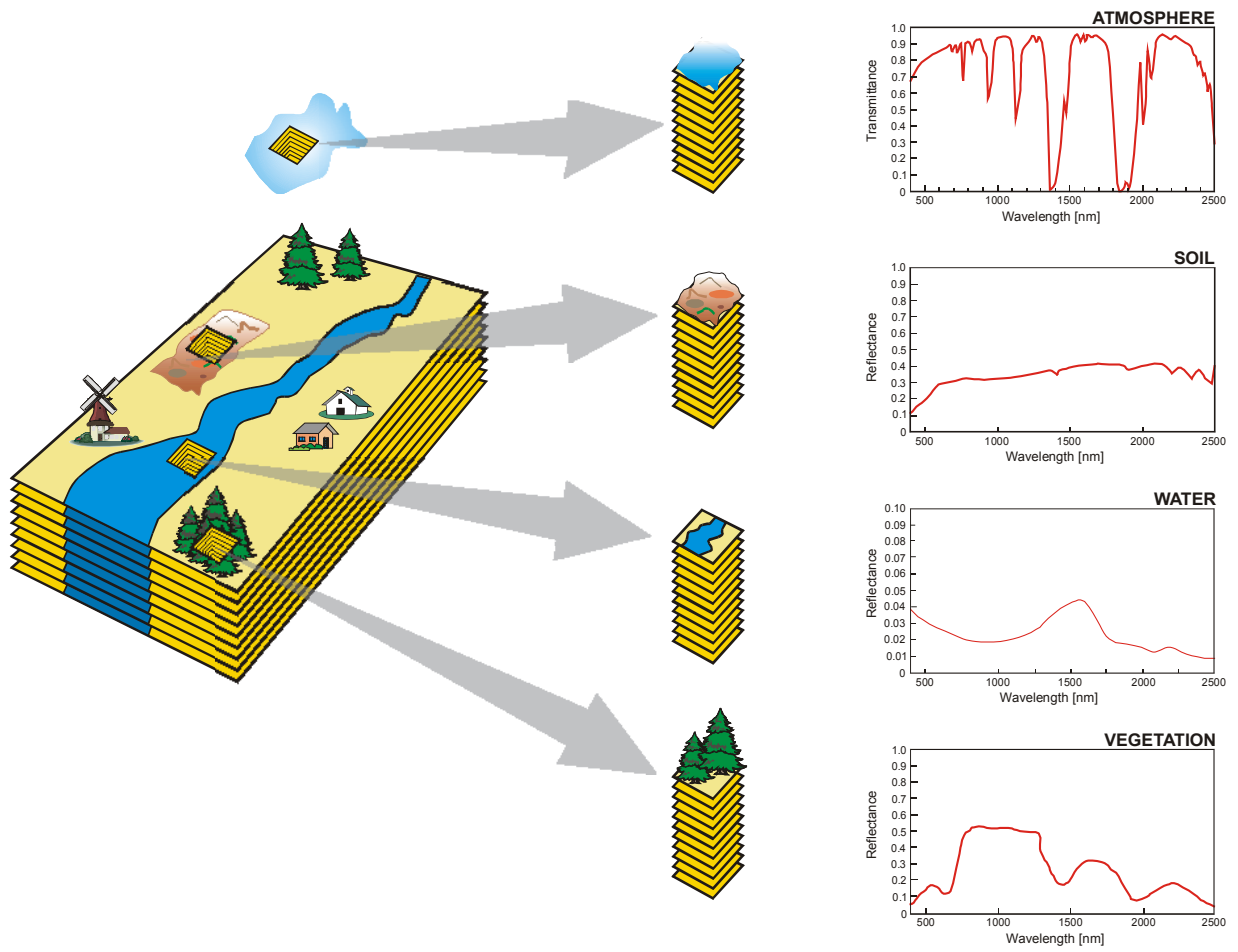
*Figure 1-4:*        *Hyperspectral image cube (based on NASA diagram; cartography: V.Falck)*

## *1.2 Importance of Chlorophyll and Nitrogen*

Chlorophyll is the pigment primarily responsible for harvesting light energy used in photosynthesis. Photosynthesis is unique in utilising light as a source of energy for the incorporation of carbon dioxide and water into an energy-rich product, sugar that can be metabolised by the plants (equation (1.1)) (Kaufman et al., 1989):

$$6\,CO_2 + 12\,H_2O \rightarrow C_6H_{12}O_6 + 6\,H_2O + 6\,O_2 \uparrow \qquad\qquad (1.1)$$
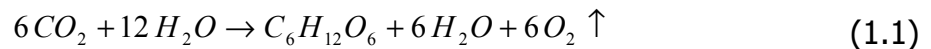
The common denominator in all photosynthetic plants is the occurrence of chlorophyll a. Special molecules of chlorophyll a are believed to accept light energy (electrons) from surrounding pigments and transfer it to an acceptor molecule, resulting in the conversion of light energy to a stable form of chemical energy, which is stored in the form of assimilated carbon. For this, chlorophyll a is viewed as playing the key role in the transfer of light energy. The other pigments are referred to as accessory pigments and include chlorophylls b, c and d, carotenoids, photocyanin and photocoerythrin (Kaufman et al., 1989). The specific structure as well as the absorption features of the chlorophylls are described in more detail in section 5.1.

The primary event in photosynthesis is the absorption of light by the photosynthetic pigments, i.e. the chlorophylls, which are located in the chloroplasts. Chlorophyll primarily is located in the leaves. Mainly this proportion is also viewed by a remote sensing system due to the more or less horizontal alignment of the leaves. The chlorophyll content is correlated with the depth and width of its absorption feature and can be measured by hyperspectral remote sensors.

As mentioned above, photosynthesis forms the basis of plant growth, development and primary productivity. A clear and detailed knowledge of bio-chemical processes as well as their change due to climatic and anthropogenic pressure is essential for the understanding of the environment. Therefore chlorophyll is an important parameter for an accurate characterisation of these processes as well as for their inclusion into hydrological or vegetation modelling.

There are four atoms of nitrogen in each molecule of chlorophyll. This close relation together with the fact that nitrogen itself does not absorb or reflect radiation leads to the derivation of nitrogen content via the chlorophyll content of the plant or leaf respectively.

Most plant tissues contain between 1 and 5% nitrogen on a dry weight basis, and its content tends to decline during the maturation. About 80% of the initial leaf nitrogen content is recycled before leaf abscission. The fraction in dead leaves presumably corresponds to structural leaf nitrogen, whereas the fraction remobilised corresponds to the metabolic pool. For the optimisation of canopy photosynthesis, the metabolic nitrogen pool can be remobilised to vivid parts of the plants (Lemaire, 1997).

Nitrogen is very important in plant nutrition. It is a component of all amino acids and proteins, including the enzymes vital to plant metabolism. It is a constituent of the building blocks of nucleic acids and is found in vitamins and many other plant constituents. Nitrogen is required in relatively large amounts for optimum growth and it is the availability of nitrogen that often causes the limitation to growth. To be available for the plants, it must be fixed, meaning that it must be combined with some other element to form a nitrogen compound. Examples for compounds are nitrate ($NO_3^-$) or ammonium ($NH_4^+$), which are available to plants (Kaufman et al., 1989) and are absorbed through the roots. In addition to that, plants can absorb some forms of nitrogen (particularly gaseous ammonia and nitrogen dioxide) through their leaves, but absorption through the leaves contributes only a small proportion (<5%) of the total uptake (Whitehead, 1995).

The knowledge of the impact of nitrogen to the plant as well as the low prices for nitrogen fertiliser led to increasing fertilisation with nitrogen during a period from about 1950 to the mid 1980s (Whitehead, 1995). Although other factors were involved, the increasing rate of nitrogen fertiliser was responsible for much of the amounts of nitrogen leached through the soil and lost in gaseous forms to the atmosphere. Nitrogen that is leached from soils into groundwater is almost entirely in the form of nitrate and, if the groundwater is used for domestic supplies, the nitrate may constitute a health risk to consumers. In 1980 the European Community adopted a directive, which includes a maximum concentration of nitrate in water intended for human use. This directive as well as the perception of the negative impact of overfertilisation to the yield led to a more sensitive handling of nitrogen fertilisation. Therefore the nitrogen content of plants is an important parameter for the nutrition management by farmers to optimise the plant development and thus yield.

In recent years, the spatial distribution of the nitrogen within the fields becomes increasingly important in the scope of optimising the field management. GPS-based yield measurements showed the heterogeneity of the yield within a field and therefore non-uniform plant nutrition status and enabled the spatially distributed employment of fertiliser. The advantage of hyperspectral remote sensors for this task is obvious as soon as they have shown their ability to derive plant constituents and the generation of two-dimensional data.

# 2 AVIS – the Airborne Visible/Near Infrared Imaging Spectrometer

The costs for the use of existing imaging spectrometers such as DAIS, AVIRIS or HYMAP are high. Also, it is difficult to obtain these sensors for multitemporal applications such as monitoring of vegetation. Therefore, there is a need for a cost effective as well as available tool in hyperspectral remote sensing.

To fill this gap, the imaging spectrometer AVIS (**A**irborne **V**isible / near **I**nfrared imaging **S**pectrometer) was built at the Chair of Geography and Geographical Remote Sensing of the Ludwig Maximilians University Munich, Germany.

The characteristics of AVIS, which include radiometric, spectral and spatial properties, depend strongly on the characteristics of its individual components. The quality of each property, which determines the performance of the AVIS system, is limited by the quality of the parameters of the individual components. Therefore, the most important characteristics of the AVIS components, related to the subject of this study, will be described as well as the resulting overall performance of the system. The calibration procedure as an important part for the assessment of the capabilities of the system will also be described.

## 2.1 System Description

The system was developed using commonly available components, leading to the Airborne Visible/near Infrared imaging Spectrometer AVIS (Figure 2-1 and Figure 2-2). AVIS is a line imaging spectrometer consisting of two main parts: the camera unit, which includes the camera, spectrometer, lens and filter, and the storage unit, which includes the PC, frame grabber and dGPS.
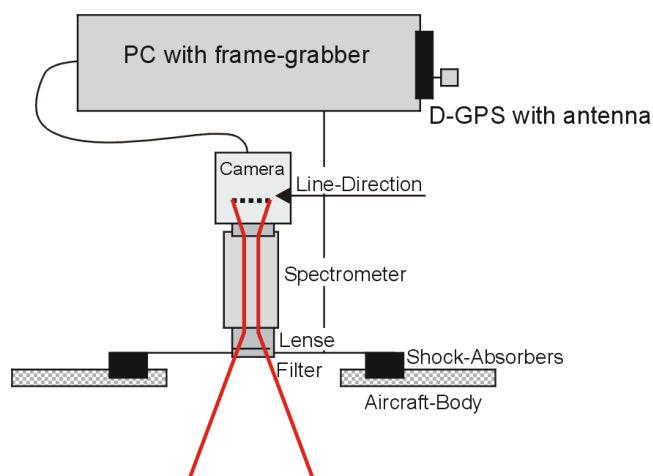


Figure 2-1:     AVIS schematic (Oppelt & Mauser, 2000)

The power supply of AVIS is ensured by two 12V led batteries, which provide power for a runtime for at least three hours.



*Figure 2-2:    AVIS mounted into the aircraft*

### 2.1.1    Camera Unit

The main part of the camera unit is the spectrograph, which is directly coupled to a standard B/W CCD camera via a C-mount. A lens is mounted in front of the spectrograph, and finally a filter is mounted in front of the lens (see also Figure 2-3).

The incoming light passes the filter and is focussed by the lens. Then it passes the spectrograph and is dispersed into the different wavelengths along its spectral axis. Finally, it is registered on the CCD element of the camera as an electrical charge, which is then read out and sent to the storage unit in form of a voltage signal.
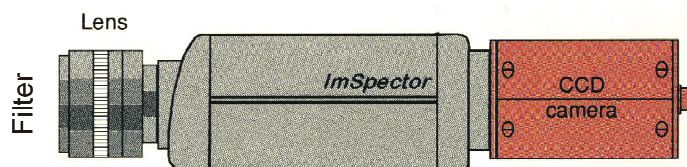


*Figure 2-3:    AVIS camera unit with CCD camera, spectrograph, lens and filter (SPECTRAL IMAGING LTD., 1998a)*

### 2.1.1.1    Spectrograph

The spectrograph (ImSpector V9-M-897, SPECTRAL IMAGING LTD.) is a direct sight spectrograph and the heart of AVIS. It is composed of a narrow slit (entrance slit), a PGP (prism-holographic transmission grating-prism) dispersive element and focussing lenses (see Figure 2-4).
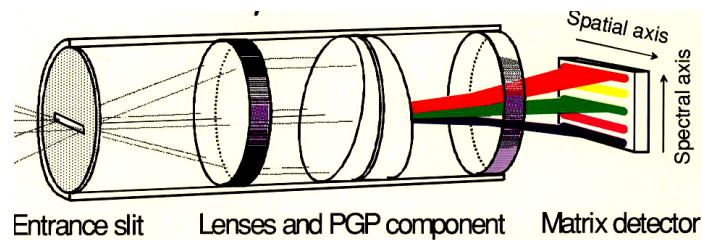


Figure 2-4:    Schematic diagram of spectrograph ImSpector (SPECTRAL IMAGING LTD., 1998a)

Radiation entering the slit is collimated by the first lens and refracted at the prism surface to the correct incident angle of the holographic grating. The grating disperses the light according to the common grating equation (2.1).

$$s \cdot \sin\theta_m = m \cdot \lambda \qquad (2.1)$$

where
| | |
|---|---|
| $s$ | grating spacing [nm], |
| $\theta_m$ | angle between the direction of wave travel and direction of m-order [°], |
| $m$ | order of spectrum, |
| $\lambda$ | wavelength [nm] (SPECTRAL IMAGING LTD., 1998a; Whelan & Hodgson, 1985). |

Spatial information at the entrance slit is transferred to the imaging plane along the axis parallel to the slit length direction. The spectrum is formed perpendicular to the optical axis into 240 spectral bands with a spectral sampling rate of 2nm. The nominal spectral resolution is 5nm (SPECTRAL IMAGING LTD., 1998a). The terms are described in section 2.3.

A scene is imaged one line at a time. The slit width and length are the determining elements for the width and length of a scene line, respectively (see section 2.5.2).

The parameters of the spectrograph are summarised in Table 2-1:

Table 2-1:    Parameters of spectrograph ImSpector V9-M-897 (SPECTRAL IMAGING LTD., 1998b)

| Parameter | Value |
| --- | --- |
| Spectral coverage | 553–1037nm |
| Number of pixels per image line | 390 |
| Slit width | 25µm |
| Effective slit length | 9mm |
| Field of View (FOV) | ±29° |
| Numerical aperture | f/2.8 |

The diffraction efficiency of the spectrograph grating is given in Figure 2-5. It decreases slowly from 57% at 550nm to 49% at 750nm, then increases to 60% at 900nm, after which it decreases again to 54% at 1040nm.

Any tubular optical construction is sensitive to ghost images and stray light caused by reflections from the optical surfaces of the spectrograph. There is also a risk of stray light caused by transmitted unwanted orders of diffraction in the holographic grating. These have been taken into account by using critically positioned baffles inside the tube. All the air/glass surfaces have multi-layer coatings to reduce backward reflections. The tilted surfaces of the prisms also refract remaining forwarded reflections to blackened walls of the spectrograph (SPECTRAL IMAGING LTD., 1998a).
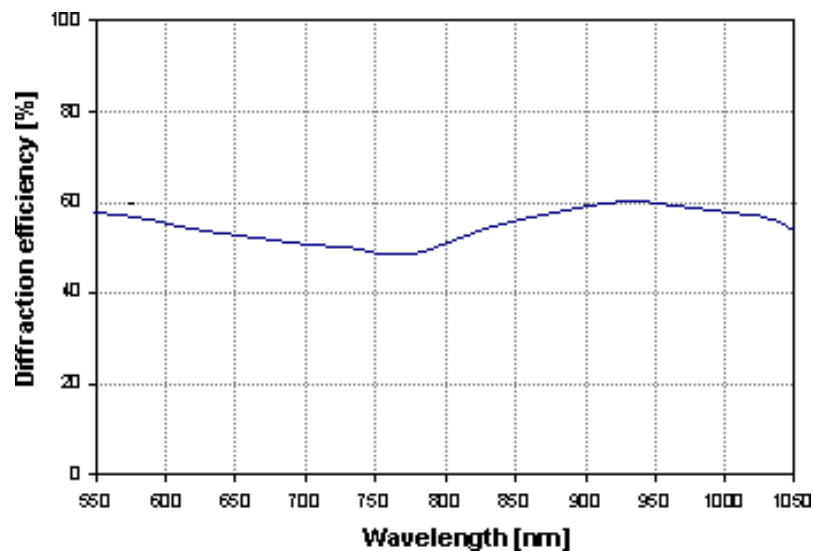


Figure 2-5:    Diffraction efficiency of spectrograph grating (SPECTRAL IMAGING LTD., 1998c)

### 2.1.1.2    Camera

The spectrograph is fixed via a C-mount to a 2/3" B/W CCD camera (HAMAMATSU C5999). Detector arrays are described by the physical camera parameters, such as sensor size,

pixel size and number, and shutter settings, as well as signal characteristics, such as spectral sensitivity and responsivity, and dynamic range (Holst, 1998). These parameters are given in Table 2-2.

The HAMAMATSU C5999 is back-illuminated and has a standard 15MHz EIA Video signal as its output with a signal to noise ratio of 57dB. The CCD element has a sensing area of 8.8 x 6.6mm with a pixel size of 11 x 13µm, which leads to a resolution of 754 x 484 pixels.

The camera operates in interlaced mode. This means that each second 30 even and 30 odd lines are stored in separate frames. Any vertical image movement smears the interlaced image, whereas horizontal movement serrates vertical lines. With excessive movement, the two frames are displaced one from another. Because of these image motion effects, with AVIS only one frame (half-image) is stored and used for image processing. The integration time is fixed at 1/60 seconds (s).

The spectral sensitivity of the camera used is improved in the near infrared compared to standard CCD cameras and records a spectral range from 400 to 1300nm (HAMAMATSU, 1998).

*Table 2-2:    Camera C5999 (HAMAMATSU) specifications (HAMAMATSU, 1998)*

| Parameter | Value |
| --- | --- |
| CCD sensor size | 2/3″ = 8.8 x 6.6mm |
| Pixels (active) | 754 x 484 |
| Pixel size | 11 x 13µm |
| Sensing area | 6.6 x 8.8mm |
| Spectral sensitivity | 400–1300nm |
| Dynamic range | 57dB (illumination 400 lux) |
| Lens mount | C-mount |
| Output signal | Video signal EIA standard, 75Ω |
| Power supply | 12V |

The relative spectral responsivity of the camera over the spectrum is shown in Figure 2.6. It increases from below 10% at 400nm to nearly 100% at 800nm. Beyond 800nm it drops continuously to nearly 5% at 1300nm. This curve is typical for a NIR enhanced silicon photo detector. Above 800nm, the quantum efficiency drops because of recombination of electrons in the CCD array before reaching a storage unit. Another reason is that the CCD silicon becomes more transparent as the wavelength increases. Thus, photons with a longer wavelength are more likely to pass through the CCD without being absorbed (Holst, 1998).
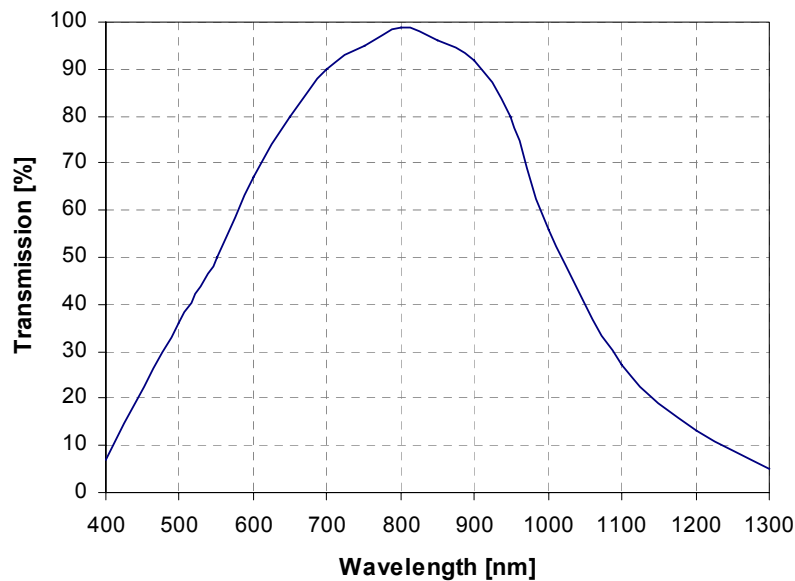
*Figure 2.6:      Spectral responsivity of camera C5999 (HAMAMATSU, 1998)*

The dynamic range is defined as the maximum signal [$V_{max}$] divided by the noise [$V_{noise}$]. It depends on integration time, binning and frame integration. In addition, the spectral content of the source and the array spectral responsivity affect the camera output voltage. Thus, the camera dynamic range can be quite variable depending on test conditions (Campbell, 1996; Holst, 1998).

$$ DR = 20 \log\left(\frac{V_{max}}{V_{noise}}\right) \tag{2.2} $$

where

| | |
|---|---|
| *DR* | dynamic range [dB], |
| $v_{max}$ | maximum signal [DN], |
| $v_{noise}$ | noise [DN]. |

The given dynamic range of 57dB at an illumination level of 400lux implies a ratio of 813:1. This means that a range of 813 grey values, which are close to saturation, can be accurately recorded under illumination conditions comparable to a relatively dark day with overcast sky (Holst, 1998).

The camera heats up during image capture and produces thermal noise (see section 4.1.3.1). To reduce the thermal noise the camera is cooled by a Peltier device mounted onto the camera.

### 2.1.1.3   Lens

The lens (SCHNEIDER CNG 1.4/8mm) is mounted in front of the spectrometer. The main characteristics are its spectral range and responsivity, focal length and the view angle (see also Table 2-3).

Table 2-3:   Parameters of lens SCHNEIDER CNG 1.4/8 (SCHNEIDER, 1998)

| Parameter | Value |
| --- | --- |
| Spectral range | 400–1000nm |
| Focal length | 8.4mm |
| View angle | 68.2° |

Figure 2-7 shows the spectral responsivity of the lens. In the 550 to 850nm range it remains relatively stable at a level above 90%, afterwards it decreases slowly towards longer wavelengths. Therefore the lens contributes the limitations of the spectral responsivity of AVIS towards the NIR at 1000nm.
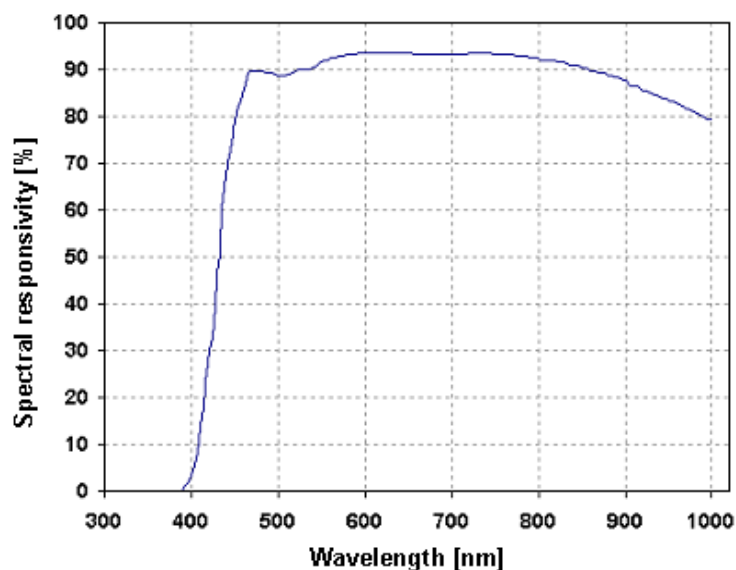


Figure 2-7:       Spectral responsivity of lens SCHNEIDER CNG 1.4/8 (SCHNEIDER, 1998)

### 2.1.1.4   Filter

The resulting spectral responsivity of AVIS is the product of the responsivities of the components, which is shown as the blue line in Figure 2-8.

To adjust the dynamics of the spectral responsivity to nearly the same level throughout the wavelength range, a filter is mounted in front of the lens. During image capture, the filter limits the danger of saturation and blooming due to a high spectral sensitivity of the

wavelength region between 650 and 900nm in comparison to the sections below and above.
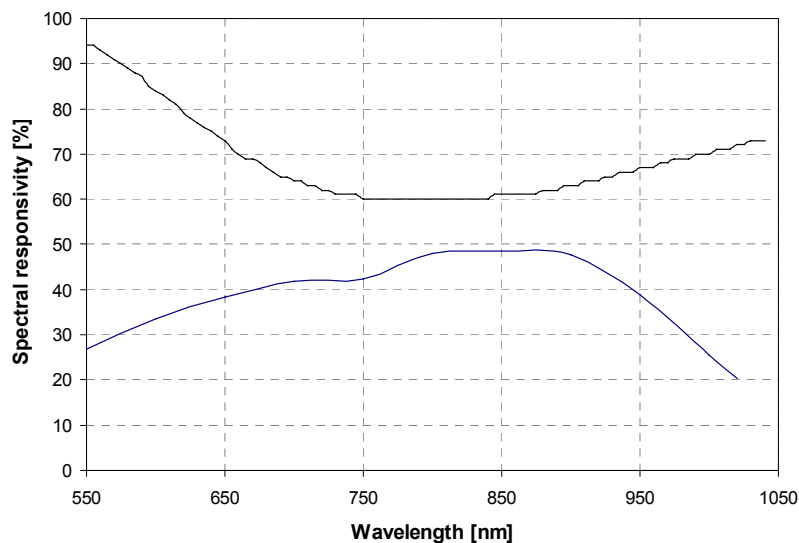


Figure 2-8:    Spectral responsivity product of lens, spectrograph and camera (blue) and transmission curve of filter SCHOTT BG 26 (SCHOTT, 1999)

The filter SCHOTT BG 26 proved best for this task (see black line in Figure 2-8). BG 26 is a belt filter made of ionic coloured glass. It shows an almost diametrical curve to the responsivity product. This results in an almost horizontal curve of the resulting spectral responsivity of AVIS (see also Figure 2-9). The spectral responsivity lies near 28% from 550nm to 700nm. It decreases slightly to 25% at 700nm and shows an increase to 29% towards 800nm, where it remains stable until 900nm. Then there is a decrease to 18% towards 1000nm.
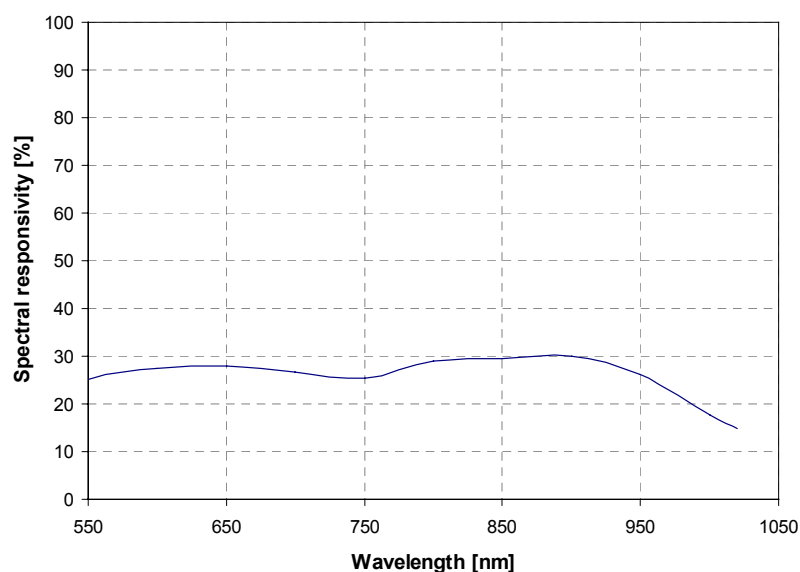


Figure 2-9:    Spectral responsivity of AVIS

### 2.1.2    Storage Unit

The storage unit of AVIS consists of the PC and the Global Positioning System (GPS), which is mounted onto the PC.

As for the camera unit, the 12V led batteries guarantee the power supply of the storage unit.

#### 2.1.2.1    Personal Computer

The PC is a standard dual Pentium II, 400MHz, with a 12V power supply unit. The analogue output signal of the camera is digitised by the integrated frame grabber with a data depth of 10bit and then stored on the hard disk. The frame grabber defines a number of 780 pixels within the standard Video signal.

In addition, a temperature card is installed to measure the temperature of the camera for the dark current correction of the data. A temperature probe, which is mounted on the camera, transmits the sensor temperature to the card, where it is stored in a header for each image line.

#### 2.1.2.2    Differential GPS (dGPS)

The GPS employed is AFUSOFT RAVEN 3, which uses dGPS data from the System RASANT. RASANT transmits correcting data for the GPS measurements from permanent reference stations via the radio data system RDS (EN 50067) operating in VHF-sound broadcasting radio. AFUSOFT decodes the incoming GPS signal and corrects it with the permanently sent RASANT data. The positioning accuracy in motion is claimed at 3 m (HY-LINE, 1998).

The dGPS outputs are time, latitude and longitude, flight altitude, velocity and number of received satellites. This output is stored in the header of each image line, as it is essential information for both radiometric and geometric correction of the captured image data.

## *2.2 Radiometric Properties*

The system was tested in the laboratory to examine its radiometric and spectral properties. This includes the assessment of the dark current and the homogeneity of the CCD element of the sensor. Both measurements must be examined at least after each modification of the system.

For an homogeneous measurement over the whole area of the CCD both the dark current and the homogeneity must be determined for each pixel. Therefore two matrices are needed for the preprocessing, each made of 390 columns and 240 lines. The column direction corresponds to the imaged area covered by the spectrograph, the 240 lines to the number of spectral bands. The grey value of each pixel is calculated:

$$DN = A_{i,j} \times (DN_{Original} - B_{i,j})$$

(2.3)

where

$DN$          grey value [DN],
$A_{i,j}$          relative sensitivity of the pixel in column i and band j,
$B_{i,j}$          dark current of the pixel in column i and band j [DN].

The measurements and results of both the dark current and the homogeneity of the CCD regarding AVIS are described in the following sections.

### 2.2.1    Dark Current

Thermally generated electrons within the system cause dark current. The main sources are the depletion region of the CCD and diffusion in the neutral bulk material of the camera. As the dark current is thermally generated, its amount is dependent on the sensor temperature (Holst, 1998).

The measurements of the dark current were performed with closed aperture of the lens. For a given temperature the average values for 100 image lines were used to determine the corresponding dark current level. These measurements were carried out both in 1999 and 2000. Figure 2-10 shows the matrix of the CCD elements for a sensor temperature of 15° Celsius, which is a typical temperature reached during the AVIS flights.

Both dark current matrices are very similar. One feature is the readout pattern. It is column dependent and does not change with line. It is superposed by an increasing dark current with increasing number of columns.
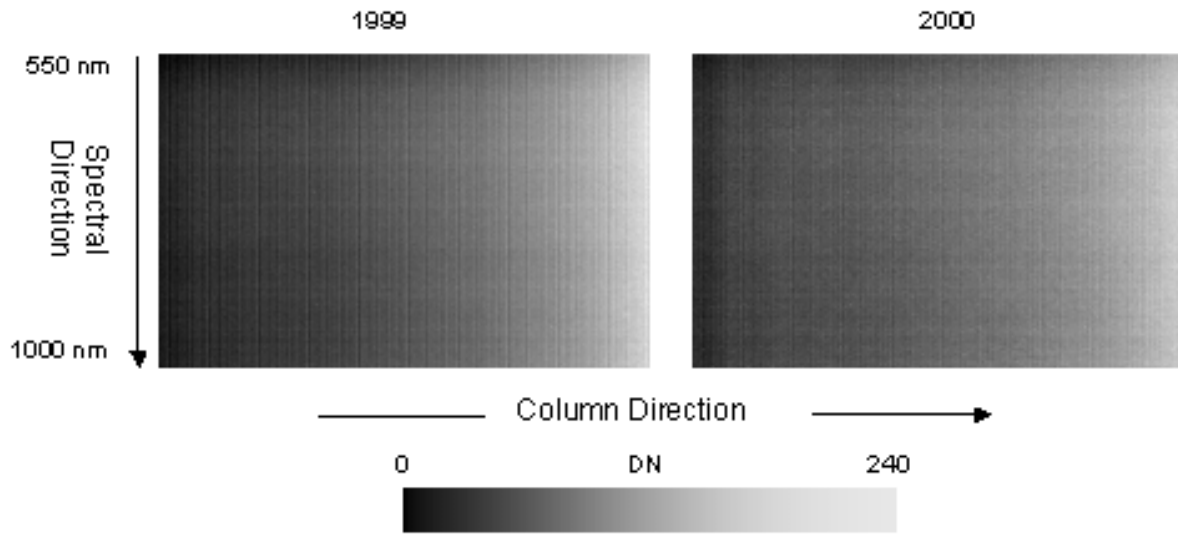
Figure 2-10:   *Dark Current matrix measured for 1999 (left) and 2000 (right) at a sensor temperature of 15°C*

The measured amount of mean dark current at different sensor temperatures for 1999 and 2000 are shown in Figure 2-11. The blue points represent the measured dark current at different camera temperatures, which are the basis for the black regression curve. As expected, an increasing dark current can be observed with increasing temperature. For both 1999 and 2000 a linear trend fits very well.
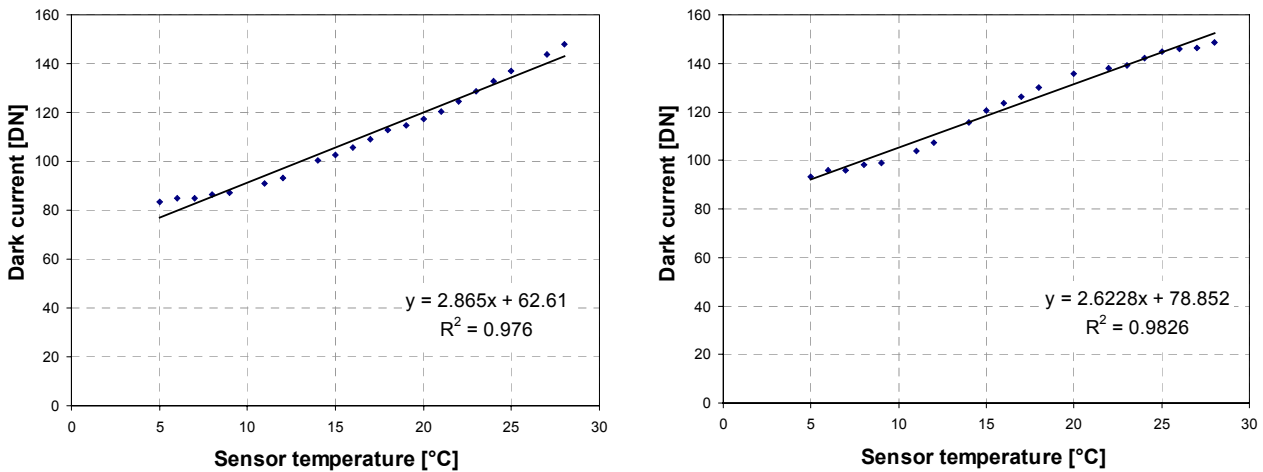


Figure 2-11:   *Dependency of mean dark current on sensor temperature measured for 1999 (left) and 2000 (right)*

The trend of both dark current functions is the same, but for 2000 the amount of dark current lies at a higher level than in 1999. The shift lies at about 16 DNs. This difference is caused by different lens settings in 2000 (see section 2.4).

To reduce the influence of dark current the camera is cooled by a Peltier device (see section 2.1.1.2). The cooling is software-controlled. A temperature probe measures the actual sensor temperature, and if a predefined value is exceeded, the Peltier device is

switched on. Thus it was possible to reduce the range of sensor temperatures from 5-26°C to 5–16°C. The maximum difference from 26°C to 14°C leads to a dark current decrease of 30%.

Under flight conditions the sensor temperature could not be stabilized at a given value. The reason is found in the size of the Peltier device that is limited by the space in the standard mount, where the AVIS is fitted into the aircraft. With this given size of the Peltier element the surrounding temperature of the air influenced the cooling. It was possible to cool the sensor to a temperature level 15°C below the surrounding air temperature. The resulting sensor temperatures lie in the range of 5°C to 16°C.

## 2.2.2     Homogeneity of the CCD Array

Array detectors such as CCD elements have defects. These defects are regions with reduced sensitivity or with increased dark current. For scientific applications such as spectroscopy, these variations affect results and must therefore be corrected (Holst, 1998).

Another aspect is the light falloff or vignetting, which is an important effect for the illumination of an array through a lens. The frame of the lens shades the part of the light, which is arriving with high incidence angles (Pellikka, 1994).

For the derivation of sensor homogeneity and vignetting the radiation was measured under homogeneous light conditions for the years 1999 and 2000. For this purpose, measurements were performed using an integrating sphere and a Tungsten halogen lamp as illumination source. At least 500 image lines were imaged for the analysis, which was carried out with dark current corrected data.

Figure 2-12 shows the resulting matrices of the AVIS CCD element for 1999 and 2000. For a better visualisation the grey values are stretched from 0 to 255. In both matrices an overlapping of several phenomena can be seen.

On the right-hand margin darkened pixels on the CCD can be seen as a black-and-white column.

Several bright spots can be observed within the matrix. Their size varies and their shape is irregular with diffuse edges, which leads to the conclusion that they are most probably inhomogeneities in the silicon crystal of the CCD. They reduce the sensitivity of the sensor, so these pixels are darker compared with their surroundings. Therefore they must be multiplied with a higher (brighter) value (Oppelt & Mauser, 2000).
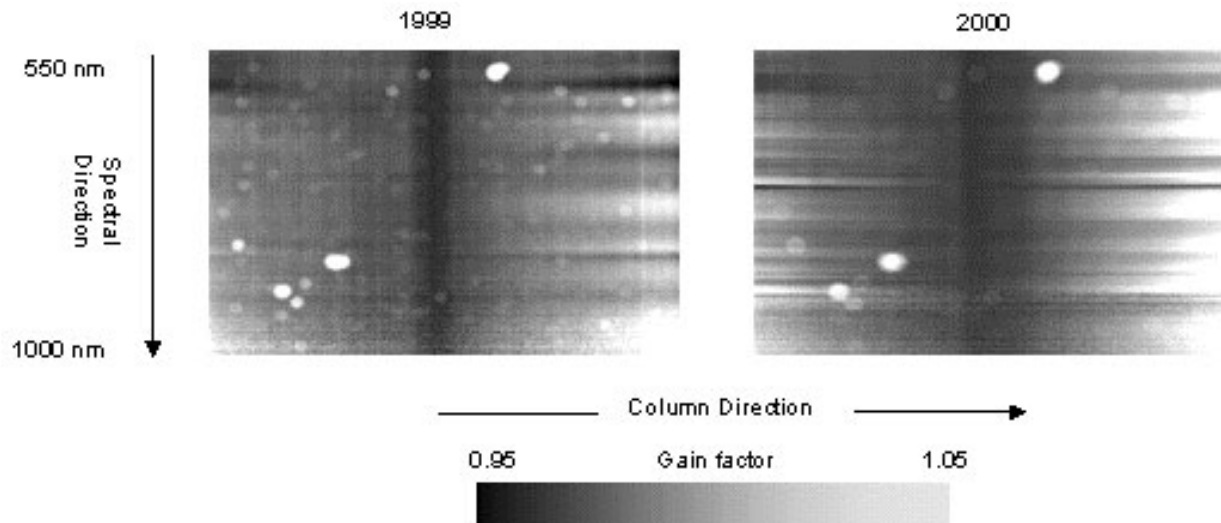
*Figure 2-12:*     *Gain matrices for 1999 (left) and 2000 (right)*

The spots are superimposed by a decrease in sensitivity towards the left and right edges of the CCD. This decrease is mainly due to the effect of vignetting (Oppelt & Mauser, 2000). This effect seems to be larger in the year 2000, especially on the right edge of the CCD. This is caused by the different lens settings in 2000. To increase the amount of radiation in the NIR, the aperture was widened in 2000 in comparison to 1999. This lead to a decrease of the gain factor in the NIR region, but an additional effect seems to be an increasing vignetting at the margins of the CCD.

## *2.3 Spectral Properties*

In the discussion of spectral properties of imaging spectrometers the terms spectral resolution, spectral sampling interval and centre wavelength are the basic parameters. Given a Gaussian shaped response function, the spectral resolution is defined as the full width half maximum (FWHM) of the function. The spectral sampling interval is the measure of distance between two adjacent points sampled in the spectrum. The centre wavelength, finally, is the peak response of the spectrometer to an infinitesimally small emission line (Figure 2-13) (Schaepman, 1998; Wolfe, 1997).
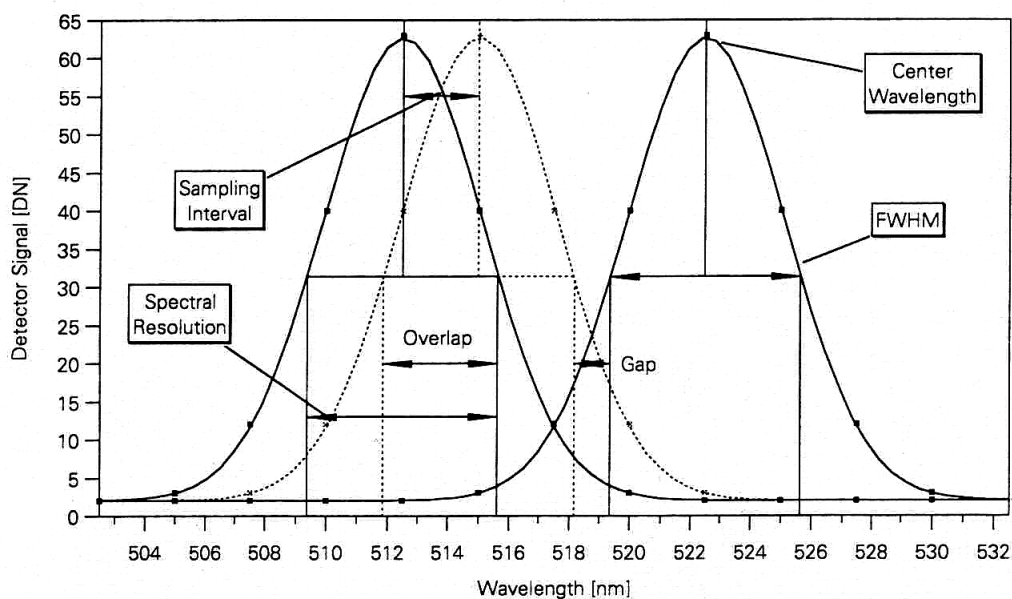


*Figure 2-13:*     *Spectral resolution, spectral sampling interval, FWHM and centre wavelength of a Gaussian response function (Schaepman, 1998)*

### 2.3.1     Spectral Resolution

Several methods exist to measure the spectral resolution of a spectrometer. With AVIS this was done using the radiative transfer model LOWTRAN-7 (Kneizys et al., 1988). This procedure requires already calibrated data, whereby the calibration is described in section 4. The basic idea is to correlate measured and modelled at sensor radiances of the oxygen absorption at about 760nm. This feature is suitable for this task because of its characteristic shape with two absorption peaks. Therefore, measurements of skylight were performed with AVIS, and these radiances were compared with modelled radiances, carried out with spectral resolutions from 0.5 to 8nm in steps of 0.5nm. The comparison is shown in Figure 2-14 with two modelled resolutions, 0.5nm and 6nm. The modelled shape at a spectral resolution of 6nm fits best with the measured feature (Oppelt & Mauser, 2000).
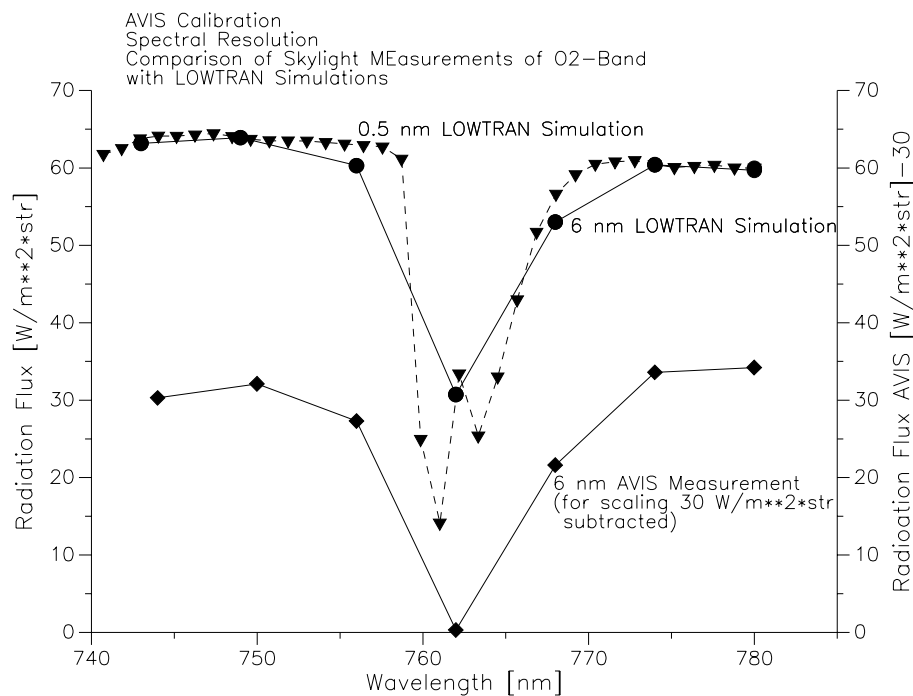
*Figure 2-14:*    *LOWTRAN simulation of radiances of skylight for 0.5 and 6nm spectral resolution compared with AVIS spectrum (Oppelt & Mauser, 2000)*

Thus, the spectral resolution or the FWHM of AVIS can be determined at 6nm.

### 2.3.2    Spectral Sampling Interval

The original spectral sampling rate of AVIS is 2nm, while the spectral resolution is 6nm. Thus the data are oversampled by the factor 3. Therefore the resampling of the bands to a spectral sampling rate corresponding to the spectral resolution enables the reduction of the huge amount of data as well as the increase of the Signal to Noise Ratio without loss of spectral information. The resampling to 80 spectral bands is described in section 4.2.2. Thus this step is not discussed here furthermore.

### 2.3.3    Centre Wavelengths

The centre wavelengths of the spectrograph are defined by the manufacturer. The centre wavelengths for the data of the 2nm data are given in Appendix 1.

The first centre wavelength lies at 553.3nm for the 240 band data, and with the given spectral sampling interval of 2.0452nm the centre wavelengths can be determined with the following equation:

$$\lambda_{n\,centre} = \lambda_1 + 2.0452 \cdot n_b \qquad\qquad (2.4)$$

where

$\lambda_1$            centre wavelength of band 1 [nm],

$\lambda_{ncentre}$         centre wavelength of band $n_b$ [nm],

$n_b$          number of band (Oppelt & Mauser, 2000).

The averaging of bands leads to an 80-band data set with new centre wavelengths. The averaging was calculated using equation (4.1) (section 4.2.2). The actual number of band is 74 because the lens limits the spectral sensitivity at 1000nm.

The positioning of the centre wavelengths must be calibrated. In general this is done using one or more atomic emission lines from either a discharge lamp or an hollow cathode lamp. The wavelengths of most atomic emission lines are known with an accuracy that exceeds the requirements of calibration (Schaepman, 1998; Chen, 1997). The calibration of the centre wavelengths of AVIS was performed using an Argon emission lamp (Electro-Technoic Inc.). The description of its emission lines is based on the National Bureau of Standards – National Research Council, Committee of Line Spectra of the Elements (NBoS) (Reader & Corliss, 1976). The measurements were performed in the darkened laboratory with the Argon lamp as illumination source. The data were dark current and homogeneity corrected before the analysis. The results are shown in Figure 2-15.

The measured grey value peaks of AVIS correspond well with the emission lines of the Argon lamp. The deviation is smaller than the original spectral sampling interval of 2nm.



| Emissionline NBoS | Reflection peak AVIS |
|---|---|
| 695.54 | 696.76 |
| 706.72 | 705.88 |
| 738.39 | 738.28 |
| 750.39 | 750.43 |
| 763.51 | 762.58 |
| 801.48 | 801.05 |
| 811.53 | 811.17 |
| 842.46 | 841.55 |
| 866.79 | 865.87 |
| 912.29 | 912.41 |
| 922.45 | 922.54 |
| 965.78 | 965.06 |
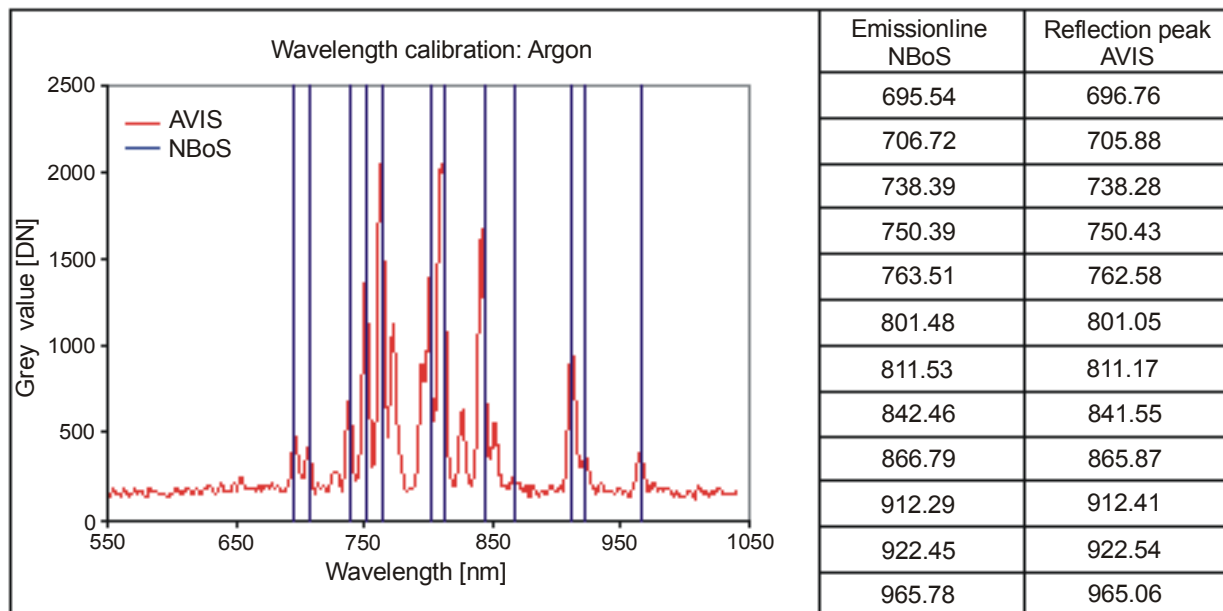
Figure 2-15:    Wavelength calibration of AVIS using an Argon emission lamp; the table presents the wavelengths of the reflection peaks in [nm]; NBoS = National Bureau of Standards (Oppelt & Mauser, 2000)

These results confirm the good quality of the spectrograph. They also demonstrate that no spectral shift occurs from the 650nm to the 1000nm region. Spectral shift refers to the

nonlinearity of the sampling interval as well as spectral resolution in the region of the instrument's sensitivity. Spectral shifts normally occur mainly towards longer wavelengths. Between 670nm and 950nm no such effects can be observed, thus it can be expected that AVIS shows no spectral shift.

Table 2-4: Centre wavelengths for the averaged band AVIS setup with a spectral resolution of 6nm

| Band No. | Centre wavelength [nm] | Band No. | Centre wavelength [nm] | Band No. | Centre wavelength [nm] | Band No. | Centre wavelength [nm] |
|---|---|---|---|---|---|---|---|
| 1 | Header | 21 | 673.97 | 41 | 796.68 | 61 | 919.39 |
| 2 | 557.39 | 22 | 680.11 | 42 | 802.82 | 62 | 925.53 |
| 3 | 563.53 | 23 | 686.24 | 43 | 808.95 | 63 | 931.67 |
| 4 | 569.67 | 24 | 692.38 | 44 | 815.09 | 64 | 937.80 |
| 5 | 575.80 | 25 | 698.51 | 45 | 821.23 | 65 | 943.94 |
| 6 | 581.94 | 26 | 704.65 | 46 | 827.36 | 66 | 950.07 |
| 7 | 588.07 | 27 | 710.78 | 47 | 833.49 | 67 | 956.21 |
| 8 | 594.21 | 28 | 716.92 | 48 | 839.63 | 68 | 962.34 |
| 9 | 600.34 | 29 | 723.06 | 49 | 845.77 | 69 | 968.48 |
| 10 | 606.48 | 30 | 729.19 | 50 | 851.90 | 70 | 974.62 |
| 11 | 612.61 | 31 | 735.33 | 51 | 858.04 | 71 | 980.75 |
| 12 | 618.75 | 32 | 741.46 | 52 | 864.17 | 72 | 986.89 |
| 13 | 624.87 | 33 | 747.60 | 53 | 870.31 | 73 | 993.02 |
| 14 | 631.02 | 34 | 753.73 | 54 | 876.45 | 74 | 999.16 |
| 15 | 637.16 | 35 | 759.87 | 55 | 882.58 | 75 | 1005.29 |
| 16 | 643.29 | 36 | 766.00 | 56 | 888.72 | 76 | 1011.43 |
| 17 | 649.43 | 37 | 772.14 | 57 | 894.85 | 77 | 1017.57 |
| 18 | 655.56 | 38 | 778.28 | 58 | 900.99 | 78 | 1023.70 |
| 19 | 661.69 | 39 | 784.41 | 59 | 907.12 | 79 | 1029.84 |
| 20 | 667.84 | 40 | 790.55 | 60 | 913.26 | 80 | 1035.98 |

## 2.4 Signal to Noise Ratio (SNR)

Noise may be present in the radiant flux arriving at the detector. This external noise may be generated in the processing of the optical signal by mechanical vibrations of the optical components, inadequate spectral filtering, or random scattering of stray light. In addition electrical noise may be generated in the system by electromagnetic fields originating from chopper motors and other sources. Quantum noise generated by the random arrival of photons from a constant light source cannot be eliminated. Internal noise is produced by the detectors and during signal processing. The major sources are the detector and the preamplifier. The other components of the measured input signal are defined as the signal. This noiseless part of a measurement carries the information of interest (Schaepman, 1998; Schowengerdt, 1997). For effective use, an instrument must be designed so that the noise level is small relative to the signal. This is measured by the Signal to Noise Ratio (SNR), the ratio of the measured brightness to the variation of the noise (Campbell, 1996).

The SNR definition used here relies on noise in a signal of the AVIS instrument, which is defined as the standard deviation of that signal. This definition is based primarily on a laboratory calibration of an instrument (Schaepman, 1998) assuming a Gaussian distributed signal:

$$SNR = \frac{DN}{\sigma}$$                                             (2.5)

where

$DN$              measured signal (dark current corrected) [DN],

$\sigma$              standard deviation [DN].

The SNR in the laboratory is measured using an integrating sphere and a constant radiation source. The advantage of laboratory determined SNR is the absence of significant changes in the optical path. The integrating sphere as an inherently stable radiance source exhibits only a very small standard deviation in luminescence over time. The expected SNR values are therefore high and are not comparable to vicarious calibration experiments derived SNR values using the sun as illumination source (Schaepman, 1998). The AVIS setup used in the laboratory was optimised for flight conditions. The illumination source was a Tungsten halogen lamp. The data were corrected for dark current and CCD homogeneity. The results of the measurements for 1999 are shown in Figure 2-16:  .

The range of DNs is 2048, because two neighbouring pixel with each 10bit data depth are added. With a maximum grey value of 1800 DNs the detector is not saturated. This is an important fact, because under flight conditions the illumination is at a lower level. Saturation during a flight is thus unlikely to occur.
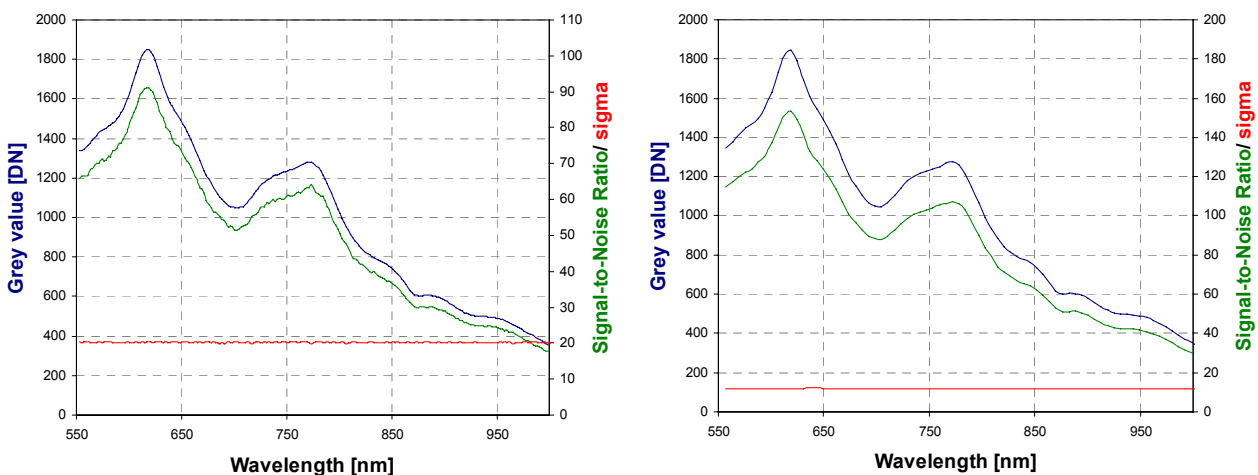
*Figure 2-16:* *AVIS SNR analysis 1999 for a spectral sampling interval of 2nm (left) and 6nm (right); sigma is the standard deviation; illumination source: Tungsten halogen lamp (Oppelt & Mauser, 2000)*

The standard deviation, sigma, represents the system noise. In the diagrams the independency of sigma from the corresponding grey value can clearly be seen. The system noise is therefore independent of the incoming radiation.

The SNR decreases with the amplitude of the signal. This behaviour is characteristic for array detectors at a relatively low flux level (Holst, 1998). The maximum grey values appear at 630nm and 800nm respectively, which corresponds both to the maximum signal of the lamp at 630nm and to the spectral sensitivity of the system (see Figure 2-9) (Oppelt & Mauser, 2000).

With the 2nm resolution the SNR above 900nm becomes very low, and the measured signal is near the level of the system noise. The interpretation of the signal may thus cause problems because of its uncertainty.

With the 6nm resolution the SNR values lie at a level 1.7 times higher than with 2nm, which is caused by the averaging of the bands. Presuming a Gaussian error distribution, the signal increases three times by the averaging of three bands, while the noise increases with the square root of three. This corresponds to the increase of the SNR caused by averaging (Oppelt & Mauser, 2000).

Nevertheless, the SNR, especially in the NIR, is low considering the good illumination conditions during the measurement. The less ideal illumination conditions during flight, compared to those in the laboratory, have to be taken into account. These considerations and experiences, which were made during the first year of operation, led to a change of the camera settings for the year 2000. To increase the amount of incoming radiation the aperture of the lens was increased. To avoid saturation in the lower wavelength region the gain factor for the camera output signal was reduced. This change of settings necessitates a SNR analysis for the 2000 data.

The measurement procedure was the same as in 1999. Figure 2-17 provides the results of the SNR analysis in 2000 for the spectral sampling interval of 6nm. The grey values lay at a level one third of 1999, which is due to the lowered gain factor of the camera. Yet the standard deviation lie with an average value of 6.3 on a lower level than in 1999, which leads to an increased SNR. The maxima still lay at 630nm and 800nm, but the SNR is 220 and 150 respectively. At 900nm the SNR is 58, compared to 50 in 1999. The factor of SNR 2000/1999 decreases from 1.47 at 600nm to 1.16 at 900nm. This is due to the slight increase of the standard deviation from 6.1 to 6.8 along this wavelength region.
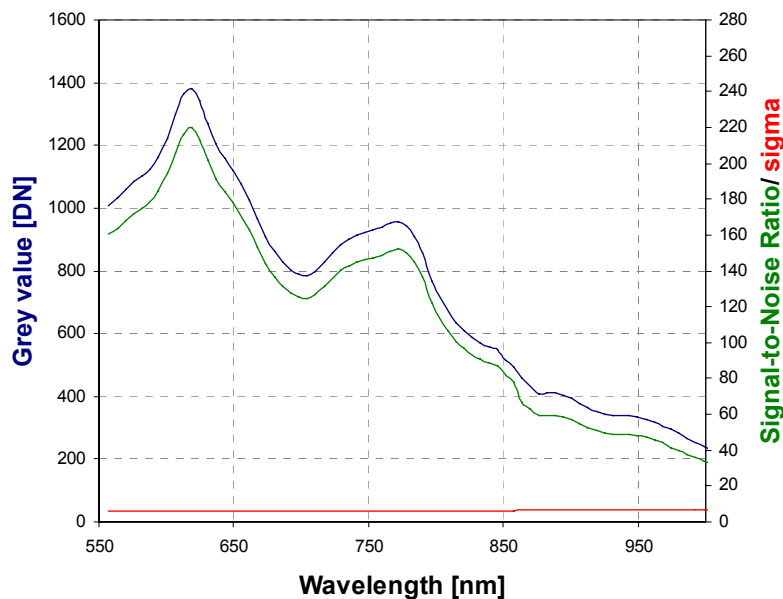


Figure 2-17:    AVIS SNR analysis 2000 for a spectral sampling interval of 6nm; sigma is the standard deviation; illumination source: Tungsten halogen lamp

Additionally, a SNR analysis was performed in 2000 using the integrating sphere with the sun as illumination source. These measurements should act as a vicarious calibration and give information about the signal-to-noise behaviour under natural illumination conditions. The measurements were taken in the field under weather conditions suitable for image acquisition, and the illumination entrance of the sphere was oriented towards the sun. The analysis procedure was equal to these conducted in the laboratory. Figure 2-18 shows the results of this vicarious calibration.

The shape of the curve is different from those made with the halogen lamp. It has a larger slope and the first maximum is shifted toward the blue wavelength region. Also the curve shows absorption features of oxygen at 760nm and water vapour at 940nm. The signal drops steeply above 850nm, until it reaches 75DN at 943nm. The low signal level causes the decrease of sigma from 7.6 at 630nm to 5.8 at 900nm. Thus, the SNR decreases from 150 at 600nm to 30 at 900nm, and even 17 at 940nm.
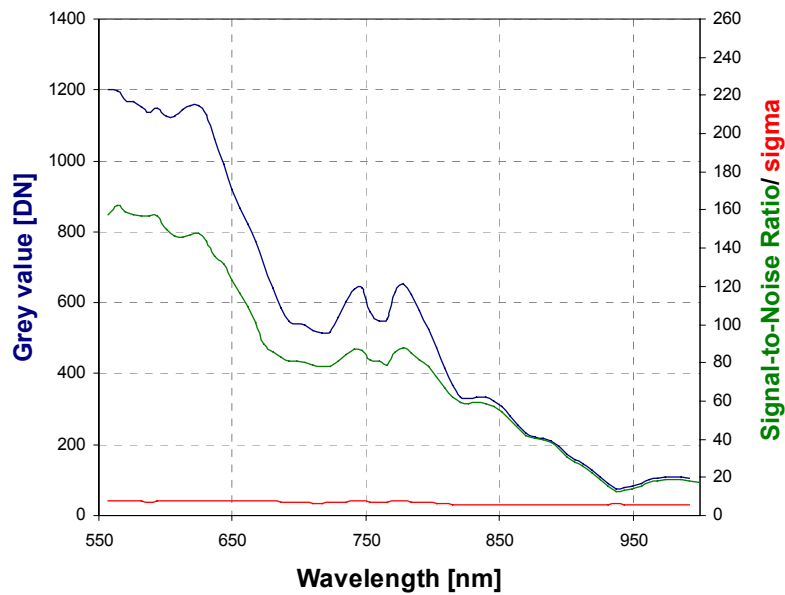
*Figure 2-18:    AVIS SNR analysis 2000 for spectral sampling interval of 6nm; sigma is the standard deviation; illumination source: sunlight*

This experiment shows a good SNR behaviour of AVIS in the VIS range. The low signal level above 850nm leads to a strongly reduced SNR in this region, where the incoming light limits the interpretation capability of the data.

The resulting SNR values in dB are calculated using equation (2.6) and are summarised in Table 2-5. It has to be noted that the SNR values are valid only for targets with a reflection identical to the integration sphere, which is close to 100%.

$$SNR_{dB} = 20\log\left(\frac{DN_{max}}{DN_{noise}}\right)$$   (2.6)

where

*DN_{max}*        maximum signal [DN],

*DN_{noise}*      noise level [DN] (Holst, 1998).

*Table 2-5:    AVIS SNR*

| AVIS setup / sampling interval | Illumination source | SNR [dB] |
|---|---|---|
| 1999 / 2nm | Tungsten halogen | 39 |
| 1999 / 6nm | Tungsten halogen | 45 |
| 2000 / 6nm | Tungsten halogen | 47 |
| 2000 / 6nm | Sun | 44 |

## 2.5 Geometric Properties

The most important geometric parameters are the spatial resolution, the field of view (FOV) and the instantaneous field of view (IFOV). The spatial resolution is the resolving power of an instrument while the terms FOV and IFOV describe the spatial sampling behaviour of a remote sensing system as detailed below.

### 2.5.1    Spatial Resolution

The spatial resolution provides valuable information regarding the finest spatial detail that can be discerned by a system. An electronic imaging system is composed of many subsystems and its spatial resolution is determined by each of them (Holst, 1998).

With AVIS, the spatial resolution is mainly influenced by the geometry of the lens, slit length and point spread size of the spectrograph and the camera size. The spatial resolution is determined by the lowest parameter value mentioned above, whereby it has to be differentiated between the spatial resolution along and across the direction of the aircraft motion (SPETRAL IMAGING LTD., 1998a; Oppelt & Mauser, 2000).

The spectrograph has a resolution of 300 pixels (SPECTRAL IMAGING LTD., 1998c). The frame grabber samples 780 pixels per image line. This oversampling produces superfluous data. Therefore two consecutive pixels are added which leads to a resulting number of 390 pixels per image line (Oppelt & Mauser, 2000).

This configuration is used to test the signal transfer function of AVIS. The test was carried out in the laboratory using a black/white ramp. The results are shown in Figure 2-19.
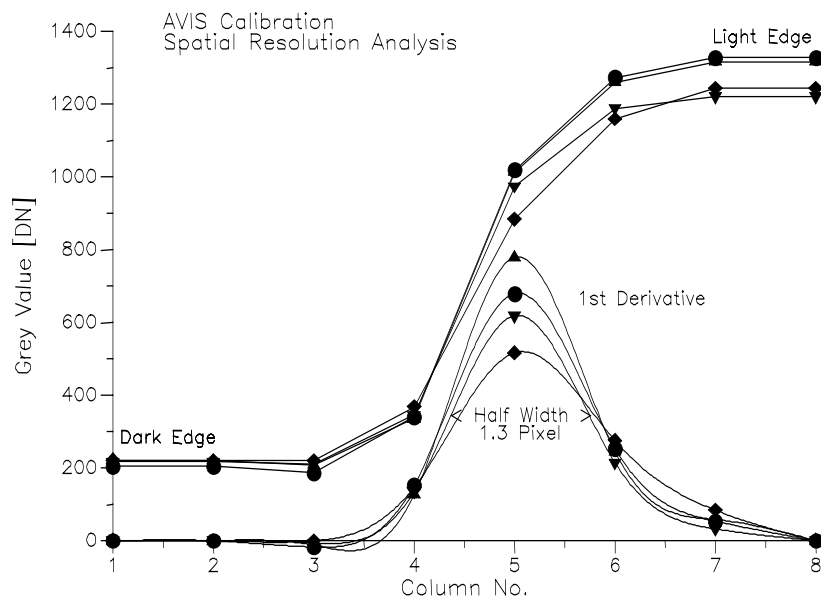


*Figure 2-19:      Illustration of a brightness ramp (Oppelt & Mauser, 2000)*

A spline was fitted for the first derivative of the ramp. Figure 2-19 illustrates the change of the brightness within 1.3 pixels. The new value is reached at the third pixel. Thus the actual spatial resolution of the system lies at real 300 pixels per image line (390/1.3=300) (SPECTRAL IMAGING LTD., 1998c; Oppelt & Mauser, 2000).

## 2.5.2    Field of View and Instantaneous Field of View

The Field of View (FOV) is the solid angle through which radiation is accepted by an optical system. The FOV of AVIS of 68.2° is sized by the lens.

The instantaneous field of view (IFOV) represents the area viewed by the instrument for each pixel. With an airborne instrument it can be distinguished between the IFOV on the sensor and the IFOV on the ground. In addition, the IFOV along an image line is different from the IFOV in the direction of aircraft motion.

The instantaneous field of view along an image line ($IFOV_{across\ track}$) is determined by the field of view ($FOV$) of the lens and the number of pixels per image line as follows:

$$IFOV_{across\ track} = \frac{FOV_{lens}}{N_c} = \frac{1.19}{390} = 3.1 \cdot 10^{-3}$$

(2.7)

where

$IFOF_{across\ track}$        instantaneous field of view along an image line [rad],
$FOV_{lens}$           field of vies of the lens [rad],
$N_c$              number of columns (pixel) per image line.

Thus the $IFOV_{across\ track}$ of the AVIS system is 3.1mrad.

The IFOV on the ground along the image line is dependent on the $IFOF_{across\ track}$ and the flight height of the aircraft as follows:

$$IFOV_{across\ track, ground} = IFOV_{across\ track} \cdot D$$

(2.8)

where

$IFOV_{across\ track, ground}$  IFOV on the ground along the image line [m],
D                distance between system and target = flight height above ground [m].

The IFOV of one pixel in direction of the aircraft movement ($IFOV_{along\ track}$) is determined by the width of the spectrograph slit and the focal length of the camera as followed:

$$IFOV_{along\ track} = \frac{W_s}{f} = \frac{25 \cdot 10^{-6}}{8.4 \cdot 10^{-3}} = 2.98 \cdot 10^{-3}$$

(2.9)

where

$IFOV_{along\ track}$       instantaneous field of view along the movement [rad],
$W_s$             slit width of spectrograph [m],

$f$                    focal length of the camera [m].

Therefore the AVIS IFOV along the aircraft movement is 2.98mrad.

The along track IFOV on ground is determined by the instantaneous field of view along the movement and the velocity of the aircraft.

$$IFOV_{along\ track\ ,ground} = IFOV_{along\ track} \cdot v_{aircraft} \tag{2.10}$$

where

$IFOV_{along\ track,\ ground}$     along track IFOV on the ground [m],

$v_{aircraft}$             velocity of the aircraft [ms$^{-1}$].

To provide a nearly square pixel size with a given aircraft speed, it is important to adapt the frame rate at different flight levels. Under flight conditions the aircraft speed is often not constant, because the pilot has to consider both changing wind and thermals. This as well as slight variations of the ground elevation cause variations in the pixel spacing. Therefore during the flight only approximately square pixels can be obtained. The variations in pixel size have to be corrected afterwards during the processing of the data.

Thus at an aircraft velocity of 50ms$^{-1}$, corresponding to 180kmh$^{-1}$, the resulting values for the IFOV on the ground and across track FOV on the ground are given in Table 2-6 as well as the frame rate required.

Table 2-6: Pixel size, spatial resolution and FOV at different flight altitudes with resulting frame rates

| Flight altitude [m above ground] | $IFOV_{across\ track,\ ground}$ [m] | $IFOV_{along\ track,\ ground}$ [m] | $FOV_{across\ track}$ [m] | Frame rate [images/s] |
|---|---|---|---|---|
| 300 | 0.93 | 0.89 | 363 | 50 |
| 600 | 1.86 | 1.79 | 725 | 25 |
| 1000 | 3.10 | 2.98 | 1209 | 15 |
| 1500 | 4.65 | 4.47 | 1814 | 10 |
| 3000 | 9.30 | 8.94 | 3627 | 5 |

During operation it turned out that the upper limit of the frame rates is 22 images/s. Lapsed lines occur at frame rates above this value. With decreasing flight height and increasing aircraft speed the number of lapses increased. Thus, the flight height was limited on its lower boundary at about 600m above ground.

## 2.6 Summary

The previous sections describe the AVIS components and their behaviour in their radiometrical, spectral and geometrical manner. The properties of the system AVIS is a composition of its components. Table 2-7 summarises the most important characteristics of AVIS for the years 1999 and 2000.

AVIS operates with 240 bands in the 550-1000nm wavelength region. The original spectral sampling rate is 2nm, but with a real spectral resolution of 6nm the data are resampled with a spectral sampling rate of 6nm. The last 6 bands of the resulting 80 band data set cannot be used because the lens limits the spectral range of AVIS at 1000nm. Therefore 74 bands of AVIS can be used for analysis.

Table 2-7:   AVIS parameters

| Parameter | Description |
|---|---|
| Spectrograph | ImSpector V9-M-897 |
| Slit width spectrograph | 25µm |
| Camera | HAMAMATSU C5999; 2/3" |
| Lens | SCHNEIDER CNG 1.4/8 |
| Focal length | 8.4mm |
| Filter | SCHOTT BG26; belt filter |
| Spectral range | 553–999nm |
| Spectral resolution | 6nm |
| Spectral sampling rate / resampling | 2nm / 6nm |
| Number of bands used | 74 |
| SNR (illumination: Tungsten halogen lamp) | 45dB (1999); 47dB (2000) |
| Spatial resolution | 300 pixels per image line |
| Spatial sampling rate | 390 pixels per image line |
| FOV | 1.19rad |
| IFOV across track | 3.10mrad |
| IFOV along track | 2.98mrad |

The lens settings were changed in 2000 leading to different SNRs for the years 1999 (45dB) and 2000 (47dB).

The spatial resolution across track is 300 pixel with a spatial sampling rate of 390 pixel. The FOV of the system is 1.19rad, which is determined by the lens. The across track IFOV can be rated at 3.10mrad, while the along track IFOV is 2.98mrad. The spatial resolution

on the ground is dependent on the flight altitude. It varies from about 2m flown at 600m above ground to 10m at 3000m.

The spectral sensitivity of AVIS is shown in Figure 2-20. It is a smooth shaped curve with an average sensitivity of 30%. Two slight maxima exist at 630nm and 900nm; beyond 900nm the spectral sensitivity drops towards 18%.
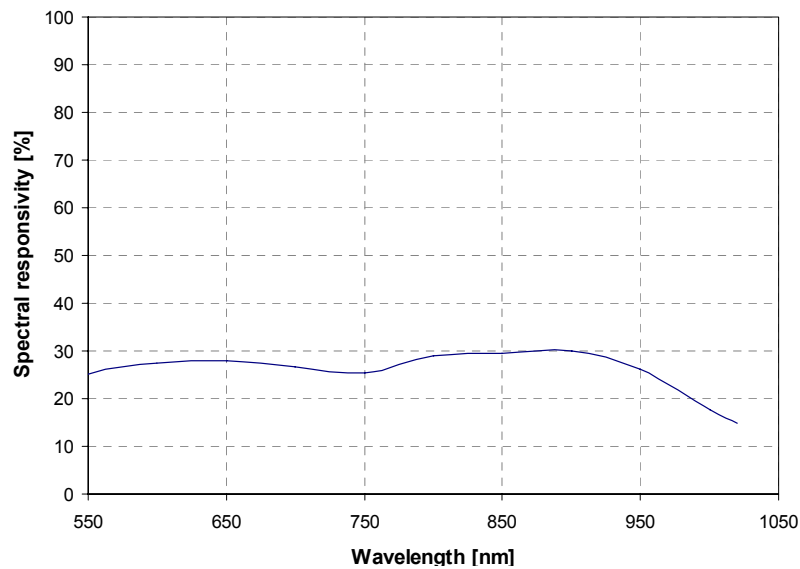


*Figure 2-20:     Spectral responsivity of AVIS*

# 3   Test Sites and Ground Measurements (Ground Truth)

Field measurements are important for the development of empirical methods regarding the derivation of biological compounds of the biosphere with remote sensing data as well as for the validation of existing approaches. Beside the measurements of biological parameters on the ground there is a need for validation measurements with field spectrometers for investigation and comparison of a new system with established ones.

To provide an extensive data base for the analysis of the remote sensing data, the following investigations were made on ground within three test sites throughout the years 1999 and 2000.

1.    Land cover mapping (main fruits), which were integrated in a Geographical Information Systems (GIS) in addition to the information about soils and elevation:

|               |        |
|---------------|--------|
| Test site Gilching | 1999 |
|               | 2000 |
| Test site Inning | 1999 |
|               | 2000 |
| Test site Frieding | 1999 |

2.    Detailed measurements at several test fields to ascertain plant parameters:

|               |      | Time period |
|---------------|------|-------------|
| Test site Gilching | 1999 | $19^{th}$ April – $27^{th}$ September |
|               | 2000 | $25^{th}$ April – $21^{st}$ August |
| Tets site Inning | 1999 | $19^{th}$ April – $27^{th}$ September |
|               | 2000 | $25^{th}$ April – $21^{st}$ August |
| Test site Frieding | 1999 | $19^{th}$ April – $27^{th}$ September |

A description of the test sites, the investigated plant species as well as the selected parameters and ground truth measurements follow in the sections below. The measurements with field spectrometers are also illustrated.

## 3.1 Test Area Starnberg

Three test sites were chosen for the ground truth campaigns, which all are located in the Starnberger county, in this study called test area Starnberg. The whole region will be characterised regarding its location, integration into natural units and climate, whereas these parameters cover all of the three test sites. Others such as soil, land cover and description of the test fields have to be discussed separately.

The test area for this study is located in the northern Bavarian foothills, 25km southwest of Munich, Germany. It is embedded between the Ammersee in the west and the Starnberger See in the east. The municipalities Gilching and Andechs limit the test area at the northern and southern edge respectively. The corners are given in Table 3-1.

Table 3-1:    Location of the test area Starnberg

| Geographical coordinate | East | North |
|---|---|---|
| Upper left corner | 11° 09' | 48° 06' |
| Lower right corner | 11° 20' | 47° 57' |

The reasons for the choice of this area are manifold. First of all, this site is characterised by a large variability in land use in combination with similar growing conditions. The small extent as well as the proximity to the Institute for Geography in Munich makes ground truth measurements much easier. Additionally, the proximity to the German Aerospace centre DLR enables the use of its reflection standard (see section 3.4.4.1).

The main land use types are grassland, maize and grain, which are the crops of interest for this study. Thus a wide selection of feasible test fields exists.

The variation in ground elevation is less than 120m. High relief energy affects the illumination conditions, which influence the radiometric processing and interpretation of the remote sensing data. Additionally, the relief, among other things, influences the geometric resolution of the image data. Differences of the relief alter the spatial resolution on ground and complicate geometric processing. Thus the subdued relief simplifies the processing of the hyperspectral data.

An important factor was the possibility to cooperate with the local office for agriculture, the *Amt für Landwirtschaft*. In this region most of the farmers are under contract to this office. This includes accounting of fertiliser and herbicide application as well as the date of sowing, soil treatment and harvest. The collaboration enabled access to the file system, so-called "Schlagkartei", where the treatment data are stored. The access to this file is on the basis of field numbers and includes information for the interpretation of both ground and AVIS data.

Last but not least two weather stations of the Bavarian network of agro-meteorological stations in this region enable access to local weather monitoring. A network of 119 weather stations throughout Bavaria provide information about precipitation, soil and air temperature, total radiation and air humidity with an hourly resolution. This information is available free of charge via Internet. The station numbers 72 "Gut Hüll" and 80 "Rothenfeld" provide information about the weather during the field campaigns. Their locations are given in Figure 3-11.

The integration of the test area into natural entities leads to a differentiation into two units: the young moraine region of the Ammer-Loisach glacier (I, see Figure 3-1) and the alluvial cover of the Munich plain (II) (Graul, 1962).
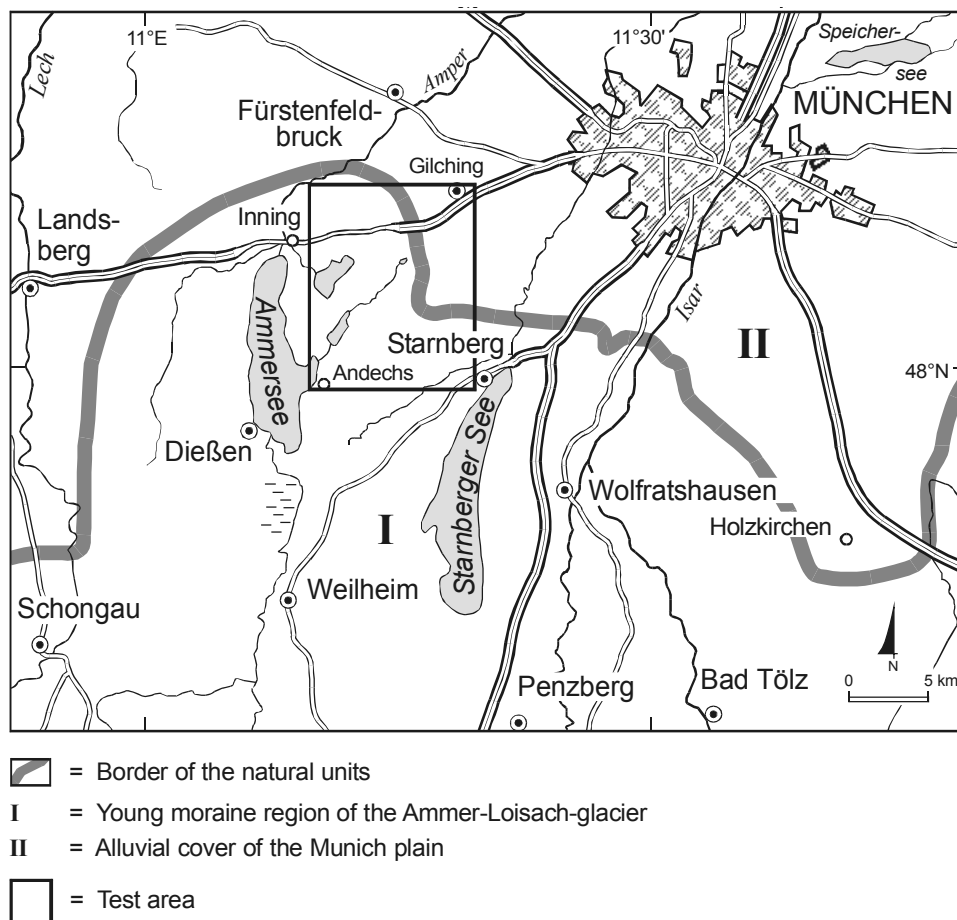


*Figure 3-1:*      *Location of the natural units of the test area Starnberg (cartography: V. Falck)*

The hilly area of the young moraines, which originates from the late Pleistocene, is embedded between the Fürstenfeldbruck older moraine region with higher relief in the north and the flysch zone in the south. The ground elevation lies between 530m and 650m above sea level. The succession of three circles of moraines with characteristic hilly forms and numerous dead ice kettles dominates this landscape. The drainage is mostly underground (Graul, 1962).

The Munich plain is an alluvial accumulation of gravels that covers the area of an oblique triangle. Its corners lie at Holzkirchen (Taubenberg) south of Munich, 60km north-west near Fürstenfeldbruck and near Moosburg, a small town 50km north of Munich. The ground elevation is 700m above sea level in the south-east, 500m in the north-west and 400m in the north corner (Michler, 1994).

According to the climatic classification of Köppen & Geiger (1961) the test area can be assigned to the cool and ever moist temperate climate *Cfb*. Summers are influenced by the prevailing north–west wind and are characterised by high amounts of rainfall, which are due to the barrier effect of the Alps. Within the 30-year period 1931-1960 the maximum is reached in July. The autumns and winters are deficient of precipitation. This is due to the foehn occurring with south–west wind as well as high-pressure weather. The annual amount of precipitation lies between 900 and 1100mm, increasing towards the alps (Keller, 1956; Andres & Pfeiffer, 1955).
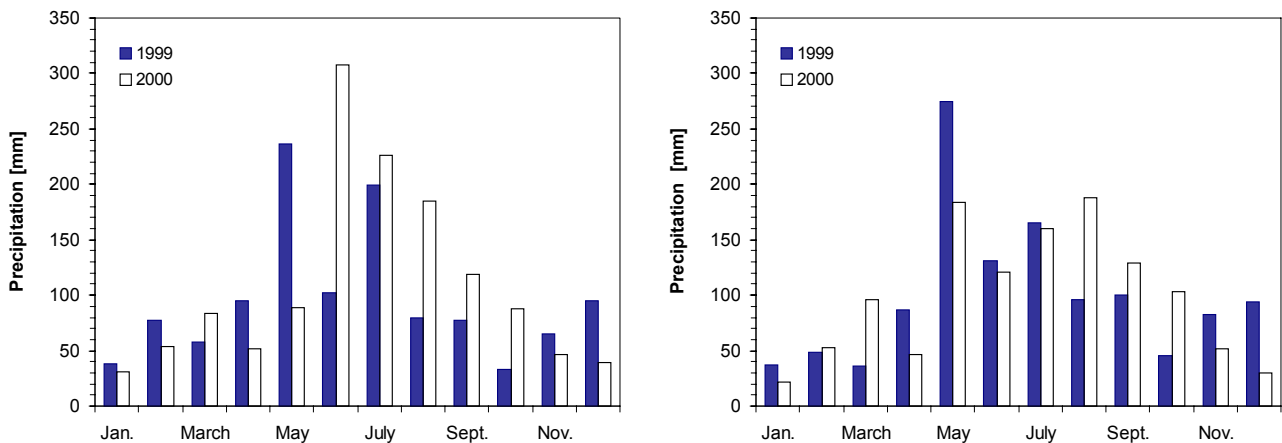


Figure 3-2:      *Monthly precipitation measured at the weather stations Hüll (left) and Rothenfeld (right) during 1999 and 2000*

Compared to the precipitation distribution described above, the weather stations Hüll and Rothenfeld show an earlier maximum of precipitation in 1999, which lies in May. This is due to the heavy rainfalls from 19th to 22nd of this month, leading to flooding in this region. In 2000, Hüll monitored a strong maximum in June (307mm), in Rothenfeld two maxima in May (183mm) and August (188mm) lay close together. Compared to the measuring period of 1931 to 1960 (see also Table 3-2), 1999 and 2000 are years with a high level of rainfall. Especially in 2000 this area is characterised by a very wet summer and autumn. This is noteworthy considering the fact that in 1999 the high amounts of rainfall in the second May decade led to flooding with the highest waters of the 20th century. But while several events happened in 1999 (May) and 2000 (June), in 2000 steady rainfall over a period of months led to a very high level of annual precipitation. In 1999 the water passed the watersides and vitiated the flooded fields near the lakes and

rivers. In 2000 the steady rain led to a mouldering and rotting of crops on the fields. Due to this the ground truth campaign was concluded at the end of August 2000.

Whereas the precipitation increases towards the south, the mean annual temperatures decrease slightly towards the Alps. The average temperatures in the time period 1931 to 1960 lie between 7°C and 8°C. The annual variations of temperature lie between 17°C and 19°C (Traub et al., 1956; Grottenthaler, 1980). The measured variations 1999 and 2000 are within this range, whereas the mean temperatures are raised, which can be explained by the inter-annual variability of weather data.

Table 3-2:    Mean average precipitation and average temperature within the test area (time period 1931 – 1960) measured at the weather stations Hüll and Rothenfeld (1999 and 2000) (Demircan 1995; Grottenthaler, 1980; Stolz, 1998; data of the "Agrarmetereologisches Messnetz Bayern" 1999 and 2000)

| Parameter | 1931 - 1960 | Hüll | | Rothenfeld | |
|---|---|---|---|---|---|
| | | 1999 | 2000 | 1999 | 2000 |
| Precipitation [mm] | 900 – 1100 | 1160 | 1320 | 1200 | 1180 |
| Ratio summer – winter precipitation | 1.9 | 1.7 | 3.3 | 2.1 | 3.0 |
| Month of precipitation maximum | July | May | June | May | August |
| Mean temperature [°C] | 7.0 – 8.0 | 8.3 | 8.5 | 7.5 | 8.4 |
| Annual temperature variation [°C] | 17 - 19 | 19.2 | 19.4 | 18.1 | 18.9 |

### 3.1.1    Test Site Gilching

The test site Gilching includes two adjacent water protection areas and ensures the water supply of the municipality. It covers an area of 19.4km² and is therefore the largest of the three test sites. Its position within the test area is presented in Figure 3-11.

According to the classification of the natural units (Meynen & Schmidthüsen, 1953; Graul, 1962) this test site is located in the "Gilchinger Platten", a subunit of the Munich alluvial plain (see Figure 3-1).

Between the hilly region of the Ammer–Loisach glacier and the Munich gravel plain there remains a strip of moraines of the Riß diluvium. Glacial waters cut their way through the moraines and formed the spillway of Gilching. This process can be seen in the topographic relief of the test site, which is given in Figure 3-3.

The glacial spillway of Gilching covers most of the area. Its elevation rises softly from 560m above sea level in the north to 620m in the south. In the south-west and south–east the moraines can be seen as terraces. The south–western terrace is made up of older moraines, originating from the Riß diluvium, and is more evident with differences in elevation of up to 30m towards the spillway of Gilching. The south–eastern part is formed

of younger moraines of the Würm diluvium and shows differences in elevation of up to 10m (Graul, 1962; Grottenthaler, 1980).

The parent material is also visible in the existing soil textures (see Figure 3-3). A paddy field soil exists at the spillway while medium silt and silty loam dominate on the terraces. Braunerde developed mainly as a soil type, corresponding to cambisols in the FAO system, which covers 90% of this test site. The other 10% are covered with rendzina, which is located on the south–west terrace.
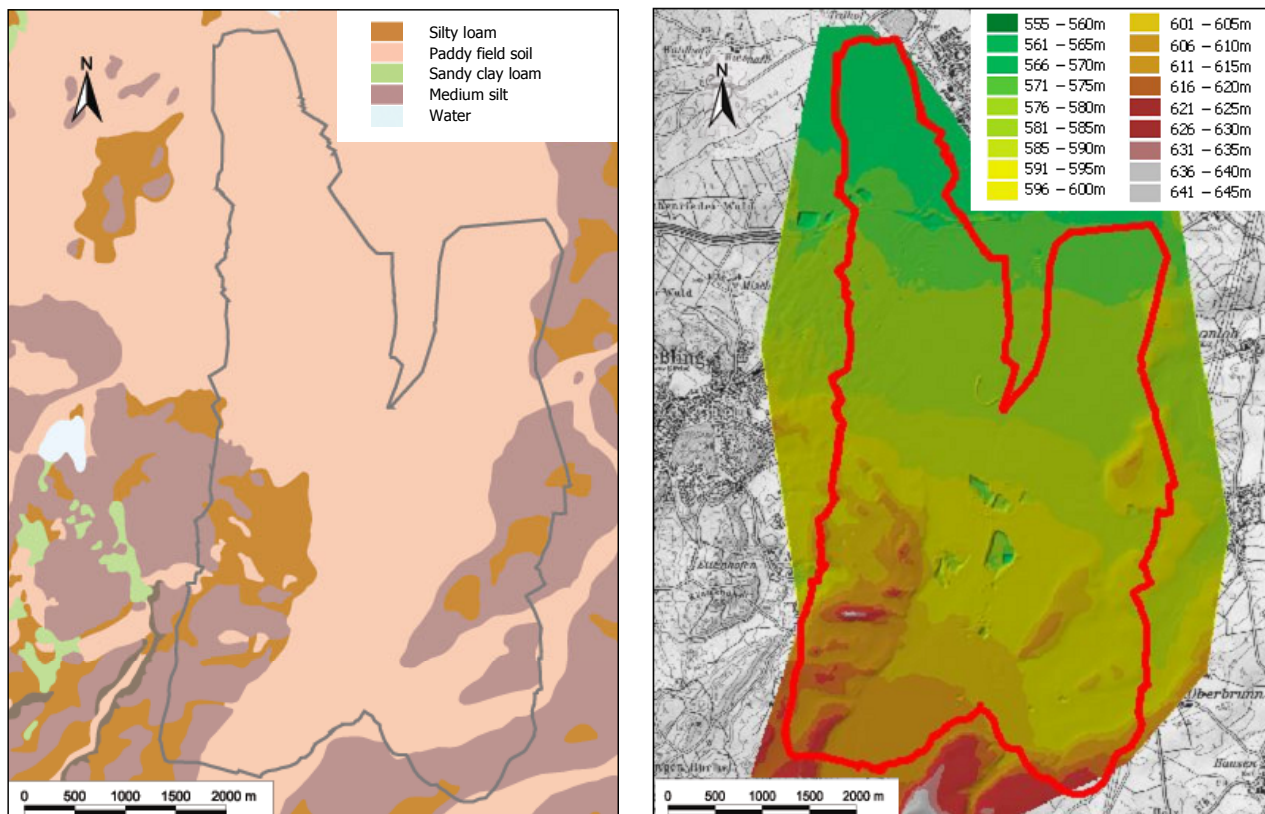


*Figure 3-3:*      *Soil texture (left) (source: Geologisches Landesamt, 1980) and elevation (right) in the test site Gilching (data source: Bayerisches Landesvermessungsamt, 1999)*

As mentioned above, the land cover is very heterogeneous. Land cover mappings in 1999 and 2000 showed that 35% of the test site is used as arable land, which is located on the braunerde with its high agricultural potential. The dominating crop types are wheat, maize and barley, but oat and rye can be found as well. About 27% of the area is occupied with permanent grassland, nearly 29% is classified as forest. 9% is sealed or residential and 4% is gravel pits. Figure 3-4 and Table 3-3 show the results of the land cover mappings for 1999 and 2000.

One of the two weather stations of the Bavarian network of agro-meteorological stations is located on the north–eastern edge of the test site. The station Hüll provides the meteorological data for this thesis.

Table 3-3:    *Distribution of land cover types within the test site Gilching 1999 and 2000*

| Land use type | Percentage coverage 1999 [%] | Percentage coverage 2000 [%] |
|---|---|---|
| Forest | 28.7 | 28.7 |
| Cereals | 20.0 | 21.4 |
| Maize | 12.2 | 8.10 |
| Grassland | 26.6 | 29.0 |
| Gravel pit | 3.50 | 4.10 |
| Sealed / Residential | 8.70 | 8.70 |
| Water | 0.30 | 0.30 |
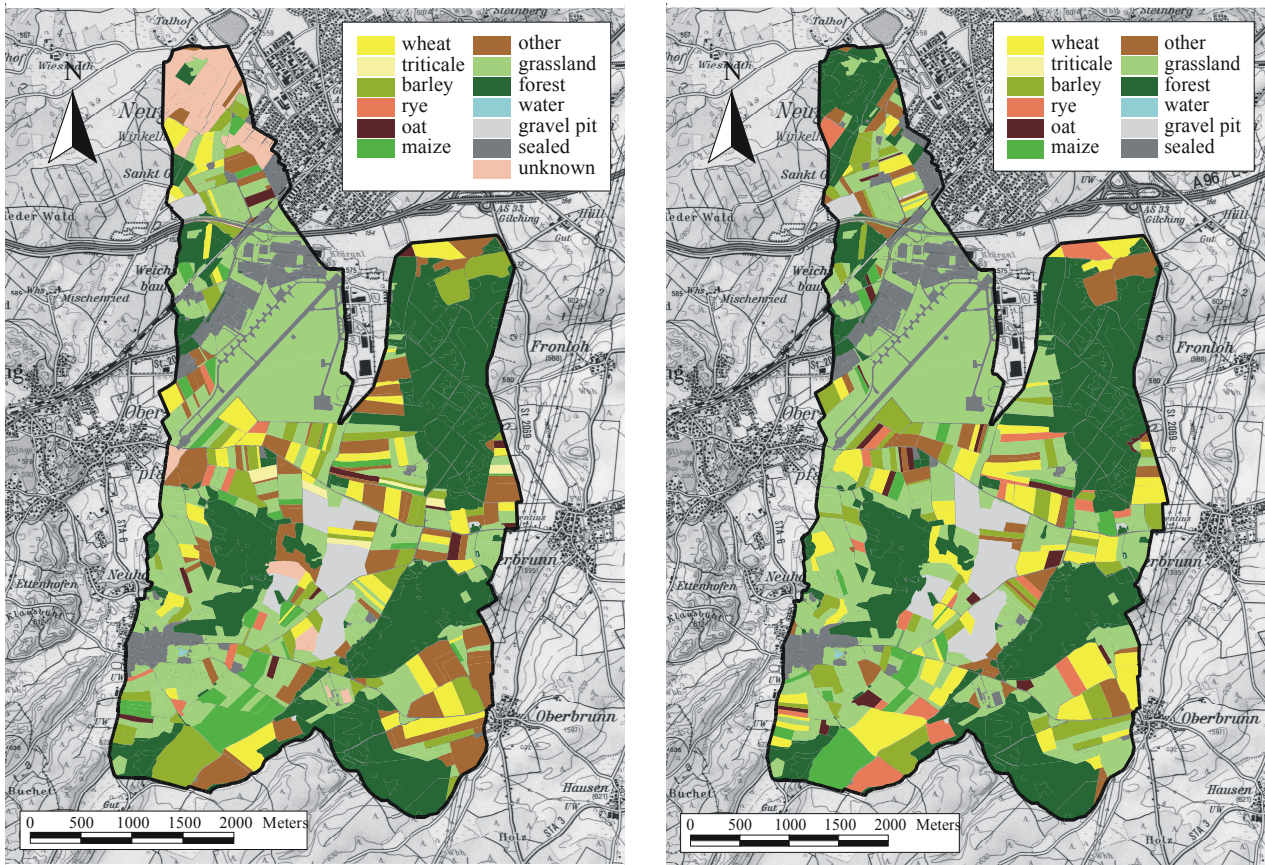


Figure 3-4:        *Land cover maps for 1999 (left) and 2000 (right)*

### 3.1.2    Test Site Inning

The test site Inning is also a water protection area and located at the north–western corner of the test area Starnberg (see Figure 3-11). It covers a relatively small area of 1.2km².
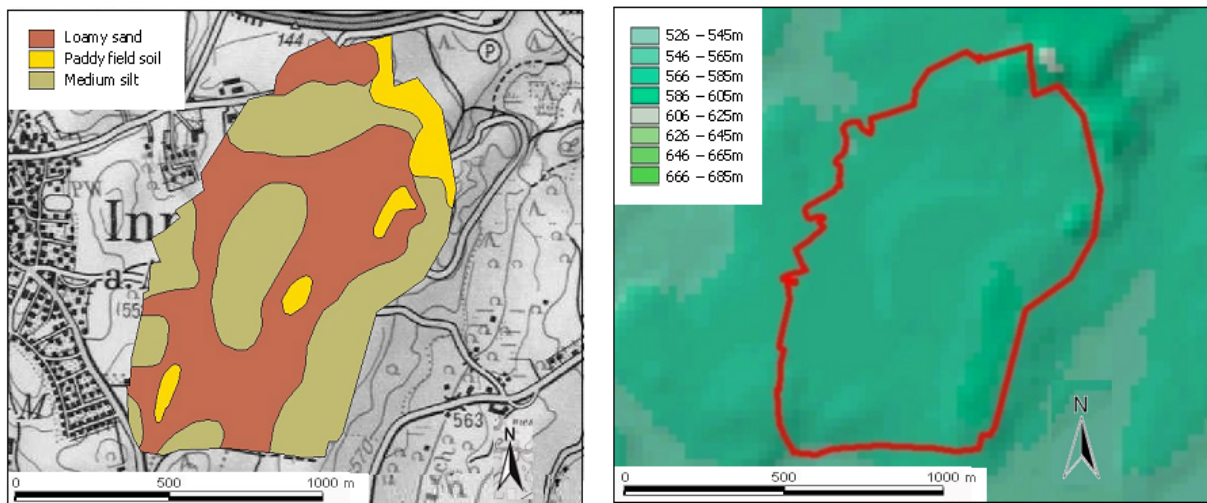
*Figure 3-5:*     *Map of soil texture (left) (data source: Geologisches Landesamt, 1986) and digital elevation (right) of the test site Inning (data source: MILGEO)*

Regarding the incorporation into the natural units, the test site Inning belongs to a subunit of the Ammer–Loisach hilly area, the Seefelderwald moraines. This area is characterised by less distinct rises, compared to the hill country (Graul, 1962). The differences in ground elevation are between 560m on the western edge and 610m in the east (see Figure 3-5). In contrast to the digital elevation map (DEM) of Gilching with a resolution of 5m, the resolution of the Inning DEM with 30m is on a lower level. Related to the small area of this test site the DEM appears to be blurred.

*Table 3-4:*     *Distribution of land cover types within the test site Inning 1999 and 2000*

| Land cover type | Percentage coverage 1999 [%] | Percentage coverage 2000 [%] |
|---|---|---|
| Forest | 64.1 | 64.1 |
| Grassland | 25.0 | 25.0 |
| Cereals | 6.90 | 6.40 |
| Unknown | 4.00 | 0.00 |
| Maize | 0.00 | 4.50 |

Both the relief and the parent material influence the soil texture as well as soil type found in this area. The hill slopes have loamy sand as soil texture, from which braunerde / cambisols developed. On top of the moraines, especially in the north-east, a paddy field soil exists and on the high slopes medium silt, which leads to rendzina (Geologisches Landesamt, 1986).

The dominant land cover type of this test site is forest, which covers 64% of the area. The depressions, where saturation after rain occurs, take up 25% and are covered with permanent grassland. The main crops in 1999 are wheat and barley, which cover about

7%. The rest of the land cover (4%) is unknown. In 2000 about 4% are covered with maize. The results of the land cover mappings in 1999 and 2000 are presented in Table 3-4 and Figure 3-6.
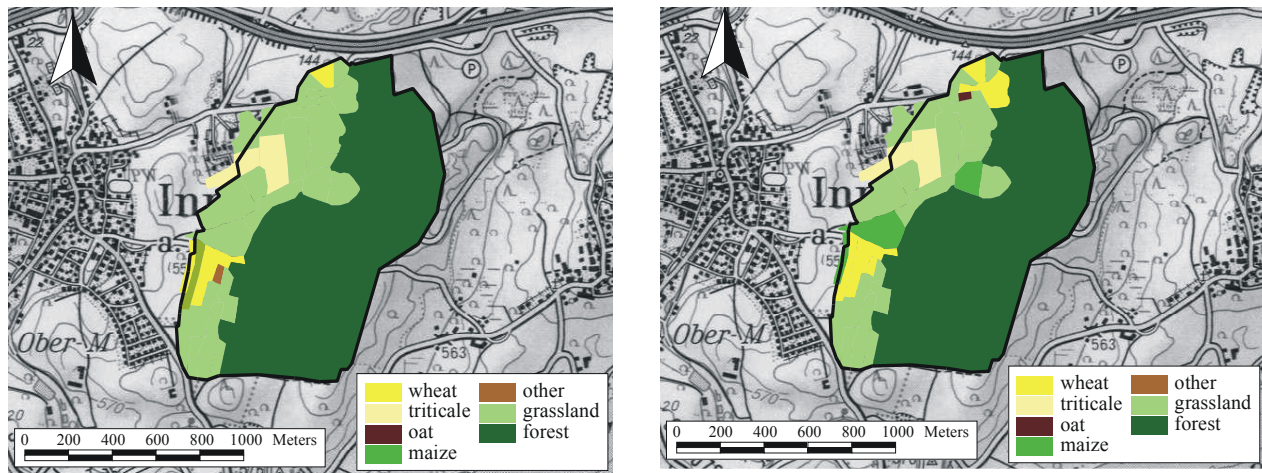


*Figure 3-6:       Land cover in the test site Inning for 1999 (left) and 2000 (right)*

### 3.1.3    Test Site Frieding

Similar to Gilching and Inning the test site Frieding is a water protection area. It covers 1.1km² and is the smallest of the three test sites. It is located at the southern edge of the test area Starnberg, north–east of the hamlet Andechs (see Figure 3-11).

This test site is classified as a part of the Ammer–Loisach hill country, namely the subunit Andechser hills (Graul, 1962). It lies on a ridge at an altitude between 650m and 700m (Figure 3-7). This subunit is characterised by small circles of end moraines with broad, alluvial fields in between.

The test site Frieding is located in one of these alluvial fields, and with an average altitude of 700m it is the highest of the test sites.

Concerning the soil texture a sandy loam dominates with a share of 99.8%, from which cambisols originate as soil type (Geologisches Landesamt, 1986). Because of the limited expressiveness of such a soil map, it is refrained from a presentation of this parameter.

The test site Frieding is outlying of the ground measurement route. Therefore this site was chosen as test site for 1999 only. To reduce the length of the route, ground truth measurements in 2000 were carried out only at the Inning and Gilching sites.
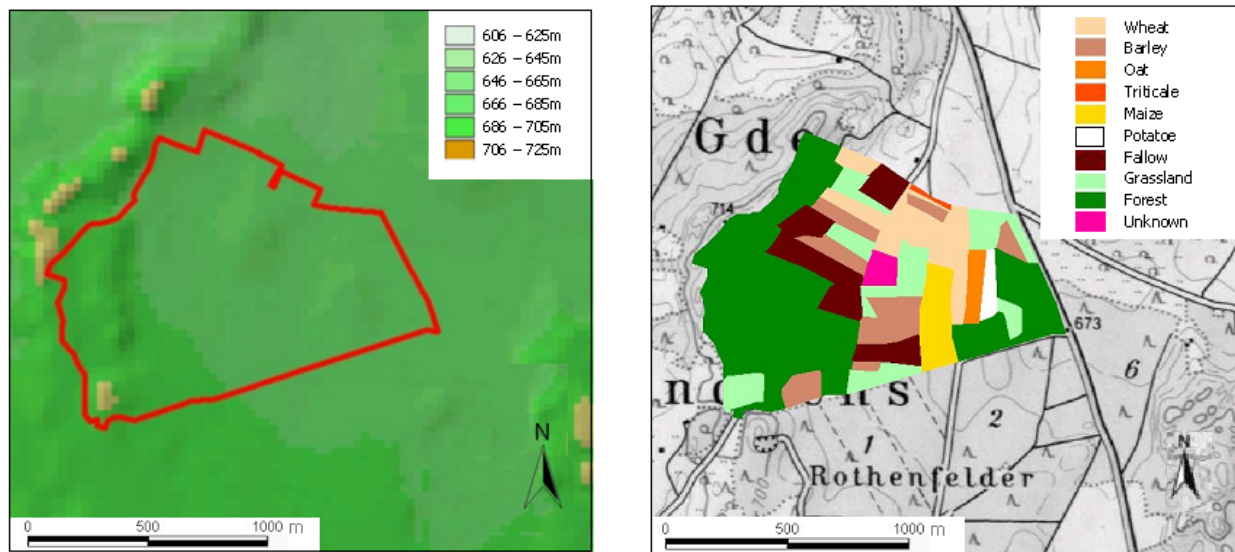
*Figure 3-7:*      *Digital elevation map (left) (Data source: MILGEO) and land cover mapping (right) for the test site Frieding 1999*

Figure 3-7 and Table 3-5 show the results of the land cover mapping for 1999. Nearly 44% of the test site are covered with forest. Cereals dominate the agricultural use with 23.6% followed by maize with 5%. Grassland and fallow land cover about 13.6% and 10% respectively. A field of potatoes occupies 1.4%.

*Table 3-5:*   *Distribution of land cover types within the test site Frieding 1999*

| Land use type | Percentage coverage [%] |
|---|---|
| Forest | 43.9 |
| Cereals | 23.6 |
| Grassland | 13.6 |
| Fallow | 10.9 |
| Maize | 5.00 |
| Potatoes | 1.40 |
| Unknown | 1.60 |

## 3.2 Investigated Land Cover Types

The plant species investigated in this thesis are maize, wheat and permanent grassland. These types of land cover about 70% of the agricultural area. This ensures a great variety of possible test fields while covering a large part of the agricultural land.

The following biological compilation of the investigated land cover types is mainly extracted from Heyland (1996), Franke (1989) and Pommer (2001). For the description of grassland, Ellenberg (1996), Heyland (1996), Spatz (1994) and Whitehead (1995) are the main sources.

The following sections are not want to be a complete description of the biology, botany or morphology of these plant species or communities. For this purpose the literature mentioned above should be consulted.

### 3.2.1     Wheat (*Triticum aestivum L.*)

Wheat is the most widely cultivated plant in the world in terms of both acreage and production.

Wheat is an annual, mostly non-aristated spiky grass (Graminaceae). In comparison to other cereals, *Triticum aestivum L.* puts higher demands on climate and soil. It yields best in climates with mild winters, warm summers with a long sunshine duration. In the cool and humid climate of the test area, winter wheat, which requires an annual mean temperature above 7.5°C, can be cultivated without restrictions.

Table 3-6:   *Requirements of winter wheat regarding climate, soil and water supply (Franke, 1989; Stolz, 1998)*

| Developmental cycle [days] | Temperature [°C] | | | Climatic requirements | Soil | Water supply |
|---|---|---|---|---|---|---|
| | min | opt | max | | | |
| 180 - 250 | 10 | 18 | 25 | Susceptible to frost during resting period | Prefers medium soil texture; tolerant to damming wetness; pH optimum 6-8 | Max. annual precipitation 1000mm |

The demand on the soil is very high: wheat prefers nutritious soils with a high water storage capacity such as loamy and silty soil. For a high yield, a well drained soil is more important than an even distribution of precipitation. Limiting factors are high amounts of precipitation during anthesis, where 34 to 40mm should not be exceeded. Otherwise the development of the grain is poor and correspondingly the yield is reduced. The annual precipitation should not exceed 1000mm. Nevertheless, the high rates of radiance of the Bavarian Alpine foothills enable the cultivation of winter wheat up to an annual precipitation of 1200mm.

### 3.2.2    Maize (*Zea mays L.*)

Concerning the world-wide cultivation of grains, maize ranks second behind wheat. Maize is an annual, non-tillering plant belonging to the family of grasses (Graminaceae). Its stalk reaches a height of 1 to 3m and a diameter of up to 5cm.

*Table 3-7:    Requirements of maize regarding climate, soil and water supply (Franke, 1989; Heyland, 1996)*

| Development cycle [days] | Temperature [°C] | | | Special climatic requirements | Soil | Water supply |
|---|---|---|---|---|---|---|
| | min | opt. | max | | | |
| 100 - 140 | 10 | 28 | 35 | Susceptible to frost; minimum temperature for germination 15°C | Well drained; No damming wetness | 500 – 700mm precipitation |

Maize can be cultivated in regions where the daily mean temperatures are above 15°C and no frost occurs during the growing season. The optimum temperature for germination is 18 – 20°C, while the minimum lies at 10°C.

*Zea mays L.* can be cultivated in all well drained soils. An annual precipitation of 500 to 700mm is sufficient for the development of the plants; damming wetness should be avoided. The root system can penetrate up to 2m into the soil. The widely branched main part lies in the upper 0.8 to 1m where 80% of the uptake of water takes place.

In the countries of the temperate zone maize is mainly used as fodder, which is offered as grain, soilage or silage. In the year 2000, only 3% of the maize harvest in Germany was taken for the production of food, 97% were used as forage.

### 3.2.3    Grassland

In central Europe grassland occupies about 35–40% of the utilised agricultural area. Grassland has a large potential for the production of plant biomass, partly because the leaf area index is higher than for crops and partly because it has the capability to regrow after cutting or grazing. Grassland is adapted to different climatic and soil conditions due to its large variety of species. Most grassland species of the temperate zone are perennial and will grow whenever the temperature is above 5°C and when there is adequate moisture. Assimilation starts at 0°C, but biomass increases significantly above 5°C until it reaches its maximum at temperatures between 17 and 25°C (see also Table 3-8). The minimum annual precipitation lies at 400 to 500mm, but precipitation up to 1000mm per year increases the yield.

*Table 3-8:  Requirements of grassland of the temperate zone regarding climate, soil and water supply (Heyland, 1996; Whitehead, 1995)*

| Developmental cycle [days] | Temperature [°C] | | | Special climatic requirements | Soil | Water supply |
|---|---|---|---|---|---|---|
| | min | opt | max | | | |
| Adapted to local conditions | 0 | 17-25 | 35 | Susceptible to frost, snow and changes of temperature | Humus content | 400 – 500mm min. annual precipitation |

In contrast to crops, the soil texture is less important for the development of grassland. The soil type, especially a well-developed humus layer, influences both yield and content of nutrients, protein and net energy lactose. Grassland is used as fodder; therefore the quantity of biomass produced is as important as its quality, wherein the latter influences the quality and yield of milk as well as meat.

The species, which compose a grassland canopy, can be divided into three groups with varying botanical characteristic features:

- o  grasses,
- o  legumes,
- o  herbs.

Grasses are monocotyledonous species with a similar structure to crops. In botanical terms, they all belong to one family, i.e. the sweet grasses (Poaceae). In temperate zones, the sweet grasses make up the largest proportion of a grassland canopy. They can be divided into two groups according to their growth height: the tall and the short grasses. The tall grasses, for example meadow fescue (*Festuca pratensis Huds.*), oatgrass (*Arrhenatherium elatius L.*) or timothy (*Phleum pratense L.*), mainly influence the development of biomass. The short grasses, for example cocksfoot *(Dactylis glomerata L.)*, bluegrass (*Poa pratensis L.*) or perennial ryegrass (*Lolium perenne L.*), have a great importance for the density and endurance of the turf. Thus the former influence the yield while the latter influence the livestock capacity.

Legumes and most herbs are dicotyledonous. Legumes live in a mutualistic symbiosis with nodule bacteria and therefore are able to bind atmospheric nitrogen. This leads to a significantly higher protein content and a heightened mineral content compared to herbs. A major advantage of growing a legume in association with grass is that the nitrogen fixed by a legume benefits not only the legume itself, but also the grass growing with it, and the mixed herbage often provides a better diet for livestock than would the legume alone. Their growth height as well as their strength is low, therefore they loose importance with increasing density of the canopy. Under these conditions white clover (*Trifolium repens L.*) and red clover (*Trifolium pratense L.*) are the most important leguminous species.

The herbs show the most variety regarding rooting, habit and persistence. Most herbaceous plants respond immediately to different environmental conditions. Therefore

the condition of a habitat can be judged by its herbaceous composition. Both protein and mineral content are higher compared to the grasses. But their importance is obliged to their amount in the canopy. Up to a proportion of 5% they have a positive influence on the protein and mineral quality of a pasture. But the yield lessens when the herbaceous plants increase to 20% and more. The high quantity of herbs in a canopy is often due to a excessive supply with organic fertiliser. This supports the occurrence of specific species, so called liquid manure flora, such as cow parsley (*Anthriscus sylvestris L*), hogweed (*Heracleum sphondylium L.*) and broadleaf dock (*Rumex obtusifolius L.*). Dandelion (*Taraxacum officinale Web.*) is a very widespread herb because of its high adaptability, but high nutrient supply nurtures its growth. On thickened ground, mainly at the entrances of pastures, species such as silverweed (*Potentilla anserina L.*) and broad-leaved plantain (*Plantago major L.*) can be found.

Some canopies have a fourth layer, covering the soil surface, which is built up of mosses and thatch. Those four layers that may occur in a grassland canopy are shown in Figure 3-8.
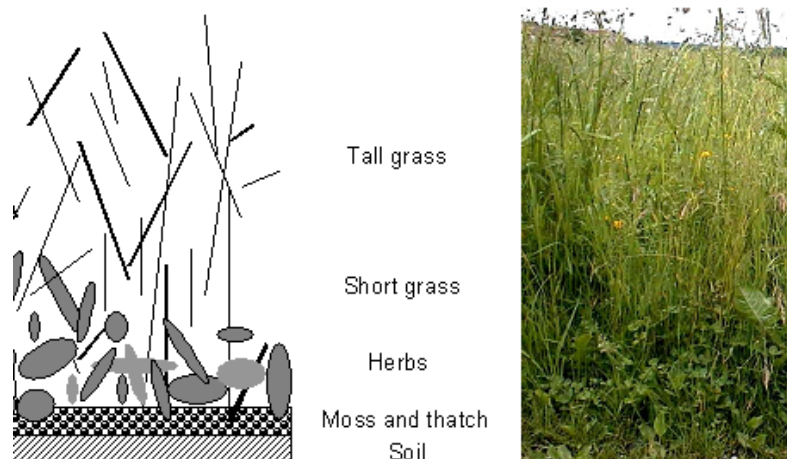


Figure 3-8:      Structure of a grassland canopy (Riegler et al., 1998; modified)

A great variety of different plant communities exist which are adapted to specific habitats. The botanical diversity increases from the straw meadow to the forage meadow that is cut twice a year. Meadows that are used more intensively, i.e. both more cuttings and fertiliser, can reach a higher yield, but their floristic composition becomes poorer. Different types of communities develop, depending on the kind of fertiliser as well the intensity of fertilisation.

The type as well as the intensity of use has a great impact on the morphology and species composition. Tall grass species for example react more sensitively to a more frequent use than small grasses and herbs. Therefore the regrowths are both richer in legumes and herbs than the first growth. Grazing is not as rapid and has a more selective effect, and nutrients are partly recycled directly by the excrements of the livestock. But with

increasing grazing intensity the number of species decreases. Figure 3-9 shows the connection between plant diversity and type of cultivation.
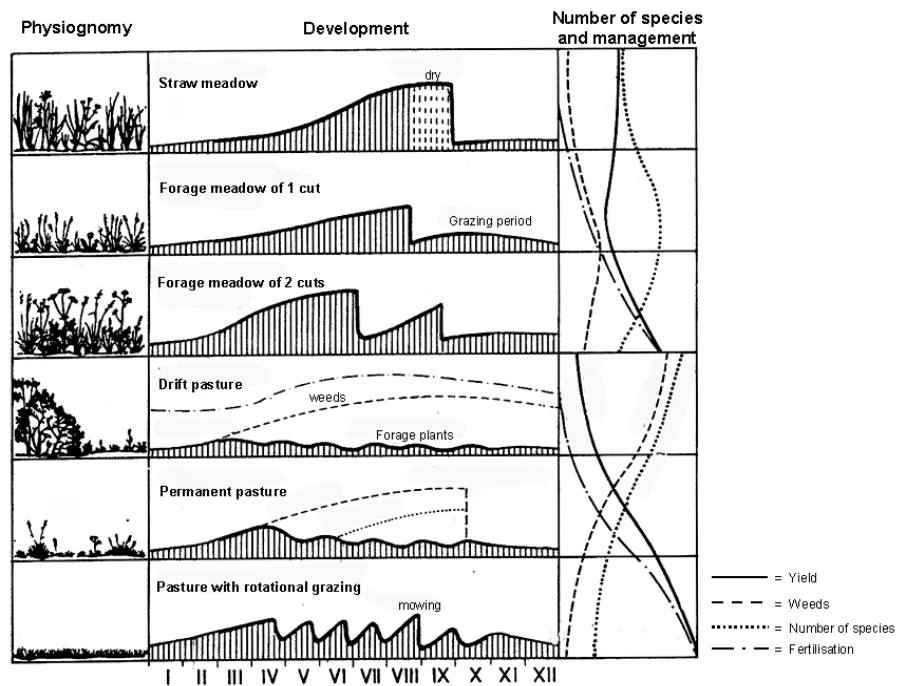


*Figure 3-9:    Effect of the type of cultivation on the biological diversity of grassland (Ellenberg, 1996; modified)*

The main effect of nitrogen fertiliser is the acceleration of growth and the increase of leaf size. A deficiency of nitrogen restricts the number of tillers that develop and, more importantly, it also restricts the growth of individual leaves and their photosynthetic capacity.

Within grassland canopies nitrogen fertiliser stimulates the growth of the biomass delivering grasses and herbs of the liquid manure flora. Thereby the illumination conditions for legumes and lower herbs are decreased and as a result their fraction recedes. When the nutrient supply is insufficient, the higher grasses as well as the tall herbs cannot develop adequately, while the short grasses and herbs can now spread under full light. This context is shown in Figure 3-10. Their dominance leads to a reduced yield, which is on the one side due to the absence of grasses biomass. On the other hand the herbs tend to crumble while drying and silaging, which reduces the quality and quantity of the forage.
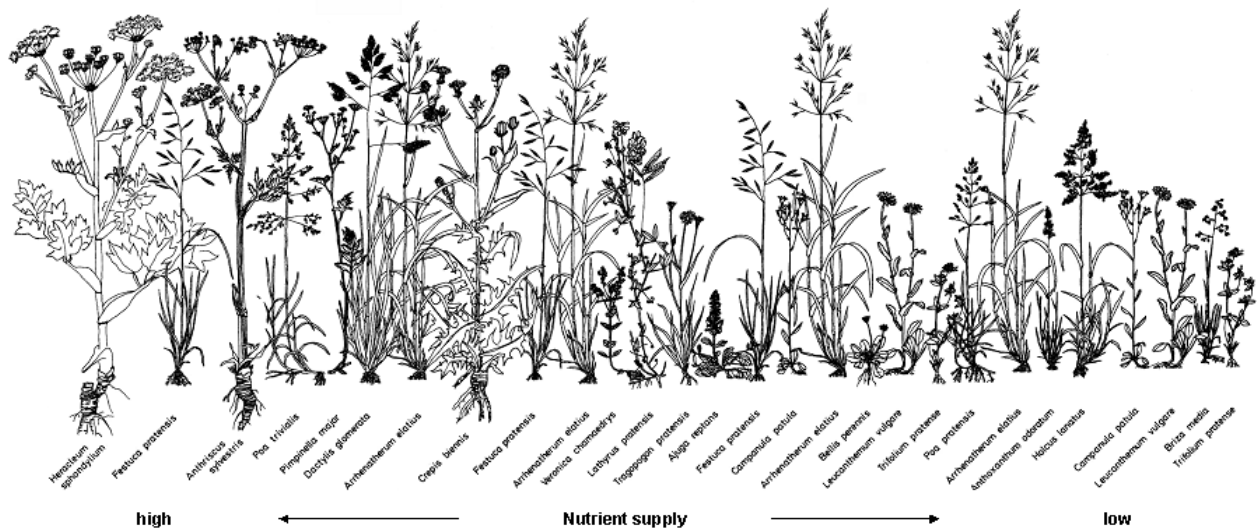
Figure 3-10:    Connection between nutrient supply and occurrence of species in a fresh (oatgrass) meadow (Arrhenatherion elatioris) (Spatz, 1994)

Intensely utilised grassland is normally fertilised at the beginning of the growing period and after each cut, except for the last one in a year. The rates of nitrogen fertilisation recommended for intensively farmed grassland in temperate regions are generally within the range of 200 to 240kg per ha, depending on soil type, weather and management. When grassland is mown or lightly grazed, the amount of nitrogen leached is normally less than 20kg per ha and year, even if fertiliser is applied. The main reason why relatively little nitrate is leached from mown grassland is that grass has a large capacity to take up nitrate, and this capacity is maintained for much of the year. However, when grassland is fertilised regularly and grazed intensively, more than 100kg nitrogen per ha and year may be leached as nitrate. In water protection areas restrictions for fertilising exist to avoid the leaching from nitrogen into the ground water.

## *3.3 Ground Measurements*

The detailed inquiry of plant parameters at selected test fields was undertaken during the vegetation periods of 1999 and 2000. Thereby 1999 three fields of wheat were registered as well as three fields of maize. In 2000 six fields of wheat and three fields of maize were observed. Furthermore four fields of permanent grassland were investigated over the years 1999 and 2000.

The selected timescale for grassland is the Day of the Year (DOY; the DOY code is given in Appendix 3). The period of plant development and growth for wheat and maize is mainly dependent on the date of sowing. Therefore the timescale for these land use types is the Days after Sowing (DAS).

The positions of the selected test fields within the test area are given in Figure 3-11.

The fields were selected in cooperation with the local office for agriculture of this area. Special attention was paid to the size, location and slope of the fields. The fields should be recognized easily from the aircraft to ensure coverage of the field during each flight. Besides the location this can be assured when the fields do not exceed or fall below a critical size. Therefore the fields should be small enough to be covered by one flight strip and avoid that the images of two or more flight strips have to be pieced together to get a full coverage of the field. On the other hand the fields should be large enough to contain as many pixels as possible in the AVIS images for the analysis (about 1ha). Additional the fields should be as plain as possible to avoid illumination and geometrical effects in the remote sensing data. All these claims are not mandatory, but they ease the acquisition and processing of the remote sensing data.

The soil on which the test fields are located seems to be of secondary importance for this task. The focus of this thesis lies on the quantification of the above-ground content of chlorophyll and nitrogen in plants. The quantification should be independent of the soil type and centred on the above-ground parts of the plants. Therefore the nitrogen in the soil is not taken into consideration.
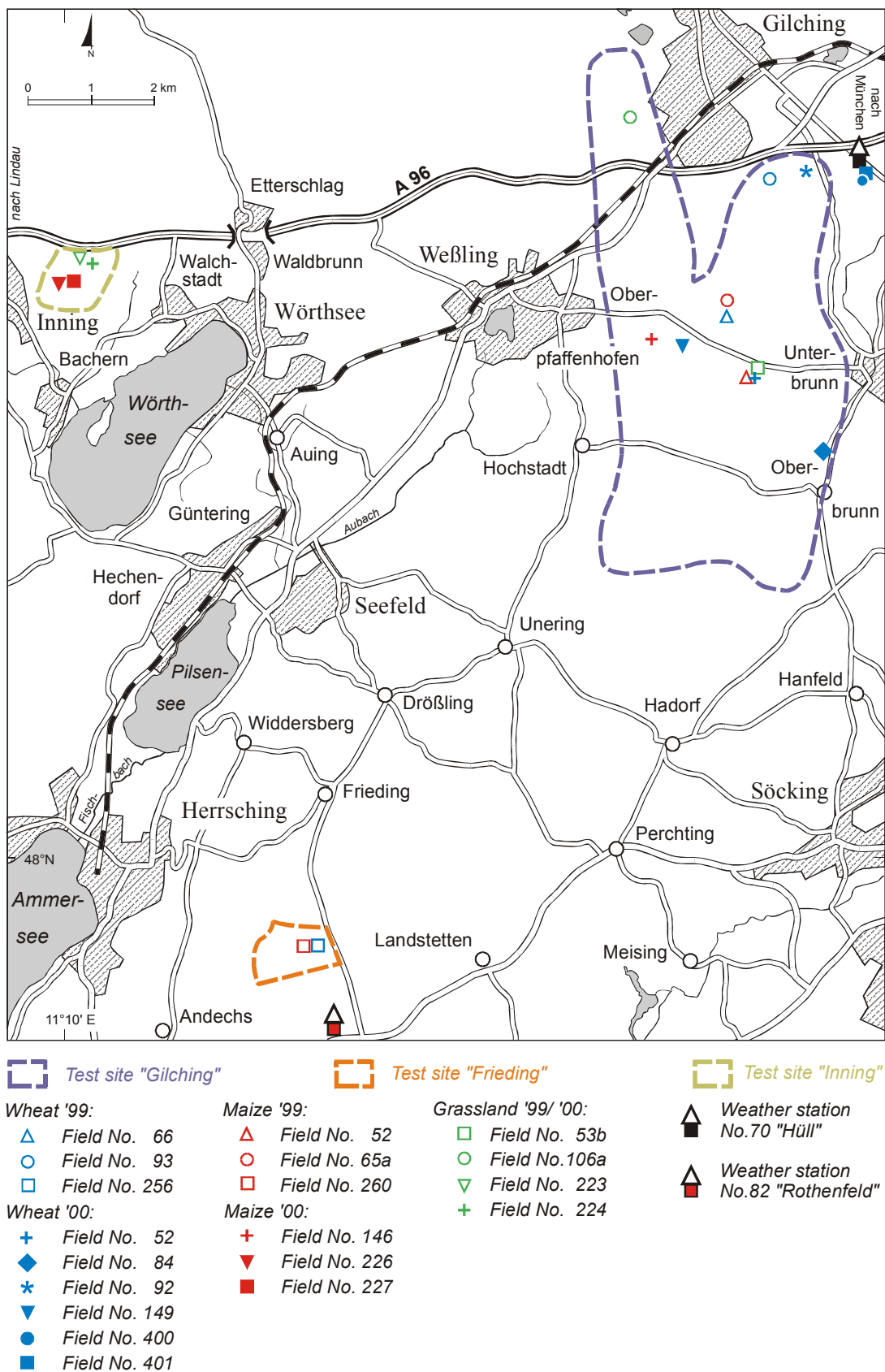
Figure 3-11:    Positions of the test fields for 1999 and 2000 as well as locations of the weather stations
                (cartography: V.Falck)

### 3.3.1 The Ground Measurements

The sampling on ground was carried out weekly. This interval guarantees that the morphological development of the vegetation can be acquired precisely enough to enable linear interpolation between the sampling dates (Demircan, 1995). Additional sampling simultaneously to the flight dates of AVIS caused logistical and personnel problems. Because of the weather dependency and the restricted availability of the aircraft, the AVIS missions were often fixed at extremely short notice. This made it difficult to provide manpower for the sampling on ground. The continuous, weekly sampling provides continuous monitoring of the plant parameters and their retrieval for each flight date.

For each test field, plant samples that showed an average development stage were taken at three sampling points. These sampling points were located along a field diagonal and were also marked in aerial photographs of the test field to ensure their clear identification in the field (Figure 3-12).
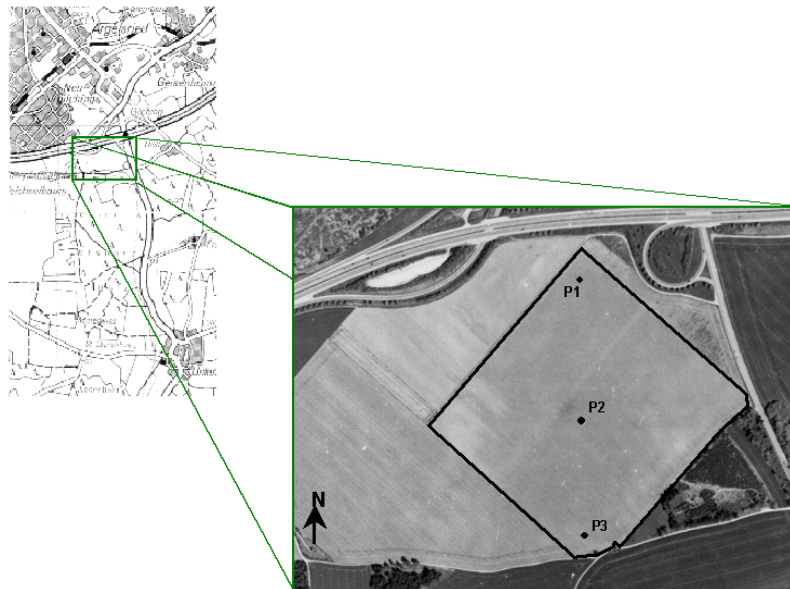


*Figure 3-12:*     *Location of the sampling points within a test field of wheat*

Representative samples of three maize plants and corn stalks along a row of 25cm were taken at each sampling point. Additionally, within the maize fields the number of plants per meter in a row was counted at each sampling point. Once a year the distances between the rows were measured for each field. Grassland samples were taken at four sampling points, which were spread over the test field, by cutting an area of $\frac{1}{4}m^2$. This provides a simple extrapolation to the biomass for 1m².

These limitations were necessary because the harvest of 1m² of plants leads to a bulk of material that exceeds the available capacity in the laboratory. Weekly cutting of 1m² also leads to a loss of yield, which the farmers were not willing to accept. The limited sampling

enables a simple extrapolation to a biomass of 1m² and guarantees the acceptance by farmers at the same time.

### 3.3.1.1    Weekly Measured Plant Parameters

Several plant parameters were measured regularly, including the phenological stage, the height as well as the wet and dry biomass. Additional notes regarding fertilisation, precipitation, visible diseases and/or weeds and irrigation were also recorded. An example for a measurement report is provided in Figure 3-13. For a better subsequent reconstruction of the development of the vegetation, photographs were taken of each stand.



Figure 3-13:    Measurement report for wheat

#### 3.3.1.1.1    Phenological Status

Phenological stages are periods of development during growth and maturing of plants in which marked physiological and/or morphological properties emerge (Goudie, 1994). The EUCARPIA (EC) scale for cereals and maize is used in this thesis to describe the phenological status of the plants (Zadoks et al., 1974). Principal growth stages, which are given in Table 3-9, were introduced to describe boundaries of different growth stages. A further, more detailed classification within the principal stages is realised by the secondary growth stages, which describe the continuous growth of the plants within the principal

stages. The secondary growth stages are used with a second digit, coded from 0 to 9, for each principal growth stage.

*Table 3-9:    Principal growth stages of cereals (Zadoks et al., 1974)*

| One-digit code | Description |
| --- | --- |
| 0 | Germination |
| 1 | Seedling growth |
| 2 | Tillering |
| 3 | Stem elongation |
| 4 | Booting |
| 5 | Inflorescence emergence |
| 6 | Anthesis |
| 7 | Milk development |
| 8 | Dough development |
| 9 | Ripening |

The phenological status of the meadows is not recorded because the occurrence of several plant species with different phenological properties make it very difficult to determine an average phenological status.

### 3.3.1.1.2    Plant Height of Crops

The plant height of maize and wheat is measured in cm. Maize plants being harvested, were measured separately while for wheat the average height of plants at the sampling points was derived.

Two different terms have to be distinguished: the height of the leaf and the shoot respectively.

Shoot:   maximum height; measured from the ground to the highest point of the plant, i.e. the shoot.

Leaf:    measured height from the ground to the highest unfolded leaf.

### 3.3.1.1.3    Plant Height of Grassland

This term is also measured in cm. In contrary to cultivated plants the structure of grassland consists of several layers, comparable with the strata of a forest, which are formed by different species. Grassland shows at least two strata (see Figure 3-8). These layers may be different in size, shape, density, floristic and life form composition (Küchler & Zonneveld, 1988).

Extensive grassland is characterised by a more incomplete structure and a large variety of species leading to both a strong vertical stratification and an overlapping of the particular fruit, stem, and leaf strata. With increasing cultivation the structure becomes more uniform. A reduced number of species leads to a lower stratification (Briemle et al., 1991). Therefore up to four strata may be differed in the measurement report.

### 3.3.1.1.4  Photographs

Photographs of each stand were taken weekly to document the phenological status and enable a subsequent view of the test fields. They were taken weekly and next to the same position to ensure comparability throughout the vegetation period. At least three photos were taken: one side view to display the stratification and the height of the plants, a top view picture to determine the percentage coverage of the vegetation and an overview picture to gain an insight into the homogeneity of a field (Figure 3-14).



Figure 3-14:     Photographs of wheat; side view (left), overview (centre) and top view (right)

### 3.3.1.1.5  Wet Biomass

Harvested samples of wheat and maize were separated into stem, leaf and fruit. The masses of the various constituents were determined with a dial balance (MC 1, LC4200). Their cumulated mass of the components is used as wet biomass. The wet biomass per m² was calculated using the measured row distance.

The wet biomass of grassland was measured for the whole samples, without separating stem, leaf and fruit. The wet biomass per m² was calculated by multiplying the ¼m² mass by four.

### 3.3.1.1.6  Dry Biomass

After determination of wet biomass the plant samples were dried in desiccators for 20 hours at a temperature of 105°C. The dry biomass was measured in the same way as the

wet biomass. The dry biomass per m² was also calculated in the same way as for the wet biomass per m².

## 3.3.1.2   Additional Ground Measurements

Once a year, land cover mappings were carried out in the test sites and the distances between the plant rows were determined within each test field. The data of the "Schlagkartei" provide information about the cultivation. Additional information regarding yield measurements and detailed soil investigation are also available for several fields. For the grassland test fields, a derivation of the botanical composition was carried out before the first cut in 2000.

### 3.3.1.2.1   Land Cover Mapping

The land cover mappings were carried out each year in June, including the main crops. The *Amt für Landwirtschaft* provided data of the subsequent crops. The land cover mapping included the following land use types:

- o   forest,
- o   cereals, wherein barley, maize, oat, rye, triticale and wheat were differed,
- o   potatoes,
- o   grassland,
- o   fallow land,
- o   gravel pit,
- o   impervious or residential area,
- o   water,
- o   unknown, wherever the land use could not be securely attributed.

Together with the ground elevation and the soil texture, the land cover data were integrated into a Geographical Information System (GIS) using ARC View. The results were already presented in the previous sections.

### 3.3.1.2.2   Floristic Mapping of Grassland

The term "grassland" includes a variety of vegetation types with differing compositions of species that are adapted to the particular predominating localisation factors. These factors are the length of the vegetation period, temperature, precipitation, irradiance, soil type, ground water level and management (Whitehead, 1995). The botanical composition of grassland is used for the classification into the different types of vegetation communities and therefore provides information about these factors.

The floristic mapping was carried out in May 2000 with the collaboration of Dr. Schmidtlein of the Geographical Institute of the University of Munich. For each test field two plots with a size of 4x4m were chosen to perform the investigation, including the percentage

coverage of the soil and existing plant species. The mapping of the different species was conducted using the scale from Barkman et al. (1964).

The estimation of forage quality was conducted using the Klapp value (Klapp, 1953), where the potential of the yield as forage is measured on a scale of -1 (toxic) via 0 (worthless in every respect) to 8 (significant in every respect).

The characterisation concerning the ecological site factors was conducted using the Ellenberg factors (1991), in this case the soil factors moisture (F), reaction (R) and nutrition (N). These values are relative gradations regarding the significance of their incidence in the field in a nine–level scale from 1 (least extent) to 9 (greatest extent), whereby the value 5 describes the average conditions in central Europe.

The moisture and reaction factors describe the ecological behaviour with respect to the moisture and the pH value of the soil respectively. The nitrogen or nutrition value ranges from the poorness indicators (N1 and N2) to the nitrogen indicators (N8 and N9).

The detailed results of the floristic description of the test meadows are given in Appendix 2.

### 3.3.1.2.3    Management Data



Figure 3-15:    Data sheet of the "Schlagkartei" for a field of winter wheat

The farmers who are under contract of the *Amt für Landwirtschaft* commit themselves to make records of the cultivation of their fields. These records contain information about crop rotation, cultivars, date of sowing and harvest as well as the application of fertiliser, herbicides and fungicides and the amount of donation. This information is collected in a data sheet, the "Schlagkartei". Figure 3-15 presents a "Schlagkartei" data sheet.

### 3.3.1.2.4    Yield Measurement

For several fields, GPS-based yield measurement data exist, which provide information about the heterogeneity of the yield within the field. These data were kindly placed at our disposal from Mr. Stürzer. This will be one subject of investigation in this study.

The measurement system, connected to a PC, is installed on a combine harvester. While harvesting with constant speed the fill height of the grain elevator is acquired by a light barrier radiating across the elevator paddles. The yield can be derived by the grain volume that on its side is calculated by the fill height. Every second, the position within the field is measured by a GPS and stored on the PC together with the current yield. Thus the distribution of yield can be observed.

## 3.3.1.3    Derived Plant Parameters

Derived parameters are both the chlorophyll and nitrogen content of the plants. They are not directly measured in the field, but must be analysed in the laboratory.

### 3.3.1.3.1    Plant Chlorophyll Content

The analysis was carried out in the botanical laboratory of the *Forschungszentrum für Umwelt und Gesundheit* GSF in Neuherberg near Munich, which was kindly placed at our disposal by its director Prof. Lütz.

During the weekly measurements samples of sun leaves at each sampling point were taken and pieced together in a cryo tube. Therefore one cryo tube represents the average of all sampling points within a field. The samples were immediately frozen in liquid nitrogen to avoid the chemical degradation of the chlorophyll. They were brought to the lab and were stacked there in a freezer at –50°C.

The analysis of the chlorophyll content was carried out in accordance with the method described by Porra et al. (1989). In the laboratory the frozen samples were milled with a ball mill until the plant material was fully pulverised. 70mg of the powder was admitted to 1ml of acetone (80%) and cooled for 15 minutes. Afterwards it was centrifuged for 10 minutes at 8000 revs./min. The supernatant was then filled in a graduate. The pellet was again drugged with 3ml of acetone (80%) and centrifuged until the pellet was white. The supernatants were filled up to 8ml with acetone (80%), decanted into a 1ml cuvette and placed into the photometer (SOPRA DW 2000). The photometric measurement was carried out using 80% acetone as blind value. The absorption was investigated using the

wavelength 663.6nm for chlorophyll a and 646.6nm for chlorophyll b using equation (3.1) and (3.2) respectively.

$$Chl\ a = \left(12.25 \cdot A_a - 2.55 \cdot A_b\right) \cdot \frac{vol}{w_i} \tag{3.1}$$

$$Chl\ b = \left(20.31 \cdot A_b - 4.91 \cdot A_a\right) \cdot \frac{vol}{w_i} \tag{3.2}$$

where

| | |
|---|---|
| $Chl\ a$ | chlorophyll a content [µg/g], |
| $Chl\ b$ | chlorophyll b content [µg/g], |
| $A_a$ | absorption at 663.6 nm [%], |
| $A_b$ | absorption at 646.6 nm [%], |
| $vol$ | final volume in which the chlorophyll is dissolved [ml], |
| $w_i$ | initial mass of the solved plant powder [g] (Porra et al., 1989). |

Figure 3-16 shows an example of two absorption spectra of the extracted chlorophyll of grassland. Compared to corn probes the sampling of grassland is more complicated. While wheat and maize probes contain leaves of a specific type, grassland contains a variety of different species. To average over the canopy, sun leaves of as many species as possible were collected at each sampling point and blended together. In the laboratory, the whole plant material was milled to provide absorption coefficients, which represent the average of the canopy.
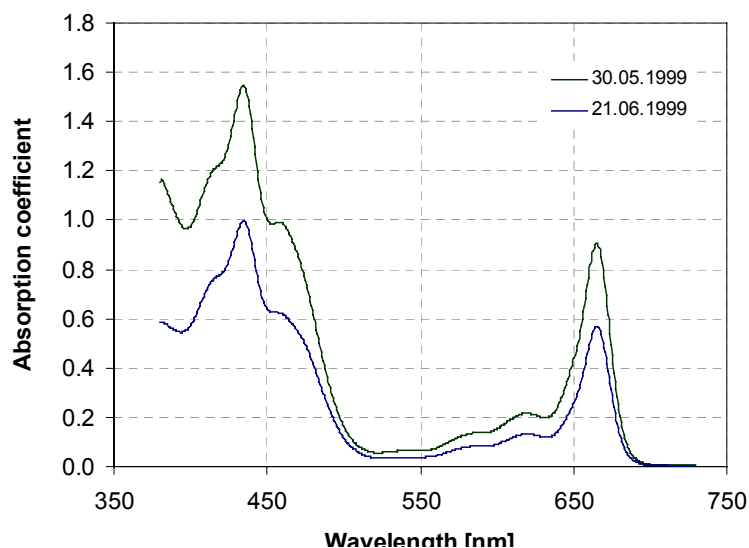


Figure 3-16:    Chlorophyll absorption spectra of sun leaves of grassland at two different sampling dates

Besides the chlorophyll content per mass [µg/g], the chlorophyll content per area [mg/m²] was calculated using the measured dry biomass $DM$ either of the leaves (cereals) or as a whole (grassland) (see equation (3.3)). The former, for example, can be used to evaluate

the overall photosynthetic capacity or productivity of a canopy, while the latter may be an indicator of plant physiological status or level of stress (Blackburn, 1998). Therefore information on both concentration per unit area and concentration per unit mass is valuable.

$$Chl\,a,b[mg/m^2] = Chl\,a,b[\mu g/g] \cdot DM \cdot 1000 \qquad (3.3)$$

About 300 samples were investigated for both 1999 and 2000. As mentioned above, the derived chlorophyll content represents a mean value for each field. The separate sampling and analysing of each sampling point was discarded because of the large number of resulting probes. The limitation of both the access to the laboratory and the required manpower enforced the mean sampling.

### 3.3.1.3.2    Plant Nitrogen Content

The dried samples of the three cereal sampling points, divided into stems, leaves and fruits, were put together. The measurements are assumed to be the mean field value of the nitrogen content of stems, leaves and fruits. The reason for the separation into stem, leaf and fruit is the sustaining translocation of nitrogen within the plant during growth and maturity. The grassland samples were not partitioned, but measured in total.

The dried samples were sent to the central laboratory of the *Bayreuther Institut für Terrestrische Ökosystemforschung* (BITÖK), where the analysis was carried out.

First the samples were milled in a bill mill. The resulting powder of each sample was analysed in the CHN-O Rapid (Foss Heraeus) according to the CHN elemental analysis method. Thereby the plant material was burned at 1000°C in an oxygen flow. The accumulated nitrogen is derived by a thermal conductivity measurement (Dr. Ilgen, director of the central laboratory of BITÖK, personal communication on 30th October 2000). The nitrogen content in percentage of dry matter [%DM] is the resulting value from this analysis. About 500 samples were analysed in this manner in 1999 and 2000.

The nitrogen content per area [g/m²] can be calculated with the equivalent fraction of measured dry biomass per m² using the following equation:

$$N\,[g/m^2] = \frac{N[\%DM] \cdot DM}{100} \qquad (3.4)$$

were
*DM*          dry biomass [g] (of the stem, leaf or fruit fraction when using cereals and total with grassland).

## 3.4 Investigated Plants

The following section describes the results of the measurements of the different plant parameters for each land cover type on the basis of their development during a vegetation period.

As mentioned already in section 3.2, the biological background of the investigated land cover types is mainly extracted from Heyland (1996), Franke (1989) and Pommer (2001). For the description of grassland, Ellenberg (1996), Heyland (1996), Spatz (1994) and Whitehead (1995) are the main sources.

### 3.4.1    Wheat (*Triticum aestivum L.*)

Various cultivars of winter wheat have been breeded to ensure the best quality and yield for different regions. For this study, two varieties were investigated. In 1999 the variety "Bussard" was on focus with three test fields (see Figure 3-11 and Table 3-10) while in 2000 three test fields of each "Bussard" and "Capo" were investigated. Both cultivars are top varieties, so called elite (E) wheat. E-wheat has the highest quality and its flour is used for baking and to improve lower-graded wheat. The most interesting aspect for the investigation of these two cultivars is the different "colour" of the two varieties. "Bussard" is dark green while "Capo" has a brighter green hue. The greenness is supposed to be the visible copy of the chlorophyll content of the leaves that is directly related to the nitrogen content. Thus the variety "Capo" is expected to show lower chlorophyll levels than "Bussard".

Table 3-10:  *Test fields for winter wheat and availability of additional data (acronyms: S = Schlagkartei; Y = yield estimation; - = no data available)*

| Year | Field number | Cultivar | Size [ha] | Test site | Sowing | Harvest | Additional data |
|------|------|------|------|------|------|------|------|
| 1999 | 66 | Bussard | 3 | Gilching | 22.10.1998 | 26.08.1999 | S |
| 1999 | 93 | Bussard | 8 | Gilching | 22.10.1998 | 27.08.1999 | S, Y |
| 1999 | 256 | Bussard | 15 | Frieding | 28.10.1998 | 04.09.1999 | S |
| 2000 | 52 | Bussard | 2 | Gilching | 16.10.1999 | 10.08.2000 | S |
| 2000 | 84 | Bussard | 4 | Gilching | - | 12.08.2000 | - |
| 2000 | 92 | Capo | 18 | Gilching | 15.10.1999 | 10.08.2000 | S, Y |
| 2000 | 149a | Capo | 2 | Gilching | - | 12.08.2000 | - |
| 2000 | 400 | Bussard | 6 | Gilching | 15.10.1999 | 10.08.2000 | S, Y |
| 2000 | 401 | Capo | 6 | Gilching | 15.10.1999 | 10.08.2000 | S, Y |

Table 3-10 summarises the test fields of winter wheat investigated for this thesis in 1999 and 2000. The corresponding dates of sowing and harvest within the years provide the

comparable development stages throughout the vegetation period, which is important for the comparison with the AVIS data and further analysis. The recorded phenological stages have a parallel development of the plants during the years 1999 and 2000. The maximum divergence, which occurred in 1999, lies between three secondary growth stages between the first two measurements dates for field No.256 (EC 26; tillering – main shoot and six tillers) on the one side and No.93 and 66 (EC 29; tillering – main shoot and nine tillers) on the other.

Concerning the quality of the wheat grain, the fertilisation with nitrogen is the "engine of development". An underdosed supply leads to both a reduced yield and grain quality. Excessive fertilising leads to an increased susceptibility to diseases and pests while increased vegetative growth of the leaves leads to a lower yield.

The development of wheat during the growing period is demonstrated with the data available for the test field No.93 in 1999 as an example (see also Figure 3-17 and Figure 3-18).



Figure 3-17:    Photographs of field No.93 for the year 1999: left=during stem elongation (EC 37) (DAS 200=10$^{th}$ May); centre=end of emergence of the inflorescence (EC 59) (DAS 228=7$^{th}$ June); right=beginning of ripening (EC 91) (DAS 284=2$^{nd}$ August)

The sowing date of winter wheat is in October, in this case 22$^{nd}$ October 1998. The germination should be completed and at least the third leaf of the plants (EC 13) should be enfolded before winter, when the plantlets are resting. At the beginning of the vegetation period in the following spring the first donation of nitrogen encourages development, but at this time the need for nitrogen is low. 40 to 70kg/ha are normally applied to ensure the development of a limited but efficient number of shoots. 42kg of nitrogen per ha were spread over field No.93 at this time, when the main shoot and the first tiller emerge (EC 21). At the end of tillering (EC 29) and the beginning of stem elongation (EC 30–32) a second donation of nitrogen is applied. Further fertilising with 30 to 70kg/ha of nitrogen can influence growth as well as the yield. In field No.93 the second

nitrogen donation was divided into three lower donations given during tillering and stem elongation. Fertilisation (14kg nitrogen/ha) during tillering (EC 25) stimulates the development of spiked stalks while a donation at EC 30 (5kg/ha), when the flag leaf is just visible, increases the number of grains per spike.

At this development stage the measurements begin for 1999. The first measurement date was 26th April (DAS 186), which corresponded to the beginning of stem elongation (EC 30). During this stage the third nitrogen donation with 60kg/ha was given. During stem elongation and booting a healthy, dense wheat canopy assimilates about 2kg nitrogen per ha. This development can be seen in the steady growth up to 80cm accordingly with the increase of dry biomass, nitrogen and chlorophyll content per area as well as chlorophyll per mass, which is shown in Figure 3-18. The left photograph in Figure 3-17 shows the plants during stem elongation, where soil can be seen through the canopy and the plants have a bright green colour.

At the beginning of booting the fourth donation of 30 to 50kg/ha nitrogen ensures the high requirements of the plants during this developmental stage. 45kg nitrogen per ha was spread over field No.93 at EC 40 (DAS 218). The plants grow rapidly up to 80cm and the inflorescence is formed. The total dry biomass as well as the total nitrogen and chlorophyll content per area also show a constant increase due to the enduring growth. Both leaf and stem nitrogen in % of dry biomass decrease at this stage, partly because the nitrogen is displaced into the forming inflorescence.

After booting the inflorescence emerges in June (EC 50; until DAS 230). The leaf height stops increasing, but the emerging flower begins to elongate. Total biomass, nitrogen and chlorophyll content are still increasing, but the dry biomass as well as the nitrogen content per area of the stem, compared to the leaf, increases more rapidly. All leaves are already developed, they just increase slightly in size, but the stalks are thickened to carry the inflorescence and therefore nitrogen is deposited. So the stem proportion increases both with biomass and nitrogen content per area, while the leaf portion increases slightly. The nitrogen content in %DM of the leaves lies relatively constant at about 3.8 up to this stage, while the stem nitrogen content decreases from 3 to 1.6% of dry biomass. The chlorophyll content per area of the leaves reaches its maximum at 4500mg/m² during this stage due to the fact that the leaves are fully developed and their dry biomass shows a maximum at 314g/m². This stage is presented in the centred photograph of Figure 3-17. The high chlorophyll content is apparent in the dark green colour of the leaves. In the upper left corner an emerged inflorescence can be seen.
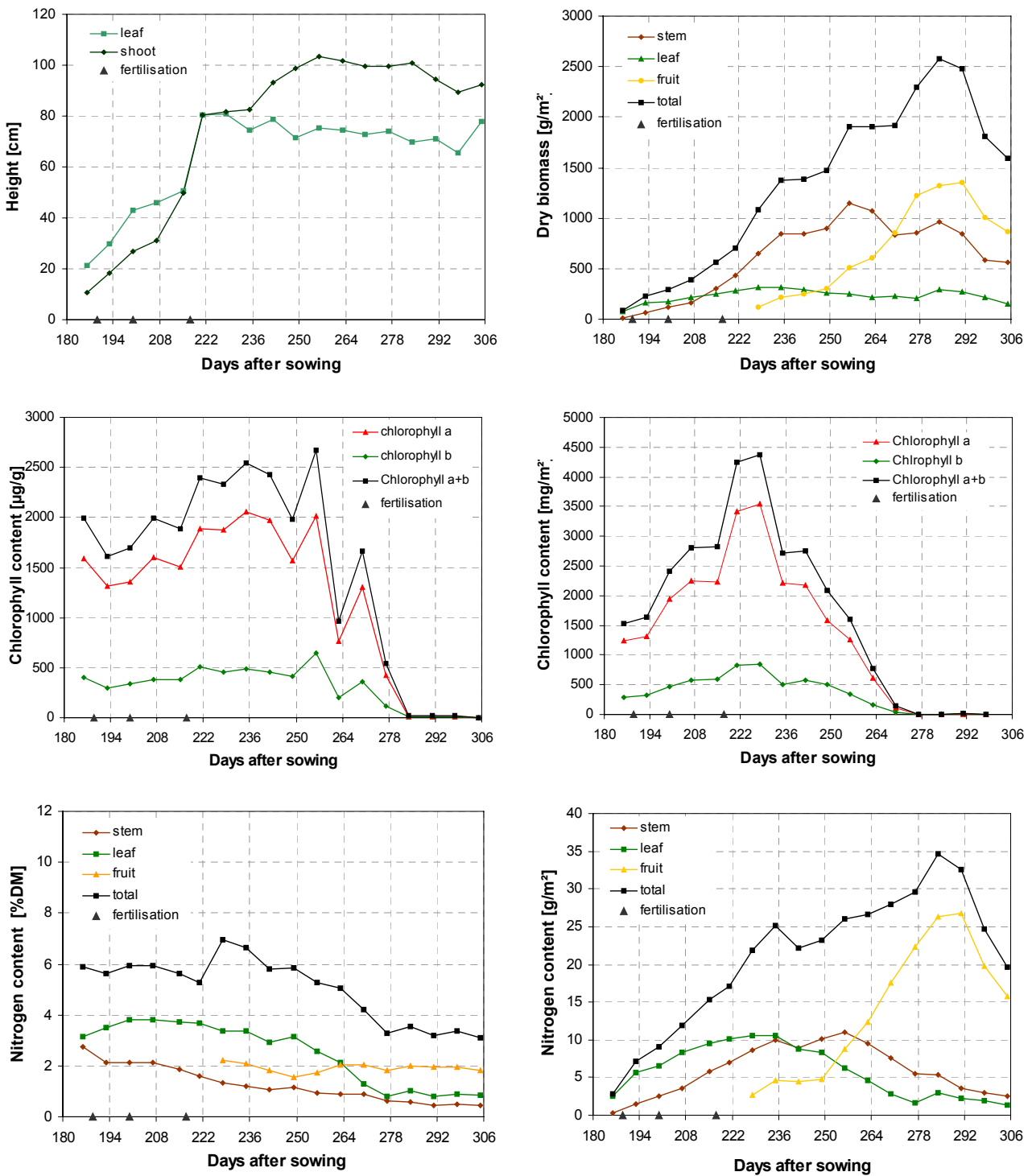
*Figure 3-18:*    *Development of plant height, dry biomass, nitrogen and chlorophyll content for wheat during the growing period 1999 as measured on field No.93*

At about DAS 230 the plants of the test field begin to flower. The stalks bend slightly under the weight of the inflorescence, which still elongates. The total dry biomass as well as total nitrogen content per area increase continuously. The stems grow in diameter to carry the forming fruits and therefore the weight of the stalks increases. The fruits begin

to increase the amount of total biomass and nitrogen per area. The leaves slowly begin to wither and their biomass decreases slightly. The percentage nitrogen content of the stems and leaves both decrease, which is due to the transfer of nitrogen into the developing fruits. The chlorophyll content per area of the leaves decreases rapidly according to their biomass, while the chlorophyll content per mass continues to rise, although more slowly than before. Chlorophyll b stays nearly constant at a level of 500µg/g until it increases to its maximum (652µg/g) simultaneously with chlorophyll a.

At DAS 240 anthesis is completed and maturation begins. The first stages of maturity are milk development (EC 70-79) and dough development (EC 80–89). The grains are fully developed in size, and they begin to harden. The grain filling, which at first is a milky liquid, becomes hard and dry. Before hardening of the grain, the height of the shoot reaches its maximum at 103cm, while the leaves are loosing height because of progressive withering. This withering is also visible in the breakdown of the leaf chlorophyll per mass, which reaches its maximum (2667µg/g) at DAS 256. The chlorophyll content per area decreases further. The biomass of the stems and leaves decrease. The fruit becomes heavier because of the growth and the filling of the grains. The nitrogen of the leaves and stems continues to be moved to the fruits, where it is stored as starch. Therefore the nitrogen content per area increases because of the increase in biomass, while the nitrogen content in %DM remains constant at a level of 2%.

At the beginning of August (DAS 284) the plants are dead, the grains hard and yellow-coloured (see right photograph of Figure 3-17). During the following ripening (EC 90-99) the grains dry further. The straw is dead and collapses. This dying and drying can be seen in the decrease of plant height, biomass and nitrogen content. At this point the wheat is ready for harvest, which was carried out on 13th August.

## 3.4.2    Maize (*Zea mays L.*)

Because of their significantly higher yields in contrast to former varieties, today the cultivation of hybrids is common. For this thesis the silage varieties "Narval" and "Magister" were cultivated on the test fields. Additionally, a mixture of the varieties "Korus" and "Bristol" was investigated in 1999. The position of the test fields is given in Figure 3-11, while the field numbers and the availability of data is shown in Table 3-11.

The first measurements of the maize fields were carried out on 7th June 1999 and 15th May 2000 respectively, at the beginning of tillering. The parallel development of the plants during their growing periods is primarily ensured by the similar dates of sowing. The comparison of phenological stages throughout the two years showed a maximum divergence of three secondary growth stages in the first measurement week. This divergence occurred between the field No.52 and No.65/260, which is mainly due to the late sowing date of No.52. However, this field catches up with the others two weeks later.

The simultaneous phenological development guarantees a homogeneous data basis for the analysis with remote sensing data.

*Table 3-11: Test fields for maize and availability of additional data (acronyms: EC=electric conductivity; S=Schlagkartei; Y=yield estimation; - = no data available)*

| Year | Field number | Cultivar | Size [ha] | Test site | Sowing | Harvest | Additional data |
|------|--------------|----------|-----------|-----------|--------|---------|-----------------|
| 1999 | 52 | Narval | 2 | Gilching | 16.05.1999 | 10.10.1999 | S |
| 1999 | 65a | Bristol/Korus | 3 | Gilching | 30.04.1999 | 28.09.1999 | S |
| 1999 | 260 | Narval | 8 | Frieding | 02.05.1999 | 27.09.1999 | S |
| 2000 | 146 | Magister | 7 | Gilching | 20.04.2000 | 03.10.2000 | - |
| 2000 | 226 | Magister | 2 | Inning | 25.04.2000 | 05.10.2000 | S |
| 2000 | 227 | Magister | 2 | Inning | 25.04.2000 | 05.10.2000 | S |

The development of maize during its growing period will be described with measurements made at one of the test fields as an example, namely field No.260 in 1999 (see Figure 3-19 and Figure 3-20).



*Figure 3-19: Photographs of field No.260 for the year 1999: left=during tillering (EC 25) (DAS 65=5th July); centre=begin of milk development (EC 73) (DAS 93=2nd August); right=dough development (EC 82) (DAS 128=6th September)*

In the region of the Bavarian Alpine foothills the maize plants are sowed at the end of April / beginning of May. The sowing date for field No.260 was 2nd May 1999. The growth of the plant is extremely light dependent. Only five to six leaves, which lie near to the ear, provide its grain filling. To provide the illumination of these leaves, the seedlings are planted in rows between 70cm and 80cm apart. Seven to twelve seeds per m are sowed in these rows. After sowing, a first basic fertilisation of the seeds provides the development of roots and ears. In this case 27kg nitrogen per ha were applied. The small uptake of

nutrients, especially nitrogen, until tillering (EC 20) is due to the slow juvenile development and the low number of plants.

The measurements start at 7th June (DAS 36), when the plantlets have already unfolded the 4th leaf (EC 22). It takes another 35 days until all the leaves are fully unfolded. During this period the plant height as well as the biomass and chlorophyll content per area and mass are rising. While the nitrogen content per area rises because of the accumulation of biomass, the nitrogen content in % of dry matter of both stem and leaf decreases from the beginning of the measurements. When reaching EC 24 to EC 26, i.e. the 6th/8th leaf is unfolded, a second donation of nitrogen is normally applied, in this case 38.8kg/ha at EC 24. At this time the left photograph of Figure 3-19 was taken. The coverage of the soil is sparse during this development stage, while the plantlets unfold their leaves. By now the dark greenish colour is an indicator for the high chlorophyll content per leaf mass, which is measured on that date.

The fertilisation provides the nutrients for the period of stem elongation, booting and emergence of the inflorescence (EC 30 to 59), where the plants grow rapidly until they reach the maximum leaf height of 2m. Accordingly the biomass as well as the nitrogen and chlorophyll content per area increase steeply. The chlorophyll content per mass also reaches its maximum at DAS 63 with 2125µg/g; afterwards it decreases slowly. When the ear starts to grow (DAS 78; EC 40), both leaf biomass and nitrogen content decrease to the benefit of the fruit. The nitrogen content of the dry stem biomass now increases more steeply than that of the leaves. The stems thicken to be able to carry the increasing weight of the fruit. Chlorophyll a per unit area rises steeply until it reaches its maximum (4500mg/m²) when the inflorescence has emerged (DAS 93). Now the nitrogen content of the stems reaches its minimum level of 0.5% DM, where it remains stable until the plants mature. Chlorophyll b per area, which is relatively stable compared to the chlorophyll a content, also shows a maximum at 183mg/m² at the end of booting (DAS 84).

The centre photo of Figure 3-19 shows the maize plants at the transition between the developmental stages, where the inflorescence is fully emerged and the milk development begins. The faded tassels can be seen on top of the plants and at the lower right corner a female inflorescence is visible, which will be filled during the following milk development.

In the period 15 days before and after the emergence of the inflorescence (EC 50) the maize plants assimilate 70 to 75% of their total uptake of mineral nutrients.

The male tassels begin to flower. To provide cross-pollination the tassels flower first and afterwards the female inflorescences flower until DAS 114 (EC 60-69). The height of the leaves is decreasing slightly, while the shoots are still elongating up to 2.20m. The increase of total dry biomass as well as total nitrogen content is due to the forming fruits. The stems remain constant, while the leaves' biomass and nitrogen content begin to

decrease. The chlorophyll content of the leaves decreases accordingly; they start to wither.
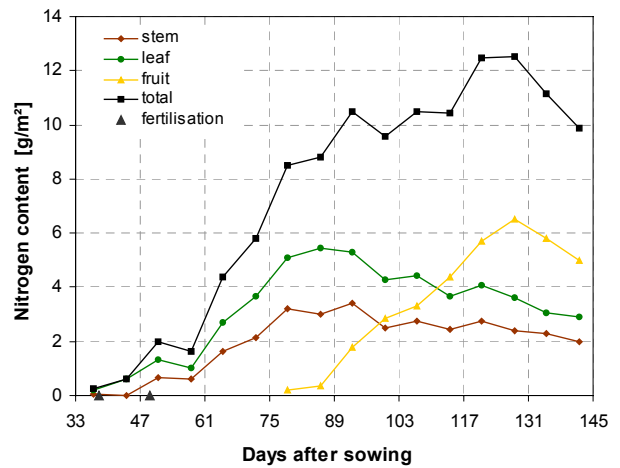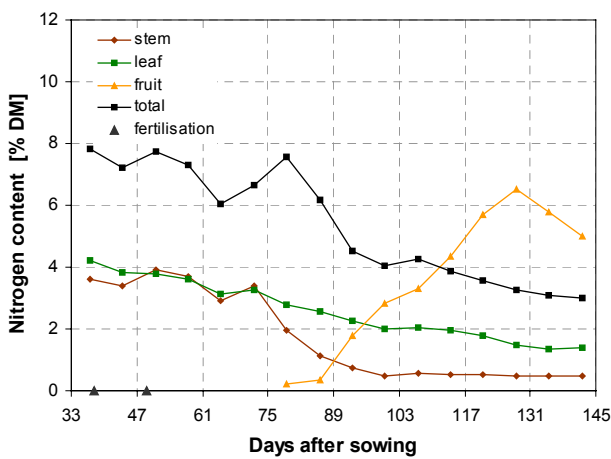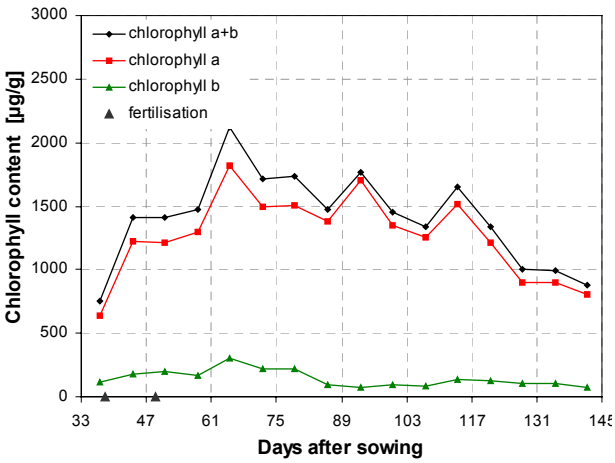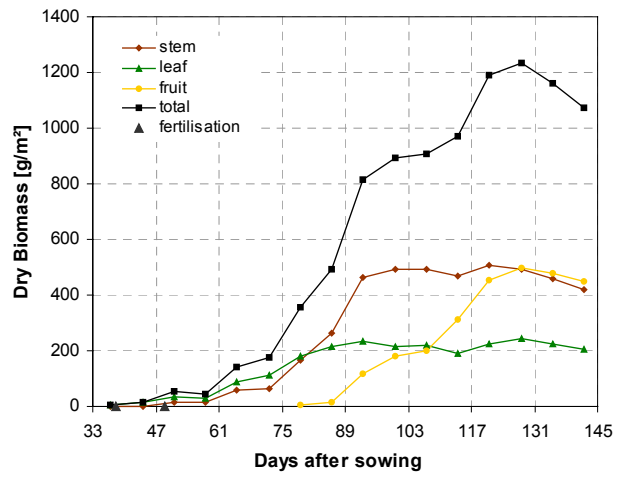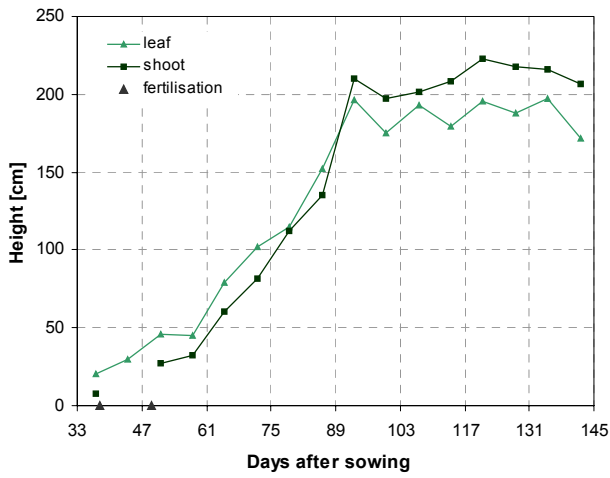


*Figure 3-20:*   *Development of plant height, dry biomass, nitrogen and chlorophyll content for maize during the growing period 1999 as measured on field No.260*

During anthesis and maturity the ears require considerable quantities of nitrogen, but it is provided by the transfer from the leaves and stalks into the grains. Nitrogen uptake from the soil hardly occurs. Therefore the nitrogen content of leaves and stalks decreases for the benefit of the fruits. Accordingly the leave chlorophyll continues to break down. The period of milk and dough development takes three more weeks, where similarly to wheat the grains fill and harden. The shoots also begin to bend. The total biomass still increases because of the increase of fruit mass, whereas the stems and leaves remain relatively stable. The right picture in Figure 3-19 presents a view of the plants at the beginning of dough development. The formerly dark green colour is faded and the ears have reached their full size.

The following ripening completes the growing period of maize. The straw is dead, the leaves are fully withered and yellow–brown coloured. The ears are ready for harvest, which took place on 27th September 1999.

Depending on the yield 160 to 280kg nitrogen per ha has been assimilated in total. But maize is known as a "heavy feeder" and tolerates heavy applications of nitrogen fertiliser without yield reduction. This behaviour often leads to a excessive fertilisation especially with nitrogen. The investigated test fields are fertilised with 60 to 100kg nitrogen per ha. This is due to the fact that these fields are located in water protection areas. Excessive fertilisation leads to an increased outwash of nitrogen into the ground water. Especially with maize the low coverage of the soil surface promotes outwash, which threatens the quality of the ground water and therefore the supply of drinking water of this area. This fact and the menacing of fines, leaded to a responsible treatment of the fields with nitrogen fertiliser.
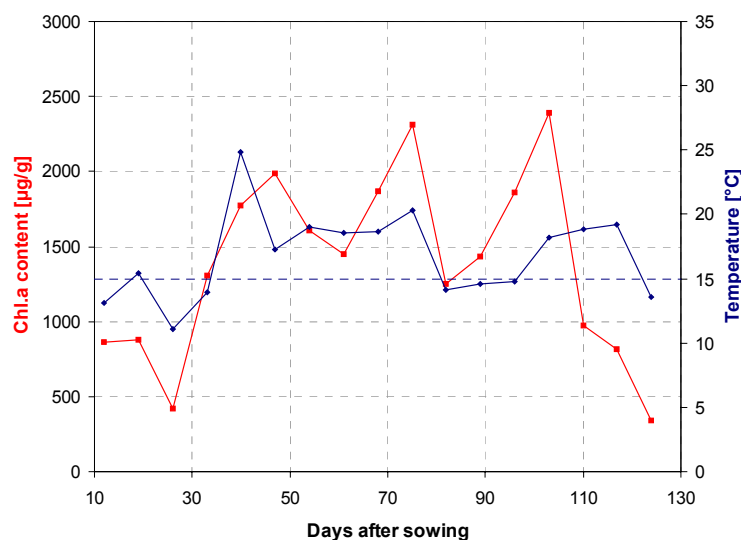


Figure 3-21:   Dependence of chlorophyll a content per mass of the daily mean temperature derived from field measurements of maize field No.52 and weather station Hüll (the dotted blue line represents 15°C)

A noticeable behaviour is the variation of the chlorophyll content per mass, which shows distinct variations during the vegetation period. Pigment contents per mass are more variable than contents per area for all investigated land covers (see Figure 3-18, Figure 3-20, Figure 3-23, Figure 3-24, Figure 3-27 and Figure 3-29) but the maize canopies show the highest variations up to 500µg/g between two sampling dates. Moreover, these variations differ between the cultivars. These fluctuations in the field have also been observed by Baker when temperatures are fluctuating (Prof. Baker, University of Essex, UK, Dept. of Biological Science; personal communication on 16th January 2002). Certain maize varieties can become chlorotic when temperatures drop, but the chlorophyll levels recover when temperatures rise again. The response time to the temperature changes depends on the cultivar. Wheat and grass do not show such distinct effects since they are more chilling tolerant. The comparisons between the temperatures and the chlorophyll content per mass confirm this suspicion. The chlorophyll content per mass and the temperatures show the same trend, especially below 15°C. Figure 3-21 depicts an example for this phenomenon. The decrease of the chlorophyll content after DAS 103 (7th September) is caused by the ripening of the plants and the successive degradation of the chlorophyll.

### 3.4.3    Grassland

For this thesis, four test fields of grassland were investigated in the years 1999 and 2000. In 1999 the measurements were carried out from 19th April to 27th September, in 2000 from 25th April to 21st August.

The utilisation intensity of the test fields varies between extensive use with no application of fertiliser (field No.224) to intensive use with four to five cuts per year (Field No.223). The botanical analysis of the indicator values identifies the field No.223 as having the highest nitrogen level, while field No.224 shows the lowest nitrogen factor of the four test meadows (Table 3-12). Nevertheless, the N values for the extensive meadows are still high compared to the average in central Europe. Even the unfertilised fields show no poorness indicators. The biological description leads to the conclusion that all investigated meadows can be assigned to the same plant community, i.e. a species-poor, fragmental fresh (oatgrass) meadow (*Arrhenatherion elatioris*), merely field No.224 shows a higher saturation with grassland flora species of *Arrhenatherion elatioris* (see Table 3-12).

Oatgrass meadows are the most common type of mown grassland in the Alpine foothills, so the selected test fields represent an important community in the test area. The development of the meadows during the growing season will be described below.

*Table 3-12: Characterisation of the grassland test fields in 1999/2000 and availability of Schlagkartei data (S) (- = no data available) (the Klapp value is weighted and normalised to maximum)*

| Field No. | Test site | Size [ha] | Plant community | Type of use | Level of utilisation | Klapp value | Ellenberg values | | | Add. data |
|-----------|-----------|-----------|-----------------|-------------|----------------------|-------------|------|------|------|-----------|
| | | | | | | | F | R | N | |
| 106a | Gilching | 2 | Species-poor Arrhenatherion elatioris | Mown meadow | 1 cut | 1.0 | 4.9/ 5.0 | 6.4/ 6.0 | 6.3/ 5.7 | - |
| 224 | Inning | 2 | Species-poor Arrhenatherion elatioris | Mown meadow | 2 cuts | 0.8/0.7 | 5.1/ 5.1 | 6.8/ 6.7 | 5.6/ 6.1 | - |
| 53b | Gilching | 2 | Species-poor Arrhenatherion elatioris | Mown pasture | 3 cuts + 2 grazing | 0.7 | 4.9 | 6.5 | 5.9 | S |
| 223 | Inning | 1 | Species-poor Arrhenatherion elatioris | Mown meadow | 4 - 5 cuts | 0.8/0.5 | 5.0/ 5.7 | 6.7/ 6.3 | 6.7/ 6.8 | S |

### 3.4.3.1    Meadow with one cut

Field No.106a is mowed once a year, at the beginning of July (1st in 1999 and 3rd in 2000). Therefore it must be fertilised to provide yield, but this field is not treated with mineral fertiliser. To supply the necessary nutrients this meadow was mulched with bark at the beginning of the vegetation period in April in both years. The nutrients are dissolved by mineralisation of the organic material and so the nutrient cycle can be closed.



*Figure 3-22:    Photographs of meadow No.106a for the year 1999: left=first growth on DOY 123 (3rd May); centre=first regrowth on DOY 200 (19th July); right=first regrowth on DOY 263 (20th September)*

Field No.106a is an extensive fresh meadow with percentage coverage of 95% at the relevés. The numbers of species found in the two measurement plots are 11 and 9, respectively. Facies-bearing grasses are meadow foxtail (*Alopecurus pratensis L.*) and

cocksfoot (*Dactylis glomerata L.*). Dandelion (*Taraxacum officinale Web.*) and red clover (*Trifolium pratense L.*) can also be found frequently. The moderate occurrence of dandelion can be seen in Figure 3-22, where the photo was taken in spring while flowering. In addition, low hop clover (*Trifolium campestre L.*) can be found at some plots, especially in the tyre tracks where the soil is compacted. Nevertheless, the botanical analysis assigns this meadow the highest forage quality of the four test fields.
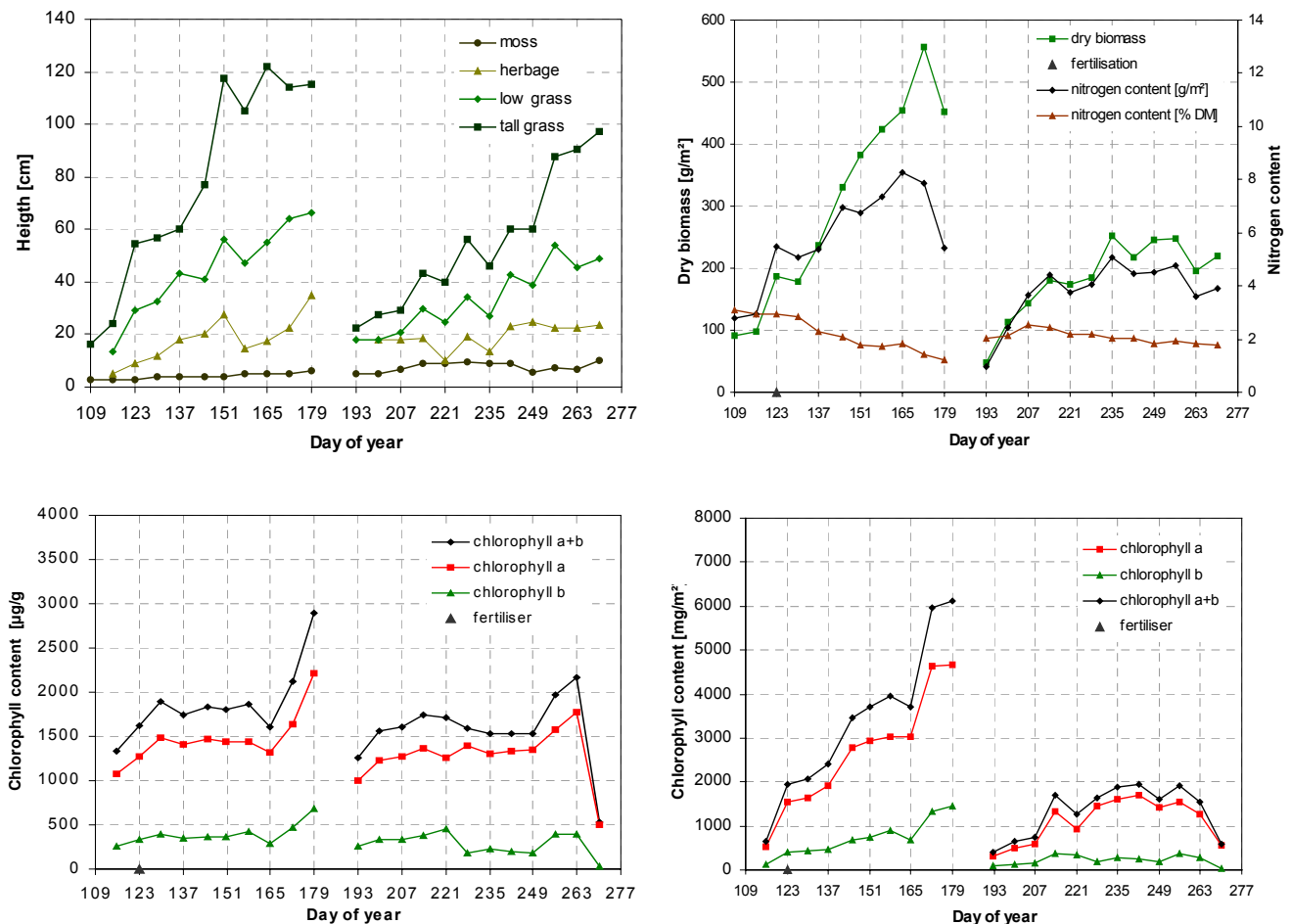


Figure 3-23:    *Development of plant height, dry biomass, nitrogen and chlorophyll content for the extensively used meadow No.106a during the growing period 1999*

Figure 3-23 shows that the parameters plant height, chlorophyll content per mass and chlorophyll content per area rise until the cut on 4th July (DOY 185). Dry biomass and nitrogen content per area show a parallel course, but they decrease in the week before mowing. This is partly due to the translocation of nitrogen from senescent leaves and partly due to death and decay of older leaves while the chlorophyll content of the young leaves on top of the canopy is still increasing. The nitrogen content in % of the dry matter decreases constantly from 3 to 1.2%.

The biomass measurements show stronger variations compared to those of wheat and maize. This can be mainly attributed to the less homogeneous but patchy coverage of

swards (see also Figure 3-22) and the different development of plant species during the year leading to a patchy coverage of the ground. Therefore the measured biomass is varying depending on the sampling point chosen.

The cut is carried out on a date during the anthesis of the grasses, where the digestibility of the dry matter is still high enough to use it as high quality forage.

All parameters rise again during the second upgrowth, but as expected they reach a lower level. This time the plants undergo the whole growing cycle and mature, which is visible in the breakdown of plant chlorophyll content both per mass and area in September. Defoliation of grassland canopies during the growing season causes a major though temporary reduction in nitrate uptake. This phenomenon can also be seen in the profile of the percentage nitrogen curve in Figure 3-23. This also leads to a reduced production of biomass and primarily causes the reduced level of chlorophyll content per area. In contrast, the chlorophyll content per mass almost attains its previous level.

### 3.4.3.2   Meadow with two cuts

Meadow No.224 is mainly located in the aquifer protection zone II of a water protection area, but partly covers zone I. In zone I no fertilising is allowed, while in zone II the application of fertiliser in moderate donations is permitted. Meadow No.224 is not fertilised, but cut twice a year, namely in June and at the end of August.

Field No.224 belongs to the oatgrass meadows (*Arrhenaterion elatioris*) and has coverage of 98% at the relevés. The numbers of different species at the relevés were 15 and 11. Facies-bearing species are wild oat (*Bromus hordeaceus L.*), Italian ryegrass (*Lolium multiflorum Lam.*) and rough meadow grass (*Poa trivialis L.*). Dandelion (*Taraxacum officinale Web.*), red clover (*Trifolium pratense L.*) as well as mouse-ear chickweed (*Cerastium holosteoides Fr.*) and less numerously daisy (*Bellis perennis L.*) can also be found in this field. The prevalent occurrence of dandelion can be seen in Figure 3-25 where it flowers at the beginning of May. Indicator plants for soil compaction or an oversupply of nutrients cannot be found in this meadow.

The development of measured plant parameters is very similar to that for meadow No.106a and is shown in Figure 3-24 for 1999. Differences can be recognised in the curves of the plant height and the chlorophyll content per mass before the first cut. The height of the low and tall grasses show a significant decrease after DOY 153, which corresponds to the 2nd June. This behaviour can be explained by flat wind throw, which mainly affects the top layer of the canopy. This may be the reason for a reduced illumination, which leads to a reduced chlorophyll concentration per mass in the leaves. Biomass still increases because of continuous growth especially of the small grasses and herbs.
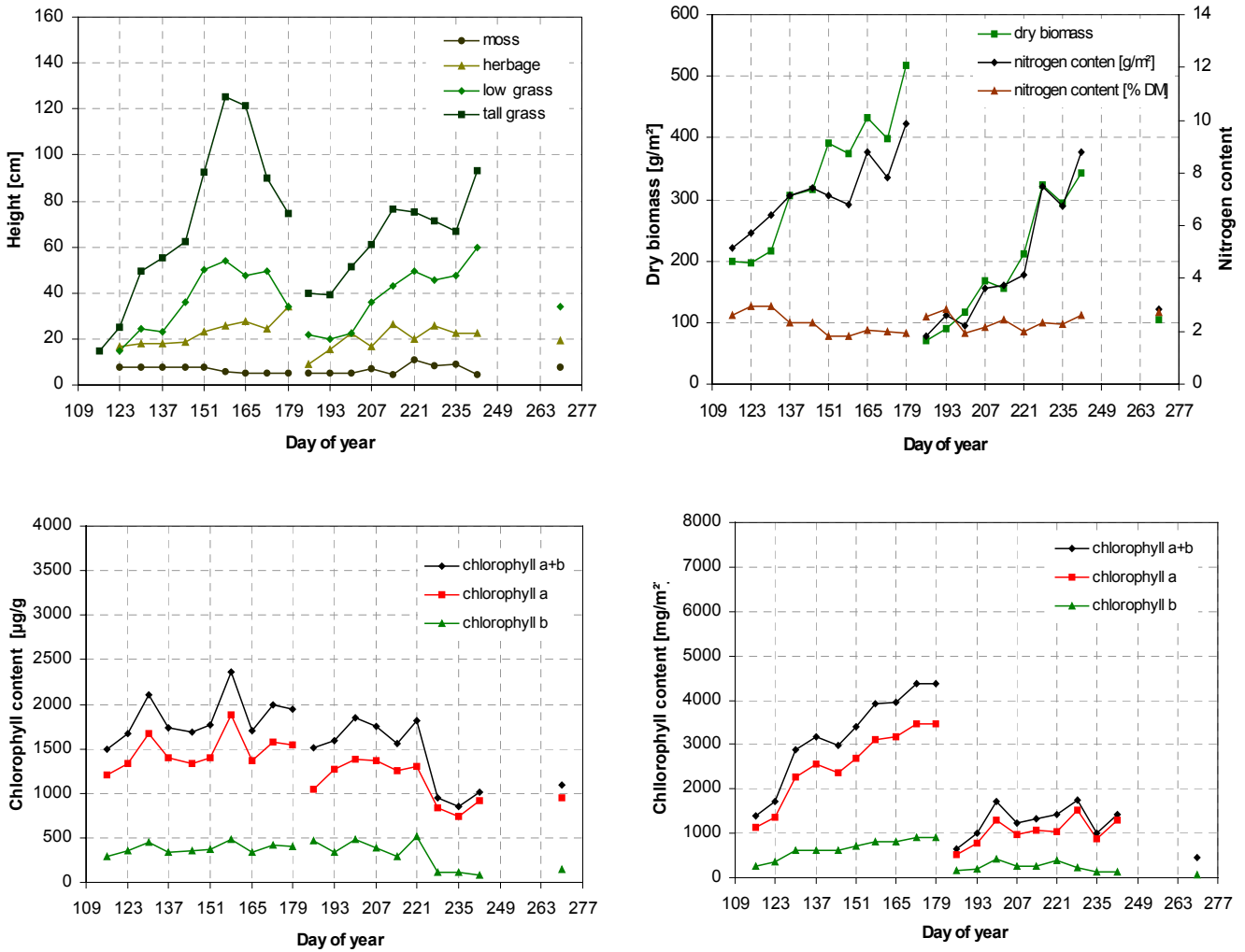
Figure 3-24:    Development of plant height, dry biomass, nitrogen and chlorophyll content for the extensive meadow No.224 during the growing period 1999

During the first regrowth the chlorophyll content per mass shows a comparable trend to field No. 106a. A minor breakdown of the chlorophyll concentration occurs in the middle of August (DOY 221 to 228), but remains on a relatively high level of 1000 µg/g until the second mowing. This is possibly due to the reduced nutrient supply compared to the mulched sward. The reason for the reduction lies in the fact that the nutrient reserve in an unfertilised soil begins to deplete earlier than in a fertilised sward. The fact that the chlorophyll concentration shows the same phenomenon in 2000 supports this explanation as much as the slow second regrowth of the plants (see also Figure 3-25), which prevented measurements in the first two weeks of the second regrowth.

*Figure 3-25:*     *Photographs of the test meadow No.224 for the year 1999: left=first growth at DOY 123 (3rd May); centre=first regrowth at DOY 200 (19th July); right=second regrowth at DOY 263 (20th September)*

### 3.4.3.3    Meadow with rotational grazing

Field No.53b is an intensively used meadow that is cut three times a year with grazing periods after the second and third cuts.

This field also belongs to the fresh grass meadows (*Arrhenaterion elatioris*) with percentage coverage of 100% and, compared to the other test fields, a moderate number of species with 13 at plot one and 14 at the second plot.

Facies-bearing grasses are rough meadow grass (*Poa trivialis L.*), wild oat (*Bromus hordeaceus L.*), Italian ryegrass (*Lolium multiorum Lam.*) and to a lesser degree cocksfoot (*Dactylis glomerata L.*). Herbs such as yarrow (*Achillea millefolium L.*) and dandelion (*Taraxacum officinale Web)* are numerous, which can be seen in the left photograph of Figure 3-26, which was taken during the flowering of dandelion at the beginning of May. The legumes are represented by red clover (*Trifolium pratense L.*), mouse-ear chickweed *(Cerastium holosteoides Fr.)* and wall speedwell *(Veronica arvensis L.)*.

The high level of utilisation requires the application of fertiliser as well as additional maintenance of the topsoil. Fertiliser is applied at the beginning of the vegetation period and each regrowth to compensate for the loss of nutrients due to mowing. After the grazing period in July organic fertiliser is applied, while mineral nutrients are donated at the beginning of the vegetation period and the other regrowths.

Additional maintenance work after grazing is necessary to repair the trampled topsoil and to distribute the cowpats. The field is levelled and rolled after the summer grazing period at the beginning of August (see Figure 3-26 centre right) as well as after the autumn grazing period in following spring.

Figure 3-26:     Photographs of the test meadow No.53b for the year 1999: far left=first growth at DOY 123 (3rd May); centre left=first regrowth at DOY 172 (21st June); centre right=second regrowth after grazing at DOY 208 (26th July); far right=third regrowth at DOY 242 (30th August)

The measurements start on 26th April 1999 (DOY 116). Results for 1999 are shown in Figure 3-26. The first upgrowth quickly reaches a plant height of 70cm. The parameters chlorophyll and nitrogen content show similar curves both per area and mass. The first cut was on 18th May (DOY 138). The canopy reaches the same height just four weeks later with high nitrogen content in the dry matter, which mainly is due to the nitrogen fertilisation of the meadow on 29th May (DOY 149). Even so, the dry biomass only attains two-thirds of the highest level, which is mainly caused by the reduced growth of the small grasses. The development of the biomass is similar for the further upgrowths. The increase of plant height, chlorophyll content per mass as well as the nitrogen content in the dry matter immediately after fertilisation is very conspicuous. As expected, the tall grass species especially exhibit the growth-stimulating effect of nitrogen fertiliser, but also the herbs show a much better development. In contrary to the plant height both the chlorophyll content per mass and the nitrogen content in the dry matter seem to return slowly to the previous level after the sudden rise. This phenomenon is very distinct during the second upgrowth and especially during the third regrowth, where the initial chlorophyll content is already higher compared to the other upgrowths. The reduced chlorophyll content can be noticed when comparing the colour in the photographs in Figure 3-26. The first regrowth has the brightest green compared to the first and third upgrowths.

The measurements were not carried out during grazing because firstly, the canopy is extremely inhomogeneous and secondly, the young grazing stock complicated the measurements.

The third cut on the 7th October lies beyond the measurement period, which ends on 27th September.
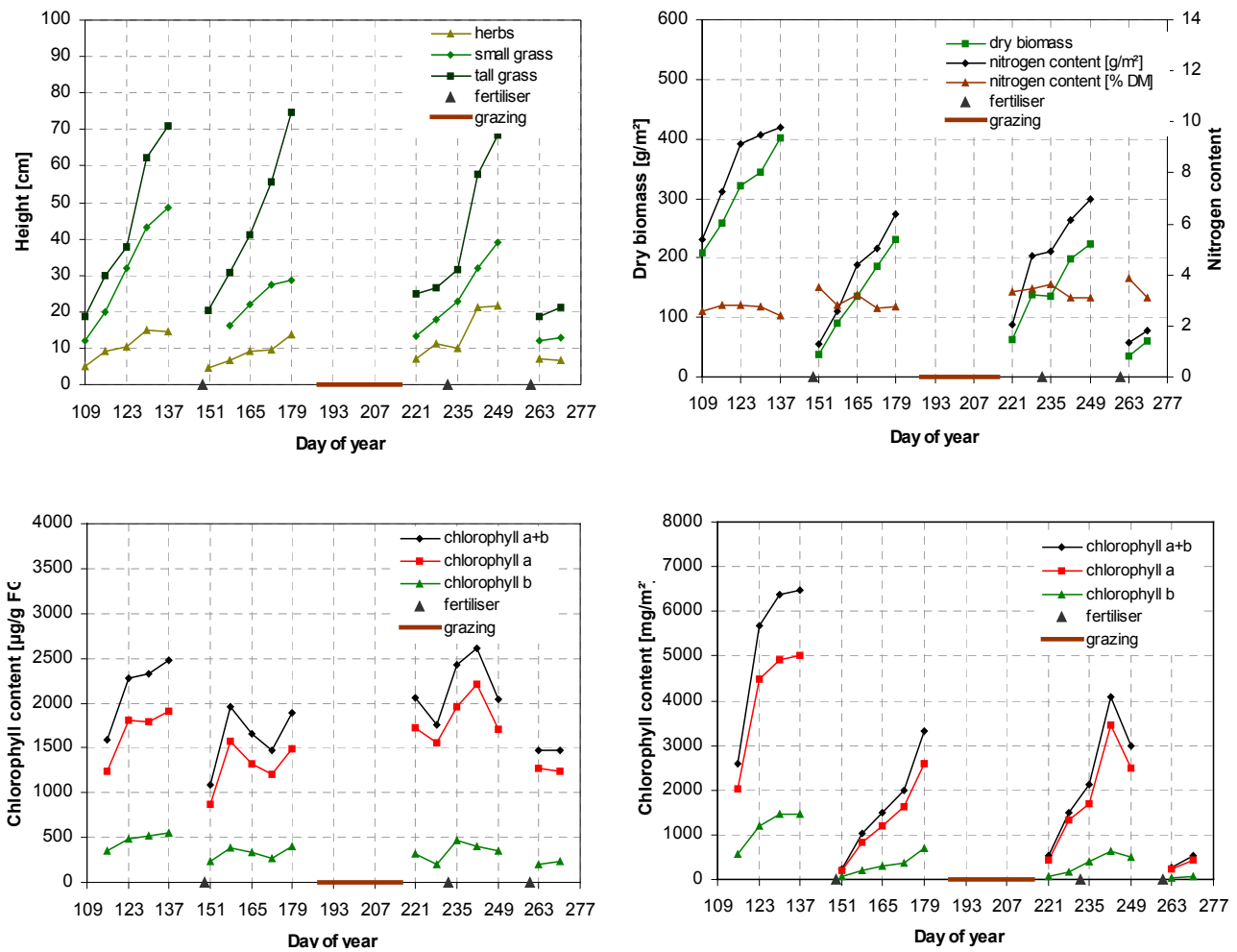
Figure 3-27      *Development of plant height, dry biomass, nitrogen and chlorophyll content for the intensive meadow No.53b during the growing period 1999*

### 3.4.3.4    Meadow with four to five cuts

Test field No.223 is a mown meadow that is cut four (1999) and five (2000) times a year, respectively. The main reason for the lower intensity of use in 1999 is the unfavourable weather conditions, namely the flooding in May (see also Figure 3-2), leading to partial flooding of that field. Therefore in 1999 the meadow could not be cut at the end of July, but only in August and October.

The meadow No.223 is also classified as fresh meadow (Arrhenatherion elatioris). The number of mapped species is 13 and 14. Most of the ground is 100% covered, but a depression within the meadow forms an area of disturbance where the coverage only lies at 70%. This depression covers about one fifth of the meadow and is flooded when heavy rainfall occurs. The botanical analysis also assigns the plot within that area both the highest moisture (F) and nitrogen (N) value. This leads to differences in the botanical composition that will be described separately.

The facies-bearing grasses of the undisturbed part of the meadow are bluegrass (*Poa pratensis L.*), perennial ryegrass (*Lolium perenne L.*), and to a lesser degree cocksfoot (*Dactylis glomerata L.*). The herbal and legume fraction is mainly composed of red clover (*Trifolium pratense L.*), dandelion (*Taraxacum officinale Web*) (see Figure 3-28) and cow parsley (*Anthriscus sylvestris L*). Creeping buttercup *(Ranunculus repens L.),* hogweed (*Heracleum sphondylium L.*), and mouse-ear chickweed (*Cerastium holosteoides Fr.*) also occur.



*Figure 3-28:      Photographs of the test meadow No.224 for the year 1999: far left=first growth at DOY 116 (26<sup>th</sup> April); centre left=first regrowth at DOY 158 (7<sup>th</sup> July); centre right=second regrowth at DOY 207 (26<sup>th</sup> July); far right=third regrowth at DOY 263 (20<sup>th</sup> September)*

The disturbed plot shows a different botanical composition. The grass species recede, while those species dominate that indicate a disturbance, flooding and/or over-fertilisation of the soil. The former are represented by a limited number of meadow foxtail (*Alopecurus pratensis L.*) and bluegrass (*Poa pratensis L.*). Numerous broadleaf docks (*Rumex obtusifolius L.*), annual meadow-grass (*Poa annua L.*), and to a lesser extent shepherd's-purse (*Capsella bursa-pastoris Med.*), chickweed (*Stellaria media L.*), thyme leaved speedwell (*Veronica serpyllifolia L.*), broad-leaved plantain (*Plantago major L.*), creeping bent (*Agrosis stolonifera L.*), and mouse-ear chickweed (*Cerastium holosteoides Fr.*) represent the latter.

The harvest of this meadow is used for silage. To reduce the species that crumble while drying or silaging and therefore lessen the yield, an herbicide is applied with the fertilisation at the beginning of the second regrowth. The affected species are dicotyledonous, so primarily herbs and legumes are reduced. The primary objective is the reduction of toxic plants such as creeping buttercup *(Ranunculus repens L.).*
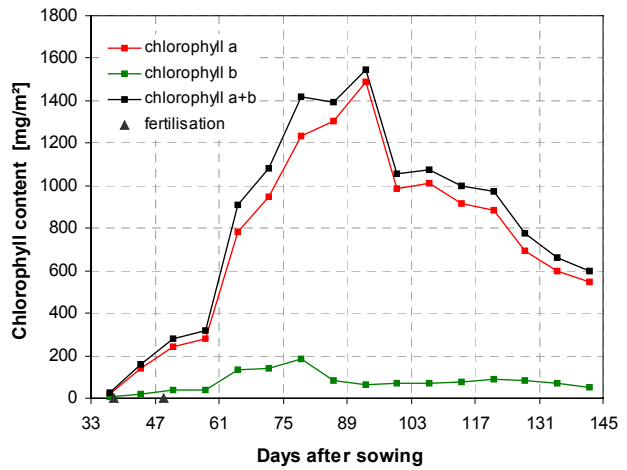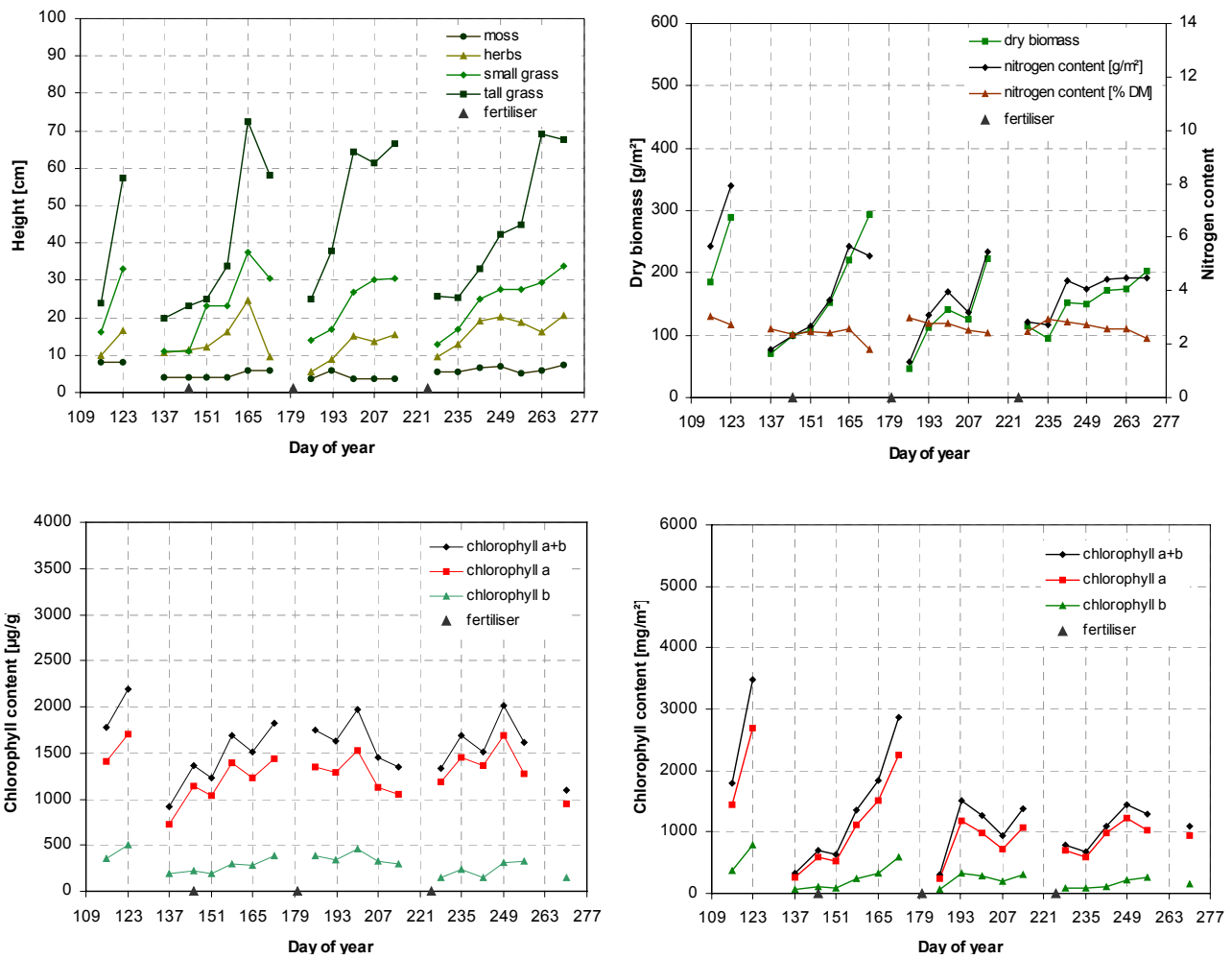
Figure 3-29:     *Development of plant height, dry biomass, nitrogen and chlorophyll content for the intensive meadow No.223 during the growing period 1999*

Field No.223 was fertilised at the beginning of the growing season as well as after each cut to provide a sufficient supply of nutrients. The measured plant parameters are shown in Figure 3-29. Comparable to field No.53b an immediate increase of plant height, especially of the tall grass and herbage layer, can be observed after the fertilisations. The strong decrease of plant height at the end of the second upgrowth is caused by wind throw that was also observed at field No.224 in the same test site. Nevertheless, the height of the canopy is similar for each upgrowth, although the biomass is reduced at the last two upgrowths. A possible reason may be a decreased density of the canopy after the application of herbicides.

The nitrogen content of the dry matter decreases as expected during each upgrowth from a level of 2.9% to 1.8% respectively. The nitrogen content per area as well as the chlorophyll content per area also take a course according to the biomass.

The weekly variations of the chlorophyll content per mass of this meadow up to 500µg/g are conspicuous and occur also in the 2000 results of this meadow. These fluctuations

may be due to various factors such as low irradiance, rainfall and low temperatures or problems during sampling and analysis. The low irradiance may be probable on DOY 165 (14th June) where a relative minimum was observed for all investigated meadows. The analysis of the temperature, irradiance and precipitation data of the weather stations showed no correlation with these parameters on this date. In fact, on DOY 172 (21st June) the chlorophyll content is higher, although both the irradiance and temperature are lower and even more rainfall occurred on that day and in the period five days beforehand. The influence of the weather conditions seems not to cause this minimum. The patchy canopy, which can be seen in the photographs of Figure 3-28 may cause this effect. The proportion of senescence and therefore yellow and brown leaves during the regrowths is high, most likely because of the herbicide application. The chlorophyll analysis is very sensitive to dead plant material and therefore even leaves that begin to mature can reduce the chlorophyll content.

### 3.4.4    **Field Spectrometer Data**

Ground truth activities with respect to spectroradiometric measurements in support of imaging spectrometer overflights are an important tool in validating and calibrating the acquired data sets. A well characterised and calibrated set of ground-based instruments is necessary to develop methods to compare the operational environment of the imaging spectrometer to its laboratory calibration environment. In this case, where an imaging spectrometer has no specific inflight calibration and no inflight characterisation before and after the data acquisition can be performed, the spectroradiometric behaviour of the instruments relies fully on the laboratory calibration and on its stability. Recent advances have proven the need of in situ measurements to predict the at sensor radiance and to allow a validation of calibration coefficients (Schaepman et al., 1997; Strobl et al., 1997).

The reflectance of a canopy can differ greatly from the reflectance on leaf level measured on the ground. The direct comparison of the spectra is very difficult to realise because shadowing effects, vegetation scattering and illumination differ with the variation in both observation height and area. Ground based spectrometer data must be employed very carefully to interpret the airborne derived measurements (Prof. J. Miller, University of York, Canada; Dept. of Physics; personal communication at 13th November 2001).

For this study field spectrometer measurements are used for both the prediction of the at-sensor radiances and validation of the AVIS data. The former was performed using the reflectance target of the DLR while the latter was carried out through measurement of several test fields simultaneously to the airborne data acquisition.

### 3.4.4.1    DLR Reference Target

A part of the hangar at the airfield of the DLR in Oberpfaffenhofen, near Munich, is measured regularly by the German Remote Sensing Data Centre (DFD) with a field spectrometer (GER 3700). Mr. Beisl of the DFD kindly placed these measurements at our disposal. The optical system consists of three spectrometers (512 element SI array, 128 element PbS array, 64 element PbS array) and covers the 350–2450nm wavelength range. The instrument has a spectral sampling interval of 1.5nm (359–1050nm), 6.8nm (1030–2100nm) and 8nm (2100-2450nm) respectively. The spectral resolution of the three wavelength regions is 2.3, 10.4 and 12.3nm respectively.

Figure 3-30 shows the location of the hangar on the terrain of the DLR and a reflectance spectrum for the 550–1040nm wavelength region measured in 1999. The spectrum is an average of 48 individual measurements carried out at a height of 1m above ground.

The main advantage of using this target is firstly its location within the test area. Secondly the use of a concrete target does not require simultaneous measurements during each flight, because the temporal variation as well as the bi-directional scattering of a concrete

target compared to vegetation is very low (Prof. J. Miller, University of York, Canada; Dept. of Physics; personal communication at 13th November 2001).
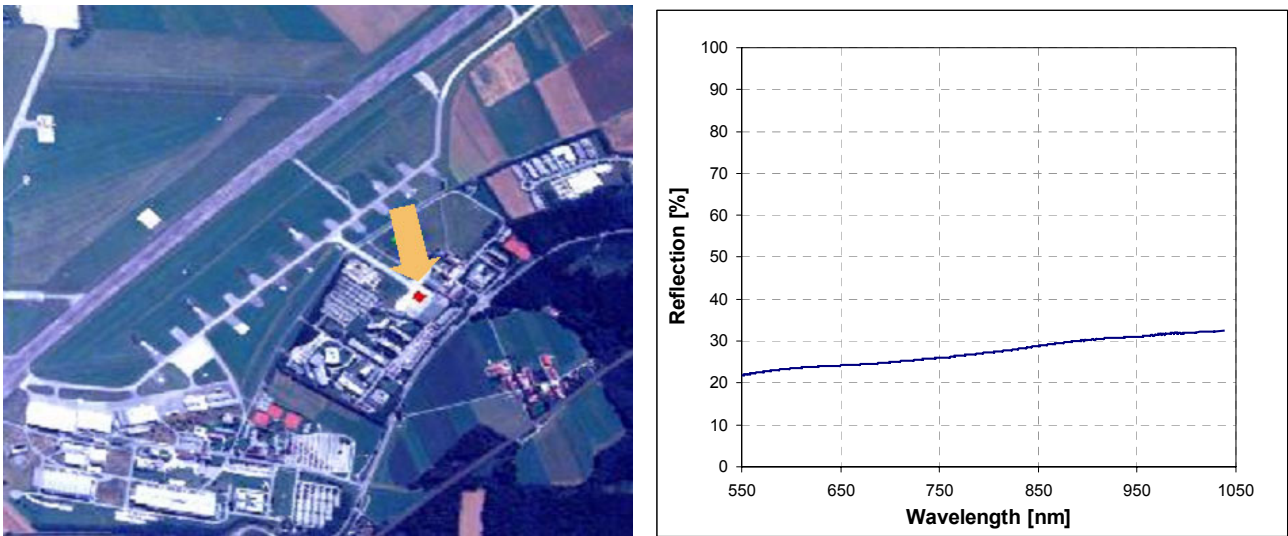


*Figure 3-30:    Position of the DLR reference field (left) and a reflectance spectrum measured in 1999*

## 3.4.4.2            Ground Measurements of Test Fields

In addition to the spectrum of the DLR hangar, measurements simultaneous to the AVIS overflight were conducted using the Institute for Geography's GER SIRIS field spectrometer. The SIRIS instrument consists of three separate diffraction gratings and covers the 400–2500nm wavelength region (400–1000nm, 1000–1800nm, 1800–2500nm) with a spectral sampling of 2, 4 and 6nm respectively (Bach, 1995).
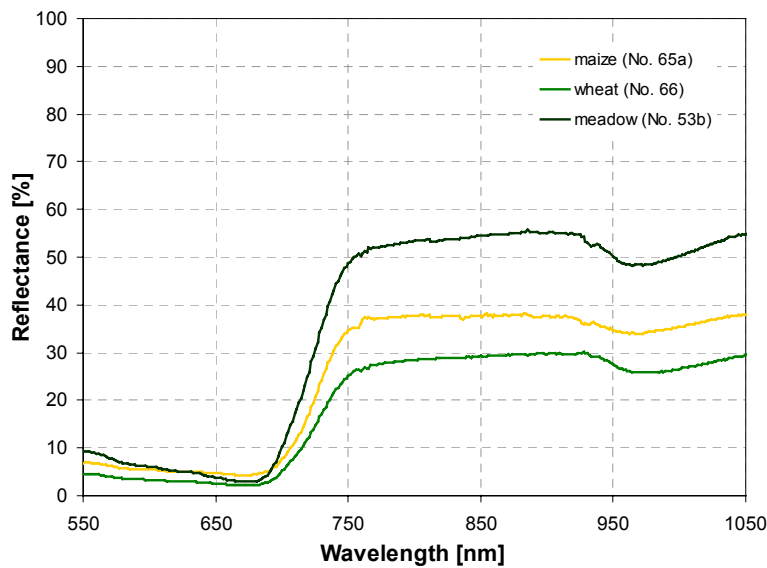


*Figure 3-31:    SIRIS reflectance spectra of different land covers measured on 3rd July 1999*

In 1999 SIRIS measurements were performed on two dates, namely 3rd July and 18th July. On both dates the measurements were carried out on six test fields (wheat: No.66 and 93; maize: No.52 and 65a; meadow: No.53b and 106a). Figure 3-31 provides reflectance spectra of the different land cover types measured on 3rd July 1999.

Field reflectance measurements were performed with the spectrometer looking from a distance of 1m in nadir direction onto the ground. A barium sulfate ($BaSO_4$) panel was used as the reflectance standard. For each reflectance spectrum two measurements were taken, first the reference and subsequently the target was measured. The correction to absolute reflectance was done by ratioing the target and the reference measurement. At least three measurement sequences were averaged and further used to validate the AVIS data.

# 4   Airborne Measurements and Preprocessing of the Data

As shown in section 3 vegetation parameters are highly dynamic and their development depends, besides the crop type, on many different factors such as management or weather conditions. This facts and the aim of finding the most suitable dates for airborne measurements require a multitemporal approach for the monitoring of vegetation parameters. Over the two years of this study as many airborne measurements as possible were carried out to obtain the largest possible data set.

Before the data could be analysed, they had to pass through several preprocessing steps. During these steps system errors were corrected and each band was assigned to a specific wavelength.

Optical data are not only dependent on the characteristics of the sensor or observed pixels on the ground. The irradiance, the atmospheric conditions and the pixel environment have a large influence on the measured data and therefore must be corrected as well. Especially for multitemporal approaches an atmospheric correction is essential for a quantitative analysis of the data (Bach & Mauser, 1994; Roberts et al., 1997; Staenz et al., 2000). During the correction process grey values are converted into absolute reflectance values, which solely contain information about the observed target on the ground.

In the following section design planning and realisation of the overflights will be described. The preprocessing steps including the atmospheric correction will be explained as well, followed by a discussion of the results. Finally, the geometric rectification of the image data will be described.

## 4.1 The flight campaigns 1999 and 2000

The airborne measurements with the AVIS system were conducted in collaboration with the flying group of the *Luftwaffe* (German Air Force) located at the air base Fürstenfeldbruck, 25km west of Munich. The aircraft used was a Do 27 (Dornier), which is equipped with a standard camera mount onto which the sensor could be installed (see Figure 2-2 in section 2.1).

To obtain as much as possible airborne measurements at all sorts of phenological stages a weekly repetition of AVIS was desired. However, imaging spectrometers are optical systems and thus their use is weather-dependent. During the two years of monitoring, bad conditions with cloudy and rainy weather periods prevented AVIS measurements. Especially in June and August 1999 as well as in April and June 2000 the weather led to longer gaps between measurement sets. Thus, twelve and nine flights were carried out in 1999 and 2000 respectively, which is presented in the flight calendar shown in Figure 4-1. Providing that the phenological developments of the plants over the two years are comparable, the combination of all measurements may still enable the assessment of the vegetation parameters throughout a growing period.
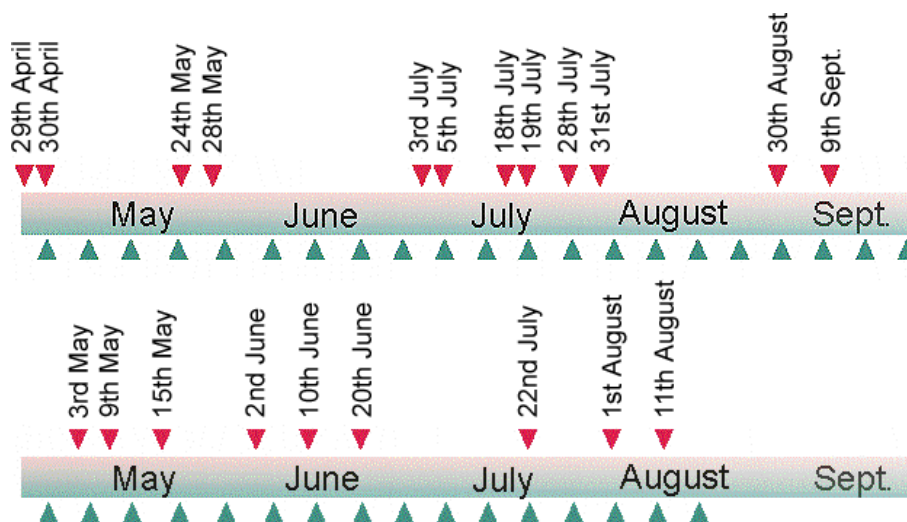


Figure 4-1:    Campaigns calendars for 1999 (top) and 2000 (bottom) (green triangles=ground measurements; red triangles= AVIS measurements)

The flight stripes were chosen in such a manner that as few different stripes as possible cover all the test fields. The relatively small size of the test area was helpful in minimising the flight duration, which reduced the costs for one mission.

Measurements were carried out in N–S and S–N direction at two different altitudes, namely 4000 and 10000ft above sea level (asl) (see Figure 4-2). The 4000ft level enables a more detailed monitoring of the test fields while the 10000ft level is easier to conduct in terms of the field coverage.

The area lies within the approach corridor of the Munich airport, so the airspace at 10000ft is governed by its traffic control. Due to the traffic volume this altitude could not always be flown, while the 4000ft could be flown without any restrictions. In 1999 both altitude were flown, but waiting periods often occurred before the flying permissions were obtained, so in 2000 only the 4000ft were flown.

To provide the coverage of the test fields, the flight navigation first was GPS based. With time it turned out that the alignment of the aircraft for a correct GPS position after the turns was very time-consuming and the flights stripes had to be extended. On the other hand, the local knowledge of the pilots enabled a much better coverage of the test fields than by using the GPS, and so flight navigation was carried out visually.
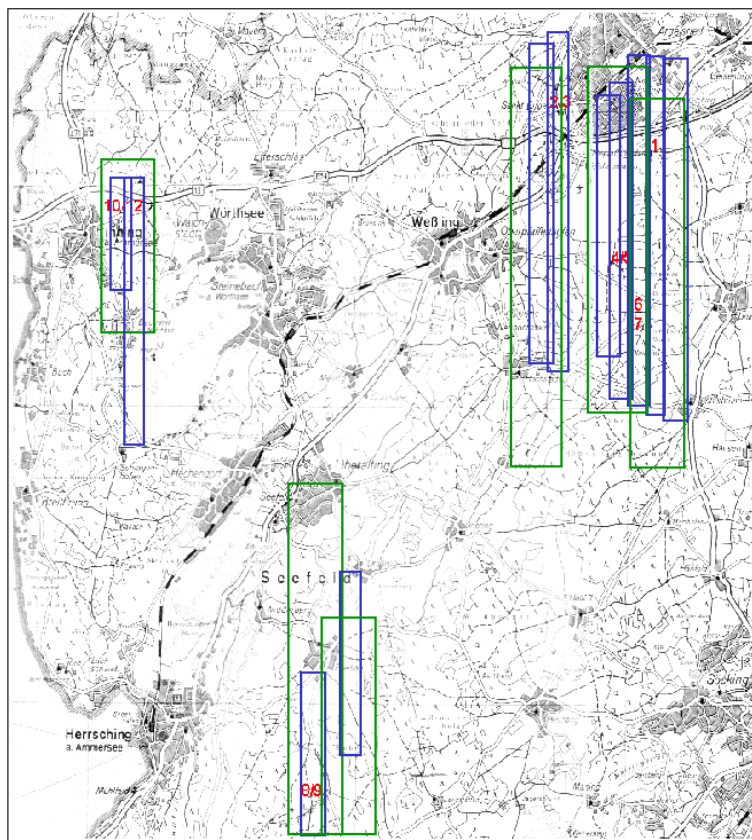


*Figure 4-2:      Flight stripes within the test area on 18<sup>th</sup> July 1999, flown at 4000ft (blue) and 10000ft asl (green); the red numbers represent the position of the test fields*

## *4.2 Data Preprocessing*

During the flight the raw data are stored onto the hard disk of the computer. Afterwards they were transferred to exabyte tapes. The large number of 240 spectral bands, each containing 390 lines with a data depth of 16 bits, leads to a huge amount of data. With an average length of 2000 lines per flight stripe, the resulting amount of data is about 125MBs per stripe. The number of flight lines depends on the chosen altitude and lies between 9 and 18 per overflight. In total, about 35GB of AVIS raw data had to be preprocessed.

The data passed several processing steps before they could be analysed quantitatively. These preprocessing steps are shown in Figure 4-3 and will be described in more detail below.

### 4.2.1 Dark Current and Flat Field Correction

As first processing step the inherent errors of the system must be minimised, which is done by the correction of the dark current as well as the flat field. Thereby the sensor temperature-dependent dark current signal is subtracted from the raw data. During the flat field correction the data is corrected for the individual sensitivity of each pixel in the CCD to derive a homogeneous registration area. Both procedures as well as the corresponding correction equation (2.3) used are already described in section 2.2. Therefore these preprocessing steps will not be discussed in further detail here.

*Figure 4-3: AVIS preprocessing steps*

Dark current correction

Flat field correction

Resampling to 80 bands

Atmospheric correction

Reflectance calibration

### 4.2.2 Resampling to 80 Bands

The original sampling interval of the AVIS spectrograph is 2nm. As the spectral resolution is 6nm (see section 2.3.1), the data is oversampled by the factor 3. Therefore a mean value for three bands can be calculated without any loss of spectral information. The averaging was done assuming a Gaussian-shaped response function represented by different weights for the adjacent bands:

$$DN_{new} = \frac{A_1 \cdot DN_{i-2} + A_2 \cdot DN_{i-1} + A_3 \cdot DN_i + A_4 \cdot DN_{i+1} + A_5 \cdot DN_{i+2}}{\sum A_i}$$

(4.1)

where
$DN$          digital number [DN],

| | |
|---|---|
| *A1* | 0.135, |
| *A2* | 0.606, |
| *A3* | 1.000, |
| *A4* | 0.606, |
| *A5* | 0.135. |

By incrementing *i* by three a total of 80 resampled bands with a nominal bandwidth of 6nm is produced from the original AVIS bands. Advantages of the averaging are the reduction of the amount of data and the number of bands by the factor 3, as well as the resulting increase of the SNR (see also section 2.4) (Oppelt & Mauser, 2000). An example of these effects of the averaging is presented in Figure 4-4 for a vegetation grey value spectrum.
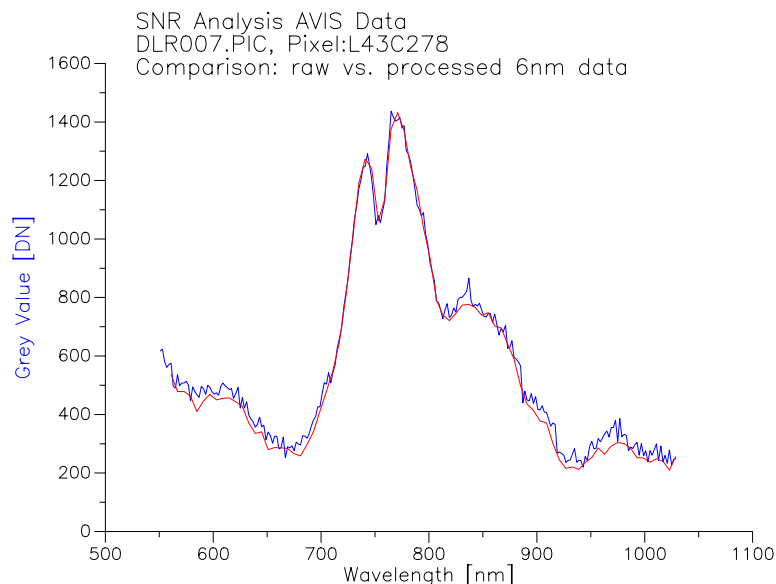


*Figure 4-4:        Effects of averaging for an AVIS grey value spectrum (Oppelt & Mauser, 2000)*

In the course of the first resampling runs, a number of pixels showed shifted spectra, which was particularly conspicuous around the oxygen absorption feature at 761nm. In the AVIS raw data, the position of the absorption changes with increasing column and depends on the observed target as well as the state of the viewed surface, which is shown in Figure 4-5. The position varies most when comparing the measurements of skylight and natural surfaces, but also the comparison of the same area measured at two different dates shows differences.

To correct this shift a wavelength alignment was added to the resampling procedure. An oxygen-fitting algorithm that takes advantage of the changing position of the oxygen absorption feature, which has two minima centred around 761nm, was applied to remove this effect. Six spectral bands, which are located around 761nm, are searched for their absolute minimum, which then is set to the spectral band No. 103.7 (761nm) within the

240 band data. Afterwards follows the resampling procedure as described above, whereas the minimum of the oxygen absorption feature was used to align the spectra of the resulting 80 band data. The graph on the right in Figure 4-5 shows the enhancement due to the oxygen alignment, especially in the range of columns 50 to 340. Although the oxygen waveband scatters, the values lie within the range of one band, namely No.103. In the first and last 50 columns respectively, the position of the oxygen absorption shows higher deviations of up to one/three band(s). These deviations lead to a wavelength shift in the data and therefore must be excluded from the analysis (borders of analysis in Figure 4-5).
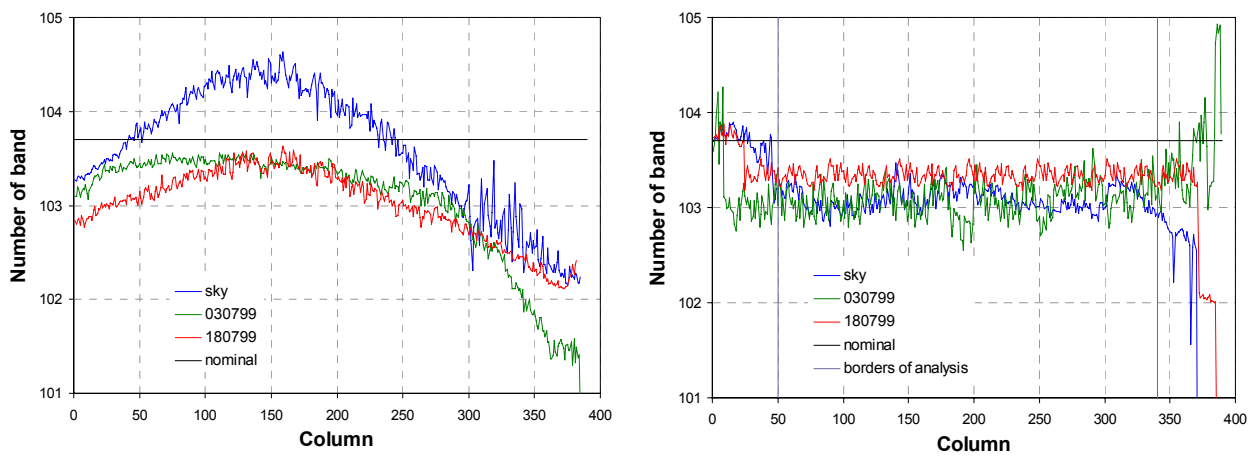


*Figure 4-5:*     *Deviation of the oxygen absorption position from the nominal band No.103.7 (=761nm; left) and corrected wavelength shift after the oxygen alignment (right)*

### 4.2.3     **Atmospheric Correction and Reflectance Calibration**

Surface reflectance retrieval from hyperspectral remote sensing is an important step in the data processing chain leading to the extraction of quantitative information. Atmospheric effects due to scattering by dry air molecules and particulate matter and absorption by air molecules influence the signal, which is received by the sensor.

The scattering component, which is to be removed from the signal, is the path radiance, which is the amount of radiation that is reflected by the atmosphere without any interaction with the ground or surrounding pixels of the observed target on the ground. Scattering by air molecules (Rayleigh scattering) decreases rapidly with wavelength ($\sim\lambda^{-4}$) whereas scattering by particulate matter (Mie scattering) decreases less rapidly (Schanda, 1986).

Absorption of solar radiation by air molecules is a selective process that occurs only at discrete wavelengths. The main molecular absorbers are shown in Figure 4-6. The atmosphere in the Visible is influenced by molecular absorbers such as water vapour, carbon dioxide and oxygen in the Infrared part of the spectrum. The most dominant absorption features associated with water vapour are at 940, 1120, 1400 and 1900nm

(Jacobson, 2000). In the VIS and NIR spectral region, which are of concern in this study (550-850nm), minor water vapour absorption features occur at 720 and 820nm. Other dominant absorbers in this region are $O_2$ and $O_3$. $O_2$ has a major absorption feature centred at 760nm and two minor absorptions at 630 and 690nm. $O_3$ absorbs in the range 450-770nm.
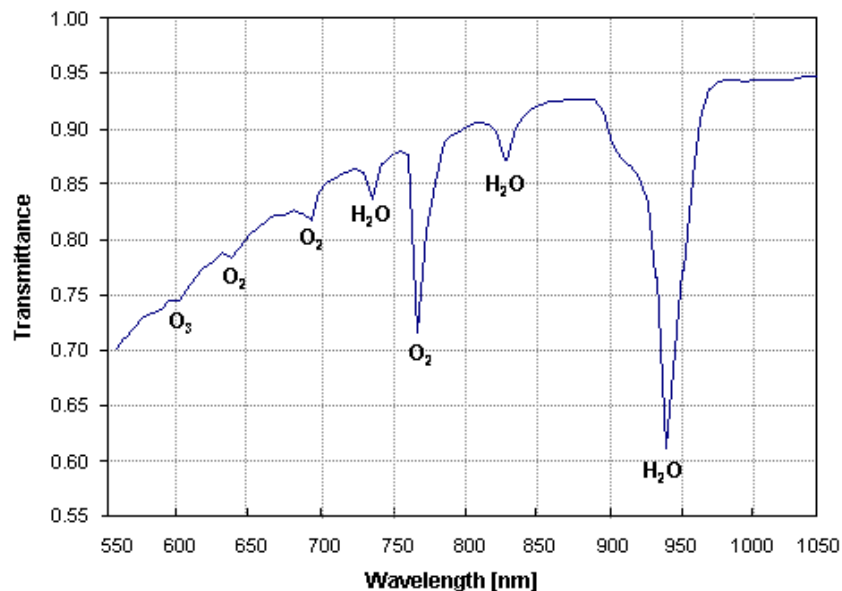


Figure 4-6: *Atmospheric transmittance and main absorbers in the VIS and NIR spectral region, modelled with a spectral resolution of 6nm using LOWTRAN-7*

In order to calculate surface reflectance from remotely measured radiance, radiative transfer codes play an important role in the removal of atmospheric scattering and gaseous absorption effects. Given the high volume and complexity of hyperspectral data, the surface reflectance retrieval results depend strongly on the selected code as well as on the radiometric and spectral calibration of the sensor (Staenz et al., 2000).

For this study the atmospheric correction was carried out using PULREF (Procedure to Use Lowtran for Reflectance Calibration) (Bach, 1995), which is based on the radiative transfer code LOWTRAN-7 (Kneizys et al., 1988). PULREF is made up of a sequence of processing steps (see Figure 4-7), which combines atmospheric modelling and reflectance calibration.

First of all the sensor must be characterised in radiometric and spectral terms. In PULREF this is done by generating a sensor wavelength file as well as a calibration file.

The wavelength file provides detailed data about each spectral band including the central wavelength and the FWHM of each spectral band. This file can be defined after the laboratory calibration and is used to derive the sensor response for each spectral band.

The calibration file basically contains the same data as the wavelength file, but also additional gain values to convert the grey values into radiances. These gain values are not known and thus have to be defined, as described in the next section.
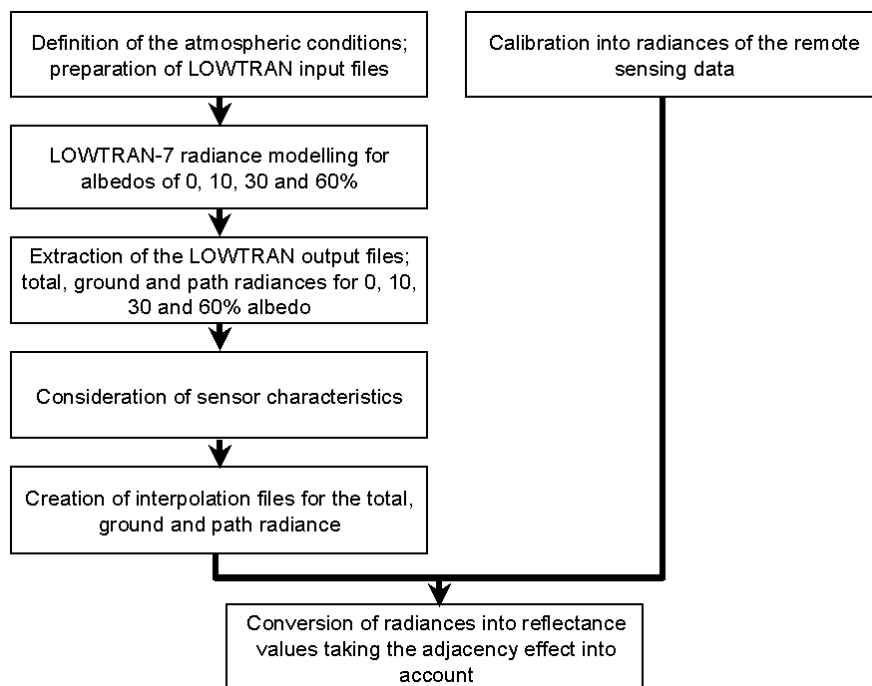
*Figure 4-7:*     *Sequence of PULREF processing steps (Bach, 1995; modified)*

### 4.2.3.1   Calibration into Radiances

This processing step was used for the conversion of grey values into spectral radiances. This is usually done by sensor-specific gain and offset values, which enable the calculation of at-sensor radiances according to the following equation:

$$SR_i = (DN_i - DC_i) \cdot g_i$$

(4.2)

where

$SR_i$          spectral radiance at the sensor for band i [W/m² sr µm],
$DN_i$         grey value for band i [DN],
$DC_i$         offset value for band i [DN],
$g_i$           gain value for band i [W/m² sr µm DN].

For most operational sensors the gain and offset values are published. However, for the new sensor AVIS these values did not exist and therefore had to be derived.

The offset value is equivalent to the dark current, which was already considered during preprocessing. Therefore the offset value did not have to be corrected here.

The gain value was derived as follows:
1.   Definition of a calibration file with the gain value set to 0.
2.   LOWTRAN-7 modelling of at sensor radiances of the DLR hangar reflectance spectrum using the calibration file, which includes the zero gain values (Figure 4-8).

3. Derivation of the gain values by division of the modelled radiance by the measured grey value for each band (Figure 4-8).

4. Replacement of the blank values by the derived gain values in the calibration file.

5. Iterative improvement of the gain values by repeating of steps 3 and 4.
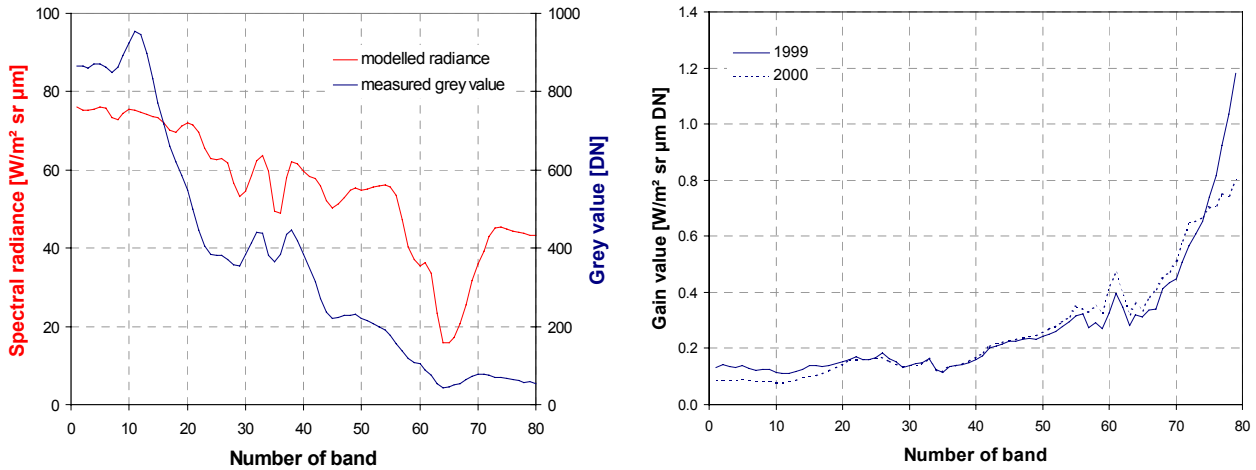


Figure 4-8:    Modelled spectral radiances and measured grey values of the DLR hangar for the 18th July 1999 (left) and gain values for 1999 and 2000 (right) for a spectral resolution of 6nm

The calibration file must be generated each time the sensor features change. For this study the procedure was carried out each year before the measurement period. In 1999 a second derivation was necessary because in May it turned out that the AVIS data, that had already been gathered, were not focussed. Therefore the system had to be refocused and the gain values had to be derived again. Figure 4-8 shows the gain values for 1999 and 2000. The comparison of the two curves shows a similar trend. The gain values above band No.70 (980nm) increase steeply, which is due to the limited transmission of the lens and the limited sensitivity of the CCD in this wavelength region (see section 2).

### 4.2.3.2    Definition of Atmospheric Conditions

Knowledge about the state of the atmosphere during the AVIS measurements is important for its precise modelling. The data needed for the parameterisation of atmospheric conditions are derived from radiosonde profiles measured by the *Deutschen Wetterdienst* (DWD) at the monitoring station Oberschleissheim, which is located about 30km north of the test area. DWD radiosonde takeoffs are carried out twice to four times a day at several monitoring stations and provide the range of vision on ground and data about air temperature, dew point temperature, relative humidity and atmospheric pressure measured at different altitudes during the ascent. These measurements serve as input parameters to LOWTRAN and provide a more accurate modelling of the atmosphere than by using one of the standard atmospheres.

### 4.2.3.3 Atmospheric Modelling with LOWTRAN-7

Based on the atmospheric input data as well as the geographical coordinates, the date, time and observation altitude, the at-sensor radiances are calculated for the 500–1000nm wavelength region using LOWTRAN-7. Calculations are conducted assuming four different ground albedo values (0, 10, 30 and 60%) (Bach, 1995).

The results for the four albedos include the ground, path and total radiances. The ground radiance is defined as the part of the radiance reaching the sensor, which is reflected by the observed target on the ground (see left graph in Figure 4-9). The path radiance is the amount of radiation that is reflected to the sensor by the atmosphere without any interaction with the ground or by the surrounding pixels of the viewed target (see right graph in Figure 4-9). The total radiance is the sum of the path and ground radiances and represents the radiance that is measured by the sensor viewing a target on the ground.
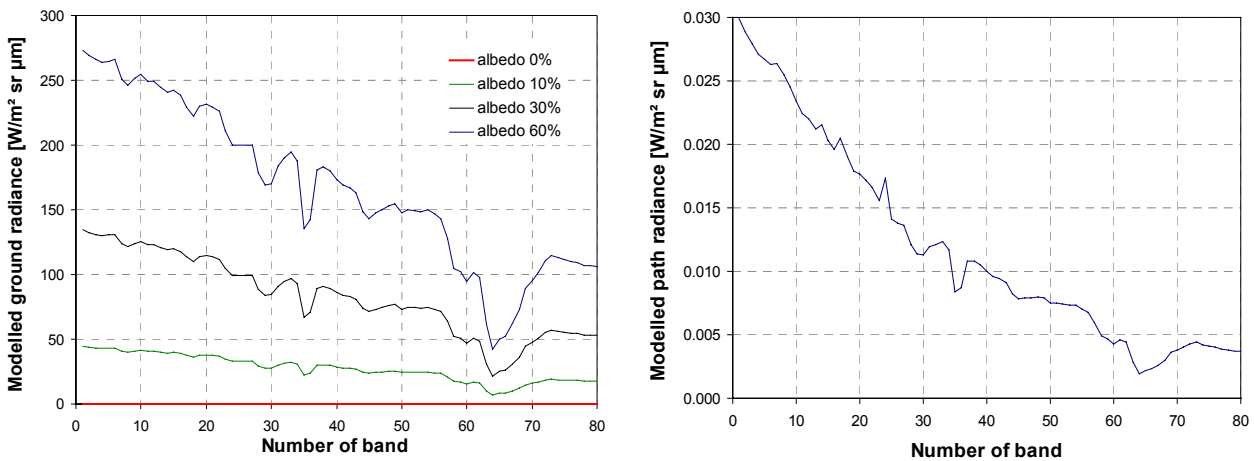


Figure 4-9: *Modelled ground (left) and path (right) radiance using LOWTRAN-7 for the 18th July 1999 with a spectral resolution of 6nm*

### 4.2.3.4 Consideration of the Sensor Characteristics

As mentioned above, the spectral characteristics of the sensor are stored in the wavelength file. This wavelength file is now convoluted with the modelled radiance spectra. The results are spectral radiances of ground albedos of 0, 10, 30 and 60%, received in the manner, which is characteristic for the specific sensor. Figure 4-10 shows an example for the total at-sensor radiance of the DLR hangar calculated for the 18th July 1999 using the AVIS sensor characteristics. The oxygen absorption and the water absorption features positioned at band No.35 (760nm) and 64 (938nm) respectively, are conspicuous features in the radiance spectra.
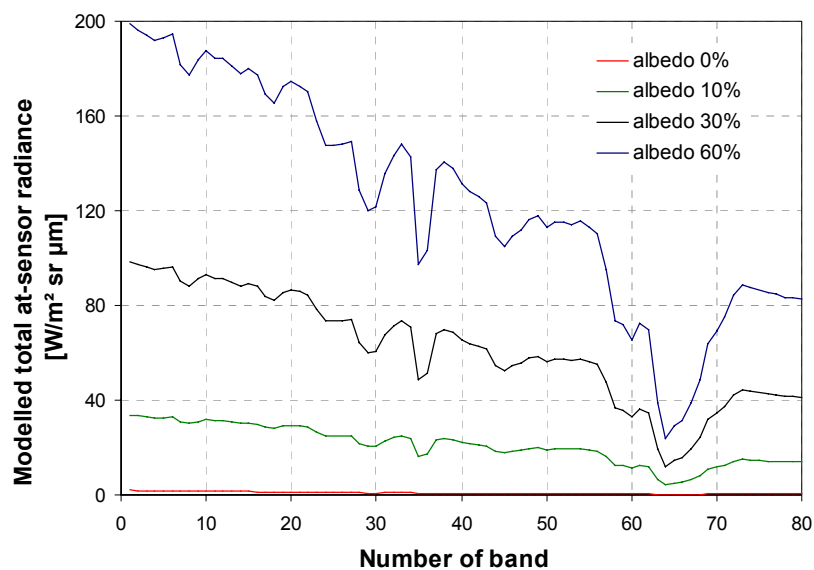
*Figure 4-10:    Modelled total at-sensor radiance using LOWTRAN-7 for the 18th July 2000 with a spectral resolution of 6nm*

### 4.2.3.5    Reflectance Calibration

The four albedo pylons are the basis for the reflectance calibration with PULREF. LOWTRAN is inverted and the spectral reflectance for each band is calculated by the linear interpolation of the measured radiance between the four pivots at 0, 10, 30 and 60% albedo. The reflectance calibration included the consideration of the adjacency effect by the derivation of a weighting function, which describes the relative contribution of surface points at a predefined distance to the observed pixel (Bach, 1995).

## 4.2.4    Validation of the Preprocessed Data

The preprocessing sequence provides atmospherically corrected spectral ground reflectance data. This enables the quantitative analysis as well as the comparison with reflectance data derived at different flight dates, because the signal contains only the part of the information which is directly related to the observed pixel on-ground and is not influenced by the atmosphere, sensor characteristics or by radiation of pixels surrounding it.

During preprocessing it turned out that the reflectance spectra of the unfocussed data showed an insufficient quality for parameter derivation. Therefore the AVIS data measured on 29th and 30th April as well as on 25th May could not be included in analysis.

The results of the preprocessing must be validated for their quality. This was done using measurements of a ground based spectrometer, in this case GER SIRIS (see section 3.4.4.2), which were carried out nearly simultaneously to the image acquisition with AVIS, namely on 3rd and 18th July 1999. The results will be discussed in the following sections.

## 4.2.4.1    1999

For 1999 the preprocessed image data show a high consistency in the VIS region, but in the NIR region the spectra show increasing variations towards longer wavelengths. The problems, which occurred, will be described on the basis of a typical example provided in Figure 4-11.

The graph on the left shows reflectance spectra of five individual pixels spread over a maize field. The course of the curves is very similar until 740nm. The NIR plateau up to 850nm is also characterised by a similar trend of the curves, but with higher variations than in the VIS. The maximum amplitude of these variations reaches 5% reflectance. In contrast to the variations, the different level of the curves at the NIR plateau is a common phenomenon. The reflectance in the NIR region is dependent on the leaf structure of the plants (Gausman, 1974), which may vary within a canopy, or their leaf angle (Price, 1994) as well as on variations in the viewing geometry such as the view angle (Kennedy et al., 1997), the multiple scattering or shadowing effects in the canopy (Kuusk, 1991). Price (1994) measured NIR reflectances in the range of 29 to 43% during a sequence of measurements within a maize canopy. The variability of spectra is described more detailed in section 5.3. The differences in the overall reflectance level of the AVIS single spectra are most probably due to the spectral variability of a maize canopy and cannot be ascribed to the preprocessing.
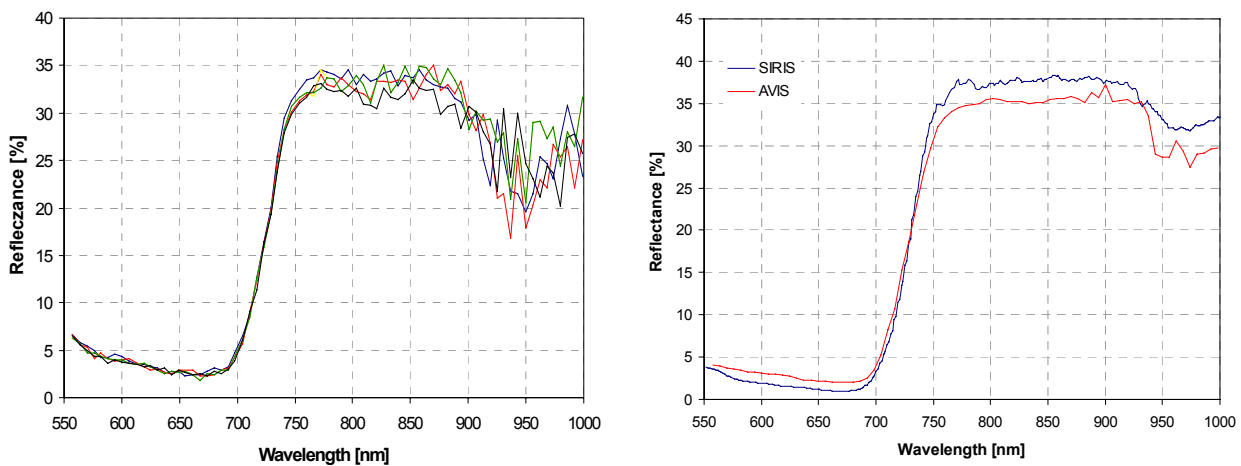


Figure 4-11:    *AVIS reflectance spectra for 1999 for individual pixels (left) and field average (right), measured at field No. 52 on 18th July 1999; altitude: 4000ft asl*

The variations between two bands in the 850–1000nm wavelength region are in the magnitude of 10% reflectance. These variations are too high for a quantitative or even qualitative analysis of the single reflectance spectra. Figure 4-11 also shows that the variations are not systematically, but appear to be random. This is confirmed when looking at the average field spectrum, which is shown in the right graph in Figure 4-11, where most of the variations are averaged. These facts led to the conclusion that the variations

are noise. The SNR of the system decreases steeply from a value of 65 at 760nm towards the longer wavelengths (see section 2.4). At 850nm the SNR is about 30 and decreases further to 20 at 1000nm. The signal in the 850–1000nm wavelength region is strongly influenced by system noise, and therefore at least the single spectra cannot be analysed in that wavelength range. The quality of the averaged spectra depends strongly on the number of pixels that are included in the averaging. This number of pixels varies with the field size and the flight altitude. Both the size of the fields being investigated and the observation altitude differ, but should be comparable within the analysis. Therefore the averaged spectra were also discarded for wavelengths above 850nm.

The comparison of the averaged AVIS field spectrum with the SIRIS spectrum (Figure 4-11) shows good results considering the fact, that point measurements are compared with two-dimensional measurements. The differences in the NIR are of the magnitude 3.5% reflectance, in the VIS they range from 1 to 1.4%. In the region of maximum chlorophyll absorption at 680nm the SIRIS measured 1.1% reflectance while AVIS measured 2.1%.

## 4.2.4.2   2000
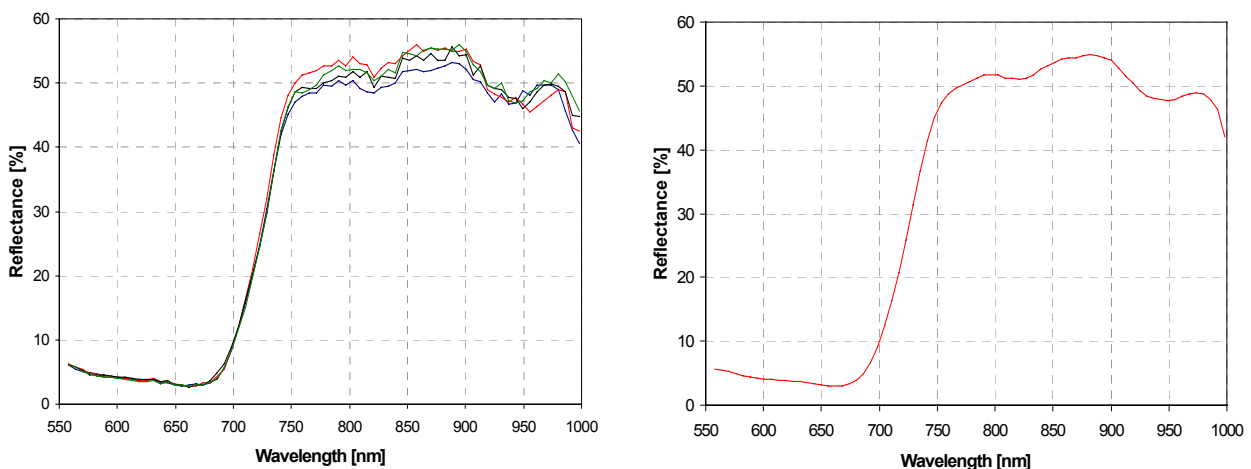


Figure 4-12:     AVIS reflectance spectra for 2000 for individual pixels (left) and mean field spectrum (right), measured at field No. 146a on 22$^{nd}$ July 2000; altitude: 4000ft asl

The results of preprocessing for the year 2000 will also be discussed on the basis of an example, which is shown in Figure 4-12. The acquisition date of the measurements is the 22$^{nd}$ July. Compared to the 1999 data, the individual pixel spectra, which are spread over a field of wheat, show a great improvement, especially in the NIR. The course of the curve is smooth up to 900nm with variations of at most 4% reflectance. The water absorption feature at 940nm can be reconstructed, but in this wavelength region the variations increase up to 8% reflectance. The reflectance values beyond 980nm drop down both in the individual pixel spectra and the averaged field spectrum. The comparison of reflectance spectra of different land use types and other acquisition dates confirmed this

observation. The reason for this artefact is most probably the decrease in system sensitivity combined with the decreased SNR that cannot be compensated during preprocessing. The 2000 data are analysed in combination with those of 1999, therefore the reflectances beyond 850nm will not be included in the further analysis.

For 2000 no field spectrometer data are available for validation. The mean field spectrum of the maize canopy therefore cannot be validated with ground-based measurements, except with the DLR hangar spectrum. This spectrum is used as a calibration target during preprocessing, thus it cannot be used as a validation target.

## 4.2.5    Directional effects

Directional effects are a function of many factors, such as the sensor view-angle, altitude, the angle between sun azimuth and sensor scan plane as well as the scatter patterning of land use types (Kennedy et al., 1997; Roberts et al., 1997).

Sensors with a large FOV are characterised by a changing view angle for every pixel in a line. The view angle increases the quantity of atmosphere through which the sensor views, which can increase the path radiance and, consequently, the overall brightness (Royer et al., 1985; Irons et al., 1987). Each change in view angle also alters the sun-sensor-object geometry of the observed surface objects. This effect is influenced by the bi-directional reflectance distribution function (BRDF, see section 5.4.1.4) of surface and atmosphere. For a given wavelength and surface type, BRDF can cause either increased or decreased observed radiance at higher view angles, depending on sun-sensor-object geometry. Cross track brightness gradients are considered to be a combination of these two view angle dependent effects (Royer et al., 1985; Roberts et al., 1997). Kennedy et al. (1997) identified the BRDF as the primary determinant of view angle effects in AVIRIS data. Currently the correction of this effect is not possible.

Most of the above studies dealt with satellite or high altitude airborne measurements where cross track brightness gradients in the AVIS data are not visible to the naked eye, when slight differences are difficult to obtain in the highly heterogeneous landscape of the test area. Therefore the AVIS data must be searched for occurring brightness gradients.

Influences, which depend on the sun azimuth and the altitude, are normally minimised by the atmospheric correction. Both parameters are included in the atmospheric correction leading to at-sensor radiance. The quality of the correction largely depends on the quality of the input parameters. The comparison of reflectances measured at different altitudes during one overflight is one possibility for examining this influence. Therefore the reflectances of AVIS measurements were compared for the maize canopies on 19th and 31st July 1999, where two altitudes were flown at almost the same daytime to provide similar sun elevation.

Table 4-1:   Differences of maize reflectances due to different altitudes for two AVIS measurement dates
(sun elevation is calculated for sea level at 47°57′N 11°17′E)

| Date | Aquisition time [CET] | Sun elevation [°] | Deviation [% reflectance] | 4000ft asl | 4000 - 10000ft asl |
|------|------------------------|--------------------|----------------------------|-------------|---------------------|
| 19th July 1999 | 10:30-11:45 | ca. 54.9-61.9 | Mean | 0.79 | 1.39 |
| | | | Maximum | 2.94 | 5.78 |
| 31st July 1999 | 10:00-11:30 | ca. 48.8-58.6 | Mean | 1.51 | 3.35 |
| | | | Maximum | 5.73 | 6.99 |
| Total | | | Mean | 1.15 | 2.72 |
| | | | Maximum | 5.73 | 6.99 |

Table 4-1 presents the deviations for all maize fields that were covered on these two dates. Figure 4-13 shows one example of spectra flown on the 19th July. Figure 4-13 also illustrates that the differences between the two altitudes are wavelength dependent. The maximum difference between the spectra flown at 4000ft is 5.73% reflectance whereas the difference between 4000 and 1000ft spectra is 6.99% indicating that the maximum difference between the two altitudes is 1.26% reflection. The mean difference is 1.15% reflection for spectra derived at the same altitude and 2.72% for different flight levels. This small difference allows the comparison of spectra derived at the two altitudes, whereas the differences may also be due to the BRDF of the vegetation.
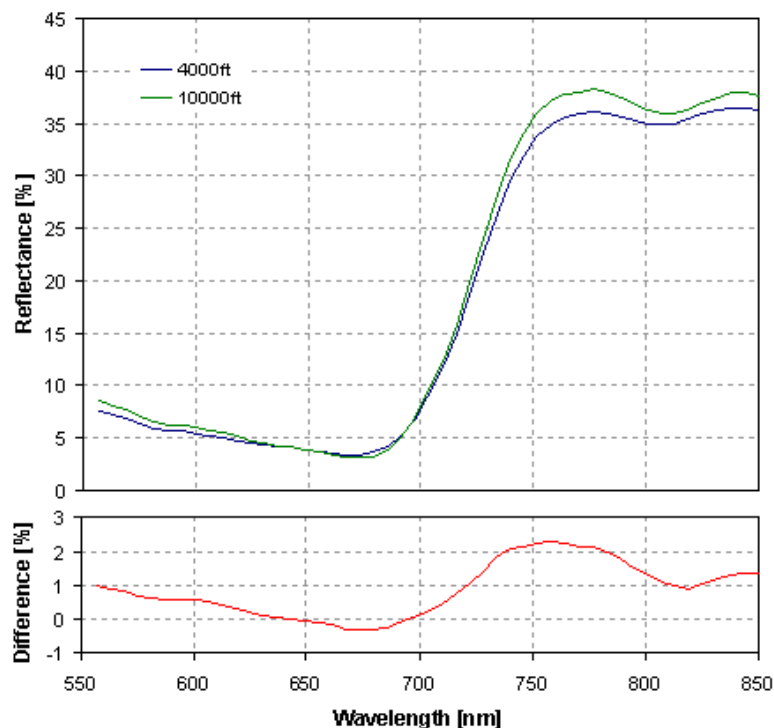


Figure 4-13:   Field average spectra of maize field No.260 at 4000 and 1000ft asl, flown on 19th July 1999 (upper graph) and differences between the two spectra (lower graph)

The course of the difference spectrum is similar to vegetation indicating an incompletely correction of the adjacency effect. The adjacency effect depends on the altitude flown due to scattering in the atmosphere and a different IFOV. The spectra of a target acquired in an altitude of 1000ft resulting in a small IFOV, are more affected by a superimposition of adjacent targets than a 4000ft spectrum with larger pixel spacing. When the adjacency effect is not completely eliminated for the 10000ft flight level a vegetation-shaped difference spectrum remains after subtracting.

A simple approach for the investigation of brightness gradients occurring across track, which are due to the large FOV of the sensor, is the comparison of reflectance spectra of the highway, which crosses the N-S oriented flight stripes transversally. The left graph in Figure 4-14 shows a sequence of highway spectra within one AVIS scene recorded on 9th May 2000 and shows the difficulty in obtaining isolated asphalt spectra, which is mainly due to the perturbing effect of the centre strip of the highway. Therefore some of the spectra show slight signs of a red edge between 700 and 740nm as well as water absorption at 820nm. This also accounts for the higher deviation from the mean value in the NIR, which is shown in the right graph of Figure 4-14. The mean deviation ranges between 0.6 and 1.18% reflectance in the NIR, while in the VIS the values are located between 0.2 and 0.8%. On the 9th May, the maximum deviation from the mean reflectance is 1.4% while the value for the comparison of the three acquisition dates ranges at 2.6%. This result indicates that no radiometric distortion due to the FOV of the sensor occurs.
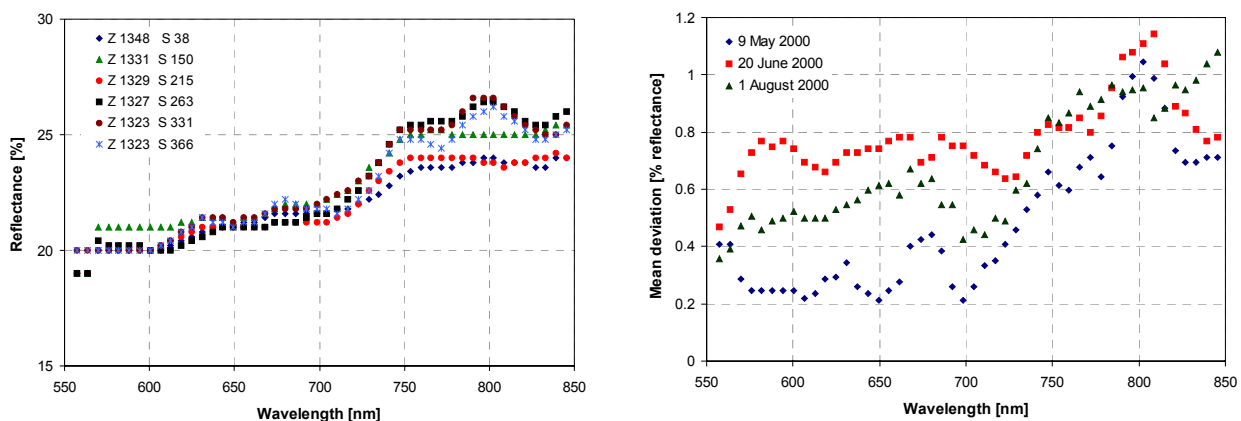


Figure 4-14:    Mean highway spectra from 9th May 1999 (left; position of the pixel in Z=row; S=column) and comparison of different acquisition dates (right)

### 4.2.6    Results of the Preprocessing

Figure 4-15 provides the preprocessing results on the basis of an example acquired on 22nd July 2000. The image shows the DLR terrain near the highway A96 Munich–Lindau, which passes through the upper part of the image. The left image represents a false

colour composite of the 240 band AVIS grey value raw data, while the right image shows the equivalent bands of the 80 band preprocessed reflectance data
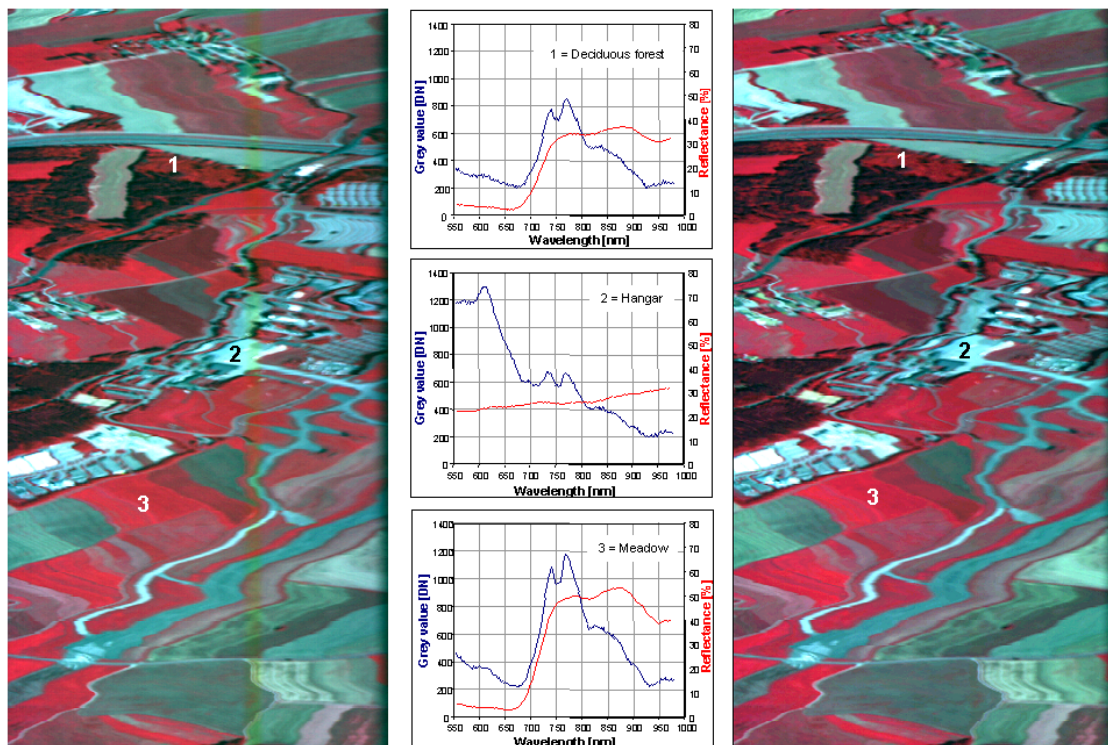


Figure 4-15:    AVIS raw data image (left) and processed image (right) (R/G/B = 582/674/729nm) with associated grey value (blue) and reflectance (red) spectra of different land cover types, acquired on 19$^{th}$ July 1999

A conspicuous feature in the raw data sequence is the yellowish stripe along track. This is a feature that is also visible in the flat field file (Figure 2-12), and locates an area of reduced sensitivity on the sensor CCD. The vignetting effect, which occurs especially on the right margin of the flight stripe, is already described in section 2.2.2. The stripe is minimised in the preprocessed image during the flat field correction, while the light falloff could not be completely corrected. This is the part of the image, which is already excluded from the analysis because of the poor results during oxygen alignment. The preprocessed image also seems darker coloured. The faded colours of the raw image are due to the atmosphere between surface and sensor, which is also removed in the processed image.

The AVIS campaigns provide a bulk of radiometric measurements of the test fields. These measurements enable the comprehension of the plant development throughout the vegetation period as well as the differences between the investigated species. The reflectance spectra resulting from preprocessing are presented in the following for the different land covers in 1999. The reason for discussing the 1999 data lies in the longer measurement period within this year.

### 4.2.6.1    Wheat

During each AVIS overflight 1999 and 2000 the test field were covered at least once. Each coverage provides a mean field reflectance spectrum for the given date. In total, 134 spectra are therefore available for the analysis of the wheat data. Table 4-2 provides the coverage of the test fields.

*Table 4-2:    Coverage of wheat test fields during the flight campaigns 1999 and 2000*

| AVIS overpasses 1999 | Wheat No. 65a | | Wheat No. 93 | | Wheat No. 256 | |
|---|---|---|---|---|---|---|
| Altitude [ft asl] | 4000 | 10000 | 4000 | 10000 | 4000 | 10000 |
| 28th May (DOY 148) | - | - | 1 | 1 | 1 | 1 |
| 3rd July (DOY 184) | - | 3 | - | 2 | - | 2 |
| 5th July (DOY 186) | 3 | - | 3 | - | 1 | - |
| 18th July (DOY 199) | 1 | - | 1 | - | 1 | - |
| 19th July (DOY 200) | 2 | 1 | 3 | 2 | 1 | 1 |
| 28th July (DOY 209) | 2 | - | 2 | - | 1 | - |
| 31st July (DOY 212) | 1 | 1 | - | - | 1 | 1 |

| AVIS overpasses 2000 | Wheat No. 52 | Wheat No. 84 | Wheat No. 92 | Wheat No. 149a | Wheat No. 400 | Wheat No. 401 |
|---|---|---|---|---|---|---|
| 3rd May (DOY 124) | 1 | 1 | 3 | 2 | 1 | 1 |
| 9th May (DOY 130) | 2 | 3 | 3 | - | 2 | 2 |
| 15th May (DOY 136) | 3 | 2 | 4 | 2 | 1 | 1 |
| 2nd June (DOY 154) | 2 | 4 | 3 | 2 | 2 | 2 |
| 10th June (DOY 162) | 2 | 2 | 3 | 2 | 3 | 3 |
| 20th June (DAS 172) | 2 | 3 | 3 | 2 | 2 | 2 |
| 22nd July (DAS 204) | 1 | 1 | 1 | 1 | 2 | 2 |
| 1st Aug. (DOY 214) | 1 | 3 | 2 | 2 | - | - |

The development of wheat during the vegetation period is discussed on the basis of the averaged field spectra of field No.93 in 1999, which is presented in Figure 4-16. The spectral behaviour of the wheat canopy during its development is marked by a conspicuous change, especially in the NIR. The first measurement took place during stem elongation, when chlorophyll content is high and therefore the chlorophyll absorption is distinct. During the later measurements the chlorophyll content decreases and the reflectance in the VIS is doubled from stem elongation until dough development. In the NIR region the reflectance rises during stem elongation until anthesis and decreases during maturity to a level of a soil spectrum.

This development is caused by the chlorophyll of the plants, further explanations see section 5.1.
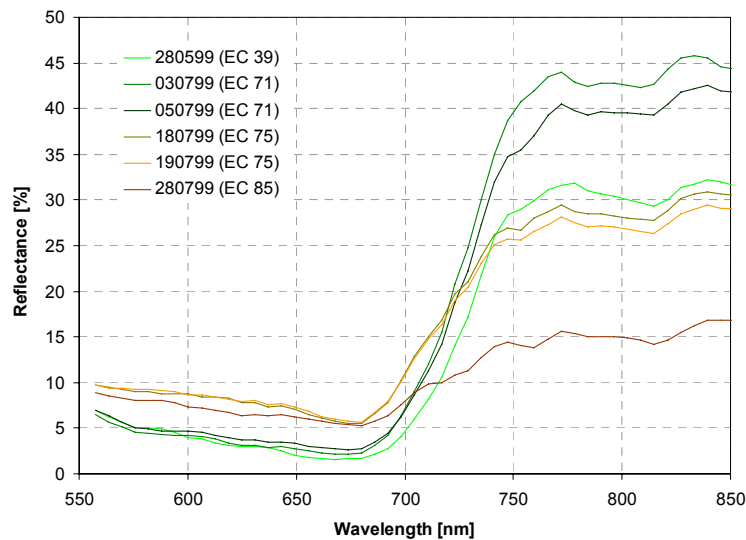


*Figure 4-16:*     *Development of a wheat canopy (field No.93) throughout the vegetation period 1999*

### 4.2.6.2    Maize

During the measurement periods the investigated maize fields were covered 75 times in total. A survey of the data acquisition and therefore of the number of reflectance spectra which were used in this study is presented in Table 4-3.
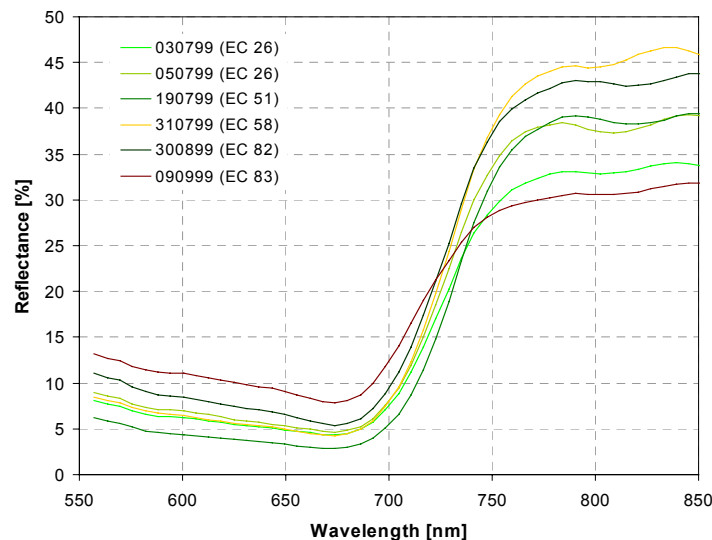


*Figure 4-17:*     *Development of a maize canopy (field No.65a) throughout the vegetation period 1999*

Figure 4-17 shows the spectral development of maize during the growing season of 1999 on the basis of one test field, namely No.65a. In contrast to wheat, the AVIS measurements can reproduce the whole developmental cycle from tillering to senescence.

During tillering and stem elongation, when the maize plants are growing fast and a lot of biomass is built up, the reflectance in the red wavelength region decreases. This is caused by the increasing absorption by chlorophyll, which is now accumulated in the plants. After anthesis the chlorophyll begins to degrade and so the reflectance in the VIS increases. The NIR reflectance shows the same behaviour as with wheat, i.e. an increase until anthesis and a decrease after flowering. These radiometric measurements are in good qualitative accordance to the chlorophyll content per area measured on the ground (see section 3.4.2).

Table 4-3:   Coverage of maize test fields during the flight campaigns 1999 and 2000

| AVIS overpasses 1999 | Maize No.52 | | Maize No. 65a | | Maize No.260 | |
|---|---|---|---|---|---|---|
| Altitude [ft asl] | 4000 | 10000 | 4000 | 10000 | 4000 | 10000 |
| 3rd July (DOY 184) | - | 2 | - | - | - | 1 |
| 5th July (DOY 186) | 1 | - | 3 | - | 1 | - |
| 18th July (DOY 199) | 2 | - | 2 | - | 1 | - |
| 19th July (DOY 200) | 3 | 2 | 1 | 1 | 1 | 1 |
| 28th July (DOY 209) | 2 | - | 2 | - | 1 | - |
| 31st July (DOY 212) | 2 | 1 | 2 | 1 | 1 | 1 |
| 30th Aug. (DOY 243) | 1 | - | 2 | - | 1 | - |
| 9th Sept. (DOY 252) | 1 | - | 2 | - | 1 | - |
| AVIS overpasses 2000 | Maize No.149 | | Maize No. 226a | | Maize No.227 | |
| 2nd June (DOY 154) | 2 | | 1 | | 1 | |
| 10th June (DOY 162) | 1 | | 2 | | 2 | |
| 20th June (DAS 172) | 1 | | 1 | | 1 | |
| 22nd July DAS 204) | 2 | | 2 | | 2 | |
| 1st August (DOY 214) | 1 | | 2 | | 2 | |
| 11th August (DOY 224) | 1 | | - | | - | |

### 4.2.6.3   Grassland

The grassland fields were covered 91 times during the AVIS campaigns. The dates, altitudes and number of coverages are provided in Table 4-4.

The development of a representative grassland canopy (No.106a), which is derived from AVIS measurements in 1999, is described in Figure 4-18. It shows the extensive meadow with one cut. At the end of May the meadow is vital, which can be seen from the strong chlorophyll absorption, leading to a low reflectance in the red wavelengths. The meadow was cut at the end of June, so the soil and litter mainly influence the measurement of 5th July. The chlorophyll absorption feature deteriorates and the red edge is flattened. The

increase of reflectance in the green region is due to the influence of the soil, which is visible in a freshly cut meadow.

Table 4-4:    Coverage of test meadows during the flight campaigns 1999 and 2000

| AVIS overpasses 1999 | Meadow No. 106a | | Meadow No. 53a | | Meadow No. 223 | | Meadow No. 224 | |
|---|---|---|---|---|---|---|---|---|
| Altitude [ft asl] | 4000 | 10000 | 4000 | 10000 | 4000 | 10000 | 4000 | 10000 |
| 28th May (DOY 148) | 2 | - | 1 | - | 1 | - | 1 | - |
| 3rd July(DOY 184) | - | 1 | - | 2 | - | - | - | - |
| 5th July (DOY 186) | 1 | - | 2 | - | 1 | - | 1 | - |
| 18th July (DOY 199) | 1 | - | 2 | - | 1 | - | 1 | - |
| 19th July (DOY 200) | 1 | 1 | 2 | 1 | 1 | 1 | 1 | 1 |
| 28th July (DOY 209) | 1 | - | 2 | - | 1 | - | 1 | - |
| 31st July (DOY 212) | 1 | - | 2 | 1 | 1 | 1 | 1 | 1 |
| 30th Aug. (DOY 243) | 1 | - | 1 | - | - | - | - | - |
| 9th Sept. (DOY 252) | 1 | - | 1 | - | 1 | - | 1 | - |

| AVIS overpasses 2000 | Meadow No. 106a | Meadow No. 53a | Meadow No. 223 | Meadow No. 224 |
|---|---|---|---|---|
| 3rd May (DOY 124) | 1 | 1 | - | - |
| 9th May (DOY 130) | - | 2 | - | - |
| 15th May (DOY 136) | 2 | 3 | 2 | 2 |
| 2nd June (DOY 154) | 2 | 2 | 2 | 2 |
| 10th June (DOY 162) | 1 | 2 | 1 | 1 |
| 20th June (DAS 172) | 2 | 2 | 2 | 2 |
| 22nd July DAS 204) | 1 | 1 | 1 | 1 |
| 1st August (DOY 214) | 1 | 2 | 1 | 1 |
| 11th August (DOY 224) | 1 | 1 | - | - |

This observation is in accordance with Asner (1998), who found a decrease in the pigment absorption features at 450 and 680nm as the litter content on a grass canopy increases. The plants of the viewed meadow revegetate and two weeks later the canopy shows a typical vegetation spectrum, but the chlorophyll content as well as the biomass is still on a lower level compared to the first measurement. The former is visible in the higher reflectance in the red while the latter can be seen by the lesser NIR reflectance. The meadow continues to grow until September, when the plants still contain chlorophyll but the withering of the biomass leads to a increase of reflectance in the NIR. Conspicuous are the high reflectance values of the meadow in the NIR compared to those of wheat and maize. Comparisons with the other meadows show the same phenomenon, i.e. reflectances in the NIR vary between 60 and 70% when the meadows are not mown or grazed. This may be caused by the high density of the vegetation, which leads to a high

leaf area. The leaf area has a significant influence on canopy reflectance: the larger the Leaf area Index (LAI) the higher the reflectance especially within the NIR spectral region (Asner, 1998) (see also section 5.4.1.1). This may be combined with the increase of NIR reflectance, which is due to the development of the leaves, as well as with the occurrence of dead plant material and litter within the canopy. On a meadow, individual plants mature and die while new plant material is produced at the same time. But even small increases in the percentage of litter lead to disproportionately large changes in canopy reflectance (van Leeuwen & Huete, 1996; Asner, 1998).
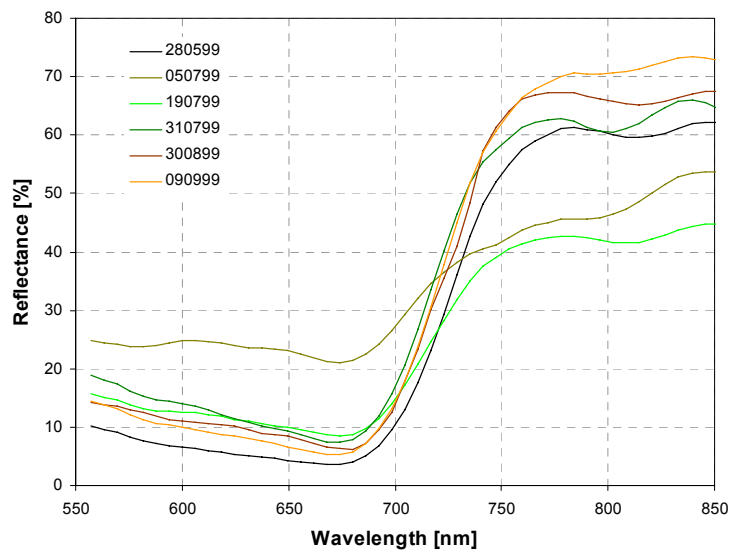


*Figure 4-18:      Development of a meadow with one cut (No. 106a) during the vegetation period 1999*

## 4.3 Geometric Rectification

For the radiometric examination of the data, geometric rectification is not mandatory but helpful for the orientation within the image as well as for the presentation of the data.

Sources of geometric distortions of particular concern to airborne sensor data are related to an unstable platform, low acquisition altitude and large FOV causing changes in pixel size as well as pixel displacements.

Low altitude acquisition combined with the large FOV causes pixels in the nadir line to be smaller than pixels on the edges of the swath due to the panoramic effect (equation (4.3), Richards, 1998):

$$p_0 = \beta \cdot h \cdot \sec^2 \cdot \theta = p \cdot \sec^2 \cdot \theta \tag{4.3}$$

where
$p_0$          across-track pixel size [m],
$\theta$          scan angle [°],
$\beta$          instantaneous field of view (IFOV) [rad],
$h$          altitude above ground [m],
$p$           pixel size at nadir [m].

The largest AVIS view angle is 34° (FOV/2), which results in $p_0$=1.45. This indicates that the geometric distortion at the edge of the swath due to the panoramic effect is 45%. The altitude is given with 600 and 1200m above ground (which corresponds to 4000 and 10000ft asl). This caused the nadir pixel size of 1.86 and 3.72m to increase to 2.49 and 5.39m respectively.

The displacement of pixels is further influenced by variations in platform velocity, altitude and attitude due to factors such as atmospheric turbulence. An increase in altitude will change the geometry of the pixel as illustrated in Figure 4-19a. Variation in velocity changes the along-track pixel size (Figure 4-19b), attitude variation in the form of roll, pitch and yaw results in along track displacement, across-track displacement and scan line rotation (Figure 4-19c, d, e).

Because of their small frames, fast frame acquisition times, low altitude and narrow swath width, airborne sensors do not cause problems in connection with earth rotation and earth curvature as do satellite based sensors.

The aircraft motions can be fully retrieved by using a dGPS and an inertial navigation system. The former provides the geographical position, velocity and altitude and the latter the roll, pitch and yaw.
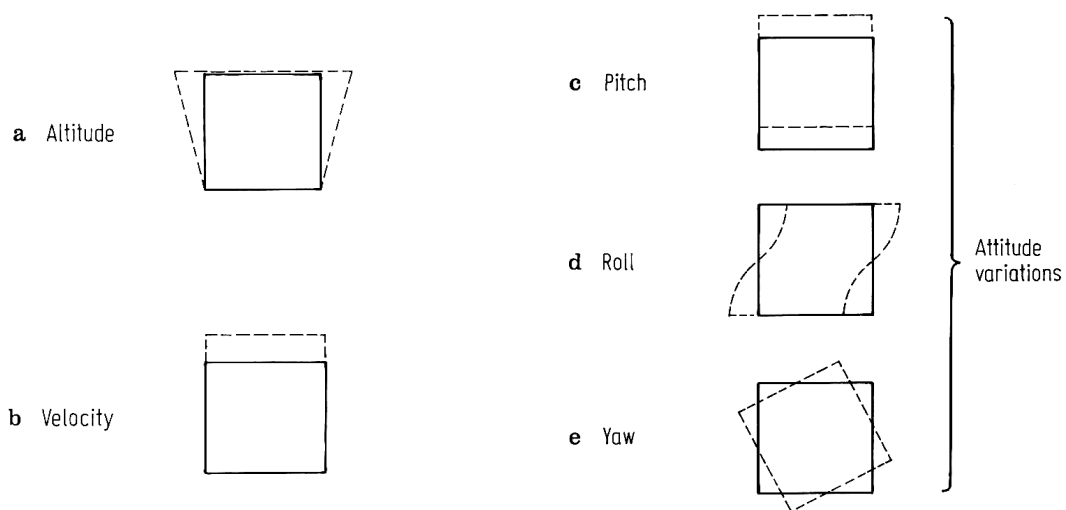
*Figure 4-19:*     *Image distortions due to altitude (a), velocity (b), pitch (c), roll (d) and yaw (e) (Richards, 1998)*

At the time of this thesis only dGPS data were available for the geometric correction of the AVIS data. Therefore the geographical position and major variations of the flight path could be corrected. Figure 4-20 shows an example of the kind of geometric correction that is possible with the available dGPS data. The selection of bands corresponds to a false colour composite. The image capture during flight is adapted to a specific velocity of the aircraft, namely 180km/h, but the real velocity lies between 180 and 195km/h. Therefore the actual along track pixel spacing is different from the nominal across-track pixel size and varies in flight direction. Thus the surface looks compressed in along-track direction. The angular motion of the aircraft is clearly visible at roads and borders between fields.

The dGPS data provide information about geographical position, altitude and velocity of the aircraft (Figure 4-20 centre). The former enables the alignment to north while the latter are used to calculate square pixels. The dGPS data are stored in the header of each image line and enable the correction of each pixel within that line.

The geometrically corrected image stripe is aligned to geographic north and has a square pixel spacing, which is consistent over the whole image. In this case the resulting pixel spacing is 3x3m.The angular aircraft motion could not be corrected and is still noticeable.

The remaining distortions in the flight stripes can only be corrected with the aircraft angular motion data and a topographic map. This distortion correction by ground points is very time-consuming and was carried out for just a few flight stripes. The results can be combined to form a mosaic, which is shown in Figure 4-21 for the test site Gilching.
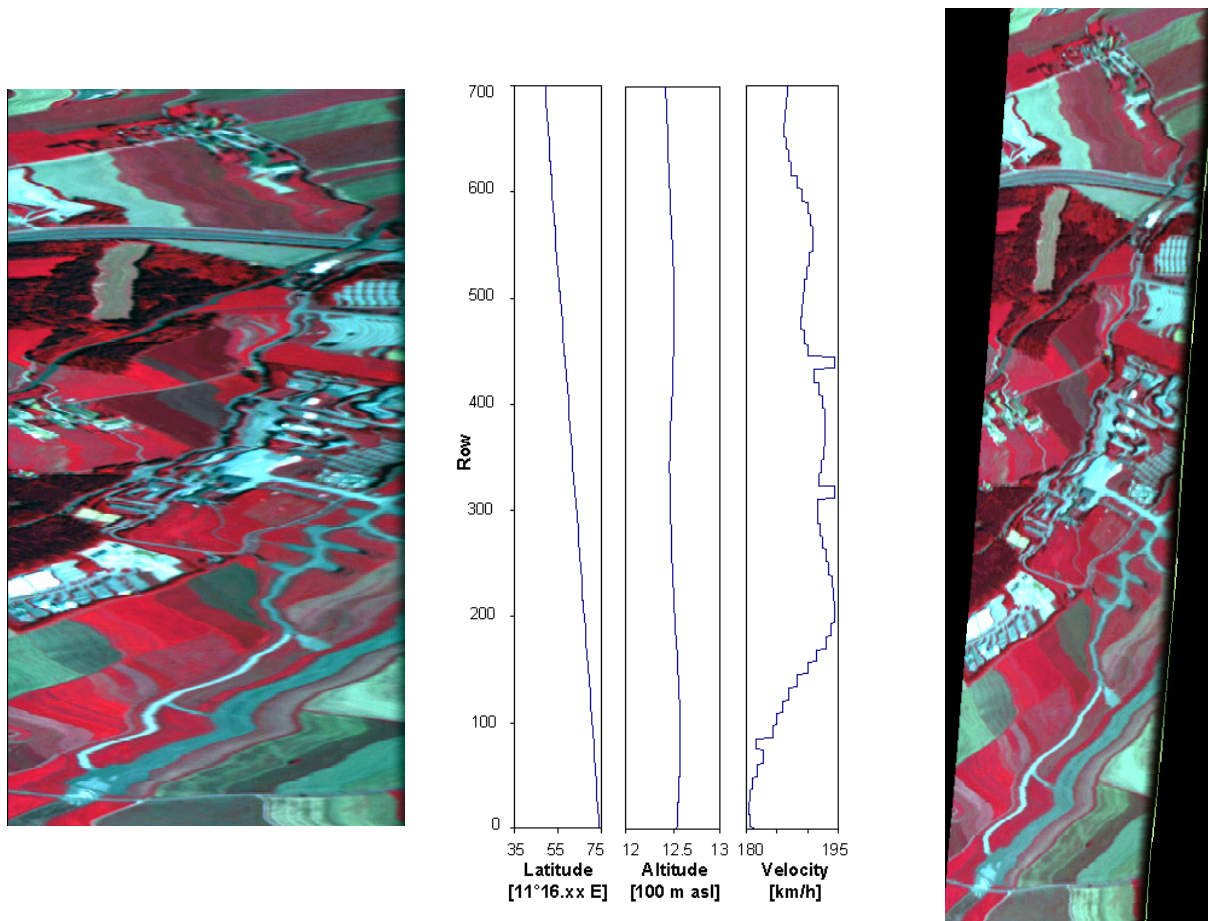
Figure 4-20:    Geometric correction of preprocessed AVIS data (left) with dGPS data (geographical
                position, flight altitude as well as velocity of the aircraft) and resulting geometrically
                corrected image (right) (R/G/B = 582/674/729nm), acquired on 19<sup>th</sup> July 1999

The rectified scenes can be used for the examination of some system parameters such as the FOV, which can be derived using equation (4.4).

$$FOV_{real} = 2 \cdot \sin^{-1}\left(\frac{D}{2h}\right)$$
(4.4)

where

$FOV_{real}$        Field of view derived in the field [°],

$D$                 across-track distance covered on the ground [m],

$h$                 flight altitude above ground [m].

The altitude above ground can be derived from flight height above sea level, which is measured with the dGPS and stored in the image header. The ground level as well as the across track distance on ground can be derived from a topographic map or from the DEM. The $FOV_{real}$ was calculated for several AVIS scenes and the results were in the range of 66° to 68°. Therefore the specifications of the contractor could be confirmed.

Figure 4-21:    Mosaic of the test site Gilching assembled using flight strips acquired on 3$^{rd}$ and 10$^{th}$ May 2000 (R/G/B = 582/674/729nm)

# 5 Derivation of Plant Chlorophyll and Nitrogen Status with Hyperspectral Remote Sensing

Plant optical properties are characterised by reflectance, transmittance and absorption. These quantities correspond to the fraction of incident radiation reflected, transmitted or absorbed by the plant, especially by the leaves (Figure 5-1). Thus, two main processes govern the radiative transfer in the plant: scattering and absorption (Lemaire, 1997).
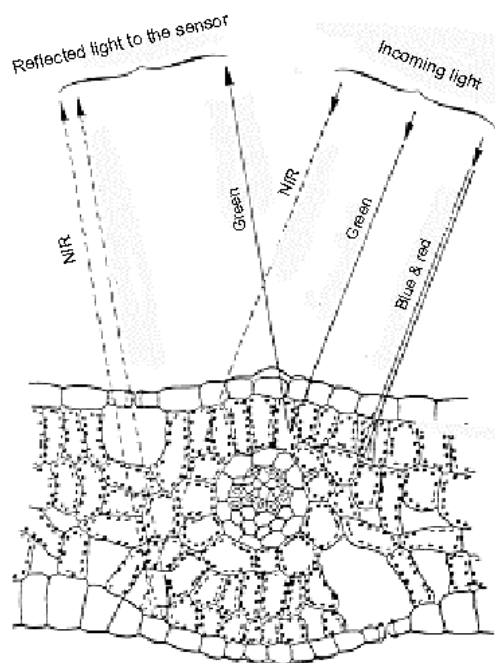


*Figure 5-1: Scattering processes of light in a leaf (Guyot et al., 1992)*

Scattering is mainly due to refraction discontinuities at the interfaces between air, cell walls and cytoplasmic water. The spectral variation of optical properties due to scattering is not as important since it is governed by the spectral variation of the refraction index which does not vary significantly with wavelength (Gausman, 1974; Lemaire, 1997).

Elementary processes of absorption are due to electronic transitions or biochemical bond vibration, rotation and stretching. Electronic transitions occur at shorter wavelengths, mainly in the visible spectral domain. Pigments such as chlorophyll, carotenoids or xanthophylls absorb in this manner. Biochemical bonds between low-mass atoms such to C, N, O or H absorb at specific frequencies and their harmonics, corresponding to vibration, rotation or stretching of the bonds. These processes occur mainly in the short wave infrared domain. However, the nitrogen in leaves is bound to C, H or O atoms, mainly within protein molecules. This implies that it is possible to infer the nitrogen content from the absorption features of proteins, or from those constituents that have characteristic absorption features and are strongly correlated to the nitrogen content (Gausman, 1977; Gates et al., 1965). Several studies demonstrated that nitrogen in dried, ground leaves could be determined accurately from the reflectance with laboratory spectrometers in the VIS and NIR (Card et al., 1988; Curran, 1989; Peterson et al., 1988; Wessman et al., 1988). Other studies elicited that the nitrogen content is also correlated with the chlorophyll content on leaf area or canopy level of different plant species such as maize (Costa, 1991; Ercoli et al., 1993), potato (Vos & Bom, 1993) or bigleaf maple (Yoder & Pettigrew-Cosby, 1995) and several deciduous and conifer species (Card, 1988; Johnson & Billow, 1996). In the 1990's, commercial instruments used for precision farming, measured the leaf nitrogen status and deficiency based on their strong

correlation to the chlorophyll content. Examples are chlorophyll meters such as SPAD 502 (Spectrum Technologies Inc., 2002) and the N-Tester (URL1), which are used mainly for crops such as maize (Wood et al., 1992; Piekielek & Fox, 1992), cereals (Peltonen et al., 1995; Wollring, 1995) or rice (Takebe, 1994). In use since the year 2000, the N-Sensor (Hydro Agri) is the first commercial tractor-mounted system for both the measurement of the nitrogen status of crops and the simultaneous application of fertiliser, whereby the nitrogen measurement is comparable to that of the N-Tester.

The most promising approach to derive the nitrogen content is indirectly via the chlorophyll content, especially of the leaves (Lemaire, 1997). This is due to the fact that the plant leaves are responsible for the photosynthetic capacity on the one hand and for the development of the ears or grains, which influences both the quality and quantity of yield, on the other.

The following sections investigate the relationship between the chlorophyll and nitrogen content of plant leaves, the characterisation of the chlorophylls as well as their influence on reflectance spectra. Further parameters that may influence the spectral behaviour of both leaves and canopies are discussed. The interaction of these parameters determines the reflectance spectra, which form the basis for the derivation of the pigment content in plants, especially the leaves. The approaches that are used within this thesis are described, followed by the results derived from the AVIS data.

## 5.1 Chlorophylls
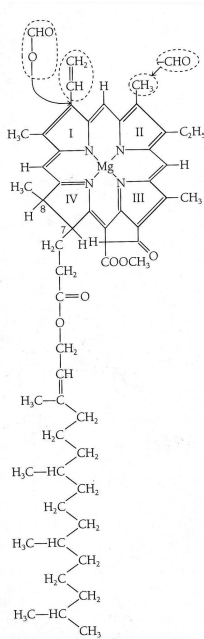


*Figure 5-2: Chemical structure of chlorophyll (Hopkins, 1995)*

Chlorophyll is the pigment primarily responsible for harvesting light energy used in photosynthesis. The chlorophyll molecule consists of two parts, a porphyrin head and a long hydrocarbon, phytol tail. The cyclic porphyrin is made up of four pyrrole rings. Four species of chlorophyll, designated chlorophyll a, b, c and d, are known. The chemical structure of chlorophyll a is shown in Figure 5-2, which also demonstrates the close relation between nitrogen and chlorophyll within the molecule.

The common denominator in all photosynthetic plants is the occurrence of chlorophyll a ($C_{55}H_{72}MgN_4O_5$) and chlorophyll b ($C_{55}H_{70}MgN_4O_6$), which is synthesized from chlorophyll a. The difference between the two structures is in a formyl group (-CHO) substitutes for the methyl group (-$CH_3$) on ring II (Hopkins, 1995; Kaufman et al., 1989). Chlorophyll c (found in diatoms, brown algae and flagellates) and d (found only in red algae) are not involved in the photosynthesis of higher plants and therefore are not described further. The natural ratio of abundance between the blue-green chlorophyll a and the yellow-green chlorophyll b is approximately 3:1 to 5:1.

The bulk of the chlorophylls functions as antenna chlorophyll, which associates with specific proteins to form a number of different chlorophyll protein complexes. Antenna pigments absorb light but do not participate directly in photochemical reactions. However, the antenna chlorophylls lie very close together so that excitation energy can easily pass between adjacent pigment molecules by a radiative transfer process. The energy of absorbed photons thus migrates through the antenna complex, passing from one chlorophyll molecule to another until it arrives at the reaction centre. The reaction centre consists of one or two molecules of chlorophyll a, which are associated to proteins, and is the site of the primary photochemical redox reaction, where light energy is converted to chemical energy (Hopkins, 1995).

A typical in vitro absorption spectrum of chlorophyll a and b is shown in Figure 5-3 (dotted line). Two major absorption bands appear for each of the two versions, one at about 430/450nm, and the other at 660/640nm. In between, the normal chlorophyll pigmented leaf shows a characteristic green reflection peak around 550nm.

The absorption spectra of the free pigment in solution are different from those of chlorophyll-protein complexes in the plants. The chlorophyll a and b in vivo absorption is opposed to 678/435nm, the second absorption maxima are shifted to 650/470nm. This behaviour must be considered by measurements in the laboratory and in the field (Hopkins, 1995; Schellberg, 1990).

The spectral behaviour of chlorophyll is also influenced by its adaptability. In weak light protochlorophyll is created as a preliminary stage from chlorophyll a,

Figure 5-3: In vivo (continuous line) and in vitro (dotted line) chlorophyll absorption of an vital plant leaf (Schellberg, 1990)

while under intense light chlorophyll becomes bleached and inactive. However, it is able to regenerate its full activity. If it is partly decomposed, the products of the decomposition become available again for the creation of protochlorophyll (Schanda, 1986). Other factors, which influence the chlorophyll content and its variations are the carbon and oxygen concentration in the air, the temperature, the availability of water and nutrients as well as the level of environmental pollutants or stress (Kaufman et al., 1989). The $CO_2$ content in the air limits photosynthesis in C3 plants (for example wheat) to the extent that light saturation occurs at fluence rates about 25% of full sunlight (400-500 µmole photons $m^{-1}s^{-1}$). At very low fluence rates the rate of $CO_2$ evolution due to dark respiration exceeds the rate of photosynthetic $CO_2$ uptake. As fluence rates increase, photosynthesis also increases, as does $CO_2$ uptake, until the rate of $CO_2$ exchange equals zero. This light compensation point lies for most plants in the range 10 to 40µmols photons $m^{-1}s^{-1}$. At fluence rates above the compensation point, the rate of photosynthesis saturates because the $CO_2$ level becomes limiting. C4 plants such as maize never really achieve light saturation, even at full sunlight. Even so, C4 photosynthesis is not necessarily more efficient than C3 photosynthesis. At temperatures below 30°C the quantum yield for C4 plants is actually lower than for C3 plants (Table 5-1) (Hopkins, 1995).

Schulze & Caldwell (1995) propose that shade leaves tend to have a much greater ratio of light-harvesting chlorophyll to stromal enzymes than do leaves that have developed in bright light. This is accompanied by a high capacity for the harvesting of light in relation to the photosynthetic capacity. It is also well established that even fully developed leaves are able to respond to altered environment by changing this relationship within a few days. Although each chloroplast in a sun leaf intercepts a relatively smaller fraction of incident light than each chloroplast in a shade leaf, this is compensated by a larger number of chloroplasts across the leaf section, and there is no consistent difference in the amount of
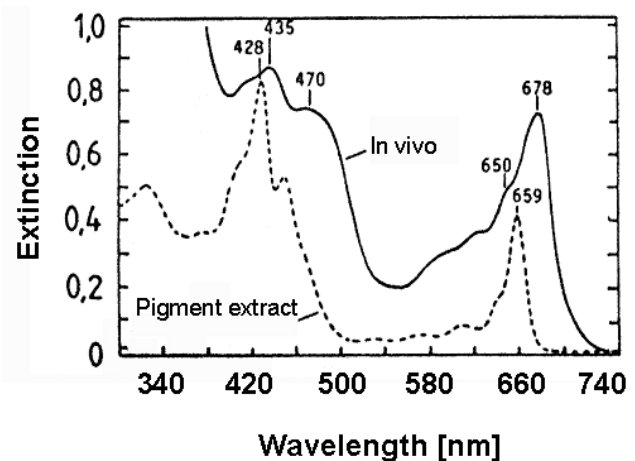
chlorophyll per unit leaf area between the two types of leaves. On the other hand Yamazaki et al. (1999) observed a decrease of the chlorophyll content per leaf area from the top to the bottom leaves of rice seedlings. However, in this thesis mainly the sun leaves are monitored both with the sampling on ground and the AVIS measurements, which leads to observations of the upper canopy layer. Therefore eventually existing differences will be neglected.

An interesting feature of C4 plants is their general low-temperature sensitivity. Most C4 species perform poorly, if at all, at low temperatures. Zea mays, for example, will not grow below 12-15°C. This lower limit for growth is probably caused by special enzymes, which are cold labile and experience a substantial loss of activity below 15°C (Prof. Neil Baker, University of Essex, UK; Dept. of Biological Science; personal communication on 16th January 2002) (see also section 3.4.2).

Table 5-1:    Comparison of significant features of C3 and C4 plants (Hopkins, 1995)

|  | C3 (*Triticum aestivum*) | C4 (*Zea mays*) |
| --- | --- | --- |
| $CO_2$ compensation point (µl $CO_2$ $l^{-1}$) | 20-100 | 0–5 |
| Light saturation (µmols photons $m^{-1}s^{-1}$) | 400-500 | Does not saturate |
| Temperature optimum (°C) | 20-25 | 30-45 |
| Quantum yield as a function of temperature | declining | steady |

The availability of water is an important factor in determining the plant metabolism and therefore the degree of chlorophyll absorption. The absorption declines or may even cease under conditions of water stress, which is due to the stomatal closure and the resulting decrease of $CO_2$ supply (Hopkins, 1995). Excessive precipitation or even flooding also have severe effects on the net photosynthesis rate. The deficiency of $O_2$ in a saturated or flooded soil decreases root activity and subsequently inhibits the supply of water and minerals for the above-ground parts of the plant (Lerch, 1991).

Although the degree of leaf photosynthesis as well as chlorophyll absorption show strong variations, they are generally highest in plants adapted to resource-rich environments. Reduced photosynthesis is a consequence of deficiencies in virtually all essential elements, but is particularly sensitive to the nitrogen supply. As a basic constituent of chlorophylls, redox carriers in the photosynthetic electron transport chain, and all of the enzymes involved in carbon metabolism, nitrogen plays a critical role in primary production. In addition to nutrient supply, the chlorophyll content of leaves is also subjected to stress by invading pathogens and environmental pollutants such as sulphur dioxide, oxides of nitrogen, ozone and heavy metals (Hopkins, 1995).

## *5.2 Measured Nitrogen – Chlorophyll Correlation*

Several studies are available which deal with the relationship between the nitrogen and chlorophyll content of leaves for different plant species. Both parameters were measured within the scope of the ground campaigns conducted for this thesis. The correlation between the chlorophyll and nitrogen content per mass as well as per area, which were measured during this study, are able either to support or refute previous results or thirdly produce new results. Therefore the correlation between nitrogen and chlorophyll is presented for each investigated plant species or land cover and for the total sample size including all investigated land covers.

The statistical analysis was carried out using the software STATISTICA (StatSoft Version 6.0, 2001). A precondition for the analysis was that the chlorophyll and nitrogen data sets are distributed normally. To check for normal distribution the level of significance $p$ as well as the Kolmogorov-Smirnov-test were computed.

The following chlorophyll–nitrogen correlations include only results that showed significant correlations ($p<0.05$), i.e. the probability of error that is involved in accepting the observed results as valid is less that 5%. The confidence interval of the coefficient of correlation was calculated as an additional test for significance using the Fisher transformation (Schönwiese, 2000). Results, which failed the Fisher-transformation, are not mentioned in the following discussion.

The investigation of the total sample size, including all land cover types, showed no significant results. Therefore it will not be discussed in the following sections.

### 5.2.1     Wheat

Few studies exist that focus on the relationship between the nitrogen content and chlorophyll meter values of winter wheat, which confirm that these parameters are highly correlated (Peltonen et al., 1995; Wollring, 1995).

The sample size for the wheat analysis included 127 measurements each of nitrogen and chlorophyll content, which were carried out during the ground truth campaigns 1999 and 2000 in the test area Starnberg. The analysis was conducted by comparing contents per area and per mass. The results are given in Table 5-2.

The correlation quality depends on the measuring unit of the parameters, whereby correlation with the chlorophyll content per area showed the highest coefficients. The best results were achieved when comparing the nitrogen content per area with the chlorophyll content per area ($r^2=0.83$ for chlorophyll a and $r^2=0.77$ for chlorophyll b, which is also presented in Figure 5-4). The other results showed significant, but poor correlations with coefficients of determination lower than 0.50, indicating that less that 50% of the variation in the data set of the nitrogen values can be explained by the chlorophyll measurements.

Presuming the preconditions mentioned above as well as a correlation, which describes at least two thirds of the variance, a predication can only be derived for the parameter contents both per area ($r^2 > 0.67$).

Table 5-2:    *Significant correlations between nitrogen and chlorophyll content of leaves for wheat canopies (r=coefficient of correlation, r²=coefficient of determination, p=statistical significance level)*

|  | r | r² | p |
|---|---|---|---|
| N [g/m²] versus Chl a [g/m²] | 0.91 | 0.83 | < 0.01 |
| N [g/m²] versus Chl b [g/m²] | 0.88 | 0.77 | < 0.01 |
| N [g/m²] versus Chl a+b [g/m²] | 0.91 | 0.83 | < 0.01 |
| N [g/m²] versus Chl a [mg/g] | 0.67 | 0.45 | < 0.01 |
| N [g/m²] versus Chl b [mg/g] | 0.66 | 0.44 | < 0.01 |
| N [g/m²] versus Chl a+b [mg/g] | 0.68 | 0.47 | < 0.01 |
| N [%DM] versus Chl a [g/m²] | 0.65 | 0.43 | < 0.01 |
| N [%DM] versus Chl b [g/m²] | 0.56 | 0.32 | < 0.01 |
| N [%DM] versus Chl a+b [g/m²] | 0.64 | 0.40 | < 0.01 |
| N [%DM] versus Chl a [mg/g] | 0.56 | 0.31 | < 0.01 |
| N [%DM] versus Chl b [mg/g] | 0.44 | 0.19 | < 0.01 |
| N [%DM] versus Chl a+b [mg/g] | 0.54 | 0.29 | < 0.01 |

The separation of the two different cultivars investigated did not lead to an improvement of the correlation, neither for the Bussard nor the Capo cultivar. The relationshisp between nitrogen and chlorophyll content per area are provided in Figure 5-4.
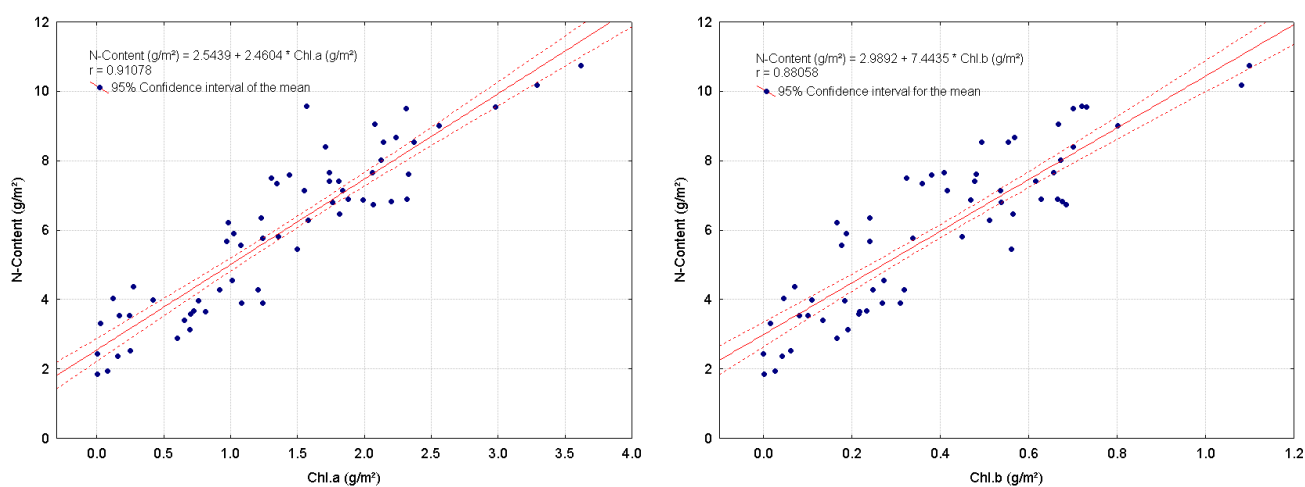


Figure 5-4:       *Relation of chlorophyll a (left) and b (right) content per area to nitrogen content per area for wheat measured during the ground measurements 1999 and 2000*

Comparable results are described by Yoder & Pettigrew-Cosby (1995) and Johnson & Billow (1996) for bigleaf maple and Douglas fir foliage, respectively. Both found the reason for the correlation of nitrogen and chlorophyll content per mass in nitrogen treatment. Mean chlorophyll content was significantly larger under high treatment than under the medium and low treatment, which were not significantly different. With Douglas fir foliage, the coefficients of correlation within each treatment varied between 0.92, 0.74 and 0.51 for the low, medium and high fertilisation respectively. Assuming comparable behaviour of wheat plants, the low correlation may be caused by fertilisation, which at high levels decouples the chlorophyll content from the nitrogen supply. This may happen when the compensation point is exceeded and nitrogen is mainly incorporated into other proteins than chlorophyll and into amino or nucleic acids. The proteins or *reserve proteins* are used as internal storage of reduced nitrogen and are located in the cell sap as well as the seed.

However, the development of the parameters during the years 1999 and 2000, presented schematically in Figure 5-5, clearly indicates the parallel trend of the contents per area and the uncorrelated trend of contents per mass. The moderate correlation between nitrogen per area and chlorophyll per mass can also be explained by the similar development at the beginning and end of the growing season, whereas during the phase of high and constant chlorophyll content before and during anthesis the nitrogen content decreases after reaching its maximum stage just before anthesis. An analysis of the parameters considering the phenological stage (before/after booting (EC 40)) showed improved results for the developmental stages after booting, where a highly significant correlation could be derived for chlorophyll content per area and nitrogen per mass (chl.a: $r^2=0.69$, chl.b: $r^2=0.72$, chl.a+b: $r^2=0.70$). Chlorophyll and nitrogen per area showed even higher correlations (chl.a: $r^2=0.83$, chl.b: $r^2=0.72$, chl.a+b: $r^2=0.81$) while the other parameters are not correlated.



| | | |
|---|---|---|
| $N_{mean}$ [g/m²] | 6.10 | 2.27 |
| $N_{max}$ [g/m²] | 9.55 | |
| $N_{mean}$ [% DM] | 2.74 | 0.86 |
| $N_{max}$ [% DM] | 4.30 | |
| $Chl.a_{mean}$ [g/m²] | 1.47 | 0.84 |
| $Chl.a_{max}$ [g/m²] | 3.71 | |
| $Chl.a_{mean}$ [mg/g] | 1.98 | 0.76 |
| $Chl.a_{max}$ [mg/g] | 3.40 | |
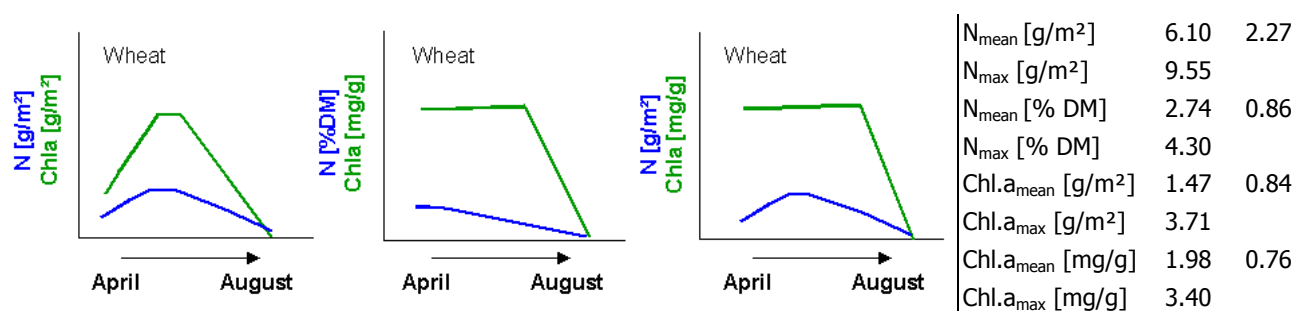
Figure 5-5:   *Schematic representation of the development of nitrogen and chlorophyll content during a vegetation period for wheat canopies derived from field measurements in 1999 and 2000 (the second number in the table is the standard deviation from the mean content values)*

The comparison of the two cultivars, which exhibit differences in their "greenness", showed that the cultivar Bussard is distinguished by a higher nitrogen and chlorophyll content both per area and per mass during the vegetative growth before booting (EC 40) (see Table 5-12 in section 5.5.4.1). This is a further indicator that the field greenness is an

indicator for the chlorophyll and nitrogen content, which was previously observed by Ma and collaborators (1996) for maize.

When considering the cultivar and its phenological stage (before/after EC 40) high correlations with both cultivars can also be found for the chlorophyll and nitrogen per mass and the chlorophyll per area and nitrogen per mass (see Table 5-3).

Table 5-3: *Significant correlations between nitrogen and chlorophyll content of leaves for wheat canopies considering the phenological stage (before/after EC 40) (r=coefficient of correlation, r²=coefficient of determination, p=statistical significance level, n.s.=not significant)*

| Bussard | Before EC 40 | | | After EC 40 | | |
|---|---|---|---|---|---|---|
| | r | r² | p | r | r² | p |
| N [g/m²] versus Chl a [g/m²] | 0.94 | 0.89 | <0.01 | 0.93 | 0.87. | <0.01 |
| N [g/m²] versus Chl b [g/m²] | - | - | n.s | 0.95 | 0.90 | <0.01 |
| N [g/m²] versus Chl a+b [g/m²] | 0.95 | 0.89 | <0.01 | 0.94 | 0.88 | <0.01 |
| N [%DM] versus Chl a [g/m²] | 0.91 | 0.82 | <0.01 | 0.83 | 0.68 | <0.01 |
| N [%DM] versus Chl b [g/m²] | 0.87 | 0.75 | <0.01 | 0.85 | 0.73 | <0.01 |
| N [%DM] versus Chl a+b [g/m²] | 0.93 | 0.87 | <0.01 | 0.84 | 0.70 | <0.01 |
| N [%DM] versus Chl a [mg/g] | 0.92 | 0.85 | <0.01. | - | - | n.s. |
| N [%DM] versus Chl a+b [mg/g] | 0.88 | 0.77 | <0.01 | - | - | n.s. |
| Capo | Before EC 40 | | | After EC 40 | | |
| | r | r² | p | r | r² | p |
| N [g/m²] versus Chl a [g/m²] | 0.95 | 0.90 | <0.01 | 0.94 | 0.88 | <0.01 |
| N [g/m²] versus Chl b [g/m²] | - | - | n.s. | 0.95 | 0.90 | <0.01 |
| N [g/m²] versus Chl a+b [g/m²] | 0.89 | 0.80 | <0.01 | 0.94 | 0.89 | <0.01 |
| N [%DM] versus Chl a [g/m²] | 0.85 | 0.72 | <0.01 | 0.83 | 0.69 | <0.01 |
| N [%DM] versus Chl b [g/m²] | - | - | n.s. | 0.85 | 0.72 | <0.01 |
| N [%DM] versus Chl a+b [g/m²] | 0.89 | 0.80 | <0.01 | 0.84 | 0.70 | <0.01 |
| N [%DM] versus Chl a [mg/g] | 0.90 | 0.81 | <0.01. | - | - | n.s. |
| N [%DM] versus Chl a+b [mg/g] | 0.83 | 0.70 | <0.01 | - | - | n.s. |

The results show that without consideration of the cultivar or phenological status, the chlorophyll and nitrogen per area are highly correlated. High correlations between chlorophyll and nitrogen per mass as well as chlorophyll per area and nitrogen per mass can only be found when both the cultivar and the phenological status are considered. These results lead to the assumption that a correlation between nitrogen and chlorophyll per mass exists for the cultivars under a given fertilisation and whenever the compensation point is not exceeded. This relationship cannot be transferred to other cultivars or fertilisation managements.

## 5.2.2    Maize

72 data pairs form the sample size of the maize analysis. Table 5-4 provides results for the correlation of maize similar to those of wheat when comparing nitrogen and chlorophyll per area, especially for chlorophyll a (Figure 5-6 left) and total chlorophyll content. Again, chlorophyll per mass shows weak but inverse dependency to the nitrogen per mass. The other correlations showed no significant dependency at all and therefore are not mentioned in Table 5-4.

Table 5-4:    *Significant correlations between nitrogen and chlorophyll content for maize leaves (r=coefficient of correlation, r²=coefficient of determination, p=statistical significance level)*

|  | r | $r^2$ | p |
|---|---|---|---|
| N [g/m²] versus Chl a [g/m²] | 0.92 | 0.84 | <0.01 |
| N [g/m²] versus Chl b [g/m²] | 0.73 | 0.53 | <0.01 |
| N [g/m²] versus Chl a+b [g/m²] | 0.91 | 0.82 | <0.01 |

The results are partly in accordance with Costa (1991), who described a very high positive correlation of leaf nitrogen with chlorophyll a and b of r=0.97 and 0.95, respectively. The strong dependency on chlorophyll b cannot be demonstrated here, though with 0.73 a moderate coefficient of correlation was determined (see also Figure 5-6 right). The results could not be improved through consideration of the phenological status during the analysis.
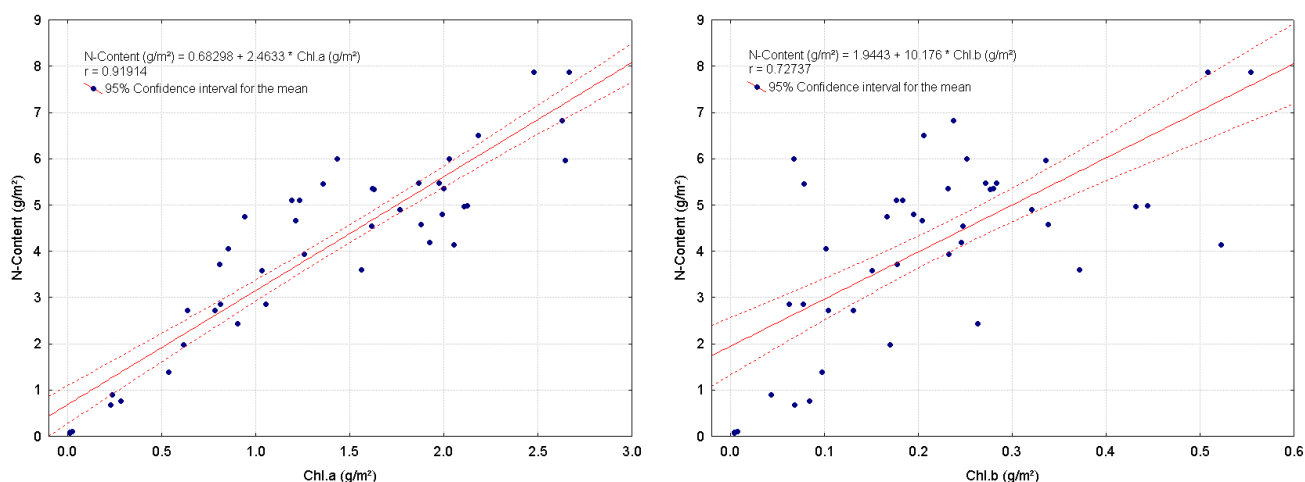


Figure 5-6:    *Relation of chlorophyll a (left) and b (right) content per area to nitrogen content per area for maize canopies derived from field measurements in 1999 and 2000*

The results were improved for the cultivars Magister and Narval when the cultivar was considered (see Table 5-5), but the mixture of Bristol/Korus failed. When the phenological status was also incorporated into the analysis, high correlations could be derived for the cultivar Magister. No improvement of the correlation coefficients could be derived except

for the nitrogen and chlorophyll b per mass correlation, which is highly correlated after the ear formation ($r^2=0.86$). The sample sizes of the other cultivars were too small for a phenological separation, thus the Fisher transformation showed no significance for the correlation coefficients.

Table 5-5:  *Significant correlations between nitrogen and chlorophyll for maize leaves considering the cultivar (r=coefficient of correlation, r²=coefficient of determination, p=statistical significance level, n.s.=not significant)*

| | Magister | | | Narval | | |
|---|---|---|---|---|---|---|
| | r | r² | p | r | r² | p |
| N [g/m²] versus Chl a [g/m²] | 0.92 | 0.85 | <0.01 | 0.88 | 0.77 | <0.01 |
| N [g/m²] versus Chl b [g/m²] | 0.82 | 0.67 | <0.01 | - | - | n.s. |
| N [g/m²] versus Chl a+b [g/m²] | 0.89 | 0.81 | <0.01 | 0.87 | 0.76 | <0.01 |
| N [%DM] versus Chl a [g/m²] | -0.93 | 0.86 | <0.01 | -0.85 | 0.72 | <0.01 |
| N [%DM] versus Chl b [g/m²] | -0.87 | 0.77 | <0.01 | - | - | n.s. |
| N [%DM] versus Chl a+b [g/m²] | -0.89 | 0.80 | <0.01 | -0.88 | 0.77 | <0.01 |
| N [%DM] versus Chl a [mg/g] | - | - | n.s. | 0.84 | 0.70 | <0.01 |
| N [%DM] versus Chl a+b [mg/g] | - | - | n.s. | 0.94 | 0.87 | <0.01. |

Figure 5-7 illustrates the relationship between the parameters nitrogen and chlorophyll during the vegetation period. The nitrogen content per mass decreases constantly during the growing period, except for the early beginning of the plant growth, and is not affected by short-term variations in environmental factors such as temperature (see centre graph in Figure 5-7). The maize canopies show distinct variations in the chlorophyll content per mass, especially of chlorophyll a (see also section 3.4.2). These variations reduce the correlation between nitrogen and chlorophyll per mass as well as the correlation of nitrogen per area and chlorophyll per mass. This leads to the assumption that only values that represent the trend of the chlorophyll content during the vegetation period can be compared with the nitrogen content per mass. This trend was derived by calculating a fitting function fourth order of the chlorophyll per mass values. The correlation between the nitrogen content and the fitted chlorophyll curve showed no improvement when all cultivars are investigated together.

Calculated separately for each cultivar, the correlation between the nitrogen content and the fitted chlorophyll curve showed improvements between nitrogen per area and chlorophyll per mass. Nitrogen and chlorophyll b per mass are now also highly correlated (see Table 5-6). The differentiation between the cultivars is necessary because they show different responses to low temperatures. Certain cultivars become chlorotic very quickly when temperatures drop, but the chlorophyll level recovers quickly when temperatures

rise again, while other cultivars show a moderate response (Prof. Neil Baker, University of Essex, UK, Dept. of Biological Science, personal communication 16th January 2002).



| $N_{mean}$ [g/m²] | 4.33 | 2.15 |
| $N_{max}$ [g/m²] | 7.80 | |
| $N_{mean}$ [%DM] | 2.97 | 0.78 |
| $N_{max}$ [%DM] | 4.46 | |
| $Chl.a_{mean}$ [g/m²] | 1.48 | 0.80 |
| $Chl.a_{max}$ [g/m²] | 3.28 | |
| $Chl.a_{mean}$ [mg/g] | 1.66 | 0.24 |
| $Chl.a_{max}$ [mg/g] | 2.44 | |
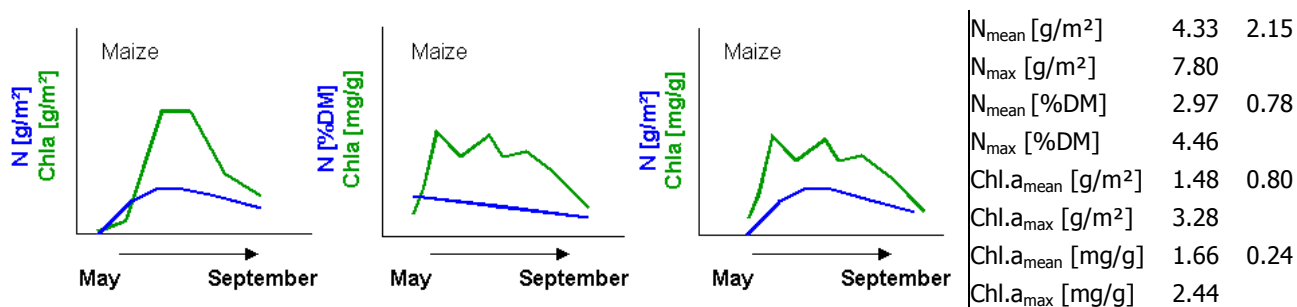
*Figure 5-7:    Schematic representation of the development of the nitrogen and chlorophyll content during a vegetation period for maize derived from field measurements in 1999 and 2000 (the second number in the table is the standard deviation of the mean content values)*

*Table 5-6:    Significant correlations between nitrogen content and chlorophyll trend per mass for the maize cultivars (r=coefficient of correlation, r²=coefficient of determination, p=statistical significance level)*

| Narval | r | r² | p |
|---|---|---|---|
| N [g/m²] versus Chl a [mg/g] | 0.92 | 0.85 | <0.01 |
| N [g/m²] versus Chl a+b [mg/g] | 0.92 | 0.84 | <0.01 |
| N [%DM] versus Chl b [mg/g] | -0.93 | 0.86 | <0.01 |
| Bristol/Korus | | | |
| N [% DM] versus Chl b [mg/g] | -0.93 | 0.86 | <0.01 |
| Magister | | | |
| N [g/m²] versus Chl a [mg/g] | 0.90 | 0.81 | <0.01 |
| N [g/m²] versus Chl a+b [mg/g] | 0.89 | 0.79 | <0.01 |
| N [%DM] versus Chl b [mg/g] | -0.90 | 0.81 | <0.01 |

Presuming the preconditions mentioned in section 5.2 and a coefficient of determination >0.67, a predictable relation could only be determined for the parameter contents both per mass for chlorophyll a and total chlorophyll (r²=0.84 and 0.82). When considering the cultivar, high correlations between chlorophyll per area and nitrogen both per mass and per area could be obtained for Magister and Narval. The results for the separation into before/after the formation of the ear (EC 40) were not significant and therefore cannot be discussed. Similar to wheat the knowledge of the cultivar enhances the resulting correlations over the whole vegetation period.

When using the chlorophyll trend a significant and high correlation could be determined between the nitrogen content per mass and the chlorophyll b content per mass. The correlation between the nitrogen content per area and the chlorophyll a and a+b content

could be improved, but the parameters were highly correlated using the original chlorophyll measurements. The correlation between nitrogen and chlorophyll b both per mass is less important for the chlorophyll-nitrogen comparison, because chlorophyll b does not show as distinct variations compared to chlorophyll a. The fact that the trend only leads to an improvement of already high correlations as well as the accurate previous knowledge required estimating the temperature dependence of the cultivar lead to the conclusion that the use of the chlorophyll trend instead of the original measurements does not lead to a significant improvement of the results.

## 5.2.3    Grassland

The sample size for the grassland sites includes 68 data pairs. The measurements of the four meadows generate results comparable to maize, both for each meadow separately and in total. They are presented in Table 5-7 and in Figure 5-8. Only the nitrogen per area and chlorophyll contents per area are highly correlated. This may be due to the fact that even these grassland canopies are well provided with nutrients and therefore show no correlation between chlorophyll and nitrogen both per mass. This is confirmed by the Ellenberg values, which for all meadows indicate a high level of nitrogen supply above the European average (see section 3.4.3).

Table 5-7:    Significant correlations between nitrogen and chlorophyll for grassland canopies (r=coefficient of correlation, r²=coefficient of determination, p=statistical significance level)

|  | r | r² | p |
|---|---|---|---|
| N [g/m²] versus Chl a [g/m²] | 0.86 | 0.73 | <0.01 |
| N [g/m²] versus Chl b [g/m²] | 0.89 | 0.80 | <0.01 |
| N [g/m²] versus Chl a+b [g/m²] | 0.89 | 0.79 | <0.01 |
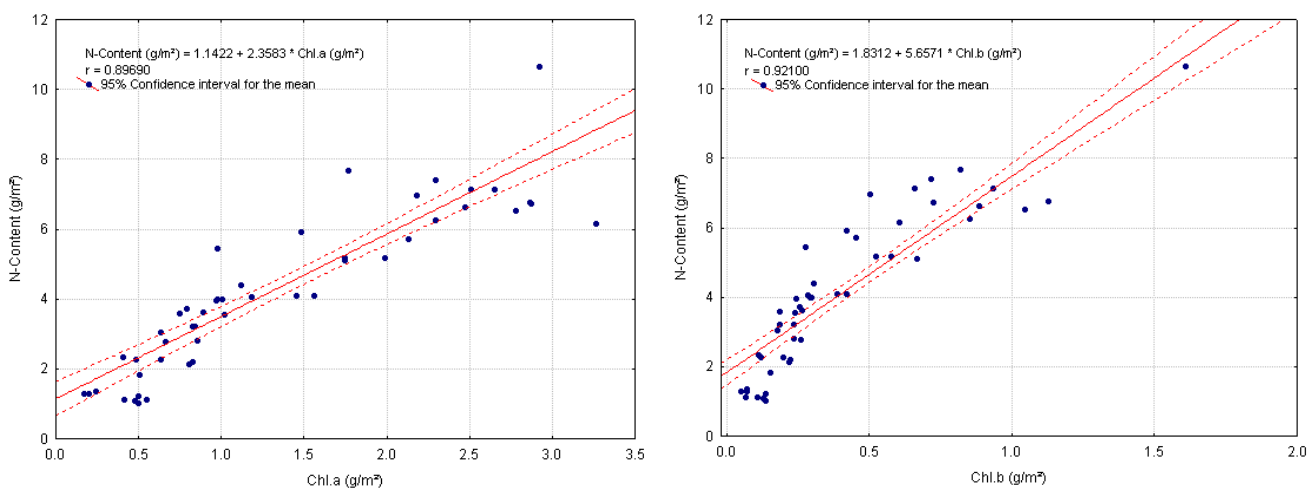


Figure 5-8:    Correlation of chlorophyll a (left) and b (right) content per area to nitrogen content per area for grassland canopies derived from field measurements in 1999 and 2000

| | | |
|---|---|---|
| $N_{mean}$ [g/m²] | 4.85 | 2.52 |
| $N_{max}$ [g/m²] | 10.6 | |
| $N_{mean}$ [%DM] | 2.34 | 0.63 |
| $N_{max}$ [%DM] | 3.80 | |
| $Chl.a_{mean}$ [g/m²] | 1.29 | 0.29 |
| $Chl.a_{max}$ [g/m²] | 2.42 | |
| $Chl.a_{mean}$ [mg/g] | 1.49 | 0.89 |
| $Chl.a_{max}$ [mg/g] | 2.09 | |
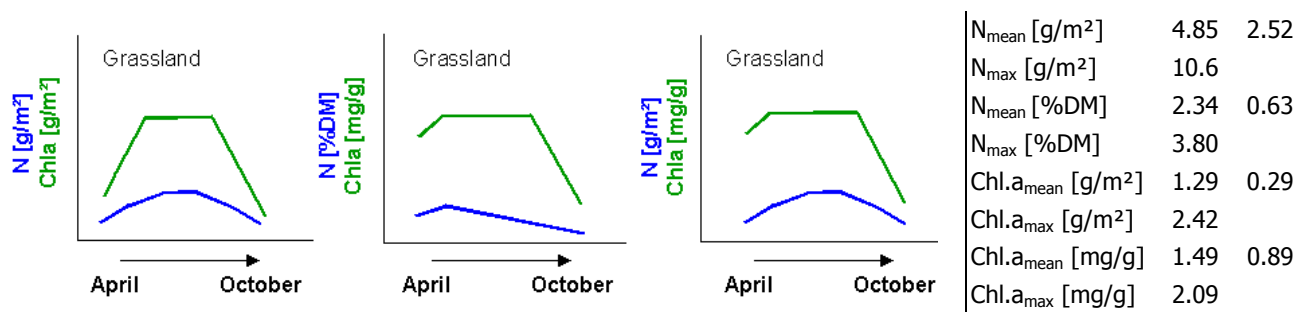
Figure 5-9:    Schematic presentation of the development of nitrogen and chlorophyll content during a vegetation period for grassland derived from field measurements in 1999 and 2000 (the second number in the table is the standard deviation of the mean content values)

Table 5-8:    Significant correlations between nitrogen and chlorophyll for the grassland sites (r=coefficient of correlation, r²=coefficient of determination, p=statistical significance level)

| Meadow No. 224 (extensive with one cut) | r | r² | p |
|---|---|---|---|
| N [%DM] versus Chl.a [g/m²] | -0.78 | 0.61 | <0.01 |
| N [%DM] versus Chl.a+b [g/m²] | -0.84 | 0.70 | <0.01 |
| N [g/m²] versus Chl.a [g/m²] | 0.94 | 0.89 | <0.01 |
| N [g/m²] versus Chl.b [g/m²] | 0.93 | 0.87 | <0.01 |
| N [g/m²] versus Chl.a+b [g/m²] | 0.92 | 0.92 | <0.01 |
| **Meadow No. 106a (extensive with one cut, mulched)** | **r** | **r²** | **p** |
| N [%DM] versus Chl.a [g/m²] | -0.63 | 0.39 | <0.01 |
| N [%DM] versus Chl.a+b [g/m²] | -0.60 | 0.36 | <0.01 |
| N [g/m²] versus Chl.a [g/m²] | 0.88 | 0.79 | <0.01 |
| N [g/m²] versus Chl.b [g/m²] | 0.86 | 0.73 | <0.01 |
| N [g/m²] versus Chl.a+b [g/m²] | 0.89 | 0.79 | <0.01 |
| **Meadow No. 53b (meadow with rotational grazing)** | **r** | **r²** | **p** |
| N [%DM] versus Chl.a [g/m²] | -0.51 | 0.26 | 0.02 |
| N [%DM] versus Chl.a+b [g/m²] | -0.53 | 0.28 | 0.02 |
| N [g/m²] versus Chl.a [g/m²] | 0.82 | 0.68 | <0.01 |
| N [g/m²] versus Chl.b [g/m²] | 0.94 | 0.89 | <0.01 |
| N [g/m²] versus Chl.a+b [g/m²] | 0.92 | 0.84 | <0.01 |
| **Meadow No. 123 (meadow with four to five cuts)** | **r** | **r²** | **p** |
| N [g/m²] versus Chl.a [g/m²] | 0.82 | 0.67 | <0.01 |
| N [g/m²] versus Chl.b [g/m²] | 0.76 | 0.57 | <0.01 |
| N [g/m²] versus Chl.a+b [g/m²] | 0.81 | 0.66 | <0.01 |

The chlorophyll and nitrogen content per area are highly correlated (Table 5-7). No correlation, which describes at least two third of the variance, could be found for the other parameters. The schematic presentation of chlorophyll and nitrogen is demonstrated in Figure 5-9. When looking at the nitrogen per area and chlorophyll per mass development, a correlation would be supposed, but could not be verified during the analysis: no significant correlation could be derived for chlorophyll per mass and nitrogen per area (see also Table 5-8). This may be also an indicator for the decoupling of the two parameters or beyond the compensation point, which was already described in section 5.2.1.

An interesting aspect lays in the differences, which may occur between the meadows with varying intensity, which are presented in Table 5-8.

With all meadows under investigation, high correlations can be found for the chlorophyll and nitrogen content both per area. A significant correlation also can be found between nitrogen per mass and chlorophyll per area. A decreasing strength of the correlation can be observed with increasing utilisation intensity. This is in accordance to the results of Yoder & Pettigrew-Cosby (1995) and Johnson & Billow (1996), which already have been described in section 5.2.1. No significant correlation could be derived for chlorophyll and nitrogen contents both per mass.

Presuming the precondition mentioned in section 5.2 and a coefficient of determination >0.67, a prediction can only be derived for the parameter contents both per area.

## 5.2.4   Conclusions

For all investigated land cover types, the chlorophyll and nitrogen content per area are highly correlated, especially for chlorophyll a and total chlorophyll content ($r \geq 0.9$). The nitrogen and chlorophyll contents per mass are uncorrelated. Significant correlations could be derived between the nitrogen per area and chlorophyll a per mass for wheat ($r = 0.76$) and grassland ($r = -0.76$).

Nitrogen per mass and chlorophyll per area and mass, respectively, of wheat are highly correlated when the phenological stage (before/after EC 40) and the cultivar are considered ($r > 0.82$).

For maize, nitrogen per mass and chlorophyll per area were uncorrelated when examining the whole population, but showed high correlations when the cultivars were analysed separately ($r > 0.85$). Similar to wheat, the knowledge of the cultivar enhances the strength of the correlation. Distinct variations of the chlorophyll content per mass during the vegetation period destroy any correlation with these parameters. The usage of a fitted chlorophyll trend curve instead of the original measurements does not lead to a significant improvement of the results.

For grassland, no significant correlation above r²=0.67 could be observed except for chlorophyll and nitrogen both per area, where a decreasing strength of correlation is observed with increasing fertilisation.

These results lead to the conclusion that the chlorophyll and nitrogen contents per mass of the investigated land covers are decoupled under the given fertilisation levels, when the compensation point for effective photosynthesis is exceeded. Beyond this limit the nitrogen in the plants is no longer incorporated into chlorophylls, but mainly into proteins, alkaloids and nucleic acids, whereas especially the proteins are used as internal storage of nitrogen.

## 5.3 Spectral Properties of Plant Leaves

Figure 5-10 presents a standardised vegetation spectrum, as observed with an imaging spectrometer. Three regions can be differentiated: The VIS, NIR and MIR wavelength region.

◊ The **VIS** wavelength range is dominated by the absorption of leaf pigments, mainly by chlorophyll a and b and to a lesser extent by carotenoids (see Figure 5-10).

o In the **NIR** region, shown in Figure 5-10, absorption has a low influence, it is characterised by high reflectance and transmittance. The high reflectance is due to diffuse scattering of light within the leaf, namely at the cell-air interfaces in leaf mesophyll (Gausman, 1974; see also section 4.2.6), which is added to the signal directly reflected at the leaf surface. The reflection level is therefore mainly influenced by the internal structure of the mesophyll, i.e. the size of the cells as well as the number of intercellular spaces (Gates et al., 1965). For example, the compact mesophyll of dicotyledonous plants leads to a lower NIR reflectance than the porous mesophyll of monocotyledons (Guyot et al., 1992).
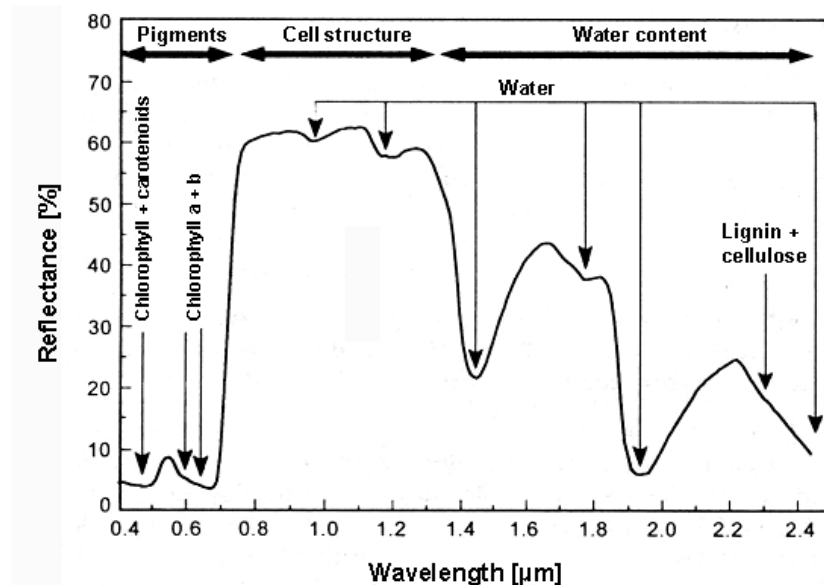


Figure 5-10:    Parameters influencing the spectral reflectance of green vegetation (Bach, 1995; modified)

The NIR region is also influenced by weak water absorptions at 820, 940 and 1150nm, respectively. Vibrations and rotations of the water molecules that are stored in the cell vacuoles cause these absorptions (Kaufman et al., 1989). Therefore a vigour leaf shows a lower NIR reflectance compared to a dehydrated leaf (Bach, 1995; Penuelas et al., 1993; Rollin & Milton, 1998), whereas the extent of difference is species dependent. Figure 5-11 shows the effect of dehydration for a lime leaf.

A special spectral feature of vegetation is located between 680 and 800nm. This sector is characterised by a steep increase of the reflection, called *red edge*. This feature is the result of the interaction between the chlorophyll absorption in the VIS and the high reflectance in the NIR, and therefore is a primary feature for the characterisation of the type as well as the condition of vegetation.
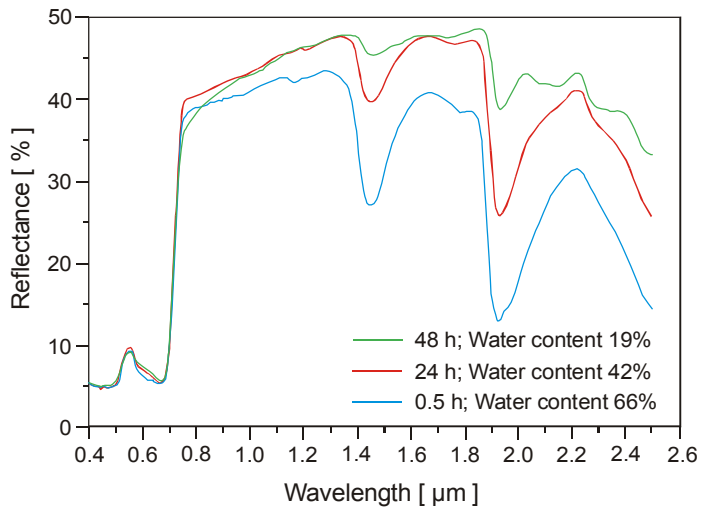


Figure 5-11: *Dependency of the spectral reflectance of a lime leaf on water content (Bach, 1995; modified)*

o The **MIR**, shown in Figure 5-10, is dominated by water absorption bands at 1450 and 1950nm, thus characterising the water content of the leaves. This wavelength region is not recorded with AVIS and therefore it is not described further here. For details it is referred to Curran (1989), Schanda (1986) and Schellberg (1990).

The dependency of leaf properties on the factors mentioned above and in the consequence of their change during plant development, results in a chronology of leaf reflectance spectra within the growing period. Figure 5-12 provides an example of this development for an oak leaf.
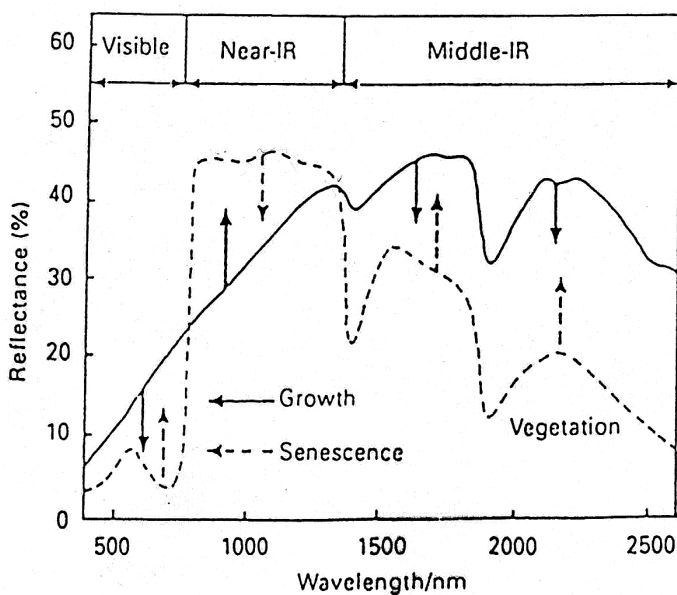


Figure 5-12: *Spectral reflectance of an oak leaf during growth and senescence (Gates et al., 1965)*

During growth, the increasing amount of chlorophyll deepens the spectrum in the VIS. Even the green peak is on a lower level compared to the initial growing stages, which is caused by the superimposition of the reflection peak at 550nm and the strong absorption features at 440 and 680nm. During senescence the chlorophyll is degraded progressively and its characteristic features are fading. The curve returns to its initial shape. In the NIR, reflectance increases during the growth and decreases again in maturity. The MIR reflection decreases during growth, when the water content of the leaf increases, and vice versa.

## *5.4 Spectral Properties of Plant Canopies*

At the canopy scale the reflectance properties of individual leaves are insufficient to describe the remotely sensed response, as it is often an assemblage of green and non-green plant parts (leaf, stem, flowers, standing litter etc.), their biomass as well as background and shadow (Blackburn, 1998). Further parameters that influence the reflectance of a canopy are the distribution of the plants and leaves as well as their orientation towards the remote sensor (Baret et al., 1994; Schellberg, 1990; Yoder & Pettigrew, 1995). Also the effects of solar and viewing geometry play a critical role in determining the reflectance characteristics of vegetation (Asner, 1998; Myneni et al., 1993).

### 5.4.1    Biophysical Attributes of a Canopy

Several studies have been carried out to evaluate the effects of biophysical parameters on reflectance values of different plant species. This was done either by empirical investigations (Huete, 1985; Huete, 1988; Tucker, 1979; Walburg et al., 1982) or more recently by modelling (Asner, 1998; Baret et al., 1994; Myneni et al., 1989; Sellers, 1985).

Examples for the spectral development of the canopies under investigation are already described in section 4.2.6 and therefore are not explained here in further detail.

#### 5.4.1.1   Canopy Density (Leaf area Index)

The density of a canopy can be described by the Leaf Area Index (LAI). The LAI is defined as the ratio of the upper leaf surface to the area of soil surface (Campbell, 1996). This means the higher the LAI the higher the biomass. Canopy LAI variation has a strong influence on reflectance signatures, with the most pronounced effect in the NIR and a smaller effect in the VIS region (see Figure 5-13). There is also a deepening of the water absorption bands at 820nm and more obviously at 940nm. While the overall NIR trend is towards increasing scattering with increasing leaf area, these NIR absorption features lag behind the rest of the plateau due to enhanced water absorption as canopy biomass increases (Asner, 1998).

Canopy reflectance is very sensitive to leaf reflectance, but for low LAIs, the sensitivity of canopy reflectance is very small and does not change significantly with leaf reflectance. Conversely, for dense canopies, canopy reflectance is very sensitive to changes in leaf reflectance. This behaviour is explained by the enhancement of the leaf signal through multiple scattering processes in the canopy (Baret et al., 1994).
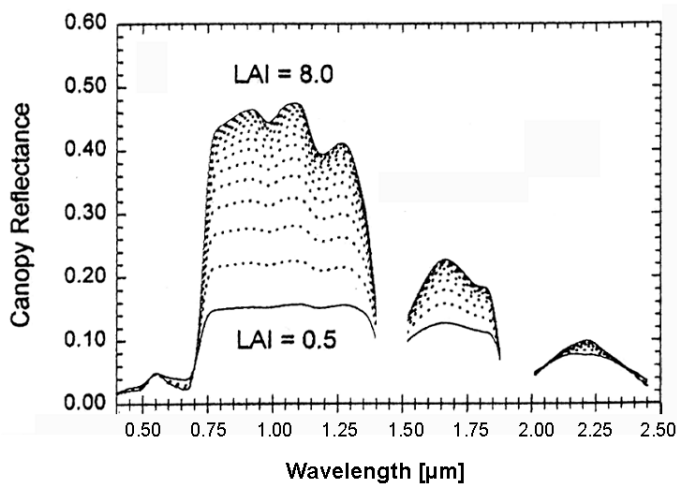
Figure 5-13: Difference in reflectance due to LAI variations (Asner, 1998)

Asner (1998) also found a sensitivity of grassland canopy reflectance to standing litter in the VIS and NIR, where the NIR showed the largest deviations. The pigment absorption features and the NIR plateau deteriorated as litter content increased. In contrast, stem optical variability plays a much smaller role in determining canopy reflectance than leaf optical properties or the occurrence of standing litter. This is due to the fact that stems and spikes make up a negligible fraction of the canopy (Schellberg, 1990). The influence of the LAI, biomass and standing litter can be minimised by the use of specially adjusted vegetation indices (Asner, 1998).

### 5.4.1.2  Soil Background

When the vegetation cover of a canopy is fractional and bare soil is visible, the resulting signal received by the sensor is a mixture of soil and vegetation. Thereby the soil moisture as well as the soil type influences the signal with its specific spectral behaviour and according to the percentage of fraction. When the soil moisture increases a deepening of the water absorption bands as well as a darkening of the whole reflectance spectrum can be observed. The soil type influences the spectrum through its specific grain size distribution and mineral composition (Bach, 1995), as illustrated in Figure 5-14.
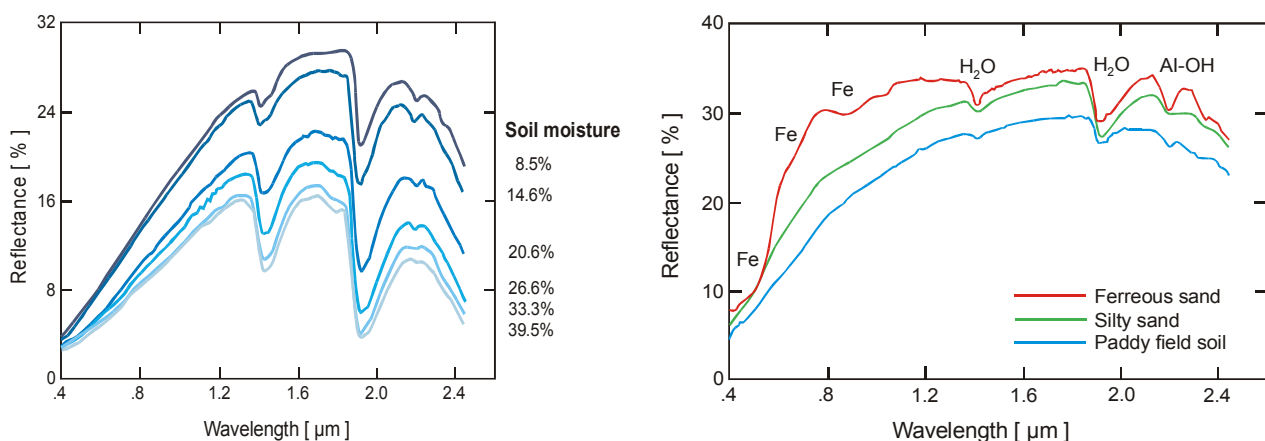


Figure 5-14:    Dependency of the reflectance of a sandy to silty soil on the soil moisture (left) and soil type (right) (Bach, 1995; modified)

The effects of soil on the reflectance can be minimised by using ratios and indices of a few wavelengths as well as by the spectral unmixing of the reflectance spectra. The relative

cover of plant canopies and bare soil patches can be separated with reasonable accuracy using a linear unmixing approach (Adams et al., 1995).

### 5.4.1.3   Leaf Orientation

Leaf orientation drives variation in canopy reflectance characteristics by ordering the scatterers (leaves and stems) in three-dimensional space, providing a means for photons to interact with multiple surfaces such as leaves, woody material and soils. The leaf orientation is described by the leaf angle, which has a strong effect on canopy reflectance (Asner, 1998; Baret et al. 1994; Sellers, 1985). For a given LAI, as mean leaf angle decreases NIR reflectance increases as it does with increasing LAI, but the water absorption

Figure 5-15: Effect of changing mean leaf angle (MLA) on canopy reflectance, simulated with a LAI=5.0 (Asner, 1998)

features at 820 and 940nm do not strengthen. This behaviour is due to the fact that, assuming vertical illumination, horizontally orientated leaves mainly reflect the incoming light vertically. Vertically oriented leaves reflect in horizontal direction towards adjacent leaves, leading to a further invasion into the canopy and therefore the signal received by the sensor decreases (Schellberg, 1990).

The effect of leaf orientation on spectral reflectances of canopies can be minimised, comparable to the soil influence, by the application of ratios and indices using certain distinct wavelengths (Bannari et al., 1995; Haboudane et al., 2002).

### 5.4.1.4   Viewing Geometry

The viewing geometry is mainly a function of the scattering behaviour of the surface, the sun zenith angle (Huss, 1984) and the position of the sensor. Huss (1984) differentiated between three basic forms for the distribution of scattering in relation to the direction of the incoming radiation, which are described graphically by Gerstl (1988) (Figure 5-16):

   a)  diffuse scattering, for example of sandy soils,
   b)  forward scattering of an agriculturally used landscape,
   c)  backward scattering of woody areas and forests (see also Figure 5-17).

Figure 5-16:     Basic forms of scattering distribution: diffuse scattering (left), forward scattering (centre); backward scattering (right) (Gerstl, 1988)

The at-sensor radiance depends on the position and inclination of the sensor relative to both sun and canopy. Guyot et al. described in 1988 the abundance of the reflected radiation in relation to the sensor inclination and demonstrated furthermore that this effect is wavelength dependent. Equation (5.1) describes this dependency within the bi-directional reflectance distribution function (BRDF), whereby the BRDF is defined as the ratio between the change of reflected to incoming radiation relative to the scattering behaviour of the canopy (Sandmeier et al., 1998).

$$BRDF(\lambda, \theta_i, \varphi_i, \theta_r, \varphi_r) = \frac{dR(\lambda, \theta_i, \varphi_i, \theta_r, \varphi_r)}{dR(\lambda, \theta_i, \varphi_i)} \tag{5.1}$$

where
$BRDF$     bi-directional reflectance distribution,
$R$         reflectance [%],
$\lambda$         wavelength [nm],
$\theta$         zenith angle [°],
$\varphi$         azimuth angle [°],
$i$         illumination direction [°],
$r$         viewing direction [°].
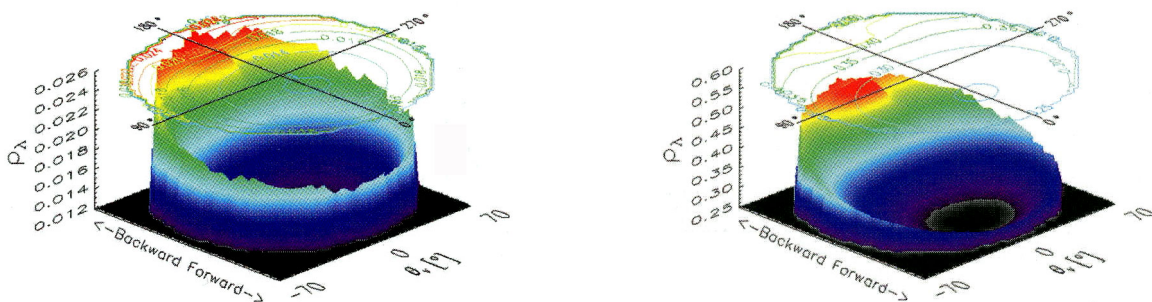


Figure 5-17: BRDF of an aspen forest in the red (670nm; left) and NIR (870nm; right) for a sun zenith angle of 50°, $\rho_\lambda$ = reflectance (ESA, 1999)

Several investigations have recently been carried out to develop approaches and instruments for the measurement of the BRDF (Camacho-de Coca et al., 2001; Leroy & Hautecoeur, 1999; Qin & Xiang, 1994) and correction (Duchemin et al., 2001; Roujean et al., 1992; Widen, 2001). Few results have been published on the spectral dependence of

the bi-directional phenomenon, which is demonstrated in Figure 5-17. Likewise, most of the presently available BRDF models do not handle the spectral variability of the BRDF effects (Sandmeier et al., 1998). Therefore the correction of the anisotropical reflectance behaviour of vegetation is not incorporated into this thesis.

## 5.5 Approaches for the Derivation of Chlorophyll and Nitrogen Content of Plants

Over recent years, the derivation of both chlorophyll and nitrogen content of plants was the subject of various investigations on multispectral (Prince & Tucker, 1986; Townshed & Justice, 1986) and hyperspectral sensors (Datt, 1998; Jago et al., 1999; Pinar & Curran, 1996; Yoder & Pettigrew-Crosby, 1995). Hyperspectral remote sensing techniques allow the differentiation of the spectral behaviour of chlorophyll a and b with their specific absorption features as well as their respective effects on vegetation reflectance spectra (Blackburn, 1998; Datt, 1998).

These characteristics have promoted the development of various approaches, based on model inversion or the use of empirical and semi-empirical methods, to estimate the chlorophyll content with remote sensing. Amongst these investigations, studies using optical indices for chlorophyll estimation have focused on evaluating the reflectance in individual bands, band reflectance ratios and combinations and the characteristics of derivative spectra. Combinations of spectral bands are widely used to minimise variations of extraneous factors and maximise sensitivity to chlorophyll content, which is based on the relationship between chlorophyll content and certain specific narrow spectral bands. The spectral regions identified as the most suitable to quantify chlorophyll are those around 680nm, corresponding to the absorption peak of chlorophyll a, and 550nm matching with the minimum chlorophyll absorption in the visible domain.

This thesis focuses on the relatively unknown Chlorophyll Absorption Integral ($CAI$), in comparison to established indices, which are the Normalised Difference Vegetation Index, which is derived either by simulated Landsat TM data with broad wavebands ($NDVI_{TM}$) and by two narrow wavebands of the hyperspectral AVIS data ($hNDVI$). The fourth index is the Optimised Soil-Adjusted Vegetation Index ($OSAVI$).

### 5.5.1 The Normalised Difference Vegetation Index (NDVI)

The NDVI is one of the evergreens in the large group of vegetation indices and was first proposed by Rouse (1973) for Landsat MSS data:

$$NDVI = \frac{(NIR - RED)}{(NIR + RED)} \tag{5.2}$$

where

*NIR*          reflectance in the near infrared wavelength region,

*RED*          reflectance in the red wavelength region.

This index was used for investigations of green vegetation (Sellers, 1985), the identification of agricultural crops (Tucker & Sellers, 1986) and precipitation in semi-arid areas (Kerr et al., 1989). Accordingly, it was used in numerous regional and global

applications for studying the state of vegetation with various sensors (Prince & Tucker, 1986; Townshed & Justice, 1986; Hame et al., 1997). The success of the NDVI as a descriptor of vegetation variations in spite of atmospheric effects and radiometric degradation in the red and near infrared bands lies in the normalisation (Holben et al., 1990). However, the NDVI has recently also been criticised because of some perceived defects:

◊ Differences between the "true" NDVI, as would be measured at the surface, and that actually determined from space are sensitive to attenuation by the atmospheric scattering and absorption. This handicap can be overcome when absolute reflectances, which are already corrected for these atmospheric effects, are used for the calculation of the NDVI (Demircan, 1995).

◊ The NDVI is sensitive to changes in the fractional vegetation cover until a full cover is reached, beyond which a further increase in LAI results in an additional small and asymptotic increase in NDVI. This saturation level of LAI ranges typically between 2 and 3, depending on vegetation type, age and leaf water content (Carlson & Ripley, 1997).

◊ Variations in soil brightness can produce large variations in NDVI from one image to the next (Liu & Huete, 1995).

Nevertheless, the NDVI is probably still the most well-known and common index, especially for multispectral remote sensing approaches. Several time-series analyses mentioned above have focused on the use of the NDVI, especially with multispectral remote sensors. For this reason, analysis of the NDVI was included in this thesis to provide a basis for comparison of multi- and hyperspectral approaches and as a well-known reference.

To calculate the multispectral NDVI, the Landsat TM bands three and four were simulated with the AVIS data using the following equation:

$$NDVI_{TM} = \frac{(TM4 - TM3)}{(TM3 + TM4)} = \frac{(AVIS_{TM4} - AVIS_{TM3})}{(AVIS_{TM4} + AVIS_{TM3})} \qquad (5.3)$$

where
*TM4*        simulated TM band 4 (700-900nm),
*TM3*        simulated TM band 3 (600-680nm),
$AVIS_{TM4}$      mean reflectance, derived from AVIS bands 25-50 (699-852nm) [%],
$AVIS_{TM3}$      mean reflectance, derived from AVIS bands 9-22 (600-680nm) [%].

Band 4 of Landsat TM could only be simulated up to 852nm due to the poor quality of the spectra in the wavelength range beyond 850nm in 1999 (see section 4.2.6).

The hyperspectral NDVI (*hNDVI*) was derived as follows:

$$hNDVI = \frac{\left(AVIS_{827nm} - AVIS_{668nm}\right)}{\left(AVIS_{827nm} + AVIS_{668nm}\right)} \qquad (5.4)$$

where

$AVIS_{827nm}$      AVIS reflectance at 827nm [%],

$AVIS_{668nm}$      AVIS reflectance at 668nm [%].

The selected bands represent the reflectance plateau in the NIR (827nm) and the maximum chlorophyll absorption (668nm) in the red spectral region respectively.

## 5.5.2    Optimised Soil-Adjusted Vegetation Index (OSAVI)

*OSAVI* belongs to the SAVI (Soil-Adjusted Vegetation Index; Huete, 1988) family, which is an evolution of the NDVI, but with an additional soil adjustment factor. The *OSAVI* is defined as follows:

$$OSAVI = (1 + 0.16) \cdot \frac{(R_{800} - R_{670})}{(R_{800} + R_{670} + 0.16)} \qquad (5.5)$$

where

$R_{800}$          reflectance at 800nm,

$R_{670}$          reflectance at 670nm.

Rondeaux and collaborators (1996) proposed the *OSAVI* to reduce the background reflectance contributions and enhance sensitivity to leaf chlorophyll content variability. The reason that this index is selected for this thesis is its easy application in the context of operational observations of agricultural landscapes. Its determination requires no knowledge of soil properties, and moreover it offered the best results for the majority of the agricultural crops that were investigated by Rondeaux et al. (1996).

## 5.5.3    Chlorophyll Absorption Integral (CAI)

The *CAI* derives the chlorophyll content by measuring the area between a straight line connecting two points of the red edge and the curve of the red edge itself. Therefore it is an approach on the basis of a spectral envelope measurement. This procedure is derived from chemical spectroscopy for the derivation of ingredients and their concentration in chemical solutions. The method is widely used in geological applications of hyperspectral remote sensing for the detection of minerals in rock, while for vegetation analysis it is relatively unknown and no literature applying it is known to the author.

The *CAI* is defined as follows (Oppelt & Mauser, 2001a and b):

$$CAI = \int_{R600}^{R735} R(EQ) \qquad (5.6)$$

where

$R_{735}$            reflectance at 735nm [%],

$R_{600}$            reflectance at 600nm [%],

$R(EQ)$            envelope quotient.

The envelope-quotient ($EQ$) is calculated according to equation (5.7):

$$EQ = \frac{Rs_i}{\mathrm{Re}_i}$$ (5.7)

where

$Rs_i$            reflectance of the vegetation spectrum at band i [%],

$Re_i$            reflectance of the envelope at band i [%].

Figure 5-18 illustrates the principle of the $CAI$ measurement. The end points of the measurement can be chosen interactively, but must remain constant for a measurement series. The end points for this thesis were chosen in such a manner that the chlorophyll absorption feature can be monitored as well as the reflectance level in the NIR. The position of the red edge is defined as the position of the inflection point along the increase of reflectance from the chlorophyll absorption toward the reflectance plateau in the NIR. Changes in the reflectance of the plants due to their developmental stage or stress, which influence the absorption depth, width and the position of the red edge can be measured using this approach (Figure 5-18).
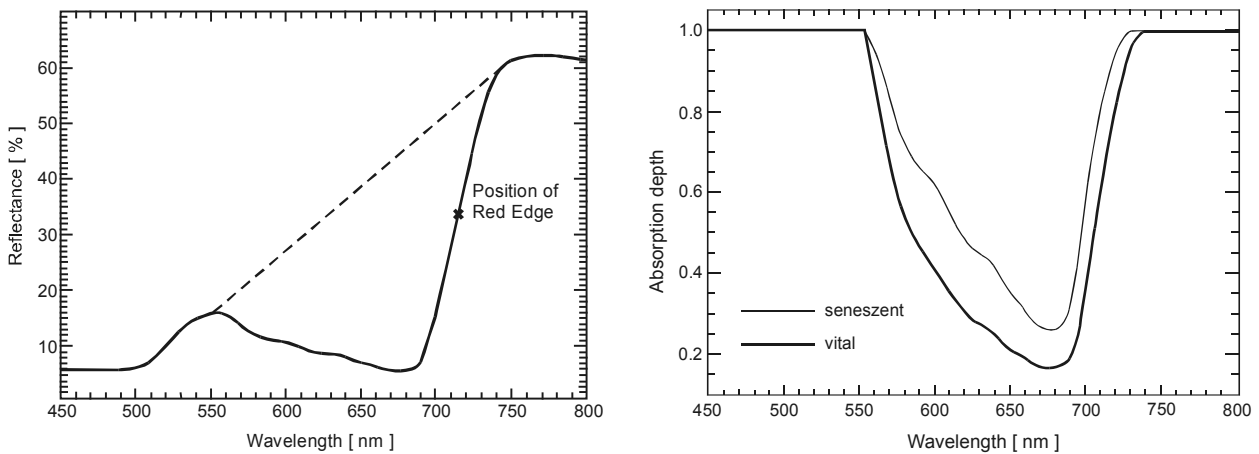


Figure 5-18:    Principle of CAI measurement (left), position of the red edge and changes in chlorophyll absorption due to plant senescence (URL2)

## 5.5.4    Results of the Chlorophyll and Nitrogen Derivation

The statistical analysis was conducted using STATISTICA (StatSoft Version 6.0, 2001). The correlation coefficients (r) were calculated based on an error probability of 5%. The following sections include only significant correlation results with a level of significance $p < 0.05$. The confidence interval of r was tested for significance using the Fisher transformation. Only results that showed a significant relationship are considered. In

addition, the correlation must describe at least two thirds of the variance (r=0.82 and r²=0.67).

No significant results could be derived investigating all measurements without any separation into the different land covers. Therefore they will not be discussed in further detail. The results for each type of land cover are divided into three parts, namely the analysis without consideration of the phenological development, the vegetative period before the formation of the ear (EC 40) and the generative growing period beyond EC 40.

### 5.5.4.1 Wheat

Considering the wheat fields as a whole, the choice of approaches is limited (Figure 5-19 and Table 5-9).

Table 5-9: *Significantly high coefficients of determination (r²≥0.67) using linear correlation equations for wheat, derived without consideration of the cultivar*

| All phenological stages | Nitrogen | | Chlorophyll [g/m²] | | | Chlorophyll [mg/g] | | |
|---|---|---|---|---|---|---|---|---|
| | [g/m²] | [%DM] | a | b | a+b | a | b | a+b |
| $NDVI_{TM}$ | | | | | | | | |
| $hNDVI$ | | | | | | 0.67 | | |
| $CAI$ | | 0.72 | 0.71 | | 0.68 | | | |
| $OSAVI$ | | | 0.67 | | | | | |
| After EC 40 | Nitrogen | | Chlorophyll [g/m²] | | | Chlorophyll [mg/g] | | |
| | [g/m²] | [%DM] | a | b | a+b | a | b | a+b |
| $NDVI_{TM}$ | | | 0.74 | 0.68 | 0.74 | 0.68 | | 0.68 |
| $hNDVI$ | | | 0.73 | 0.70 | 0.73 | 0.83 | 0.77 | 0.83 |
| $CAI$ | 0.69 | 0.73 | 0.82 | 0.81 | 0.83 | 0.73 | 0.73 | 0.74 |
| $OSAVI$ | | | 0.72 | 0.70 | 0.73 | 0.83 | 0.77 | 0.83 |

The $NDVI_{TM}$ failed for all parameters, showing coefficients of determination below 0.67. The $hNDVI$ is only correlated with the chlorophyll a content per mass (see also Table 5-9). The $CAI$ is correlated with the nitrogen content per mass and with the chlorophyll a and total chlorophyll content per area. The $OSAVI$ shows high correlation with the chlorophyll a content per area. The histograms of the indices as well as the scatter plots in Figure 5-19 show that they are saturated at high chlorophyll and nitrogen values. These saturation levels can be rated at about 2.5g/m² and 4% nitrogen. For chlorophyll they can be located at about 1g/m² and 1.5mg/g and for chlorophyll b at 0.2g/m² and 0.4mg/g. The $CAI$ is not affected by saturation as much as the other indices, although a slight accumulation of values can be observed. All indices are significantly correlated with the parameter values

below their particular saturation limit. Especially with the chlorophyll content high correlations can be observed ($r^2 > 0.67$).
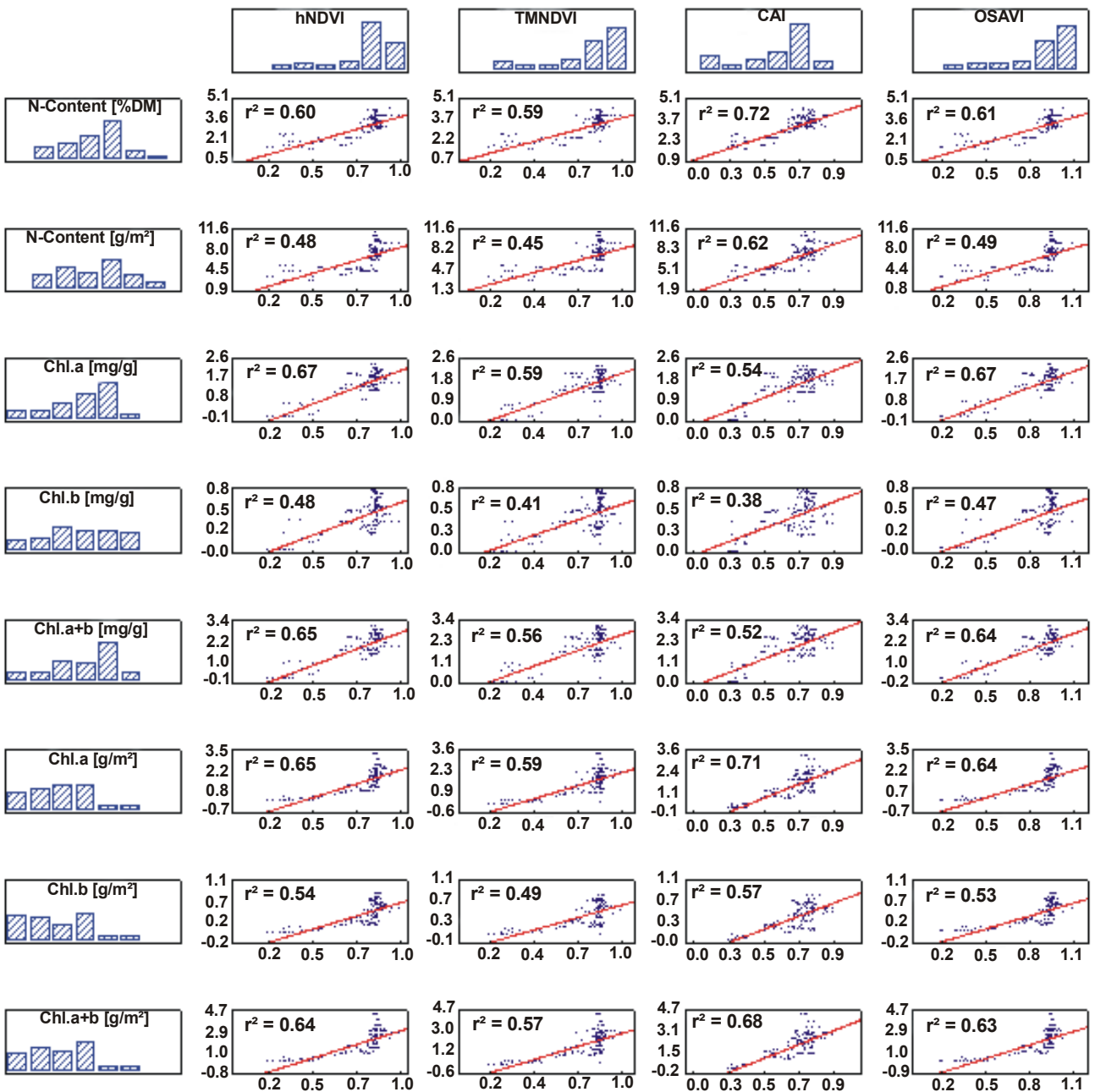


*Figure 5-19:    Plot of linear correlations between indices and chlorophyll/nitrogen content for wheat derived from field and AVIS measurements in 1999 and 2000*

When the developmental stage of the plants is considered, all approaches failed relating indices to nitrogen or chlorophylls during vegetative growth before the ears of the plants emerge. Beyond EC 40, all approaches showed high correlations with the chlorophyll content per mass and per area, except the $NDVI_{TM}$ that failed for chlorophyll b per mass. The $CAI$ was the only approach showing sufficiently high coefficients of correlation with the nitrogen content per area and mass.

These observations lead to the conclusion that without knowledge of the wheat cultivar, the approach chosen depends on either the developmental stage or the desired parameter. When the phenological status is not considered, the $CAI$ should be used for the derivation of the nitrogen content per mass and the chlorophyll content per area, while the $hNDVI$ is able to predict the chlorophyll a content per mass.

The coefficients of determination show a different behaviour when the cultivars are analysed separately. For the Bussard cultivar, chlorophyll a content is highly correlated with every index. The results for chlorophyll b as well as for the total chlorophyll content are dependent on the index used (Table 5-10). During vegetative growth, no parameter showed a sufficiently high correlation with the indices, while during generative growth all approaches are highly correlated with the chlorophyll content. Nitrogen content is only correlated with the $CAI$, while the other indices failed.

Table 5-10: *Significantly high coefficients of determination (r²≥0.67) using linear correlation equations for wheat, derived for the cultivar Bussard*

| All phenological stages | Nitrogen | | Chlorophyll [g/m²] | | | Chlorophyll [mg/g] | | |
|---|---|---|---|---|---|---|---|---|
| | [g/m²] | [%DM] | a | b | a+b | a | b | a+b |
| $NDVI_{TM}$ | | | 0.77 | 0.70 | 0.77 | 0.70 | | 0.68 |
| $hNDVI$ | | | 0.78 | 0.69 | 0.77 | 0.71 | | 0.69 |
| $CAI$ | 0.76 | 0.70 | 0.85 | 0.73 | 0.83 | | | |
| $OSAVI$ | | | 0.79 | 0.70 | 0.78 | 0.71 | | 0.69 |
| **After EC 40** | Nitrogen | | Chlorophyll [g/m²] | | | Chlorophyll [mg/g] | | |
| | [g/m²] | [%DM] | a | b | a+b | a | b | a+b |
| $NDVI_{TM}$ | | | 0.82 | 0.79 | 0.82 | 0.80 | 0.77 | 0.81 |
| $hNDVI$ | | | 0.81 | 0.78 | 0.80 | 0.82 | 0.78 | 0.82 |
| $CAI$ | 0.74 | 0.68 | 0.88 | 0.87 | 0.88 | 0.69 | 0.71 | 0.71 |
| $OSAVI$ | | | 0.82 | 0.79 | 0.82 | 0.82 | 0.79 | 0.83 |

The cultivar Capo showed a different behaviour than Bussard (Table 5-10 and Table 5-11). Without knowledge of the phenological stage the $hNDVI$, $CAI$ and $OSAVI$ are highly correlated with the chlorophyll content per mass and the nitrogen content per area, while the chlorophyll content per area showed no significant relation with the indices. The $NDVI_{TM}$ failed for all parameters. Before EC 40, the chlorophyll a content as well as the nitrogen content per area are correlated with all indices. During generative growth the $CAI$ is highly correlated with all parameters, while the $hNDVI$ and $OSAVI$ showed high correlations with chlorophyll per mass and nitrogen per area. The $NDVI_{TM}$ failed for all parameters.

This behaviour is most probably caused by the high nitrogen and chlorophyll values of Bussard during the vegetative growth that are presented in Table 5-12. Thus the Bussard parameters are often positioned beyond the saturation limit and the chlorophyll and nitrogen contents cannot be derived during this time period. In contrast, Capo showed higher mean chlorophyll contents per area during generative growth (see also Table 5-12), which causes the reduced correlation with the indices compared to Bussard.

Table 5-11: *Significantly high coefficients of determination (r²≥0.67) using linear correlation equations for wheat, derived from the cultivar Capo*

| All phenological stages | Nitrogen | | Chlorophyll [g/m²] | | | Chlorophyll [mg/g] | | |
|---|---|---|---|---|---|---|---|---|
| | [g/m²] | [%DM] | a | b | a+b | a | b | a+b |
| $NDVI_{TM}$ | | | | | | | | |
| hNDVI | | 0.71 | | | | 0.74 | | 0.68 |
| CAI | | 0.78 | | | | 0.70 | | 0.67 |
| OSAVI | | 0.70 | | | | 0.73 | | 0.67 |
| **Before EC 40** | Nitrogen | | Chlorophyll [g/m²] | | | Chlorophyll [mg/g] | | |
| | [g/m²] | [%DM] | a | b | a+b | a | b | a+b |
| $NDVI_{TM}$ | | 0.88 | 0.71 | | | 0.72 | | |
| hNDVI | | 0.92 | 0.76 | | | 0.77 | | 0.67 |
| CAI | | 0.93 | 0.79 | | | 0.81 | | 0.70 |
| OSAVI | | 0.92 | 0.75 | | | 0.76 | | |
| **After EC 40** | Nitrogen | | Chlorophyll [g/m²] | | | Chlorophyll [mg/g] | | |
| | [g/m²] | [%DM] | a | b | a+b | a | b | a+b |
| $NDVI_{TM}$ | | | | | | | | |
| hNDVI | | 0.87 | | | | 0.91 | 0.73 | 0.88 |
| CAI | | 0.90 | 0.68 | 069 | 0.69 | 0.92 | 0.83 | 0.91 |
| OSAVI | | 0.87 | | | | 0.91 | 0.72 | 0.88 |

To conclude the results for wheat, without knowledge of the cultivar grown and the phenological stage the *CAI* is highly correlated with most of the parameters, namely nitrogen per mass, chlorophyll a and total chlorophyll content per area. When chlorophyll per mass is required, *hNDVI* is the most suitable approach. The data for the vegetative growth showed no significant correlation for any index–parameter pair.

The correlation behaviour of wheat canopies is dependent on the variety grown. The cultivar Bussard showed no correlations with spectral indices during vegetative growth, while all indices are highly correlated with the chlorophyll content during the generative growing period. The nitrogen content could only be derived after EC 40 using the *CAI*.

The results could not be improved by using polynomial or exponential instead of linear correlation equations. Sometimes higher coefficients of correlation could be derived, but the results became ambiguous for low and high parameter values. Moreover, the insensitivity of the indices towards higher index values affects the results. Therefore linear regressions are used for the chlorophyll and nitrogen estimation.

*Table 5-12: Mean parameter values and standard deviations (Std) of wheat cultivars Bussard and Capo*

| Parameter | Bussard | | | | | | Capo | | | | | |
| | Before EC 40 | | After EC 40 | | Total | | Before EC 40 | | After EC 40 | | Total | |
| | Mean | Std | Mean | Std | Mean | Std | Mean | Std | Mean | Std | Mean | Std |
|---|---|---|---|---|---|---|---|---|---|---|---|---|
| N [%DM] | 3.70 | 0.29 | 2.33 | 0.84 | 2.68 | 0.95 | 3.19 | 0.77 | 2.56 | 0.53 | 2.86 | 0.71 |
| N [g/m²] | 7.38 | 1.38 | 5.47 | 2.23 | 5.96 | 2.21 | 5.39 | 1.70 | 5.61 | 2.02 | 5.52 | 1.87 |
| Chl.a [mg/g] | 1.65 | 0.27 | 1.50 | 0.71 | 1.54 | 0.63 | 1.13 | 0.46 | 1.55 | 0.61 | 1.36 | 0.58 |
| Chl.b [mg/g] | 0.42 | 0.10 | 0.46 | 0.21 | 0.45 | 0.19 | 0.29 | 0.19 | 0.46 | 0.21 | 0.39 | 0.22 |
| Chl.a+b [mg/g] | 2.07 | 0.35 | 1.96 | 0.92 | 1.99 | 0.82 | 1.43 | 0.62 | 2.01 | 0.80 | 1.75 | 0.78 |
| Chl.a [g/m²] | 1.77 | 0.51 | 1.23 | 0.84 | 1.37 | 0.80 | 1.02 | 0.41 | 1.47 | 0.85 | 1.27 | 0.72 |
| Chl.b [g/m²] | 0.45 | 0.12 | 0.38 | 0.27 | 0.39 | 0.24 | 0.26 | 0.18 | 0.44 | 0.26 | 0.36 | 0.24 |
| Chl.a+b [g/m²] | 2.22 | 0.62 | 1.61 | 1.10 | 1.76 | 1.04 | 1.28 | 0.58 | 1.91 | 1.10 | 1.63 | 0.95 |

### 5.5.4.2    Maize

The maize results are comparable to those for wheat: the $NDVI_{TM}$, $hNDVI$, and $OSAVI$ become saturated at a level of 0.8 to 0.95 (Figure 5-20). $CAI$ is not affected as much as the ratios. All approaches are negatively correlated with nitrogen content in %DM and become saturated when the dry biomass contains less than 2.5% nitrogen. For nitrogen contents higher than 2.5%DM the $OSAVI$ and the $NDVI_{TM}$ show high coefficients of determination ($r^2=0.67$). Nitrogen per area is highly correlated with all indices (Table 5-13), though in Figure 5-20 a saturation of the indices $hNDVI$, $NDVI_{TM}$ and $OSAVI$ can be observed at about 4g/m² of nitrogen.

All indices are also highly correlated with chlorophyll a and total chlorophyll content per area. Again, the indices $hNDVI$, $NDVI_{TM}$ and $OSAVI$ become saturated at a chlorophyll a content of about 1g/m² and chlorophyll b of 0.2g/m². Chlorophyll content per mass is not correlated significantly with any of the indices, which is most probably caused by the distinct temporal variations of chlorophyll, especially of chlorophyll a per mass. As the chlorophyll measurements were not carried out simultaneously to the AVIS overpasses and the chlorophyll content per mass varies with temperature, derivation of the actual chlorophyll contents per mass at the time of overflight through a linear interpolation between the sampling dates is not feasible.
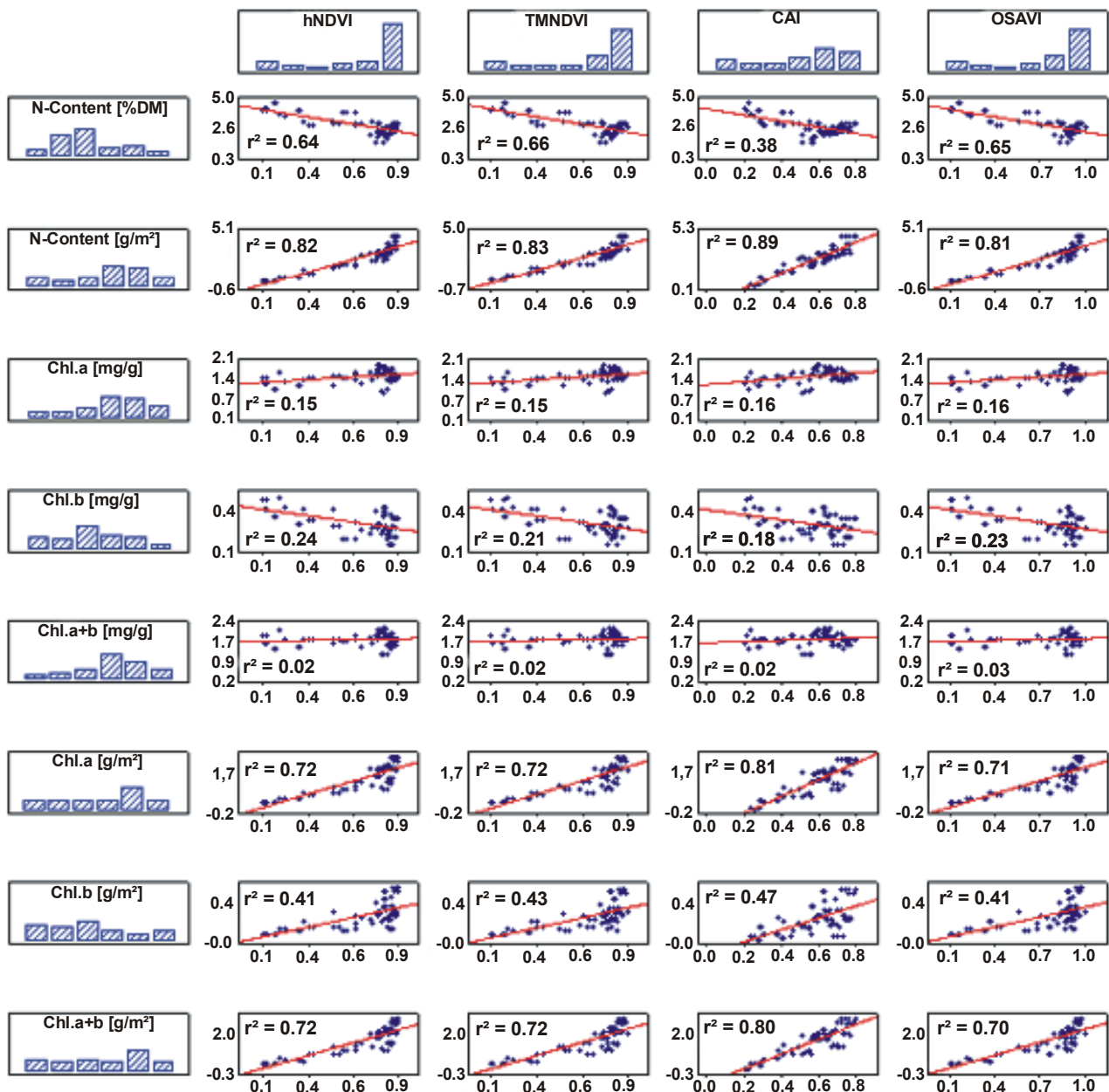
Figure 5-20:    Linear correlations between indices and chlorophyll/nitrogen content for maize derived from field and AVIS measurements in 1999 and 2000

When the phenological status is considered, as presented in Table 5-13, the nitrogen content per area as well as the chlorophyll a and the total chlorophyll content could be derived successfully with all indices for vegetative growth, while all approaches failed for the generative phase after EC 40. The high correlations for the whole growing period are therefore caused by the very high correlations between the indices and chlorophyll or nitrogen contents before EC 40.

Table 5-13: *Significantly high coefficients of determination ($r^2 \geq 0.67$) for maize, derived without consideration of cultivars*

| All phenological stages | Nitrogen | | Chlorophyll [g/m²] | | | Chlorophyll [mg/g] | | |
| | [g/m²] | [%DM] | a | b | a+b | a | b | a+b |
|---|---|---|---|---|---|---|---|---|
| $NDVI_{TM}$ | 0.83 | | 0.72 | | 0.72 | | | |
| $hNDVI$ | 0.82 | | 0.72 | | 0.71 | | | |
| $CAI$ | 0.89 | | 0.81 | | 0.80 | | | |
| $OSAVI$ | 0.81 | | 0.71 | | 0.70 | | | |

| Before EC 40 | Nitrogen | | Chlorophyll [g/m²] | | | Chlorophyll [mg/g] | | |
| | [g/m²] | [%DM] | a | b | a+b | a | b | a+b |
|---|---|---|---|---|---|---|---|---|
| $NDVI_{TM}$ | 0.88 | | 0.79 | | 0.78 | | | |
| $hNDVI$ | 0.89 | | 0.82 | | 0.81 | | | |
| $CAI$ | 0.92 | | 0.85 | 0.68 | 0.85 | | | |
| $OSAVI$ | 0.86 | | 0.78 | | 0.77 | | | |

Table 5-14: *Mean parameter values and standard deviations (Std) of maize cultivars Bristol/Korus, Magister and Narval*

| | Bristol/Korus | | | | | | Magister | | | | | | Narval | | | | | |
| | Before EC 40 | | After EC 40 | | Total | | Before EC 40 | | After EC 40 | | Total | | Before EC 40 | | After EC 40 | | Total | |
| | Mean | Std | Mean | Std | Mean | Std | Mean | Std | Mean | Std | Mean | Std | Mean | Std | Mean | Std | Mean | Std |
|---|---|---|---|---|---|---|---|---|---|---|---|---|---|---|---|---|---|---|
| N [%DM] | 3.14 | 0.18 | 2.14 | 0.50 | 2.58 | 0.61 | 3.84 | 0.68 | 2.40 | 0.14 | 3.26 | 0.89 | 3.67 | 0.50 | 2.57 | 0.58 | 3.17 | 0.59 |
| N [g/m²] | 5.39 | 0.06 | 4.77 | 1.08 | 5.08 | 0.84 | 1.47 | 1.45 | 4.73 | 0.38 | 2.79 | 2.01 | 5.36 | 2.74 | 6.06 | 2.57 | 5.39 | 2.26 |
| Chl.a [mg/g] | 1.94 | 0.16 | 1.85 | 0.08 | 1.88 | 0.12 | 1.46 | 0.16 | 1.75 | 0.31 | 1.59 | 0.27 | 1.66 | 0.06 | 1.75 | 0.14 | 1.68 | 0.17 |
| Chl.b [mg/g] | 0.27 | 0.02 | 0.25 | 0.09 | 0.26 | 0.07 | 0.37 | 0.09 | 0.33 | 0.08 | 0.36 | 0.09 | 0.23 | 0.11 | 0.19 | 0.08 | 0.22 | 0.09 |
| Chl.a+b [mg/g] | 2.21 | 0.18 | 2.09 | 0.07 | 2.14 | 0.13 | 1.84 | 0.21 | 2.08 | 0.38 | 1.95 | 0.31 | 1.97 | 0.07 | 1.95 | 0.19 | 1.93 | 0.18 |
| Chl.a [g/m²] | 1.91 | 0.15 | 1.92 | 0.22 | 1.92 | 0.18 | 0.46 | 0.43 | 1.71 | 0.39 | 0.97 | 0.76 | 1.72 | 0.91 | 2.34 | 0.31 | 1.94 | 0.85 |
| Chl.b [g/m²] | 0.27 | 0.02 | 0.25 | 0.07 | 0.26 | 0.05 | 0.10 | 0.87 | 0.33 | 0.12 | 0.19 | 0.15 | 0.29 | 0.25 | 0.29 | 0.07 | 0.29 | 0.18 |
| Chl.a+b [g/m²] | 2.18 | 0.17 | 2.17 | 0.16 | 2.18 | 0.15 | 0.48 | 0.52 | 2.04 | 0.49 | 1.12 | 0.94 | 2.06 | 1.11 | 2.64 | 0.32 | 2.64 | 0.98 |

When the cultivars are considered, as presented in Table 5-15 and Table 5-16, the results show improvements, especially with nitrogen. The nitrogen content both per mass and per area were highly correlated with all indices for the cultivars Magister and Narval before EC 40, whereas after this stage no index showed a significant correlation with nitrogen per area or mass.

The chlorophyll content per area is highly correlated with all indices, whereby the correlations before EC 40 are responsible for the significance of the correlations for all phenological stages. The results after EC 40 are poor; only the $CAI$ is significantly correlated with chlorophyll a per area of the Magister cultivar. The differences can be explained by the different chlorophyll contents of the cultivars, which lead to saturation of the indices when the chlorophyll values exceed the saturation limits. As shown in Table 5-14, the Narval cultivar shows the highest chlorophyll b content per mass. The portion of the values beyond the saturation limit is too large to derive a significant correlation for the whole sample of this parameter.

The chlorophyll a and total chlorophyll content per mass are not correlated with the applied indices before EC 40. Only chlorophyll b per mass, which does not show as distinct variations as chlorophyll a, is highly correlated to all indices for the cultivars Narval and Magister. After EC 40 all indices failed.

The field with the mixture of varieties Bristol and Korus stands out because no index is correlated either with nitrogen or with chlorophyll per mass or area. This is caused by two facts: firstly, the chlorophyll contents both per mass and area as well as the nitrogen content per area are at a very high level, thus the parameter values often exceed the saturation limit. Secondly, as demonstrated above, the chlorophyll and nitrogen contents depend on the cultivar under investigation. When two different varieties are grown at one stand, the AVIS measurements represent an average of both varieties, while the ground measurements include individual plants that cannot be attributed to a specific cultivar. Therefore the sampling may not include the same weighting of cultivars as the AVIS data. The nitrogen content in percentage of the dry biomass is also not correlated, although all values are above the saturation level of 2.5%. This is most probably caused by the small range of variation (2.9-3.2%) during the vegetative growing period. A clear statement about the cause cannot be made here. Further investigations are necessary.

As for wheat, the results could not be improved by using polynomial or exponential instead of linear regression equations. The coefficients of correlation were similar using exponential equations. Polynomial equations resulted in higher coefficients of correlation, but were ambiguous. Therefore linear regression equations are more suitable for the estimation of pigment contents because index values can be assigned unambiguously to a pigment value.

Table 5-15: Significantly high coefficients of determination (r²>0.67) for the maize cultivar Magister

| All phenological stages | Nitrogen [g/m²] | Nitrogen [%DM] | Chlorophyll [g/m²] a | b | a+b | Chlorophyll [mg/g] a | b | a+b |
|---|---|---|---|---|---|---|---|---|
| $NDVI_{TM}$ | 0.96 | 0.85 | 0.87 | 0.70 | 0.85 | | | |
| $hNDVI$ | 0.95 | 0.85 | 0.87 | 0.70 | 0.85 | | | |
| $CAI$ | 0.91 | 0.82 | 0.91 | 0.73 | 0.90 | | | |
| $OSAVI$ | 0.96 | 0.86 | 0.87 | 0.69 | 0.85 | | | |
| **Before EC 40** | Nitrogen [g/m²] | Nitrogen [%DM] | Chlorophyll [g/m²] a | b | a+b | Chlorophyll [mg/g] a | b | a+b |
| $NDVI_{TM}$ | 0.91 | 0.70 | 0.91 | 0.67 | 0.85 | | 0.69 | |
| $hNDVI$ | 0.91 | 0.72 | 0.92 | 0.67 | 0.87 | | 0.71 | |
| $CAI$ | 0.87 | | 0.91 | 0.75 | 0.87 | | 0.73 | |
| $OSAVI$ | 0.94 | 0.74 | 0.92 | 0.82 | 0.87 | | 0.70 | |
| **After EC 40** | Nitrogen [g/m²] | Nitrogen [%DM] | Chlorophyll [g/m²] a | b | a+b | Chlorophyll [mg/g] a | b | a+b |
| $NDVI_{TM}$ | | | | | | | | |
| $hNDVI$ | | | | | | | | |
| $CAI$ | | | 0.70 | | | | | |
| $OSAVI$ | | | | | | | | |

Table 5-16: Significantly high coefficients of determination (r²>0.67) for the maize cultivar Narval

| All phenological stages | Nitrogen [g/m²] | Nitrogen [%DM] | Chlorophyll [g/m²] a | b | a+b | Chlorophyll [mg/g] a | b | a+b |
|---|---|---|---|---|---|---|---|---|
| $NDVI_{TM}$ | 0.79 | | 0.85 | | 0.82 | | | |
| $hNDVI$ | 0.78 | | 0.87 | | 0.84 | | | |
| $CAI$ | 0.84 | | 0.88 | | 0.86 | | | |
| $OSAVI$ | 0.79 | | 0.88 | | 0.85 | | | |
| **Before EC 40** | Nitrogen [g/m²] | Nitrogen [%DM] | Chlorophyll [g/m²] a | b | a+b | Chlorophyll [mg/g] a | b | a+b |
| $NDVI_{TM}$ | 0.94 | 0.71 | 0.97 | 0.81 | 0.85 | | 0.69 | |
| $hNDVI$ | 0.94 | 0.72 | 0.97 | 0.81 | 0.88 | | 0.71 | |
| $CAI$ | 0.95 | 0.60 | 0.92 | 0.72 | 0.87 | | 0.75 | |
| $OSAVI$ | 0.97 | 0.74 | 0.97 | 0.82 | 0.87 | | 0.71 | |

## 5.5.4.3 Grassland

For the grassland sites, no correlation could be found for either nitrogen or chlorophyll. This is mainly caused by the parameter values, which lie beyond the saturation limits. When the sample size includes all meadows (N=67), a large number of values (30 to 51)

lie beyond the particular saturation limit. The values are summarised in Table 5-17 and also the correlation plot in Figure 5-21 illustrates this phenomenon very well. The saturation levels for grassland are comparable to those of wheat and maize and correspond to index values of about 0.8 to 0.9. When only values within the range of sensitivity are considered, significant but weak correlations could be derived for chlorophyll a and total content per area with $CAI$ (r²=0.51 and 0.58, respectively). The other indices were still uncorrelated.
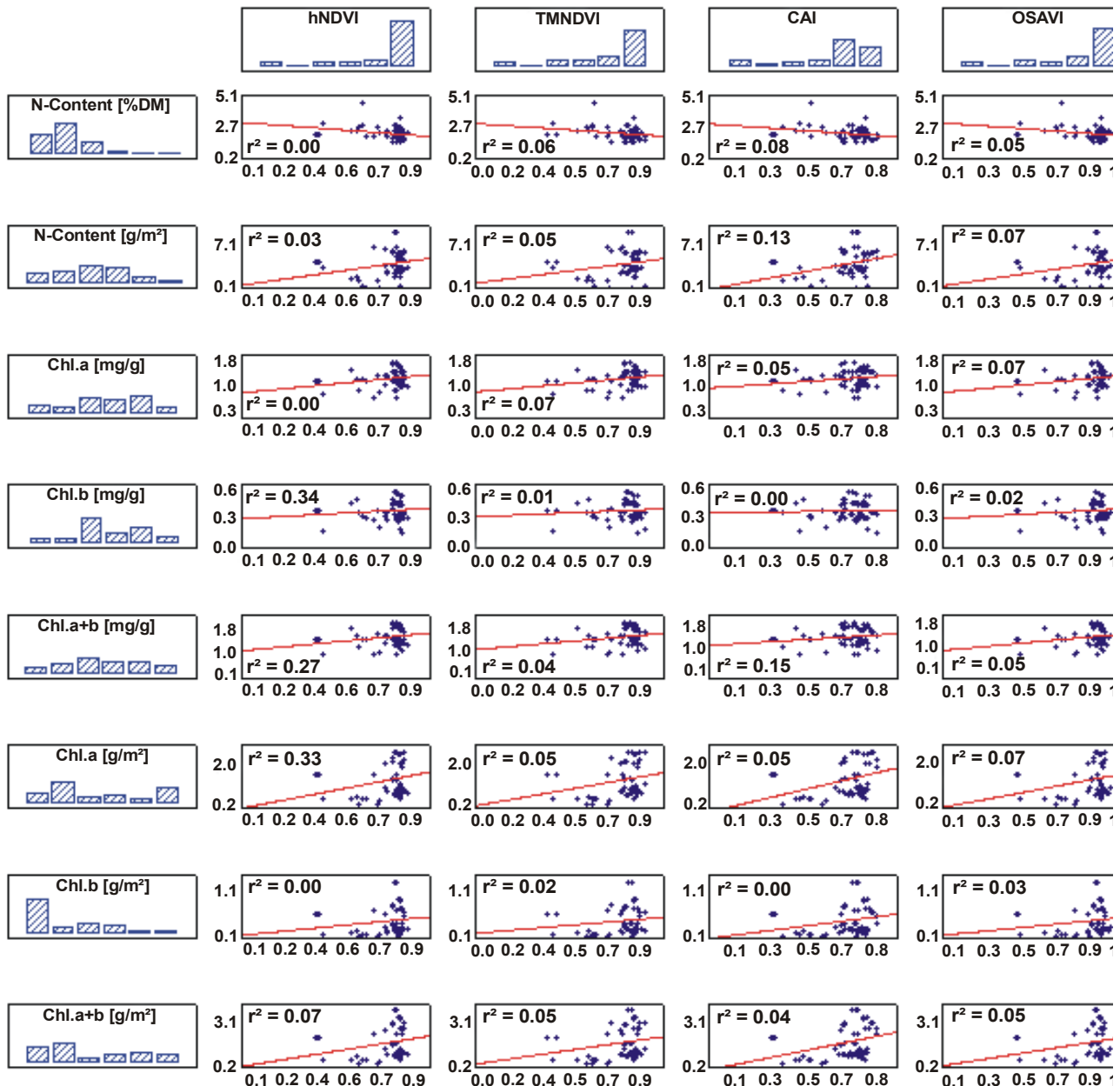


Figure 5-21:   Linear correlations between indices and chlorophyll/nitrogen content for grassland derived from field and AVIS measurements in 1999 and 2000

Table 5-17: *Significantly high coefficients of determination (r²≥0.67) for the meadow No.223 with four to five cuts*

| Field No. 223 | Nitrogen | | Chlorophyll [mg/m²] | | | Chlorophyll [µg/g] | | |
|---|---|---|---|---|---|---|---|---|
| | [g/m²] | [%DM] | a | b | a+b | a | b | a+b |
| *NDVI$_{TM}$* | | | | | | | | |
| *hNDVI* | | | | | | | | |
| *CAI* | | | 0.76 | 0.76 | 0.77 | | | |
| *OSAVI* | | | | | | | | |

When the meadows were investigated individually, sufficiently high correlations (r²>0.67) result for the intensely used meadow No.223, which is cut four to five times per year. There, the *CAI* is highly correlated with the chlorophylls per area (see Table 5-17). This is most probably caused by the fact that, except for No.223, all meadows include at least 50% of the sample values that lie beyond the saturation limits. The meadow with rotational grazing showed the highest ratio: at least 79% of the values exceed the limits. The remaining range of values was too small to form a representative sample. With meadow No.223, at most 40% of the nitrogen per area values exceed the saturation level.

The results could not be improved when polynomial or exponential instead of linear regression equations were used.

Table 5-18: *Parameter values with respect to the particular saturation limit derived for the grassland sites (Std=standard deviation)*

| | Mean | Std. | Saturation Limit (SL) | Values exceed SL | Values within SL |
|---|---|---|---|---|---|
| N [%DM] | 2.36 | 0.63 | approx 2.5 | 43 | 24 |
| N [g/m²] | 4.54 | 2.52 | approx 4.0 | 30 | 37 |
| Chl.a [mg/g] | 1.29 | 0.29 | approx 1.5 | 15 | 52 |
| Chl.b [mg/g] | 0.39 | 0.09 | approx 0.4 | 29 | 38 |
| Chl.a+b [mg/g] | 1.68 | 0.36 | approx 1.9 | 25 | 42 |
| Chl.a [g/m²] | 1.49 | 0.89 | approx 1.0 | 49 | 18 |
| Chl.b [g/m²] | 0.69 | 0.39 | approx 0.2 | 51 | 16 |
| Chl.a+b [g/m²] | 1.99 | 1.14 | approx 1.0 | 51 | 16 |

## 5.5.5    Discussion of the Results

The results of the derivation of both chlorophyll and nitrogen content of plants using different spectral indices derived from hyperspectral data depend strongly on the a priori knowledge of the canopies monitored. In general, the use of contents per area rather than contents per mass has been found to be more suitable for the investigated remote sensing

applications. These results are in accordance with Pinar & Curran (1996) and Datt (1998), who found the content per area to be a better representative for the amount of matter interacting with radiation per unit surface area. Table 5-19 identifies which of the spectral approaches investigated is most closely related to pigment content when only the plant species (maize or wheat) is known. The spectral approach and the regression model depend on the parameter investigated. The $CAI$ was found to be the most suitable approach for the estimation of chlorophyll content, especially per area, for both wheat and maize while the $hNDVI$ and $OSAVI$ enabled a good estimation of the chlorophyll content per mass of wheat. The most important criterion for the good results of the $CAI$ is the fact that this approach seems to be less insensitive at high chlorophyll contents and therefore reaches saturation at higher contents. This feature also enables its good prediction of the nitrogen content per mass of wheat, while it also became insensitive to the nitrogen content per area below values of 2.5g/m². For maize, the $CAI$ enables the estimation of the chlorophyll content per area. The other indices become insensitive for chlorophyll a contents higher than 1g/m² and 1.5mg/g. For the grassland canopies, no approach was able to fulfil the required preconditions (p<0.05, r²≥0.67, Fisher transformation).

Table 5-19: *Spectral approaches having the strongest relationship to pigment content on the basis of the coefficient of determination for wheat and maize canopies without consideration of the cultivar or phenological stage (- = no significant correlation could be derived)*

| Wheat | Chl.a | Chl.b | Chl.a+b | N |
|---|---|---|---|---|
| Content per area [m⁻¹] | | | | |
| Spectral approach | $CAI$ | - | $CAI$ | - |
| Regression model | y=-1.1368+3.818x | | y=-1.4461+4.8856x | |
| r² | 0.71 | | 0.68 | |
| Content per mass [g⁻¹] | | | | |
| Spectral approach | $hNDVI$ | - | - | $CAI$ |
| Regression model | y=-0.7187+2.8801x | | | y=-0.0643+4.3384x |
| r² | 0.67 | | | 0.72 |
| **Maize** | **Chl.a** | **Chl.b** | **Chl.a+b** | **N** |
| Content per area [m⁻¹] | | | | |
| Spectral approach | $CAI$ | - | $CAI$ | $OSAVI$ |
| Regression model | y=-0.966+4.1217x | | y=-1.1832+4.8613x | y=-2.5124+11.529x |
| r² | 0.81 | | 0.80 | 0.89 |
| Content per mass [g⁻¹] | | | | |
| Spectral approach | - | - | - | - |
| Regression model | | | | |
| r² | | | | |

Compared to the hyperspectral indices, the simulated $NDVI_{TM}$ showed the worst results for different land covers. $NDVI_{TM}$ was highly correlated with several pigment contents, but in each case the hyperspectral indices showed higher coefficients of determination. The

$NDVI_{TM}$ also became insensitive to high chlorophyll contents, as previously described by Datt (1998).

The saturation limits of the indices for wheat nitrogen have been found at 4% and 2.5g/m². The results improved when the sample sizes were limited to values, which did not exceed the saturation limits. The coefficients of correlation could not be improved using exponential instead of linear regression equations.

Higher correlations were attained when the cultivars or the phenological stage (before/after the emergence of the ear) were differentiated during the analysis, but the best results were obtained when both the cultivar and the phenological stage were known previously. The cultivar influenced the relationship between the indices and the pigment contents via its chlorophyll and nitrogen level, which may differ between the varieties. The fact that the mixture of cultivars Bristol and Korus could not be correlated significantly with any approach supports this observation. The cultivars investigated in this thesis differ in both chlorophyll and nitrogen content. The cultivar Bussard, which is dark-green coloured, is characterised by high levels of chlorophyll and nitrogen, especially during vegetative growth. This leads to a transgression of the saturation limits of the spectral derived values, resulting in poor results of pigment estimation before EC 40 (see Appendix 4). The ground measurements of the light green-coloured cultivar Capo include few values, which exceed the saturation limits. Therefore the chlorophyll and nitrogen contents could be estimated over the whole vegetation period. Thereby the $CAI$ was found to be most suitable for the retrieval of nitrogen contents as well as for the chlorophyll content per area. The chlorophyll content per mass showed best results using the $hNDVI$ for the cultivar Bussard and the $CAI$ for the cultivar Capo.

The maize results also depend on the a priori knowledge of the cultivar and its phenological stage. The $OSAVI$ was found to be most suitable for the derivation of nitrogen contents. The regression equations are given in Appendix 4. The chlorophyll content per area can be estimated using the $CAI$, $hNDVI$ or the $OSAVI$. The coefficients of determination are similar for all these approaches. The chlorophyll content per mass could not be estimated because of distinct variations, especially of chlorophyll a, which are due to temperature variations. The sampling on ground, which was not carried out simultaneously to the airborne measurements, in this case could not provide adequate validation measurements.

The results demonstrate that the optimal spectral approach for the pigment derivation is species-dependent, but also dependent on the cultivar. The chlorophyll and nitrogen level of the observed maize plants as well as their temperature sensitivity mainly causes this dependence. The investigated indices become insensitive for chlorophyll contents above about 1g/m² (1.5mg/g) chlorophyll a and 0.2g/m² (0.4mg/g) chlorophyll b, respectively. A saturation of the indices was also found for nitrogen contents above 2.5g/m². The saturation limit of nitrogen in percentage of dry matter could be rated at about 4%. The

positive correlation between the indices and this parameter for wheat lead to insensitivity at values higher this limit, while the negative correlation for maize results in saturation for values below 2.5%. The occurrence of saturation was previously observed by Blackburn (1998) and Datt (1998) with several approaches investigating Eucalyptus leaves. In fact, the *CAI* seems not to be affected by saturation as much as the other spectral indices, leading to higher coefficients of determination, especially for contents per area. The high correlations of the *CAI* and parameter per area can be ascribed to the fact that the *CAI* is based on an integral measurement over an area. Therefore the *CAI* can be used as preferred tool for the derivation of the photosynthetic capacity or productivity of a canopy with reasonable accuracy even when only the observed plant species is known.

In contrast, the chlorophyll contents per mass, which indicate the plant's physiological status or level of stress, are estimated more accurately using spectral indices such as *hNDVI* and *OSAVI*, especially for wheat. The weak correlations derived for maize are caused by its temperature dependence, leading to daily variations in the chlorophyll content per mass.

The correlations of the spectral indices with the nitrogen content, which represents the yield potential of a canopy, result in a species-dependent choice of approach. The nitrogen content of wheat showed best results using the *CAI*, while for maize the *OSAVI* was found most suitable. For both species, the separation into the vegetative and generative growing period is necessary for the derivation of the nitrogen content per mass. These results are in accordance with the observations of the chlorophyll and nitrogen content of the canopies described in section 5.2.4. There the chlorophyll and nitrogen contents per mass were only correlated when the phenological stage was considered. In contrast, chlorophyll and nitrogen content per area were highly correlated for all investigated land covers. Thus, the quality of the chlorophyll-nitrogen correlation is coupled with the quality of the derivation of both chlorophyll and nitrogen with hyperspectral approaches. The index, which was found to be most suitable for the derivation of chlorophyll content, could also be applied for the derivation of nitrogen.

The chlorophyll and nitrogen contents of the grassland canopies could not be derived with the spectral indices investigated. Although all meadows could be attributed to the same plant community (*Arrhenatherion elatioris*), they were affected by different intensities of utilisation. When the meadows were investigated separately, correlations could only be found between the *CAI* and the chlorophyll content per area for the meadow No.223 (four to five cuts). The poor potential of the investigated approaches can be mainly assigned to the following reasons: firstly, correlations between grassland chlorophyll and nitrogen could only be observed for contents both per area. Secondly, the chlorophyll and nitrogen values of the meadows mostly exceed the saturation limits of the applied indices. Only the *CAI* was highly correlated with the chlorophyll content per area of meadow No.223, which on the one side is characterised by the highest level of fertilisation, but on the other side

is affected by the highest nutrient offtake by mowing. Moreover, frequent mowing also leads to a relatively low level of chlorophyll per area resulting in a high correlation with the $CAI$, which is not influenced by saturation as much as the other indices.

# 6 Spatial Distribution of Chlorophyll and Nitrogen Content within a Wheat Canopy

The spectral indices, which were found to be most suitable for the estimation of the pigment content in section 5.5.4 are now used to derive the spatial distribution of the chlorophyll and nitrogen contents within a field of winter wheat. In this case of a Bussard canopy the *CAI* was used for the derivation of chlorophyll content per area and nitrogen content per area and per mass. The *hNDVI* was used to derive the chlorophyll content per mass.

The following section includes the description of the field and the measurements that were carried out during the vegetation period 2000. The comparison between measured chlorophyll and nitrogen on the ground and *CAI* and *hNDVI* contents derived from AVIS measurements will be discussed as well as the comparison between their spatial pattern and the yield measurements.

## 6.1 Ground Truth and AVIS Measurements

Field No.400 (Bussard), which was investigated in 2000, was chosen for this analysis. Figure 6-1 presents a survey of the test field including the dimensions and the sampling points.
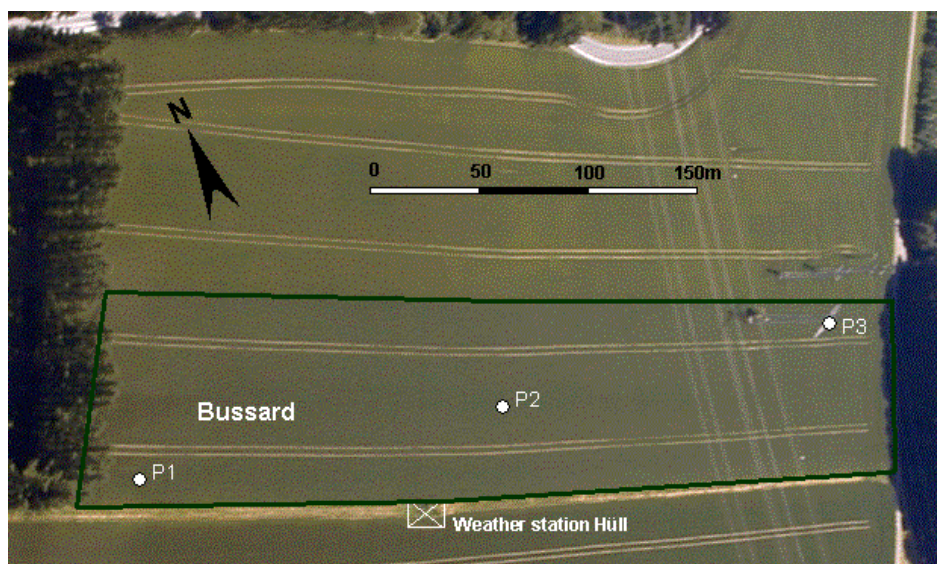


Figure 6-1:        Photograph of the test field No.400 taken during the AVIS overflight on 2$^{nd}$ June 2000

This field was selected because of the extensive data base available:
1.      Schlagkartei data are available.
2.      GPS-based yield measurements are available.

3.  Each sampling point was analysed separately for chlorophyll and nitrogen content. This enables at least three validation points per field for the spatially distributed index values.
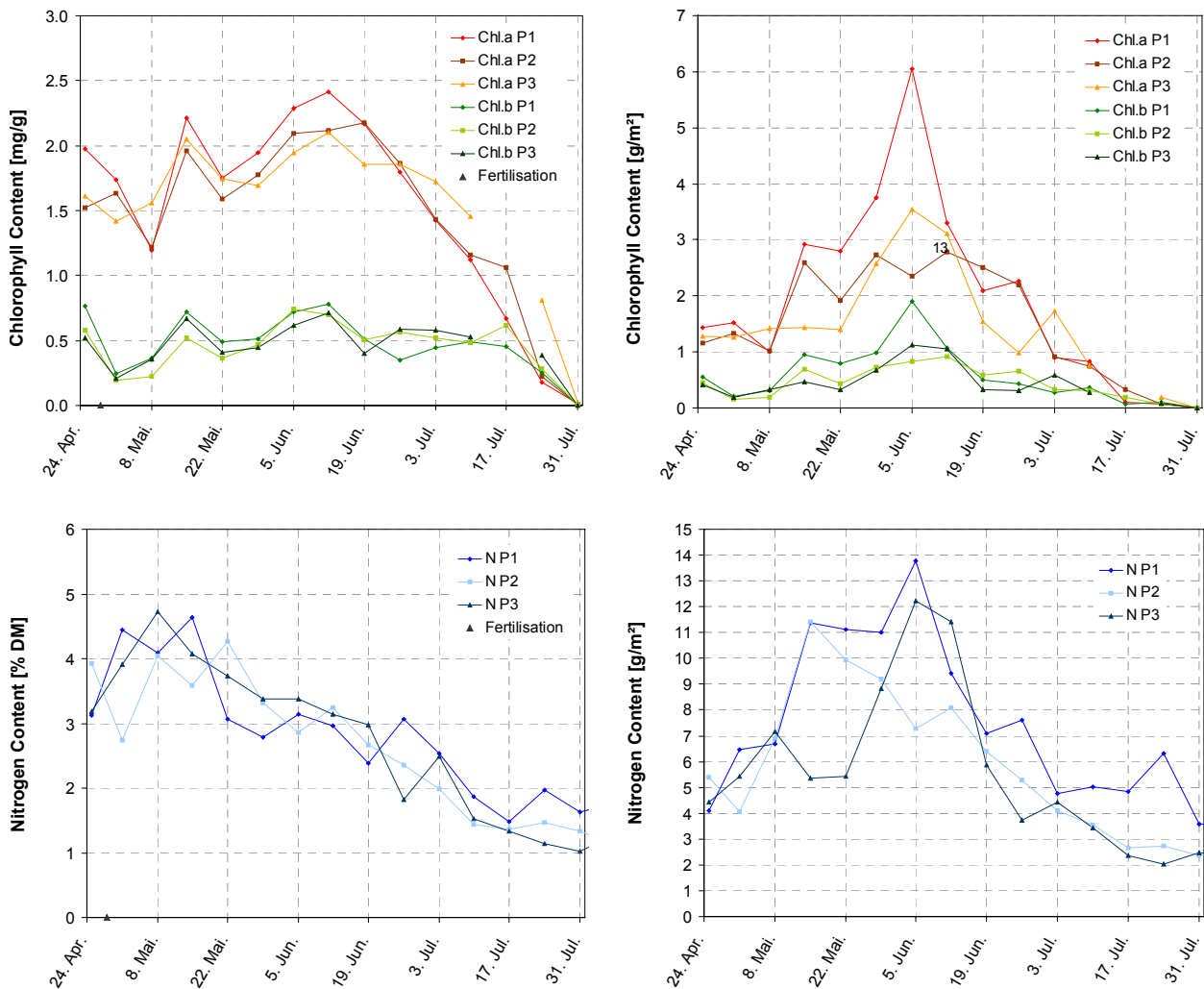


*Figure 6-2:*     *Development of the chlorophyll and nitrogen content within field No.400, cultivar Bussard, derived from field measurements in the year 2000*

The development of the chlorophyll and nitrogen contents, which were measured at the sampling points P1, P2 and P3 during the ground truth campaign in 2000, is presented in Figure 6-2. Chlorophyll and nitrogen contents show a comparable trend within the vegetation period with deviations of up to 0.7%DM nitrogen and 0.7mg/g chlorophyll a. This corresponds to variations of 27% of the chlorophyll content per mass and 61% of the nitrogen content per mass of the plant leaves. The contents per area show higher variations of up to 2.5g/m² chlorophyll a and 6g/m² nitrogen, which corresponds to 58% and 47% respectively. This gives an estimate of the variability of these parameters within the field.

Figure 6-3 illustrates the measurements that were carried out during the measurement campaign in 2000. The ground measurements were carried out weekly from the end of April (EC 37) to the beginning of August, at which time the field was harvested (11th August). During this time period seven AVIS measurements were conducted, where the field was covered. Three of the AVIS overpasses (3rd May, 9th May and 15th May) cover the time period of stem elongation and booting, which is an important phase for the yield (see also section 3.4.1).
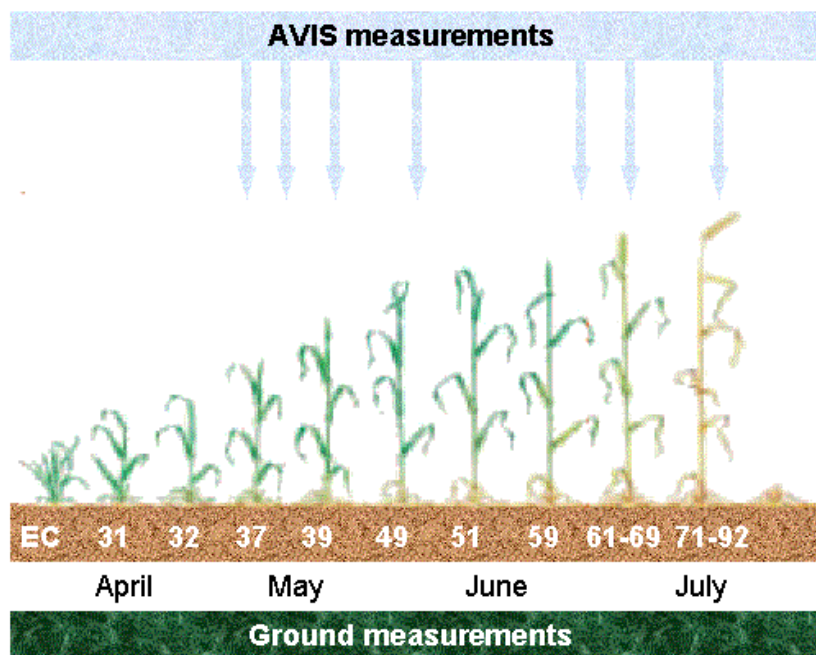


*Figure 6-3:      Campaign calendar for the wheat fields No.400 (Bussard) in the year 2000*

The fourth AVIS overflight was conducted on 2nd June during the emergence of the inflorescence, where the plants reach their maximum chlorophyll content per area. The fifth AVIS flight was carried out when the inflorescence had fully emerged (10th June) and the plants began to flower. At this time the leaves began to wither and the chlorophyll content per area decreased, but the chlorophyll per mass still increased until the beginning of milk development, which was covered with the AVIS overflight on 20th June. The last AVIS measurement (22nd July) was carried out during dough development, when chlorophyll and nitrogen contents of the leaves decreased constantly.

## 6.2 Hyperspectral Approaches Used for the Derivation of Chlorophyll and Nitrogen within the Field

The hyperspectral indices that showed the best results for the parameter retrieval in section 5.5.4 were used to calculate the chlorophyll and nitrogen content of the plants at three sampling points in field No.400. These measurements were not used for the derivation of the average field values, which were sampled separately. The following sections discuss the results of the comparison of calculated parameter values with field measurements at the three sampling points. The discussion includes parameter retrieval for chlorophyll a content per area and mass as well as nitrogen content per area and mass.

The position of the sampling points was not measured with GPS, therefore the comparison of measured and calculated values must be carried out on the basis of the analyst's visual judgement.

### 6.2.1    Chlorophyll a Content per Area

The *CAI* showed the highest coefficient of determination (r²=0.74) for the retrieval of the chlorophyll a content for the wheat sample as well as for the cultivar Bussard. The chlorophyll a content per area was calculated using the following equation, which resulted for the cultivar Bussard without consideration of the phenological stage:

$$Chl.a = -1.578 + 5.0163 \cdot CAI \qquad (6.1)$$

where
$Chl.a$        chlorophyll a content [g/m²].

Figure 6-4 presents the results of the comparison at the three sampling points. All plots show significantly high correlations (P1: r²=0.68, P2: r²=0.81, P3: r²=0.84) between measured and calculated parameter values. A high consistence can be observed at low and medium contents, where the deviation lies within the range of the standard error of the measurements. The *CAI* becomes insensitive at chlorophyll a levels higher than 2.5g/m². This behaviour can be observed at the first sampling point P1, which shows high measured chlorophyll contents in June, whereas the calculated values decrease. Filella & Penuelas (1994) supposed a saturation of the chlorophyll absorption effect for well-fertilised pepper and bean canopies. The indices *NDVITM*, *hNDVI* and *OSAVI* are ratios and therefore more affected by an increase of the reflectance in the RED at high chlorophyll contents. The *CAI* is less sensitive to the flattening and narrowing of the absorption feature, because an increase of the reflectance in the RED also results in an increase of the green reflectance peak, which is also integrated into the *CAI* measurement. It is possible that the *CAI* becomes insensitive from that point where the narrowing of the absorption feature leads to a shift of the red edge position towards

shorter wavelengths. The combination of these processes leads to a decrease of the integral area and thus of the *CAI*. This saturation limit could not be observed when the total wheat sample was investigated, because parameter values above 2.5g/m² rarely occurred (see also Figure 5.19).

The *CAI* turned out to be a good estimator for the chlorophyll content per area for the cultivar Bussard. In contrast to the other indices investigated, which become insensitive at contents higher than 1g/m² (see section 5.5.4.1), the *CAI* can be used for chlorophyll contents up to 2g/m². For chlorophyll contents above this level the *CAI* also becomes saturated.
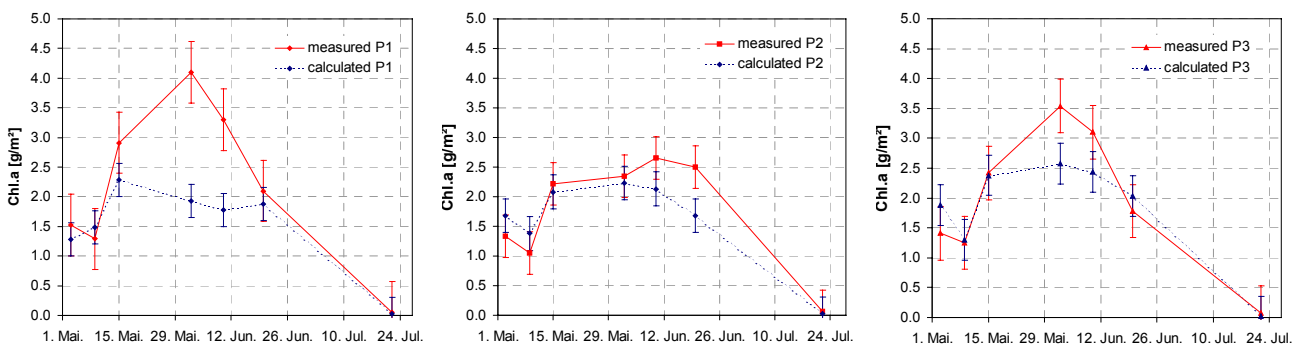


Figure 6-4:    Measured and calculated chlorophyll a content per area with rmse for field No.400 in the year 2000 (rmse=root mean square error)

### 6.2.2    Chlorophyll a Content per Mass

The results of section 5.5.4.1 showed, that the *hNDVI* was highly correlated with chlorophyll a and total chlorophyll content per mass (see also Table 5.10). The regression equation used was derived for the cultivar Bussard without consideration of the phenological stage:

$$Chl.a = -0.7268 + 3.037 \cdot hNDVI$$

(6.2)

where

*Chl.a*     chlorophyll a content [mg/g].

The measured and calculated values have a comparable trend throughout the year with high coefficients of determination (P1: r²=0.71, P2: r²=0.79, P3: r²=0.88). Figure 6-5 presents the results graphically. Especially for chlorophyll contents below 2mg/g, the measured and calculated values lie within the range of their standard errors. The *hNDVI* becomes saturated at higher chlorophyll contents, where the deviations between the measurements exceed the range of the standard errors. In contrast to the total wheat sample, where the saturation limit was rated at 1.5mg/g, the limit for the Bussard canopy can be fixed at 1.5-2mg/g.

The calculated content decreases above the saturation limit, although the measured content continues to increase. The possible reason may be a flattening of the absorption, as already mentioned in the previous section.

In this case, the *hNDVI* turned out to be a good estimator for the chlorophyll content per mass, especially below 1.5-2mg/g. The differences between the sampling points could be reproduced within the range of the standard error of the measurements.
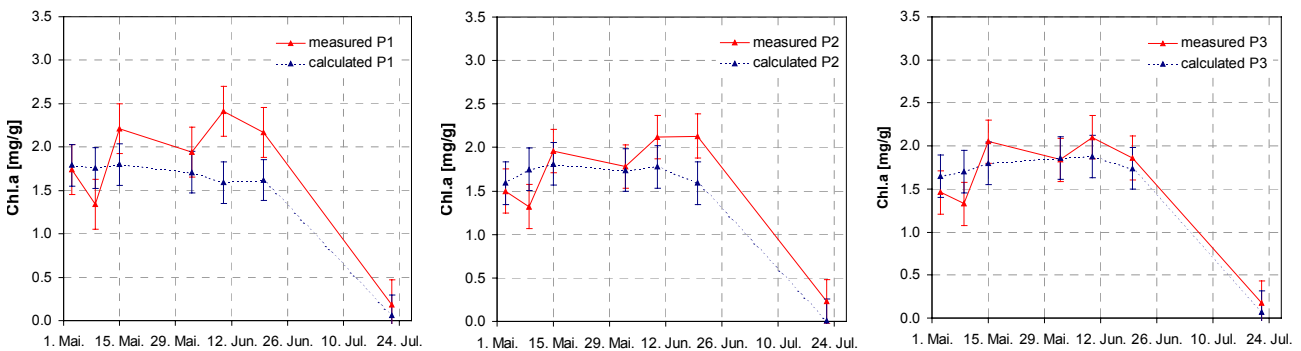


Figure 6-5:    Measured and calculated chlorophyll a content per mass with rmse for field No.400 in the year 2000

### 6.2.3    Nitrogen Content per Area

The correlation between the spectral indices and the nitrogen content per area in section 5.5.4.1 indicates that the indices become saturated at nitrogen contents above 2.5g/m². Only the *CAI* seemed to be unaffected by saturation. Therefore the *CAI* is used for the derivation of the nitrogen content per area according to equation (6.3), which was optimised for the cultivar Bussard, but does not take the phenology into consideration.

$$N = -0.8184 + 10.814 \cdot CAI$$

(6.3)

where

$N$          nitrogen content [g/m²].

The results of the three sampling points, which are presented in Figure 6-6, indicate that a saturation limit also exists, although on a higher level. This saturation limit can be rated at about 8g/m² of nitrogen. The measured and calculated values agree with the range of their standard errors for nitrogen content below that level. Deviations of up to 4.45g/m², which correspond to a difference of 60% of the measured value, occur at high nitrogen levels above 8g/m². This results in a relatively poor correlation of measured and calculated values for sampling point 1 ($r^2=0.52$), which is characterised by high measured nitrogen values at three days out of seven. The other sampling points show higher coefficients of determination (P2: $r^2=0.66$, P3: $r^2=0.68$).
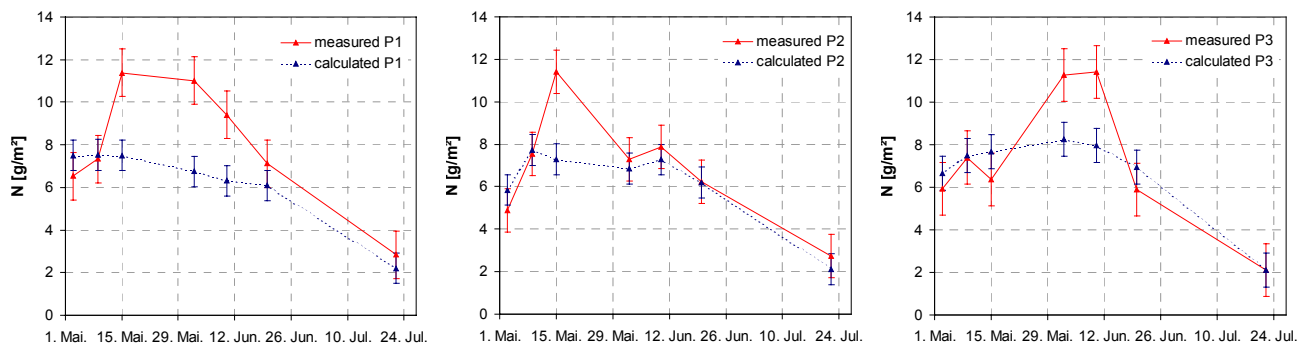
Figure 6-6:    Measured and calculated nitrogen content per area with rmse for field No.400 in the year 2000

The *CAI* is a good descriptor of the nitrogen content per area before it becomes insensitive. This saturation level can be rated at about 8g/m² of nitrogen. Compared to the other indices investigated, this is an improvement of 320%. Comparable to the chlorophyll contents, the insensitivity of the *CAI* above the saturation level is probably caused by a flattening of the absorption depth in the RED as and/or a blue shift of the red edge position.

### 6.2.4    Nitrogen Content per Mass

The *CAI* emerged as the only index investigated in section 5.5.4.1 that showed a significantly high correlation with the nitrogen content per mass. Therefore it is used for the estimation of this parameter at the three sampling points of field No.400. The regression equation chosen is optimised for the cultivar Bussard, but does not consider the phenological stage of the plants:

$$N = -0.1179 + 4.4592 \cdot CAI \qquad\qquad (6.4)$$

where

$N$          nitrogen content [%DM].

Figure 6-7 presents the results for the measured and calculated nitrogen values. Similar to the other parameters, the calculated values correspond well to the measured values below a saturation limit. For the nitrogen content per mass this limit is rated at about 4% nitrogen. The coefficient of determination of the sampling points differs depending on the nitrogen level. The first plot, which is characterised by the highest nitrogen level, shows the lowest coefficient of correlation ($r^2$=0.68). The measured and calculated values are highly correlated at plot 2 ($r^2$=0.97), where the measurements never exceed the saturation limit. Plot 3 lies in the centre with $r^2$=0.73.
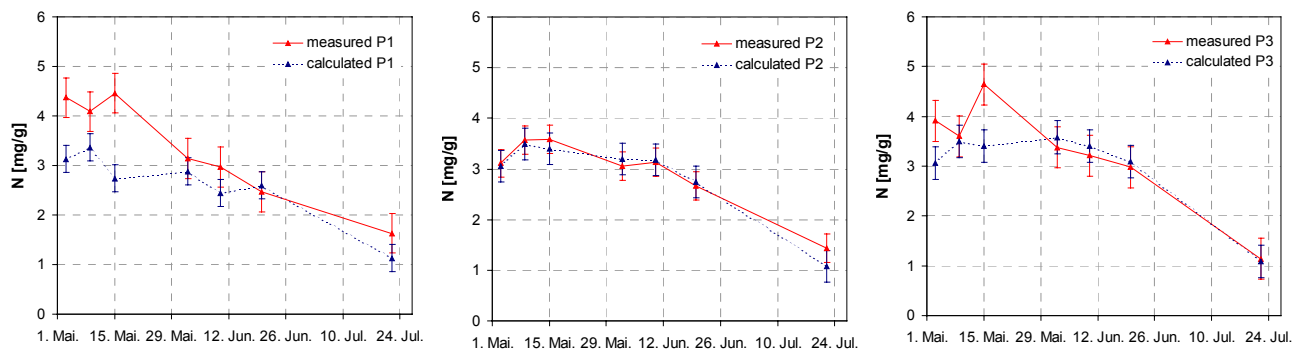
Figure 6-7:    *Measured and calculated nitrogen content per mass with rmse for field No.400 in the year 2000*

The $CAI$ turned out to be a good predictor for the nitrogen content per mass of this field as it is highly correlated with the measured parameter values. Saturation occurs at nitrogen levels beyond 4% of the dry matter. This limit was also found when the total wheat sample was investigated.

## *6.3 Spatial Patterns of Nitrogen within the Field*

The nitrogen content of plants is an important parameter for the field based agricultural management. When nitrogen supply surpasses vegetation's nutritional needs, the excess is leached leading to pollution of the ground water. This nitrogen loss represents also an economic loss for farmers. Inappropriate reduction of nitrogen can result in reduced yields and subsequently substantial economic losses. This dilemma can be overcome by the optimal and rational assessment of nitrogen status and its variability in agriculturally used areas.

As shown in the previous section, the *CAI* can be used to estimate the chlorophyll and nitrogen contents accurately for low and medium contents. This enables the differentiation of areas with different nitrogen contents within a field.

The nitrogen status of the wheat leaves can be estimated using the $CAI$. In this case the nitrogen per area was calculated using equation (6.3). Therefore the nitrogen images of field No.400 that were derived from AVIS measurements in the year 2000 are used to discuss the capability of these images for both yield prediction and the spatial patterns within the field.

Figure 6-8 presents the spatial pattern of nitrogen derived from the $CAI$ analysis of the AVIS overpasses. The images have been geometrical corrected as far as possible, but distortions due to roll motions of the aircraft could not be eliminated. Thus the images do not have exactly the same shape and may include blurred areas, which is especially conspicuous in the image for the 10th June. The yield measurement for this field in 2000 is shown as a reference for the nutrient supply.

The nitrogen-pattern images and the yield map could not be arranged in a pile to calculate correlations between the images. This is due to the remaining geometric distortions of the nitrogen images. Thus the comparison of the images can only be performed visually.

The nitrogen-pattern image of 3rd May was acquired during stem elongation (EC 37). The spatial pattern is comparable to the yield map: nitrogen pattern and yield show an increase from the southern to the northern part of the field. The brighter coloured headlands at the southern and northern edges can also be noticed. The brighter colour indicates a reduced development of the plants; this is caused by the turning manoeuvres of the tractor at the edges of the field leading to compacted soil, which reduces the plant development.

The nitrogen image of 9th May shows a higher level as well as a more balanced distribution of nitrogen. Especially the northern headland can be marked well. The field was fertilised on this day resulting in a superimposition over the whole image of wheel track patterns. The plants that grow in between the fairway of the wheels are bent leading

to a reduced growth and phenological development. This can be seen in the image as bright green coloured lines.
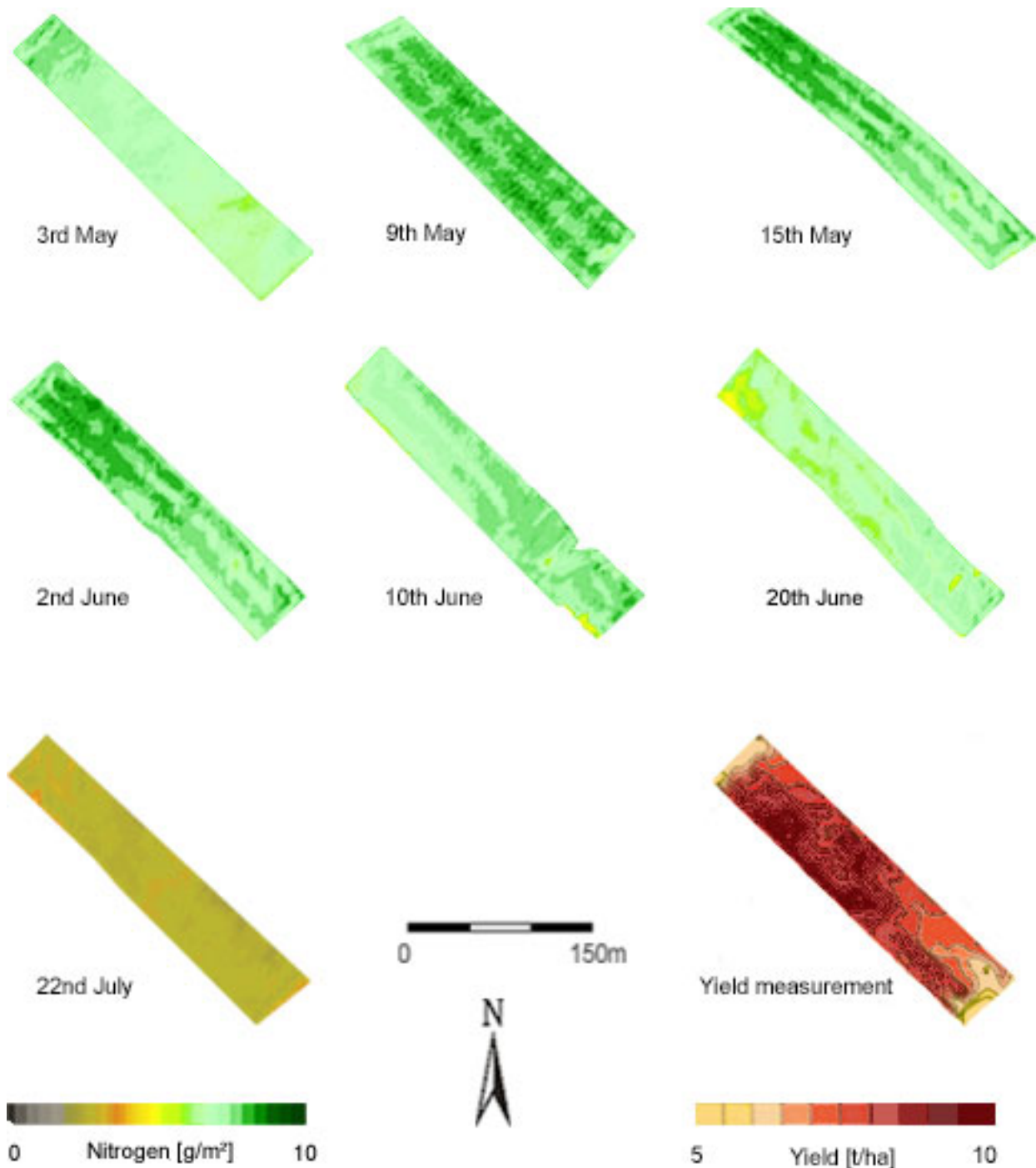


Figure 6-8:       CAI images derived from AVIS measurements in 2000 and yield measurement map of wheat field No.400

On May 15$^{th}$  the main proportion of the plants is still in the stage of stem elongation (EC 39). The wheel tracks are still noticeable in the nitrogen image, but the nitrogen pattern becomes apparent again. The nitrogen content increases from south to north and the

headlands are conspicuous. A yellow spot appears around the pylon at the south-east edge of the field indicating both a lack of vegetation at the pylon and a reduced development around it.

The nitrogen pattern of 2nd June is very similar to that of the 15th May, but the hue is darker. The wheel tracks are more faded and brighter coloured. The features such as the pylon and the headlands can also be seen at this phenological stage during the emergence of the inflorescence (EC 50).

The next image was acquired on the 10th June, when most of the inflorescences were fully emerged and the plants began to flower (EC 59-61). Now the hue pattern is inverted: the plants in the northern part began to flower resulting in a decrease of nitrogen, whereas the plants of the southern part had not reached this phenological stage leading to a relatively high nitrogen content. This fact can also be seen in Figure 6-6. From this time the nitrogen pattern images no longer represent the nutritional status, but indicate the stage of maturity.

The nitrogen pattern of 20th June even more represents the increasing maturity of the plants, but indicates the same phenomenon as in the image of the 10th June. The plants in the northern part can be assigned to the beginning of the milk development, where the grains begin to harden and the nitrogen content of the leaves decrease steeply (see also Figure 6-6). The plants in the southern part of the field were still flowering.

The 22nd July is characterised by a homogeneous brown hue, which indicates a low nitrogen level. All plants can be assigned to the dough developmental stage, where the leaves are withered. The nitrogen content of the leaves remained between 2 and 3g/m², which can be ascribed to structural leaf nitrogen.

To draw the conclusions for the temporal monitoring, the most suitable acquisition time for the derivation of the nutritional status of the plants are during the stem elongation of the plants. The patterns in the nitrogen pattern images enable the differentiation of areas with different nutritional status during these development stages. Moreover, the crop condition at these early stages of growth determine yield. Therefore it is mandatory to provide farmers with nitrogen status at those stages in order to supply appropriate rates of fertiliser based on an accurate assessment of plant growth requirements and deficiencies.

Different stages of maturity within a field can be observed with nitrogen images after anthesis. The areas where mature leaves dominate are characterised by a lower nitrogen content compared to areas with earlier phenological stages. This may be helpful to determine the most favourable date for harvest.

# 7   Summary and Outlook

Airborne hyperspectral remote sensing enables not only spatial monitoring of vegetation cover, but also the derivation of individual plant constituents such as chlorophyll and nitrogen content. These are important parameters for optimised agricultural management on a field basis through the possibility of spatially differentiated fertilisation and for hydrological and vegetation yield modelling.

The use of existing airborne imaging spectrometers is cost-intensive. Moreover, it is difficult to obtain these sensors for multitemporal applications. The imaging spectrometer AVIS (**A**irborne **V**isible/Near **I**nfrared Imaging **S**pectrometer) was built at the Chair of Geography and Geographical Remote Sensing of the Ludwig Maximilians University Munich, Germany, to overcome these difficulties. AVIS is designed as a cost-effective tool for environmental monitoring using commonly available components. AVIS enables the deployment of a hyperspectral sensor for both scientific research and educational purposes. It is based on a direct sight spectrograph coupled to a standard B/W CCD camera. The signal received by the CCD is read out and sent via a frame grabber card to a personal computer, where the data is stored on the hard disc together with additional GPS data. The radiometric, spectral and geometric properties of AVIS resulting from the calibration procedure are summarised in Table 7-1.

*Table 7-1:   AVIS characteristics*

| Parameter | Description |
| --- | --- |
| Spectral range | 553-999nm |
| Spectral resolution | 6nm |
| Spectral sampling rate / resampling | 2nm / 6nm |
| Number of used bands | 74 |
| SNR | 45dB (year 1999), 47dB (year 2000) |
| Spatial resolution | 300 pixels per image line |
| Spatial sampling rate | 390 pixels per image line |
| FOV | 1.19rad |
| IFOV across track | 3.1mrad |
| IFOV along track | 2.98mrad |

One aim of this thesis was to test the potential of AVIS for the purpose of environmental monitoring, especially of the chlorophyll and nitrogen status of plants. The land cover types under investigation were grassland, maize (*Zea mays L.*) and winter wheat (*Triticum aestivum L.*). Within this scope, a total of 21 AVIS flights were carried out during the vegetation periods of the years 1999 and 2000. The AVIS data were preprocessed before

analysis, including dark current and flat field correction, resampling as well as atmospheric correction and reflectance calibration.

The test area chosen for the validation of the AVIS data is located in the northern Bavarian foothills, 25km southwest of Munich, Germany (48° 6' N, 11° 17' E). It is situated between the Ammersee in the west and the Starnberger See in the east. The municipalities Gilching and Andechs define the northern and southern borders respectively.

Within this area, three water protection areas were chosen as test sites. In these test sites, most of the farmers are under contract to the local agricultural office "*Amt für Landwirtschaft*" resulting in detailed management data for each field. This data include useful information for the interpretation of ground and AVIS data. Two weather stations of the Bavarian network of agro-meteorological stations, namely No.72 (Gut Hüll) and No.80 (Rothenfeld), are located in the test area and provide information about precipitation, temperature and radiation. Ten and thirteen stands were selected as test fields in 1999 and 2000 respectively, including three fields each of maize and wheat in 1999 as well as three fields of maize and six fields of wheat in 2000. During both years, four meadows were investigated belonging to the same plant community (*Arrhenatherion elatioris*). The meadows differ in the utilisation intensity (non-fertilised meadow with one cut, meadow with one cut, meadow with rotational grazing and meadow with four to five cuts).

The ground truth campaigns included weekly measurements of plant parameters, such as height, dry and wet biomass, phenological stage, chlorophyll and nitrogen content, as well as a photographic documentation for each field.

The chlorophyll and nitrogen measurements, which were derived from the sampling on ground, are available in contents per area [g/m²] and in contents per mass ([mg/g] for chlorophyll and [%DM] for nitrogen). The former can be used to evaluate the photosynthetic capacity or productivity of a canopy, which is an important input parameter for hydrological or vegetation models; the latter may be an indicator for plant physiological status or level of stress, which is a valuable source of information for optimising field management.

The relationship between chlorophyll and nitrogen based on the ground measurements showed that a differentiation of the land cover types is necessary for significant correlation. When the plant species are investigated separately, the chlorophyll and nitrogen content per area are always highly correlated, especially for chlorophyll a and total chlorophyll content ($r^2 \geq 0.8$). For all investigated land cover types, the nitrogen and chlorophyll contents per mass are uncorrelated. For wheat, the results improve when the phenological state and the cultivar are considered ($r^2 > 0.67$). For maize, distinct variations in the chlorophyll content per mass during the vegetation period reduced correlation with

these parameters. The use of a fitted chlorophyll trend curve instead of the original measurements does not lead to a significant improvement of the results.

For grassland, no significant correlation above r²=0.67 could be observed except for chlorophyll and nitrogen, both per area, where a decreasing strength of correlation could be monitored with increasing fertilisation level.

These results lead to the conclusion that the chlorophyll and nitrogen contents per mass of the investigated land covers are decoupled when the compensation point for effective photosynthesis is exceeded. Beyond this limit the nitrogen in the plants is no longer incorporated into chlorophylls, but mainly into proteins, alkaloids and nucleic acids, whereas the proteins especially are used for internal storage of nitrogen.

The derivation of the chlorophyll and nitrogen content of the plant leaves on a mean field basis was conducted using three hyperspectral spectral approaches, namely the hyperspectral NDVI ($hNDVI$), the Optimised Soil Adjusted Vegetation Index $OSAVI$ as well as the relatively unknown Chlorophyll Absorption Integral $CAI$. The multispectral $NDVI_{TM}$ was simulated as established reference.

The results of the derivation of both chlorophyll and nitrogen content of plants with the investigated approaches depend strongly on a priori knowledge about the canopies monitored. In general, the use of contents per area rather than contents per mass has been found more suitable for the investigated remote sensing applications.

A significant correlation between any index and the chlorophyll or nitrogen content for the whole sample size could not be derived. The optimal spectral approach for derivation is species-dependent, but also dependent on the cultivar. The chlorophyll and nitrogen level of the plants under observation as well as their temperature sensitivity mainly caused this dependence. The $NDVI_{TM}$, $hNDVI$ and $OSAVI$ became insensitive for high chlorophyll content above about 1g/m² (1.5mg/g) chlorophyll a and 0.2g/m² (0.4mg/g) chlorophyll b, respectively. A saturation of the indices was also found for nitrogen content above 2.5g/m². The saturation limit of nitrogen in percentage of dry matter could be rated at about 4%. The positive correlation between the indices and this parameter for wheat leads to insensitivity at values above this limit, while the negative correlation for maize results in saturation for values below 2.5%.

The $CAI$ is not affected by saturation as much as the other spectral approaches, leading to higher coefficients of determination, especially for contents per area. The $CAI$ becomes insensitive at chlorophyll contents per area above 2g/m². The results lead to the assumption, that the flattening and narrowing of the chlorophyll absorption feature at 680nm most probably causes the saturation of the $NDVI_{TM}$, $hNDVI$ and $OSAVI$. The ratios are directly affected by an increase in reflectance in the red wavelength region. The high correlations between the $CAI$ and contents per area can be ascribed to the fact that the $CAI$ is based on an integrated measurement over an area and therefore is less affected by

an increase of reflectance in the red wavelengths. The *CAI* probably becomes insensitive at the point where the narrowing of the absorption feature leads to a shift of the red edge position towards the blue wavelength region. This saturation limit lies at approximately 2g chlorophyll per m².

In contrast, the chlorophyll content per mass, which indicates the plant's physiological status or level of stress, could be estimated more accurately using spectral indices such as *hNDVI* and *OSAVI*, especially for wheat. The low correlations derived for maize are caused by its higher temperature dependence, leading to daily variations in the chlorophyll content per mass.

The chlorophyll and nitrogen contents of the grassland canopies could not be derived with the spectral approaches investigated. When the meadows were investigated separately, correlations could only be found between the *CAI* and the chlorophyll content per area for the most intensely utilised meadow (four to five cuts), which on the one side is characterised by the highest level of fertilisation, but on the other side is affected by the highest nutrient offtake. The low potential of the investigated indices can be mainly assigned to the fact that the chlorophyll and nitrogen values of the meadows mostly exceeded the saturation limits of the applied indices.

The possibility of deriving chlorophyll and nitrogen accurately enough to map within field heterogeneities was discussed on the basis of a wheat field, which was analysed separately at three sampling points for chlorophyll and nitrogen content. The approaches found to be most suitable for the parameter estimation of wheat were applied. The *CAI* was used for the estimation of the chlorophyll content per area and mass as well as for the nitrogen content per area. The *hNDVI* was applied to estimate the canopy's nitrogen content per mass. Both approaches were able to reproduce the chlorophyll contents of the different sampling points accurately enough to derive the differences between the measurement points when the saturation limits were not exceeded. Beyond these limits the index values decreased with increasing measurement values.

The spatial pattern of the nutrient supply was discussed by comparing nitrogen pattern images, which were derived from *CAI* measurements acquired in 2000 with the yield measurement map of the same field. The phenological stage of stem elongation (EC 30) turned out to be most suitable for the derivation of the nitrogen pattern. On the one hand, the crop condition at these stages determine yield and on the other hand the nitrogen pattern images were able to map the inner field patterns of nitrogen supply. After anthesis the nitrogen images can map areas with different degrees of maturity. Therefore they can be used for the monitoring of maturity stages for the determination of the most favourable harvest date.

As described here, AVIS is still in its early stages. It has the potential to become a cost-effective tool for the monitoring of the environment. A modification of AVIS, namely

AVIS2, which covers the spectral range of 400-900nm, has been in commercial use since 2001.

# 8.  Zusammenfassung

Die Arbeit mit hyperspektralen Fernerkundungssensoren ermöglicht nicht nur eine flächenhafte Aufnahme der Vegetationsdecke, sondern vor allem auch die Beurteilung des phänologischen und gesundheitlichen Zustandes der Pflanzen. Dies geschieht über die Ableitung einzelner Pflanzeninhaltsstoffe, wie z. B. Chlorophyll und Stickstoff, beides bedeutende Parameter für ein optimales Feldmanagement. Daneben spielen diese Pflanzeninhaltsstoffe eine bedeutende Rolle als Inputparameter für hydrologische und pflanzenkundliche Modelle.

Da sich derzeit noch keine operationell arbeitenden, satellitengestützten Spektrometer im Orbit befinden, beschränkt sich die flächenhafte Anwendung von hyperspektralen Fernerkundungssensoren auf den Einsatz flugzeuggetragener Spektrometer. Die Arbeit mit kommerziellen Sensoren, wie AVIRIS, DAIS, HYMAP oder ROSIS, ist aber mit einem hohen finanziellen Aufwand verbunden. Eine für das Vegetationsmonitoring erforderliche multitemporale Anwendung wird sowohl durch die hohen Kosten als auch durch die limitierte Verfügbarkeit dieser Systeme erschwert. Diese Einschränkungen gaben am Institut für Geographie der Ludwig-Maximilians-Universität München den Anlass für die Entwicklung und den Bau eines institutseigenen flugzeuggetragenen abbildenden Spektrometers. Das vorrangige Ziel dabei war ein kostengünstiges System für Forschung und Lehre. Diese Vorgaben führten zur Entwicklung des flugzeuggetragenen abbildenden Spektrometers AVIS (Airborne Visible/near Infrared imaging Spektrometer).

Diese Arbeit beschäftigt sich sowohl mit der Kalibrierung als auch dem Einsatz von AVIS im Rahmen eines von der Deutschen Forschungsgemeinschaft DFG geförderten Projektes „Bestimmung des Stickstoffgehaltes von Vegetation – ein Beitrag zur deutschen BAHC Forschung" (DFG MA 875 6).

Die Kalibrierung von AVIS beinhaltet eine Beschreibung des Aufbaus mit den daraus resultierenden radiometrischen, spektralen und geometrischen Eigenschaften des Systems: AVIS ist ein Zeilenscanner, d.h. eine Bildzeile repräsentiert eine Aufnahme. Durch die Bewegung des Sensors über der Erdoberfläche hinweg entsteht durch die Aneinanderreihung mehrerer Aufnahmen ein Bildstreifen. Der Kern von AVIS ist ein *direct sight* Spektrograph, der zwischen ein Objektiv und eine Standard schwarz-weiß Videokamera montiert ist. Das einfallende Licht wird im Objektiv gebündelt und passiert dann den Spektrographen, wo es entlang einer spektralen Achse in verschiedene Wellenlängen dispergiert wird. Im Fall von AVIS wird für jeden Bildpunkt einer Zeile die spektrale Information in 240 einzelnen Wellenlängen oder Kanälen abgebildet. Die Information wird auf dem CCD der Videokamera als elektrische Ladung registriert und über eine *Frame-Grabber-Karte* auf der Festplatte eines angeschlossenen PCs gespeichert. Die Daten eines an AVIS gekoppelten GPS-Gerätes, wie z.B. geographische Länge und

Breite, Flughöhe über NN und Zeitpunkt der Aufnahme, werden in einem *header* für jede Bildzeile gespeichert.

Die radiometrischen, spektralen und geometrischen Eigenschaften, welche sich aus der Kalibrierung von AVIS ergeben, sind in Tabelle 8-1 zusammengefasst.

*Tabelle 8-1: AVIS Spezifikationen*

| Parameter | Beschreibung |
|---|---|
| Spektralbereich | 553-999nm |
| Spektrale Auflösung | 6nm |
| Spektrale Abtastrate / Resamplingrate | 2nm / 6nm |
| Anzahl verwendeter Kanäle | 74 |
| Signal-Rausch-Verhältnis | 45dB (Jahr 1999), 47dB (Jahr 2000) |
| Räumliche Auflösung | 300 Pixel pro Bildzeile |
| Räumliche Abtastrate | 390 Pixel pro Bildzeile |
| FOV | 1.19rad |
| IFOV across track | 3.1mrad |
| IFOV along track | 2.98mrad |

Der Einsatz von AVIS in der Vegetationsaufnahme, und hier speziell die Bestimmung des Chlorophyll- und Stickstoffgehaltes von Pflanzen, wird anhand drei verschiedener Landnutzungstypen erprobt, nämlich Mais (*Zea mays L.*), (Winter-) Weizen (*Triticum aestivum L.*) und Grünland. Dabei beschränken sich die Untersuchungen auf die Blätter der Pflanzen.

Die Untersuchung der Landnutzungstypen erfolgte während der Vegetationsperioden der Jahre 1999 und 2000 in einem Testgebiet im nördlichen Alpenvorland, 25km südwestlich von München. Das Untersuchungsgebiet erstreckt sich von der Stadt Gilching im Norden bis zur Gemeinde Andechs im Süden. Die westliche bzw. östliche Grenze bilden der Ammersee und der Starnberger See. Innerhalb dieses Untersuchungsgebietes wurden drei Wasserschutzgebiete gewählt, in welchen die Testfelder liegen. Diese Gebiete zeichnen sich dadurch aus, dass die Mehrzahl der Landwirte vertraglich an das örtliche Landwirtschaftsamt gebunden ist. Diese Verträge beinhalten u.a. die genaue Aufzeichnung der Bewirtschaftung im Rahmen der sog. Schlagkartei und stellen damit eine wertvolle Informationsquelle dar. Des weiteren ermöglichen zwei Wetterstationen des Bayerischen agrarmeteorologischen Messnetzes (Nr.72 „Gut Hüll" und Nr.80 „Rothenfeld") die Erfassung der meteorologischer Daten innerhalb des Untersuchungsgebietes in einer stündlichen Auflösung.

Im Jahr 1999 wurden insgesamt zehn Testfelder untersucht, wobei je drei Felder mit Winterweizen (Sorte Bussard) und Mais (Sorte Narval und Sortenmischung Bristol/Korus) einbezogen waren. Im Jahr 2000 wurden sechs Weizenfelder (Sorten Bussard und Capo) und drei Maisfelder (Sorte Magister) untersucht. Außerdem wurden über beide Jahre hinweg vier Felder mit der Nutzung als permanentes Grünland bearbeitet (einschürig ungedüngt, einschürig gedüngt, vier- bis fünfschürig und Mähweide).

Im Laufe der Vegetationsperioden von 1999 und 2000 wurden im Untersuchungsgebiet insgesamt 21 AVIS Überflüge durchgeführt. Dabei wurden die Testgebiete aus einer Höhe von 4000ft bzw. 10000ft über NN erfasst, was bei einer mittleren Geländehöhe von 680m zu einer räumlichen Pixelauflösung von 3 bzw. 10m führt. Vor der quantitativen Auswertung der hyperspektralen Daten mussten die Rohdaten vorprozessiert werden. Dies beinhaltete folgende Korrekturen: a) die Korrektur des Dunkelstromes und den Ausgleich von Inhomogenitäten des CCD's (Flatfield); b) ein Resampling der ursprünglich 240 Kanäle mit einer Abtastrate von 2nm zu einem 80-kanaligem Datensatz mit einer Abtastrate von 6nm, welche der spektralen Auflösung von AVIS entspricht; c) Atmosphärenkorrektur und Reflexionskalibrierung.

Die bodengestützte Geländekampagne beinhaltete wöchentlich durchgeführte Messungen verschiedener Pflanzenparameter wie Höhe des Triebes und der Blätter, feuchte und trockene Biomasse, phänologischer Zustand, Chlorophyll- und Stickstoffgehalt getrennt nach Blatt, Stängel und Frucht. Außerdem wurde jedes Feld zu Dokumentationszwecken wöchentlich fotografiert.

Die Chlorophyll- und Stickstoffgehalte, welche von den bodengestützten Messungen abgeleitet wurden, liegen in Gehalten pro Fläche [g/m²] und in Gehalten pro Masse (bei Chlorophyll [mg/g] und bei Stickstoff [% der trockenen Biomasse]). Mit Hilfe des Gehaltes pro Fläche können Aussagen über die photosynthetische Produktivität oder Kapazität eines Bestandes getroffen werden – ein wichtiger Eingabeparameter für hydrologische oder vegetationskundliche Modelle. Gehalte pro Masse dagegen geben Aufschluss über den physiologischen Zustand der Pflanzen sowie über Auswirkungen von Stress oder Krankheiten – wichtige Informationen für ein optimales Feldmanagement durch den Landwirt.

Der in den Pflanzen befindliche Stickstoff weist im sichtbaren und nahen infraroten Wellenlängenbereich keine spezifischen Absorptions- oder Reflexionsmuster auf. Aufgrund seines engen Zusammenhanges mit dem Pflanzenchlorophyll (jedes Chlorophyllmolekül enthält vier Stickstoffatome) wird sein Gehalt über die Menge des Chlorophylls abgeleitet.

Der erste Teil der Auswertungen beschäftigte sich deshalb mit dem Zusammenhang des Gehaltes an Chlorophyll und Stickstoff in den Blättern. Dabei konnte bei der gemeinsamen Analyse der drei Landnutzungsarten kein signifikanter Zusammenhang zwischen den beiden Parametern gefunden werden. Bei der nach Landnutzungstypen getrennten

Untersuchung konnte ein signifikant hoher Zusammenhang ($r^2 \geq 0.67$) zwischen dem Stickstoff und Chlorophyll gefunden werden, wenn beide Parameter in Gehalten pro Fläche vorliegen. Dabei korreliert insbesondere Chlorophyll a stark mit dem Stickstoffgehalt bei den untersuchten Mais-, Weizen- und Grünlandpflanzen ($r^2 \geq 0.8$). Dagegen konnten bei allen drei Landnutzungstypen keine signifikanten Beziehungen zwischen dem Chlorophyll- und Stickstoffgehalt pro Masse nachgewiesen werden. Im Fall von Weizen verbesserten sich die Ergebnisse nach der Trennung in die unterschiedlichen Sorten ($r^2 \geq 0.67$). Eine Unterscheidung der Wachstumsphasen ergab ebenfalls eine Verbesserung der Ergebnisse, wenn die Zeiten vor und nach der Blüte getrennt untersucht wurden ($r^2 \geq 0.67$).

Die untersuchten Maissorten sind dagegen durch auffällige Schwankungen im Chlorophyllgehalt pro Masse geprägt. Diese Schwankungen werden von den aktuell herrschenden Temperaturen im Untersuchungsgebiet beeinflusst. Der Mais als ursprünglich tropische Pflanze stellt bei Temperaturen unter 15° das Wachstum ein und reduziert seinen Stoffwechsel erheblich, was Auswirkungen auf den Gehalt an aktivem Chlorophyll in den Pflanzen hat. Bei steigenden Temperaturen erholt sich der Stoffwechsel und die Pflanzen beginnen wieder zu wachsen. Diese Erkältungssymptome ebenso wie die Erholungszeiten sind bei den verschiedenen Maissorten unterschiedlich ausgeprägt. Diese Temperaturabhängigkeit führt im Untersuchungsgebiet, in dem während der Sommermonate des öfteren Temperaturen unter 15°C erreicht werden, zu Variationen im Chlorophyllgehalt pro Masse, welche die Beziehung zum Stickstoff vermindern.

Bei der Analyse der Graslandflächen ergab sich, außer bei den oben bereits erwähnten Gehalten pro Fläche, kein signifikanter Zusammenhang zwischen Chlorophyll und Stickstoff.

Die Analyse dieser Resultate führen zu dem Schluss, dass die Stickstoff- und Chlorophyllgehalte pro Masse der untersuchten Landnutzungsarten ab einem bestimmten Level, dem Kompensationspunkt, entkoppelt sind. Dieser Kompensationspunkt wird dann erreicht, wenn das in der Luft enthaltene $CO_2$ limitierend auf die Photosyntheserate wirkt. Wird dieses Limit überschritten, hat ein weiterer Aufbau von Chlorophyllmolekülen keine Erhöhung der Photosyntheserate der Pflanze zur Folge. Eventuell vorhandener pflanzenverfügbarer Stickstoff wird somit nicht mehr für den Einbau in Chlorophylle verwendet, sondern vermehrt für die Synthese von Speicherproteinen genutzt.

Ein weiterer Schwerpunkt dieser Arbeit war die Ableitung des Chlorophyll- bzw. Stickstoffgehaltes der untersuchten Landnutzungsarten mit Hilfe der AVIS-Daten. Dabei wurden mehrere Ansätze verwendet, die auf ihr Potential hinsichtlich der gegebenen Aufgabenstellung überprüft werden sollten. Das Hauptaugenmerk wird auf den im Vegetationsmonitoring relativ unbekannten CAI (*Chlorophyll Absorption Integral*) gelegt. Weitere untersuchte Ansätze betrafen bereits etablierte Indices, wie den OSAVI (*Optimised Soil Adjusted Vegetation Index*) und den hNDVI (*hyperspektraler NDVI*). Der $NDVI_{TM}$ (*Normalised Difference Vegetation Index* für den Landsat TM), der mit Hilfe der

AVIS-Daten simuliert wurde, wurde als Vergleichsmöglichkeit mit einem etablierten multispektralen Ansatz berechnet.

Die Qualität der Ergebnisse der Ableitung des Gehaltes an Chlorophyll und Stickstoff unter Zuhilfenahme der AVIS-Daten hängt stark von dem Vorwissen über die untersuchten Landnutzungstypen ab. Generell können aber mit allen untersuchten Indices Gehalte pro Fläche besser erfasst werden als Gehalte pro Masse.

Die Untersuchung der gesamten Stichprobe ohne Unterscheidung in die einzelnen Landnutzungstypen ergab, dass kein Index in der Lage ist, den Chlorophyll- oder Stickstoffgehalt in signifikanter Weise zu bestimmen. Der optimale Index ist also abhängig von der Landnutzung. Da aber die Pflanzensorten innerhalb der untersuchten Landnutzungen hinsichtlich ihres Chlorophyll- und Stickstofflevels verschieden sind, spielt deren Unterscheidung eine wichtige Rolle für die Qualität der Ergebnisse. Unabhängig von der Landnutzung sind $NDVI_{TM}$, hNDVI und OSAVI insensitiv für hohe Chlorophyll- und Stickstoffgehalte. Die Grenzen für den Einsatz dieser Indices liegen bei einem Blattgehalt von 1g/m² bzw. 1.5mg/g Chlorophyll a sowie 0.2g/m² bzw. 0.4mg/g Chlorophyll b. Das Sättigungslevel für Stickstoff pro Fläche liegt bei 2.5g/m². Im Fall des Stickstoffs pro Masse ergibt die positive Korrelation mit den Indices für Weizen eine Sättigung für Werte oberhalb von 4%. Bei Mais geraten die Indices aufgrund der negativen Korrelation mit dem Flächenstickstoff für Gehalte unter 2.5% in die Sättigung.

Im Vergleich zu den oben genannten Indices zeigt der CAI deutlich größere Gültigkeitsbereiche, insbesondere bei Gehalten pro Fläche. Der CAI zeigt unabhängig von der Landnutzung bei Chlorophyll a eine Sättigung für Gehalte über 2g/m². Das Sättigungslimit für den Stickstoff pro Fläche liegt bei Werten unter 8g/m². Die Ursachen der verschiedenen Sensitivitätsbereiche des $NDVI_{TM}$, hNDVI und OSAVI im Vergleich zum CAI liegen wahrscheinlich in der unterschiedlichen Art der Messung sowie in der Verflachung und Verengung der Chlorophyllabsorption im roten Wellenlängenbereich bei hohen Chlorophyllgehalten. $NDVI_{TM}$, hNDVI und OSAVI basieren auf der Differenzbildung, d.h. bei einer Verflachung der Chlorophyllabsorption werden die Werte dieser Indices sofort beeinflusst. Der CAI dagegen stellt eine Integration über eine Fläche dar, d.h. eine Veränderung der CAI-Werte aufgrund Verflachung der Chlorophyllabsorption kann über den damit verbundenen Anstieg im grünen Wellenlängenbereich abgefangen werden. Erst wenn die Verflachung der Absorption zu einer Verschiebung der *red egde* zu kürzeren Wellenlängen hin führt, gerät auch der CAI in die Sättigung. Der Gehalt an Chlorophyll a, der zu einer Verflachung der Chlorophyllabsorption bei ca. 680nm führt, liegt demnach bei ca. 1g/m² bzw. 1.5mg/g, während eine Verschiebung der *red edge* erst bei Gehalten über 2g/m² einsetzt.

Im Gegensatz dazu zeigt die Ableitung des Chlorophyllgehalts pro Masse bei der Verwendung der Ratio-Indices hNDVI und OSAVI bessere Ergebnisse als der CAI. Insbesondere für Weizen ergeben diese beiden Indices dabei signifikant hohe

Korrelationen. Bei der Untersuchung der Maisfelder konnten keine signifikanten Ergebnisse erzielt werden, was durch die starken Schwankungen im Chlorophyllgehalt pro Masse verursacht wird.

Im Fall des Graslands konnten keine signifikanten Zusammenhänge zwischen den Indices und dem Chlorophyll- und Stickstoffgehalt festgestellt werden. Nur der CAI zeigte signifikant hohe Korrelationen mit dem Chlorophyll a Gehalt pro Fläche der intensiv genutzten 4 bis 5-schürigen Wiese. Das geringe Potential der untersuchten Indices für die Bestimmung des Chlorophyll- und Stickstoffgehaltes lässt sich durch die hohen Stoffgehalte der untersuchten Wiesen begründen, die jenseits der genannten Sättigungslimits liegen.

Zuletzt wird anhand eines Weizenfeldes die flächenhafte Verteilung des Stickstoffs und dessen Zusammenhang mit den Ergebnissen einer GPS-gestützen Erntemessung diskutiert. Die Stickstoffverteilung basiert auf CAI Berechnungen, welche von den AVIS Daten aus Überflügen im Jahr 2000 resultieren. Die Ergebnisse zeigen, dass die so berechnete Stickstoffverteilung gut mit der räumlichen Verteilung der Ernteertrages übereinstimmt. Dabei erweist sich die Phase des Schossens als am besten geeignet für die Ableitung der räumlichen Verteilung des Stickstoffes innerhalb eines Feldes. Die Möglichkeit, die Stickstoffversorgung der Pflanzen innerhalb eines Schlages abzubilden, kann dem Landwirt wertvolle Hinweise auf eine optimale Verteilung von Düngemitteln geben und damit ein verbessertes Feldmanagement ermöglichen.

# 9.  References

Adams, J.D.; Sabol, D.E.; Kapos, V.; Amelida-Filho, R.; Roberts, D.A.; Smith, M.Q.; Gillespie, A.R. (1995): Classification of Multispectral Images based on Fractions of Endmembers: Application to Land-Cover Change in the Brazilian Amazon. Remote Sensing of Environment, Vol.52, pp.137-154.

Andres, G.; Pfeiffer, D. (1955): Erläuterungen zur Hydrogeologischen Übersichtskarte 1:50 000, Blatt Augsburg. Bundesanstalt für Landeskunde, Remagen.

Asner, G.P. (1998): Biophysical and Biochemical Sources of Variability in Canopy Reflectance. Remote Sensing of Environment, Vol.64, pp.234–253.

Bach, H. (1995): Die Bestimmung hydrologischer und landwirtschaftlicher Oberflächenparameter aus hyperspektralen Fernerkundungsdaten. Münchener Geographische Abhandlungen, Reihe B, Band 21.

Bach; H., Mauser, W. (1994): Atmospheric Correction of Hyperspectral Data in Terms of the Determination of Plant Parameters. Proceedings of EUROPTO Series "Recent Advances in Remote Sensing and Hyperspectral Remote Sensing", 27-29 September, Rome, Italy.

Bannari, A.; Morin, D.; Bonn, F. (1995): A Review of Vegetation Indices. Remote Sensing Reviews, Vol.13, pp.95–120.

Baret, F.; Vanderbilt, V.C.; Steven, M.D.; Jaquemoud, S. (1994): Use of Spectral Analogy to Evaluate Canopy Reflectance Sensitivity to Leaf Optical Properties. Remote Sensing of Environment, Vol.48, pp.253–260.

Barkman, J.J.; Doing, H.; Segal, S. (1964): Kritische Bemerkungen und Vorschläge zur quantitativen Vegetationsanalyse. Acta Botanica Nederland, Vol.13, pp.394-419.

Bayerisches Staatsministerium für Ernährung, Landwirtschaft und Forsten (Hrsg.) (1999): Düngung sichert Nachhaltigkeit, Qualität, Ertrag. München.

Blackburn, G.A. (1998): Quantifying Chlorophylls and Carotenoids at Leaf and Canopy Scales: An Evaluation of Some Hyperspectral Approaches. Remote Sensing of Environment, Vol.66, pp.273-285.

Briemle, G.; Eickhoff, D.; Wolf, R. (1991): Mindestpflege und Mindestnutzung unterschiedlicher Grünlandtypen aus landschaftsökologischer und landeskultureller Sicht. Beihefte zu den Veröffentlichungen für

Naturschutz und Landespflege in Baden-Württemberg, Band 60. Karlsruhe.

Camacho-de Coca, F.; Martinez, B.; Gilabert, M.A.; Melia, J. (2001): Hot Spot Signatures in Vegetation Canopies with Varying LAI. Proceedings of the 8th International Symposium "Physical Measurements and Signatures in Remote Sensing", Aussois, France, 8-12 January; pp.303–308.

Campbell, J.B. (1996): Introduction to Remote Sensing. 2nd edition. Taylor & Francis, London.

Card, D.H.; Peterson, D.L.; Matson, P.A.; Aber, J.D. (1988): Prediction of Leaf Chemistry by the Use of Visible and Near Infrared Reflectance Spectroscopy. Remote Sensing of Environment, Vol.26, pp.123–147.

Carlson, T.N.; Ripley, D.A. (1997): On the Relation between NDVI, Fractional Vegetation Cover and Leaf Area Index. Remote Sensing of Environment, Vol.62, pp.244-252.

Chen, H.S. (1997): Remote Sensing Calibration Systems: An Introduction. Deepak Publishing, Hampton.

Costa, C. (1991): Nitrogen Rates and Chlorophyll Content in Maize Leaves. Photosynthetica, Vol.25, No.3; pp.447–450.

Curran, P.J. (1989): Remote Sensing of Foliar Chemistry. Remote Sensing of Environment, Vol.30, pp.271–278.

Datt, B. (1998): Remote Sensing of Chlorophyll a, Chlorophyll b, Chlorophyll a+b, and Total Carotenoid Content in Eucalyptus Leaves.

Demircan, A. (1995): Die Nutzung fernerkundlich bestimmter Pflanzenparameter zur flächenhaften Modellierung der Ertragsbildung und Verdunstung. Münchner Geographische Abhandlungen, Reihe B, Bd.20.

Duchemin, B.; Maisongrande, P.; Dedieu, G.; Leroy, M. (2001): A New Concept to Normalize Bidirectional Effects on Reflectances Derived from Large-Field-Of-View Sensors. Proceedings of the 8th International Symposium "Physical Measurements and Signatures in Remote Sensing", Aussois, France, 8-12 January; pp.309-313.

Ellenberg, H.; Weber, H.; Düll, R.; Wirth, V.; Werner, W.; Paulißen, D. (1991): Zeigerwerte von Pflanzen in Mitteleuropa. Scripta Geobotanica, Vol.18.

Ellenberg, H. (1996): Vegetation Mitteleuropas mit den Alpen in ökologischer Sicht. Ulmer Verlag, Stuttgart.

Ercoli, L.; Mariotti, M.; Masoni, A.; Massantini, F. (1993): Relationship between Nitrogen and Chlrophyll Content and Spectral Properties in Maize Leaves. European Journal of Agronomy, Vol.2, No.2, pp.113–117.

European Space Agency (ESA) (1999): Land-Surface Processes and Interactions Mission. Report for Mission Selection, The Four Candidate Earth Explorer Core Missions, Nordwijk, Netherlands.

Filella, I.; Penuelas, J. (1994): The Red Edge Position and Shape as Indicators of Plant Chlorophyll Content, Biomass and Hydric Status. International Journal of Remote Sensing, Vol.15, No.7, pp.1459-1470.

Franke, W. (1989): Nutzplanzenkunde. Thieme Verlag, Stuttgart, New York.

Geologisches Landesamt (Ed) (1986): Standortkundliche Bodenkarte von Bayern 1:500 000, L7932 Fürstenfeldbruck. München.

Gates, D.M.; Keegan, H.J.; Schleter, J.C.; Weidner, V.R. (1965): Spectral Properties of Plants. Applied Optics, Vol.4, No.1, pp.11–20.

Gausman, H.W. (1974): Leaf reflectance of Near–Infrared. Photogrammetric Engineering & Remote Sensing, No.40, pp.183-191.

Gausman, H.W. (1977): Reflectance of Leaf Components. Remote Sensing of Environment, Vol.6, pp.1–9.

Gerstl, S.A.W: (1988): The Angular Reflectance Signature of the Canopy Hot Spot in the Optical Regime. In: Proceedings of the 4th International Symposium of Signatures in Remote Sensing. Aussois, France, 18-22 January, pp.129–132.

Goetz, A.F.H. (1989): Spectral Remote Sensing in Geology. Asrar, A. (Ed.): Theory and Applications of Optical Remote Sensing. Wiley & Sons Inc., New York.

Goetz, A.F.H.; Heidebrecht, K.B.; Chrien, T.G. (1995): High Accuracy in In-Flight Wavelength Calibration of Imaging Spectrometry Data. In: Summaries of the Fifth Annual JPL Airborne Earth Science Workshop. Jet Propulsion Laboratory, Pasadena, California, Vol.1, pp.67–69.

Goetz, A.F.H.; Heidebrecht, K.B. (1996): Full-Scene, Subnanomenter HYDICE Wavelength Calibration. In: Proceedings of SPIE, Vol.2821, pp.85–92.

Goudie, A. (Ed.) (1994): The Encyclopedic Dictionary of Physical Geography. 2nd edition. T.J. Press, UK.

Graul, H. (1962): Die naturräumlichen Einheiten auf Blatt 180 Augsburg. Naturräumliche Gliederung Deutschlands. Bundesanstalt für Landeskunde und Raumforschung, Bad Godesberg.

Grottenthaler, W. (1980): Geologische Karte von Bayern 1:25000 – Erläuterungen zum Blatt Nr.7833 Fürstenfeldbruck Bayerisches Geologisches Landesamt, München.

Guyot, G.; Baret, F. (1988): Utilisation de la haute resolution spectrale pour suivre l'etat des couverts vegetaux. Proceedings of the 4th International Symposium "Physical Measurements & Signatures in Remote Sensing", 18-22 January, Aussois, France, pp.279-286.

Guyot, G.; Baret, F.; Jacquemoud, S. (1992): Imaging Spectroscopy for vegetation Studies. Toselli, F.; Bodechtel, J. (Eds): Imaging Spectroscopy: Fundamentals and Prospective Applications. Kluwer Academic Publisher, London.

Haboudane, D.; Miller, J.; Tremblay, N.; Zarco-Tejada, P.J.; Dextraze, L. (2002): Integration of Hyperspectral Vegetation Indices for Prediction of Crop Chlorophyll Content for Application to Precision Agriculture. Remote Sensing of Environment, Vol.81, pp.416-426..

HAMAMATSU (1998): C 5999 – IR enhanced CCD Camera-Product specifications.

Hame, T.; Salli, K.; Andersson, K.; Lohi, A. (1997): A New Methodology for the Estimation of Biomass of Conifer-Dominated Boreal Forest Using NOAA AVHRR data. International Journal of Remote Sensing, Vol.18, No.15, pp.3211–3243.

Heyland, K.U. (Ed.) (1996): Spezieller Pflanzenbau. Landwirtschaftliches Lehrbuch. Ulmer, Stuttgart.

Holben, B.N.; Kaufman, Y.J.; Kenall, J.D. (1990): NOAA-11 AVHRR Visible and Near-IR Inflight calibration. International Journal of Remote Sensing, Vol.11, No.8, pp.1511–1519.

Holst, G.C. (1998): CCD Arrays, Cameras, and Displays. 2nd edition. JDC Publishing, Winter Park, Florida, USA.

Hopkins, W.G. (1995): Introduction to Plant Physiology. John Wiley & Sons, New York.

HYLINE (1998): AFUSOFT RAVEN 3–Technical Specifications. HYLINE Communication Products.

Huete, A.R. (1985): Spectral Response of a Plant Canopy with Different Soil Backgrounds. Remote Sensing of Environment, Vol.17, pp.37-53.

Huete, A.R. (1988): Soil Adjusted Vegetation Index (SAVI). Remote Sensing of Environment, Vol. 25, pp.295-309.

Huss, J. (1984): Luftbildmessung und Fernerkundung in der Landwirtschaft. Wichmann, Karlsruhe.

Irons, J.R.; Johnson, B.L.; Linebaugh, G.H. (1987): Multiple-Angle Observations of Reflectance Anisotropy from an Airborne Linear Array Sensor. IEEE Transactions on Geoscinece and Remote Sensing, GE-25 (3), pp.128–137.

Jacobson, A. (2000): Analysing Airborne Optical Remote Sensing Data from a Hyperspectral Scanner and Implications for Environmental Mapping and Monitoring. Phd thesis, National Environmental Research Institute, Denmark.

Jago, R.A.; Cutler, M.E.J.; Curran, P. (1999): Estimating Canopy Chlorophyll Concentration from Field and Airborne Spectra. Remote Sensing of Environment, Vol.68, pp.217-224.

Johnson, L.F.; Billow, C.R. (1996): Spectrometric Measurements of Total Nitrogen Concentration in Douglas-Fir Foliage. International Journal of Remote Sensing, Vol.17, No.3, pp. 489–500.

Kaufman, P.B.; Carlson, T.F.; Dayanandan, P.; Evans, M.L.; Fisher, J.B.; Parks, C.; Wells, J.R. (1989): Plants – their Biology and Importance. Harper & Row, New York.

Kappas, M. (1994): Fernerkundung nah gebracht. Leitfaden für Geowissenschaftler. Dümmler Verlag.Keller, R. (1956): Klima und Hydrologie. Bundesministerium für Wirtschaft, Hydrogeologischer Arbeitskreis (Hrsg.): Hydrogeologische Übersichtskarte 1:500 000, Erläuterungen zu Blatt München.

Kennedy, R.E.; Cohen, W.B.; Takao, G. (1997): Empirical Methods to Compensate for a View-Angle-Dependent Brightness Gradient in AVIRIS Imagery. Remote Sensing of Environment, Vol.62, pp.277–291.

Kerr, Y.H.; Imbernon, J.; Dedieu, G.; Hautcecoeur, O.; Lagouarde, J.; Seguin, B. (1989): NOAA AVHRR and its Use for Rainfall and Evatranspiration Monitoring. Int. Journal of Remote Sensing, Vol.10, pp.847-854.

Klapp, E. (1953): Wiesen und Weiden. Verlag Paul Parey, Berlin.

Kneizys, F.X.; Anderson, G.P.; Shettle, E.P.; Gallery, W.O.; Abreu, L.W.; Selby, J.E.; Chetwynd, J.H.; Clough, S.A.. (1988): LOWTRAN-7. Air Force Geophysics Laboratory. Environmental Research Papers No.1010. Hanscom, Massachusetts.

Köppen, W.; Geiger, R. (1961): Die Klimate der Erde. Darmstadt.

Kühbauch, W. (1991): Artenerkennung und Zustandbeschreibung landwirtschaftlicher Nutzpflanzenbestände mit Fernerkundung. Berichte der Gesellschaft für Informatik in der Land-, Forst- und Ernährungswirtschaft (GIL), Band 1, pp.1–15.

Kuusk, A. (1991): Determination of Vegetation Parameters from Optical Measurements. Remote Sensing of Environment, Vol.37, pp.207–218.

Küchler, A.W.; Zonneveld, I.S. (Eds.) (1988): Vegetation Mapping. Kluwer Academic Publishers, Dordrecht.

Landgrebe, D.A.; Malaret, E. (1986): Noise in Remote Rensing Systems: the Effect on Classification Error. IEEE Transactions on Geoscience and Remote Sensing, Vol.24, pp.294-299.

Leeuwen van, W.J.D.; Huete, A.R. (1996): Effects of Standing Litter on the Biophysical Interpretation of Plant Canopies with Spectral Indices. Remote Sensing of Environment, Vol.55, pp.123–138.

Lemaire, G. (ED.) (1997): Diagnosis of the Nitrogen Status in Crops. Springer.

Lerch, G. (1991): Pflanzenökologie. Akademie Verlag, Berlin.

Leroy, M.; Hautecoeur, O. (1999): Anisotropy-Corrected Vegetation Indices Derived from POLDER/ADEOS. IEEE Transactions on Geosciences and Remote Sensing, Vol.37, No.3, pp.1698–1708.

Liu, Q.; Huete, A. (1995): A Feedback Based Modification of the NDVI to Minimize Canopy Background and Atmospheric Noise. IEEE Transactions on Geoscience and Remote Sensing, Vol.33, pp.457–465.

Ma, B.L.; Malcolm, J.; Morrison, J.; Dwyer, L.M. (1996): Canopy Light Reflectance and Field Greenness to Asses Nitrogen Fertilization and Yield of Maize. Agronomy Journal, Vol.88, pp.915–920.

Mauser, W.; Oppelt, N. (2000): AVIS – ein neuer Sensor für Umweltmonitoring und Precision Farming. Berichte der Gesellschaft für Informatik in der Land-, Forst- und Ernährungswirtschaft, Bd.13, pp.270–277.

Mauser, W.; Oppelt, N. (2001): AVIS – A New Sensor for Environmental Monitoring and Precision Farming. International Workshop on Spectroscopy Application in Precision Farming, 16–18 January, Freising, Germany, pp.41–45.

Meynen, E.; Schmithüsen, J. (1953): Handbuch der naturräumlichen Gliederung Deutschlands. Bundesanstalt für Landeskunde und, Bad Godesberg.

Michler, G. (1994): Die naturräumlichen Einheiten auf Blatt 181 München. Naturräumliche Gliederung Deutschlands. Bundesanstalt für Landeskunde und Raumforschung, Bad Godesberg.

Myneni, R.B.; Ross, J.; Asrar, G. (1989): A Review on the Theory of Photon Transport in Leaf Canopies. Agricultural and Forest Meteorology, Vol.45, pp.1-153.

Myneni, R.B.; Ross, J.; Asrar, G. (1993): A Review of the Theory of Photon Transport in Leaf Canopies. Agricultural and Forest Meteorology, Vol.45, pp.1–153.

Oppelt, N.; Mauser, W. (2000): Der Einsatz der Fernerkundung zur Bestimmung des Stickstoffgehalts von Vegetation am Beispiel Grünland – ein Beitrag zur IGBP/BAHC Forschung in Deutschland. Statusbericht über den Zeitraum Oktober 1998 bis Dezember 1999. Institut für Geographie, Lehrstuhl für Geographie und Geographische Fernerkundung der Ludwig-Maximilians-Universität München.

Oppelt, N.; Mauser, W. (2001a): The Chlorophyll Content of Maize (Zea Mays) Derived with the Airborne Imaging Spectrometer AVIS. 8th International Symposium "Physical Measurements & Signatures in Remote Sensing", 8-12 January, Aussois, France, pp.407–412.

Oppelt, N.; Mauser, W. (2001b): Derivation of the Chlorophyll Content of Maize. International Workshop on Spectroscopy Application in Precision Farming, 16–18 January, Freising, Germany, pp.52–56.

Pellikka, P. (1994): Geometric and Radiometric Corrections for Airborne Video Imagery for Land Cover Classification Applications. Presented at the First Airborne Remote Sensing Conference and Exhibition, Strasbourg, France, 11–15 September.

Peltonen, J.; Virtanen, A.; Haggren, E. (1995): Using a Chlorophyll Meter to Optimize Nitrogen Fertilizer Application for Intensely-Managed Small-Grain Cereals. Journal of Agronomy & Crops, Vol.74, pp.309–318.

Penuelas, J.; Filella, I.; Biel, C.; Serrano, L.; Save, R. (1993): The Reflectance at the 950-970nm Region as an Indicator of Plant Water Status. International Journal of Remote Sensing, Vol.14, No.10, pp.1887–1905.

Peterson, D.L.; Aber, J.D.; Matson, P.A.; (1988): Remote Sensing of Forest Canopy and Leaf Biochemical Contents. Remote Sensing of Environment, Vol.24, pp.85–108.

Piekielek, W.P.; Fox, R.H. (1992): Use of a Chlorophyll Meter to Predict Sidedress Nitrogen Requirements for Maize. Agronomy Journal, Vol.84, pp.59–65.

Pinar, A.; Curran, P.J. (1996): Grass Chlorophyll and the Reflectance Red Edge. International Journal of Remote Sensing, Vol.17, No.2, pp.351–357.

Pommer, Dr. G. (2001): Sortenempfehlungen für ökologisch wirtschaftende Betriebe 2000/2001. Bayerische Landesanstalt für Bodenkultur und Pflanzenbau. http://www.stmlf.bayern.de

Porra, R.J.; Thompson, W.A.; Kriedman, P.E. (1989): Determination of Accurate Extinction Coefficients and Simultaneous Equations for Assaying Chlorophyll a and b Extracted with Four Different Solvents: Verification of the Concentration of Chlorophyll Standards by Atomic Absorption Spectroscopy. Biochemical Biophysical Acta, Vol.975, pp.384–394.

Price, J.C. (1994): How Unique are Spectral Signatures. Remote Sensing of Environment, Vol.49, pp.181-186.

Prince, S.D.; Tucker, C.J. (1986): Satellite Remote Sensing of Rangelands in Botswana. II. NOAA AVHRR and Herbaceous Vegetation. International Journal of Remote Sensing, Vol.7; pp.1555–1570.

Qin, W.; Xiang, Y. (1994): On the Hotspot Effect of the Leaf Canopies: Modelling Study and Influence of Leaf Shape. Remote Sensing of Environment, Vol.50, pp.95–106.

Reader, J.; Corliss, C.H. (Eds) (1976): Line Spectra of the Elements. In: Handbook of Chemistry and Physics. National Bureau of Standards.

Richards, J.A. (1998): Remote Sensing Digital Image Analysis. An Introduction. Third Edition, Springer Verlag, Berlin, Heidelberg.

Riegler, G.; Stolz, R.; Mauser, W. (1998): Geometric and Radiometric Correctio of ERS SAT Data for Biomass Estimation of Meadows in Rugged Terrain. In: Proceedings of the EUROPTO Conference Barcelona, SPIE Proceeding Series, Vol.349, pp.224-235.

Roberts, D.A.; Green, R.O.; Adams, J.B. (1997): Temporal and Spatial Patterns in Vegetation and Atmospheric Properties from AVIRIS. Remote Sensing of Environment, Vol.62, pp.223–240.

Rollin, E.M.; Milton, E.J. (1998): Processing of High Spectral Resolution Reflectance Data for the Retrieval of Canopy Water Content Information. Remote Sensing of Environment, Vol.65, pp.86-92.

Rondeaux, G.; Steven, M.; Baret, F. (1996): Optimisation of Soil-Adjusted Vegetation Indices. Remote Sensing of Environment, Vol. 55, pp.95 – 107.

Roujean, J.L.; Leroy, M.; Deschamps, P.Y. (1992): A Bidirectional Reflectance Model of the Earth's Suface for the Correction of Remote Sensing Data. Journal of Geophysical Research, Vol.97, No.20, pp.455-468.

Rouse, J.W. (1973): Monitoring the Vernal Advancement and Retrogradation of Natural Vegetation. NASA/GSFCT Type II Report, Greenbelt, MD, USA.

Royer, A.; Vincent, P.; Bonn, F. (1985): Evaluation and Correction of Viewing Angle Effects on Satellite Measurements of Bidirectional Reflectance. Photogrammetric Engineering and Remote Sensing, Vol.51, No.12, pp.1899–1944.

Schaepman, M.E.; Schläpfer, D.; Müller, A.; Strobl, P. (1997): Ground Spectroradiometric Measurements in Support of the Validation of the Calibration of Digital Airborne Imaging Spectrometer (DAIS 7915) Data. Presented at the Third International Airborne Remote Sensing Conference and Exhibition, 7-10 July, Copenhagen, Denmark.

Schaepman, M.E. (1998): Calibration of a Field Spectroradiometer. Remote Sensing Series Vol.31. Remote Sensing Laboratories, Department of Geography, University of Zurich.

Schanda, E. (1986): Physical Fundamentals of Remote Sensing. Springer Verlag, Berlin, Heidelberg.

Sandmeier, S.; Müller, C.; Hosgood, B.; Andreoli, G. (1998): Physical Mechanisms in Hyperspectral BRDF Data of Grass and Watercress. . Remote Sensing of Environment, Vol.66, pp.222-233.

Schellberg, J. (1990): Die spektrale Reflexion von Weizen – ein Beitrag zur Zustandsbeschreibung landwirtschaftlicher Kulturpflanzenbestände durch Fernerkundung. Dissertation an der Hohen Landwirtschaftlichen Fakultät der Rheinischen Friedrich-Wilhelms-Universität, Bonn.

Schellberg, J.; Kühbauch, W. (1991): Reflexionsmessungen von Weizenbeständen zum Zwecke der fernerkundlichen Zustandsbeschreibung und Ertragsschätzung. Berichte der Gesellschaft für Informatik in der Land-, Forst- und Ernährungswirtschaft (GIL), Band 1, pp.61-68.

SCHNEIDER (1998): Lens CNG 1.4/8 Data Sheet.

Schönwiese, C.D. (2000): Praktische Statistik für Meteorologen und Geowissenschaftler. Gebrüder Bornträger, Berlin, Stuttgart.

Schowengerdt, R.A. (1997): Remote Sensing: Models and Methods for Image Processing. 2nd ed., Academic Press.

SCHOTT (1999): Filter BG26 Data Sheet.

Schulze, E.D.; Caldwell, M.M. (Eds.) (1995): Ecophysiology of Photosynthesis. Springer Verlag, Berlin.

Sellers, P.J. (1985): Canopy Reflectance, Photosynthesis and Transpiration. International Journal of Remote Sensing, Vol.6, No.8, pp.1335–1372.

Spatz, G. (1994): Freiflächenpflege. Ulmer Verlag, Stuttgart.

SPECTRAL IMAGING LTD (1998a): ImSpector User Manual.

SPECTRAL IMAGING LTD (1998b): ImSpector V9-M-897 – Test Report.

SPECTRAL IMAGING LTD (1998c): ImSpector V9-M-897 – Quantum Efficiency of Spectrograph Grating.

Spectrum Technologies Inc. (2002): Minolta SPAD 502 – Specifications.

StatSoft (2001): STATISTIKA Version 6.0, Kurzeinführung.

Staenz, K.; Secker, J.; Gao, B.C.; Davis, C. (2000): Radiative Transfer Codes Applied to Hyperspectral Data for the Retrieval of Surface Reflectance. Held at the 2nd EARSEL Workshop on Imaging Spectroscopy, Amsterdam.

Stolz, R. (1998): Die Verwendung der Fuzzy Logic Theorie zur wissensbasierten Klassifikation von Fernerkundungsdaten. Münchner Geographische Abhandlungen, Reihe B, Band 26.

Strobl, P.; Müller, A.; Schläpfer, D.; Schaepman, M. (1997): Laboratory Calibration and Inflight Validation of the Digital Airborne Imaging Spectrometer DAIS 7915 for the 1996 Flight Season. Algorithms for Multispectral and Hyperspectral Imagery III, SPIE Vol. 3017, Orlando, 20-25 April.

Takebe, M. (1994): Current Plant Nutrition Diagnosis. Farming Japan, Vol.28, No.6, pp.22–27.

Townshed, J.R.; Justice, C.O. (1986): Analysis of the Dynamics of African Vegetation Using the Normalized Difference vegetation Index. International Journal of Remote Sensing, Vol.7; pp.1435–1445.

Traub, F.; Gerb, L.; Keller, R. (1956): Erläuterungen zur Hydrogeologischen Übersichtskarte 1:500000, Blatt München. Bundesanstalt für Landeskunde, Remagen.

Tucker, C.J. (1979): Red and Photographic Infrared Linear Combinations for Monitoring Vegetation. Remote Sensing of Environment, Vol.9, pp.127–150.

Tucker, C.J.; Sellers, P.J. (1986): Satellite Remote Sensing of Primary Production. Int. Journal of Remote Sensing, Vol.7, pp.1395-1416.

URL1:      Hydro Agri, N-Sensor (Update of 8th March 2002): http://www.hydroprecise.com/html/ger/products/nsensor/nsensor.htm

URL2:      Internet lectures Prof. Mauser (update of 3rd March 2002) modified; http://www. geographie.uni-muenchen.de/iggf/Multimedia/Spektroskopie/as_hauptseite.htm

Vane, G.; Goetz, A.F.H. (1993): Terrestrial Imaging Spectrometry: Current Status, Future Trends. Remote Sensing of Environment, Vol.44, pp.117–126.

Vos, J.; Bom, M. (1993): Handheld Chlorophyll Meter: a Promising Tool to Assess the Nitrogen Status of Potato Foliage. Potato Research, Vol.36, pp.301–308.

Walburg, G.; Bauer, M.E.; Daughtry C.S.T.; Hously, J.E. (1982): Effects of Nitrogen on the Growth, Yield and Reflectance of Corn Canopies. Agronomy Journal, Vol.74, pp.677–683.

Wessman, C.A.; Aber, J.D.; Peterson, D.L.; Melillo, J.M. (1988): Foliar Analysis Using Near Infrared Reflectance Spectroscopy. Canadian Journal of Forestry Research, Vol.18; pp.6–11.

Whelan, P.M.; Hodgson, M.J. (1985): Essential Principles of Physics. John Murray, London.

Whitehead, D.C. (1995): Grassland Nitrogen. CAB International.

Widen, N. (2001): Directionally Independent Spectral Indices. Proceedings of the 8th International Symposium "Physical Measurements and Signatures in Remote Sensing", Aussois, France, 8-12 January; p.265.

Wilson, A.K. (1994): The NERC Integrated ATM/*casi*/GPS system. First International Airborne Remote Sensing Conference and Exhibition, Strasbourg, France, 11-15 September, Vol.II, pp.249–259.

Woledge, J.; Pearse, P.J. (1985): The Effect of Nitrogenous Fertilizer on the Photosynthesis of Leaves of a Ryegrass Sward. Grass and Forage science, Vol.40, pp.305–309.

Wolfe, W.L. (1997): Introduction to Imaging Spectrometers. SPIE Press, Bellingham, Washington, USA.

Wollring, J. (1995): Der Chlorophyllgehalt als Maßstab zur Ermittlung der 2. und 3. N-Gabe bei Winterweizen. Institut für Pflanzenernährung und Umweltforschung Hanninghof, Hydro Agri Deutschland. Unveröffentlicht.

Wood, C.W.; Reeves, D.W.; Duffield, R.R.; Edmisten, K.L. (1992): Field Chlorophyll Measurements for Evaluation of Corn Nitrogen Status. Journal of Plant Nutrition, Vol.15, No.4, pp.487–500.

Wordsworth Editions Ltd. (1995): Dictionary of Science and Technology. Mackays of Chatham PLC., Great Britain.

Yamazaki, J.; Kamimura, Y.; Okada, O.; Sugimura, Y. (1999): Changes In Photosynthetic Characteristics and Photosystem Stoichiometrics in the Lower Leaves in Rice Seedings. Plant Science, Vol.148, pp.155–163.

Yoder, B.J.; Pettigrew-Cosby, R.E. (1995): Predicting Nitrogen and Chlorophyll Content and Concentrations from Reflectance Spectra (400-2500nm) at Leaf and Canopy Scale. Remote Sensing of Environment, Vol.53, pp.199–211.

Zadoks, J.C.; Chang, T.T.; Konzak, C.F. (1974): A Decimal Code for the Growth Stages of Cereals. In: Weed Research, Vol.14, pp.415–421.

# Appendix

## *Appendix 1: AVIS Centre Wavelengths for the 2nm Resampling*

| Band. No | Centre wavelength [nm] | Band. No | Centre wavelength [nm] | Band. No | Centre wavelength [nm] | Band. No | Centre wavelength [nm] |
|---|---|---|---|---|---|---|---|
| 1 | Header | 31 | 612.59 | 61 | 673.86 | 91 | 735.14 |
| 2 | 553.36 | 32 | 614.63 | 62 | 675.91 | 92 | 737.18 |
| 3 | 555.40 | 33 | 616.67 | 63 | 677.95 | 93 | 739.22 |
| 4 | 557.44 | 34 | 618.72 | 64 | 679.99 | 94 | 741.27 |
| 5 | 559.48 | 35 | 620.76 | 65 | 682.03 | 95 | 743.31 |
| 6 | 561.53 | 36 | 622.80 | 66 | 684.08 | 96 | 745.35 |
| 7 | 563.57 | 37 | 624.84 | 67 | 686.12 | 97 | 747.39 |
| 8 | 565.61 | 38 | 626.89 | 68 | 688.16 | 98 | 749.44 |
| 9 | 567.65 | 39 | 628.93 | 69 | 690.20 | 99 | 751.48 |
| 10 | 569.70 | 40 | 630.97 | 70 | 692.25 | 100 | 753.52 |
| 11 | 571.74 | 41 | 633.01 | 71 | 694.29 | 101 | 755.56 |
| 12 | 573.78 | 42 | 635.06 | 72 | 696.33 | 102 | 757.61 |
| 13 | 575.82 | 43 | 637.10 | 73 | 698.37 | 103 | 759.65 |
| 14 | 577.87 | 44 | 639.14 | 74 | 700.42 | 104 | 761.69 |
| 15 | 579.91 | 45 | 641.18 | 75 | 702.46 | 105 | 763.73 |
| 16 | 581.95 | 46 | 643.23 | 76 | 704.50 | 106 | 765.78 |
| 17 | 583.99 | 47 | 645.27 | 77 | 706.54 | 107 | 767.82 |
| 18 | 586.04 | 48 | 647.31 | 78 | 708.59 | 108 | 769.86 |
| 19 | 588.08 | 49 | 649.35 | 79 | 710.63 | 109 | 771.90 |
| 20 | 590.12 | 50 | 651.40 | 80 | 712.67 | 110 | 773.95 |
| 21 | 592.16 | 51 | 653.44 | 81 | 714.71 | 111 | 775.99 |
| 22 | 594.21 | 52 | 655.48 | 82 | 716.76 | 112 | 778.03 |
| 23 | 596.25 | 53 | 657.52 | 83 | 718.80 | 113 | 780.07 |
| 24 | 598.29 | 54 | 659.57 | 84 | 720.84 | 114 | 782.12 |
| 25 | 600.33 | 55 | 661.61 | 85 | 722.88 | 115 | 784.16 |
| 26 | 602.38 | 56 | 663.65 | 86 | 724.93 | 116 | 786.20 |
| 27 | 604.42 | 57 | 665.69 | 87 | 726.97 | 117 | 788.24 |
| 28 | 606.46 | 58 | 667.74 | 88 | 729.01 | 118 | 790.29 |
| 29 | 608.50 | 59 | 669.78 | 89 | 731.05 | 119 | 792.33 |
| 30 | 610.55 | 60 | 671.82 | 90 | 733.10 | 120 | 794.37 |

| Band. No | Centre wavelength [nm] | Band. No | Centre wavelength [nm] | Band. No | Centre wavelength [nm] | Band. No | Centre wavelength [nm] |
|---|---|---|---|---|---|---|---|
| 121 | 796.41 | 151 | 857.69 | 181 | 918.97 | 211 | 980.24 |
| 122 | 798.46 | 152 | 859.73 | 182 | 921.01 | 212 | 982.28 |
| 123 | 800.50 | 153 | 861.78 | 183 | 923.05 | 213 | 984.33 |
| 124 | 802.54 | 154 | 863.82 | 184 | 925.09 | 214 | 986.37 |
| 125 | 804.59 | 155 | 865.86 | 185 | 927.14 | 215 | 988.41 |
| 126 | 806.63 | 156 | 867.90 | 186 | 929.18 | 216 | 990.45 |
| 127 | 808.67 | 157 | 869.95 | 187 | 931.22 | 217 | 992.50 |
| 128 | 810.71 | 158 | 871.99 | 188 | 933.26 | 218 | 994.54 |
| 129 | 812.76 | 159 | 874.03 | 189 | 935.31 | 219 | 996.58 |
| 130 | 814.80 | 160 | 876.07 | 190 | 937.35 | 220 | 998.62 |
| 131 | 816.84 | 161 | 878.12 | 191 | 939.39 | 221 | 1000.67 |
| 132 | 818.88 | 162 | 880.16 | 192 | 941.43 | 222 | 1002.71 |
| 133 | 820.93 | 163 | 882.20 | 193 | 943.48 | 223 | 1004.75 |
| 134 | 822.97 | 164 | 884.24 | 194 | 945.52 | 224 | 1006.79 |
| 135 | 825.01 | 165 | 886.29 | 195 | 947.56 | 225 | 1008.84 |
| 136 | 827.05 | 166 | 888.33 | 196 | 949.60 | 226 | 1010.88 |
| 137 | 829.10 | 167 | 890.37 | 197 | 951.65 | 227 | 1012.92 |
| 138 | 831.14 | 168 | 892.41 | 198 | 953.69 | 228 | 1014.96 |
| 139 | 833.18 | 169 | 894.46 | 199 | 955.73 | 229 | 1017.01 |
| 140 | 835.22 | 170 | 896.50 | 200 | 957.77 | 230 | 1019.05 |
| 141 | 837.27 | 171 | 898.54 | 201 | 959.82 | 231 | 1021.09 |
| 142 | 839.31 | 172 | 900.58 | 202 | 961.86 | 232 | 1023.13 |
| 143 | 841.35 | 173 | 902.63 | 203 | 963.90 | 233 | 1025.18 |
| 144 | 843.39 | 174 | 904.67 | 204 | 965.94 | 234 | 1027.22 |
| 145 | 845.44 | 175 | 906.71 | 205 | 967.99 | 235 | 1029.26 |
| 146 | 847.48 | 176 | 908.75 | 206 | 970.03 | 236 | 1031.30 |
| 147 | 849.52 | 177 | 910.80 | 207 | 972.07 | 237 | 1033.35 |
| 148 | 851.56 | 178 | 912.84 | 208 | 974.11 | 238 | 1035.39 |
| 149 | 853.61 | 179 | 914.88 | 209 | 976.16 | 239 | 1037.43 |
| 150 | 855.65 | 180 | 916.92 | 210 | 978.20 | 240 | 1039.47 |

# Appendix 2: Results of the Botanical Mapping of Grassland

| | Laufende Nummer | 1 | 2 | 9 | 8 | 7 | 3 | 4 | 6 | 5 |
|---|---|---|---|---|---|---|---|---|---|---|
| | Datum | 4.5 | 4.5 | 4.5 | 4.5 | 4.5 | 4.5 | 4.5 | 4.5 | 4.5 |
| | m² | 4 | 4 | 4 | 4 | 4 | 4 | 1 | 4 | 4 |
| | Neigung | 0 | 0 | 0 | 0 | 0 | 0 | 0 | 0 | 0 |
| | Exposition | . | . | . | . | . | . | . | . | . |
| | Höhe NN | | | | | | | | | |
| | Gesamtdeckung (%) | 90 | 95 | 100 | 100 | 100 | 100 | 95 | 100 | 70 |
| | Artenzahl | 11 | 9 | 11 | 14 | 14 | 15 | 11 | 13 | 14 |
| **Faziesbildende Gräser** | | | | | | | | | | |
| OC | Dactylis glomerata | 2a | 2a | . | . | + | 1 | . | 1 | . |
| KC | Alopecurus pratensis | 4 | 3 | 2a | 2m | . | . | . | . | 1 |
| | Poa trivialis | . | . | 1 | 3 | 3 | 2a | . | . | . |
| DV | Bromus hordeaceus | . | . | 3 | 3 | 3 | 3 | 3 | . | . |
| | Lolium multiflorum | 1 | . | . | . | 2a | 1 | 2a | . | . |
| KC | Poa pratensis | . | . | . | . | . | . | . | 4 | + |
| | Lolium perenne | . | . | . | . | . | . | . | 2a | . |
| **Bodenverdichtung/Überdüngung** | | | | | | | | | | |
| | Rumex obtusifolius | + | . | 1 | 2a | . | . | + | . | 2a |
| **Bodenverdichtung/Störung** | | | | | | | | | | |
| | Ranunculus repens | . | . | . | . | . | . | 1 | . | 1 |
| **Störung Bodenverleztzung** | | | | | | | | | | |
| | Cirsium arvense | + | . | . | . | . | . | . | . | . |
| | Trifolium campestre | 2m | 2a | . | . | . | . | . | . | . |
| | Capsella bursa-pastoris | . | . | . | . | + | . | . | . | 1 |
| | Stellaria media | . | . | . | . | . | . | . | 1 | 1 |
| | Glechoma hederacea | . | . | . | . | . | . | . | . | + |
| | Ranunculus ficaria | . | . | . | . | . | . | . | . | 2a |
| **Störung Sonstige** | | | | | | | | | | |
| | Poa annua | . | . | 2a | . | . | . | . | . | 2m |
| | Veronica sepyllifolia | . | . | . | 2m | . | . | . | . | + |
| | Plantago major | . | . | . | . | . | . | . | . | + |
| | Agrosis stolonifera agg. | . | . | . | . | . | . | . | . | + |
| **aus Einsaat** | | | | | | | | | | |
| | Medicago x varia | . | . | . | . | . | 1 | . | . | . |
| **Sonstige Kenn- und Differentialarten** | | | | | | | | | | |
| AC | Arrhenatherum elatius | . | . | . | . | . | + | . | . | . |
| VC | Galium album | + | . | . | . | . | 1 | . | . | . |
| OC | Achillea millefolium | . | . | . | 1 | 2m | . | . | . | . |
| OC | Bellis perennis | . | . | . | + | + | 1 | 1 | 1 | + |
| OC | Trisetum flavescens | . | . | . | . | . | + | . | . | . |
| DO | Heracleum sphondylium | . | . | . | + | . | . | . | + | . |
| DO | Anthriscus sylvestris | . | . | . | + | + | . | . | + | . |
| KC | Trifolium pratense | 2a | 2m | 3 | 2a | 2m | 2a | 2a | 2m | . |
| KC | Taraxacum officinale | 2a | 2a | 2a | 2m | 2a | 2a | 1 | 1 | . |
| KC | Cerastium holosteoides | 1 | 1 | 2m | 2m | 2m | 2a | 1 | 1 | 1 |
| KC | Cardamine pratensis | . | . | . | . | . | . | . | + | . |
| KC | Trifolium repens | . | 3 | . | . | . | . | . | . | . |
| KC | Ranunculus acris | . | . | + | . | . | . | . | . | . |
| KC | Rumex acetosa | . | . | . | . | + | . | . | + | . |
| KC | Holcus lanatus | . | . | . | . | . | 1 | . | . | . |
| **Sonstige Begleiter** | | | | | | | | | | |
| | Festuca rubra | . | 1 | . | . | . | . | . | . | . |
| | Veronica arvensis | 2m | 1 | 2m | 1 | 2m | 2m | 1 | 1 | . |
| | Plantago lanceolata | . | . | 2a | + | + | 2a | . | . | . |
| | Veronica persica | . | . | . | . | . | . | 1 | . | . |
| | Vicia angustifolia | . | . | . | . | . | . | + | . | . |
| **Wertzahl n. Klapp (nach Dominanz gewichtet, gegen Max normalisiert)** | | | | | | | | | | |
| | | 1,0 | 1,0 | 0,8 | 0,7 | 0,7 | 0,8 | 0,7 | 0,8 | 0,5 |
| **Ellenberg-Values** | | | | | | | | | | |
| Reihe 1 | OEK_F (dummy) | 4,9 | 5,0 | 5,6 | 5,3 | 4,9 | 5,1 | 5,1 | 5,0 | 5,7 |
| Reihe 2 | OEK_R (dummy) | 6,4 | 6,0 | 6,0 | 5,7 | 6,5 | 6,8 | 6,7 | 6,7 | 6,3 |
| Reihe 3 | OEK_N (dummy) | 6,3 | 5,7 | 6,6 | 6,5 | 5,9 | 5,6 | 6,1 | 6,7 | 6,8 |
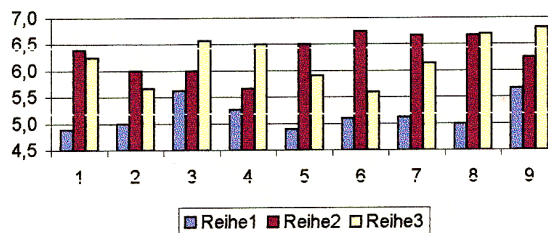
# Appendix 3: Code for "Day Of Year" (DOY) Dates

Note that in leap years "DOY+1" is valid from the 29th February!

| Tag | Januar | Februar | März | April | Mai | Juni | Juli | August | September | Oktober | November | Dezember | Tag |
|-----|--------|---------|------|-------|-----|------|------|--------|-----------|---------|----------|----------|-----|
| 1 | 1 | 32 | 60 | 91 | 121 | 152 | 182 | 213 | 244 | 274 | 305 | 335 | 1 |
| 2 | 2 | 33 | 61 | 92 | 122 | 153 | 183 | 214 | 245 | 275 | 306 | 336 | 2 |
| 3 | 3 | 34 | 62 | 93 | 123 | 154 | 184 | 215 | 246 | 276 | 307 | 337 | 3 |
| 4 | 4 | 35 | 63 | 94 | 124 | 155 | 185 | 216 | 247 | 277 | 308 | 338 | 4 |
| 5 | 5 | 36 | 64 | 95 | 125 | 156 | 186 | 217 | 248 | 278 | 309 | 339 | 5 |
| 6 | 6 | 37 | 65 | 96 | 126 | 157 | 187 | 218 | 249 | 279 | 310 | 340 | 6 |
| 7 | 7 | 38 | 66 | 97 | 127 | 158 | 188 | 219 | 250 | 280 | 311 | 341 | 7 |
| 8 | 8 | 39 | 67 | 98 | 128 | 159 | 189 | 220 | 251 | 281 | 312 | 342 | 8 |
| 9 | 9 | 40 | 68 | 99 | 129 | 160 | 190 | 221 | 252 | 282 | 313 | 343 | 9 |
| 10 | 10 | 41 | 69 | 100 | 130 | 161 | 191 | 222 | 253 | 283 | 314 | 344 | 10 |
| 11 | 11 | 42 | 70 | 101 | 131 | 162 | 192 | 223 | 254 | 284 | 315 | 345 | 11 |
| 12 | 12 | 43 | 71 | 102 | 132 | 163 | 193 | 224 | 255 | 285 | 316 | 346 | 12 |
| 13 | 13 | 44 | 72 | 103 | 133 | 164 | 194 | 225 | 256 | 286 | 317 | 347 | 13 |
| 14 | 14 | 45 | 73 | 104 | 134 | 165 | 195 | 226 | 257 | 287 | 318 | 348 | 14 |
| 15 | 15 | 46 | 74 | 105 | 135 | 166 | 196 | 227 | 258 | 288 | 319 | 349 | 15 |
| 16 | 16 | 47 | 75 | 106 | 136 | 167 | 197 | 228 | 259 | 289 | 320 | 350 | 16 |
| 17 | 17 | 48 | 76 | 107 | 137 | 168 | 198 | 229 | 260 | 290 | 321 | 351 | 17 |
| 18 | 18 | 49 | 77 | 108 | 138 | 169 | 199 | 230 | 261 | 291 | 322 | 352 | 18 |
| 19 | 19 | 50 | 78 | 109 | 139 | 170 | 200 | 231 | 262 | 292 | 323 | 353 | 19 |
| 20 | 20 | 51 | 79 | 110 | 140 | 171 | 201 | 232 | 263 | 293 | 324 | 354 | 20 |
| 21 | 21 | 52 | 80 | 111 | 141 | 172 | 202 | 233 | 264 | 294 | 325 | 355 | 21 |
| 22 | 22 | 53 | 81 | 112 | 142 | 173 | 203 | 234 | 265 | 295 | 326 | 356 | 22 |
| 23 | 23 | 54 | 82 | 113 | 143 | 174 | 204 | 235 | 266 | 296 | 327 | 357 | 23 |
| 24 | 24 | 55 | 83 | 114 | 144 | 175 | 205 | 236 | 267 | 297 | 328 | 358 | 24 |
| 25 | 25 | 56 | 84 | 115 | 145 | 176 | 206 | 237 | 268 | 298 | 329 | 359 | 25 |
| 26 | 26 | 57 | 85 | 116 | 146 | 177 | 207 | 238 | 269 | 299 | 330 | 360 | 26 |
| 27 | 27 | 58 | 86 | 117 | 147 | 178 | 208 | 239 | 270 | 300 | 331 | 361 | 27 |
| 28 | 28 | 59 | 87 | 118 | 148 | 179 | 209 | 240 | 271 | 301 | 332 | 362 | 28 |
| 29 | 29 | 59 | 88 | 119 | 149 | 180 | 210 | 241 | 272 | 302 | 333 | 363 | 29 |
| 30 | 30 | – | 89 | 120 | 150 | 181 | 211 | 242 | 273 | 303 | 334 | 364 | 30 |
| 31 | 31 | – | 90 | – | 151 | – | 212 | 243 | – | 304 | – | 365 | 31 |

## *Appendix 4: Regression Equations of the Spectral Approaches which have the Strongest Significant Relationship with the Chlorophyll and Nitrogen Content for Wheat and Maize*

### Wheat Cultivar Bussard

| All phenological stages | Chl.a | Chl.b | Chl.a+b | N |
|---|---|---|---|---|
| **Content per area [m$^{-1}$]** | | | | |
| Spectral approach | *CAI (=x)* | *CAI (=x)* | *CAI (=x)* | *CAI (=x)* |
| Regression model | y=-1.578+5.0163x | y=-0.3323+1.161x | y=-1.5667+5.317x | y=-0.8184+10.814x |
| r² | 0.74 | 0.73 | 0.83 | 0.76 |
| | | | | |
| **Content per mass [g$^{-1}$]** | | | | |
| Spectral approach | *hNDVI (=x)* | | *hHNDVI (=x)* | *CAI (=x)* |
| Regression model | y=-0.727+2.9016x | | y=-0.9037+3.853x | y=-0.1179+4.4592x |
| r² | 0.71 | | 0.69 | 0.70 |
| Spectral approach | *OSAVI (=x)* | | *OSAVI (=x)* | |
| Regression model | y=-0.6491+2.548x | | y=-0.794+3.236x | |
| r² | 0.71 | | 0.69 | |

| Bussard Beyond EC40 | Chl.a | Chl.b | Chl.a+b | N |
|---|---|---|---|---|
| **Content per area [m$^{-1}$]** | | | | |
| Spectral approach | *CAI (=x)* | *CAI (=x)* | *CAI (=x)* | *CAI (=x)* |
| Regression model | y=-1.3774+4.514x | y=-0.4498+1.431x | y=-1.8255+5.941x | y=-0.8488+10.936x |
| r² | 0.88 | 0.87 | 0.88 | 0.74 |
| | | | | |
| **Content per mass [g$^{-1}$]** | | | | |
| Spectral approach | *hNDVI (=x)* | *hNDVI (=x)* | *hNDVI (=x)* | *CAI (=x)* |
| Regression model | y=-0.9816+3.497x | y=-0.2887+1.049x | y=-1.2693+4.544x | y=0.0397+3.963x |
| r² | 0.82 | 0.78 | 0.82 | 0.68 |
| Spectral approach | *OSAVI (=x)* | *OSAVI (=x)* | *OSAVI (=x)* | |
| Regression model | y=-0.8966+2.959x | y=-0.2683+0.894x | y=-1.1639+3.851x | |
| r² | 0.82 | 0.79 | 0.83 | |

## Wheat Cultivar Capo

| All phenological stages | Chl.a | Chl.b | Chl.a+b | N |
|---|---|---|---|---|
| **Content per area [m$^{-1}$]** | | | | |
| Spectral approach | | | | |
| Regression model | | | | |
| r² | | | | |
| **Content per mass [g$^{-1}$]** | | | | |
| Spectral approach | *hNDVI (=x)* | | *hNDVI (=x)* | *CAI (=x)* |
| Regression model | y=-0.6881+2.27x | | y=-0.8963+2.933x | y=0.0334+4.138x |
| r² | 0.74 | | 0.68 | 0.78 |
| **Before EC40** | Chl.a | Chl.b | Chl.a+b | N |
| **Content per area [m$^{-1}$]** | | | | |
| Spectral approach | *CAI (=x)* | | | |
| Regression model | y=-0.672+2.4267x | | | |
| r² | 0.79 | | | |
| **Content per mass [g$^{-1}$]** | | | | |
| Spectral approach | *CAI (=x)* | | *CAI (=x)* | *CAI (=x)* |
| Regression model | y=-0.7506+2.698x | | y=-0.9491+3.412x | y=-0.2092+4.889x |
| r² | 0.81 | | 0.70 | 0.93 |
| **Beyond EC40** | Chl.a | Chl.b | Chl.a+b | N |
| **Content per area [m$^{-1}$]** | | | | |
| Spectral approach | *CAI (=x)* | *CAI (=x)* | *CAI (=x)* | |
| Regression model | y=-1.6204+4.593x | y=-0.5123+1.409x | y=-2.1325+6.001x | |
| r² | 0.68 | 0.69 | 0.69 | |
| **Content per mass [g$^{-1}$]** | | | | |
| Spectral approach | *CAI (=x)* | *CAI (=x)* | *CAI (=x)* | *CAI (=x)* |
| Regression model | y=-1.0054+3.797x | y=-0.3661+1.235x | y=-1.3712+5.031x | y=0.3702+3.305x |
| r² | 0.92 | 0.83 | 0.91 | 0.90 |

## Maize Cultivar Magister

| All phenological stages | Chl.a | Chl.b | Chl.a+b | N |
|---|---|---|---|---|
| Content per area [m$^{-1}$] | | | | |
| Spectral approach | *CAI (=x)* | *CAI (=x)* | *CAI (=x)* | *OSAVI (=x)* |
| Regression model | y=-0.9434+4.081x | y=-0.1578+0.747x | y=-1.2435+5.043x | y=-1.0018+6.103x |
| r² | 0.91 | 0.73 | 0.90 | 0.96 |
| Content per mass [g$^{-1}$] | | | | |
| Spectral approach | | | | *OSAVI (=x)* |
| Regression model | | | | y=4.8653-2.588x |
| r² | | | | 0.86 |
| Before EC40 | Chl.a | Chl.b | Chl.a+b | N |
| Content per area [m$^{-1}$] | | | | |
| Spectral approach | *OSAVI (=x)* | *OSAVI (=x)* | *OSAVI (=x)* | *OSAVI (=x)* |
| Regression model | y=-0.2772+1.939x | y=-0.0259+0.329x | y=-0.3945+2.216x | y=-1.0742+6.661x |
| r² | 0.92 | 0.82 | 0.87 | 0.94 |
| Content per mass [g$^{-1}$] | | | | |
| Spectral approach | | *CAI (=x)* | | *OSAVI (=x)* |
| Regression model | | y=0.7004+0.903x | | y=4.5391-2.281x |
| r² | | 0.73 | | 0.74 |
| Beyond EC40 | Chl.a | Chl.b | Chl.a+b | N |
| Content per area [m$^{-1}$] | | | | |
| Spectral approach | *CAI (=x)* | | | |
| Regression model | y=-3.9157+0.086x | | | |
| r² | 0.70 | | | |
| Content per mass [g$^{-1}$] | | | | |
| Spectral approach | | | | |
| Regression model | | | | |
| r² | | | | |

## Maize Cultivar Narval

| All phenological stages | Chl.a | Chl.b | Chl.a+b | N |
|---|---|---|---|---|
| **Content per area [m$^{-1}$]** | | | | |
| Spectral approach | *CAI (=x)* | | *CAI (=x)* | *CAI (=x)* |
| Regression model | y=-1.2798+4.779x | | y=-1.422+5.427x | y=-2.873+12.295x |
| r² | 0.88 | | 0.86 | 0.86 |
| Spectral approach | *OSAVI (=x)* | | *OSAVI (=x)* | |
| Regression model | y=-2.2768+4.704x | | y=-2.5432+5.330x | |
| r² | 0.88 | | 0.85 | |
| **Content per mass [g$^{-1}$]** | | | | |
| Spectral approach | | | | |
| Regression model | | | | |
| r² | | | | |

| Before EC40 | Chl.a | Chl.b | Chl.a+b | N |
|---|---|---|---|---|
| **Content per area [m$^{-1}$]** | | | | |
| Spectral approach | *hNDVI (=x)* | *OSAVI (=x)* | *hNDVI (=x)* | *OSAVI (=x)* |
| Regression model | y=-2.7108+5.954x | y=-0.8158+1.314x | y=-3.3563+7.277x | y=-6.7722+14.34x |
| r² | 0.97 | 0.82 | 0.88 | 0.74 |
| Spectral approach | *OSAVI (=x)* | 7 | *OSAVI (=x)* | |
| Regression model | y=-2.346+4.804 | | y=-2.9104+5.871x | |
| r² | 0.97 | | 0.87 | |
| **Content per mass [g$^{-1}$]** | | | | |
| Spectral approach | | *OSAVI (=x)* | | *OSAVI (=x)* |
| Regression model | | y=-0.2472+0.569x | | y=5.8997-2.635x |
| r² | | 0.75 | | 0.97 |

# Curriculum Vitae

## Persönliche Daten

Name: Natascha Maria Oppelt

Geburtstag: 25 März 1970

Geburtsort: München

Familienstand: ledig

## Schulbesuch

1976-1980 Grundschule in München

1980-1989 Pestalozzi-Gymnasium in München

## Universität

1989-1991 Studium der Agrarwissenschaften an der Technischen Universität München, Zweigstelle Weihenstephan

1991-1997 Studium der Geographie (Fachrichtung Physische Geographie) an der Ludwig-Maximilians-Universität München;
Nebenfächer: Geophysik, Geowissenschaftliche Fernerkundung, Wirtschaftsgeographie
Abschluss: Diplom Geograph (Univ.)
Thema der Diplomarbeit: Aufbereitung und thematische Auswertung von Bilddaten eines flugzeuggetragenen, multispektralen Video-Fernerkundungssystems

## Praktika und berufsrelevante Arbeiten während des Studiums

August – Sept. 1992 Praktikum bei STATTREISEN MÜNCHEN e.V.

September 1993 Praktikum beim Referat für Stadtplanung und Bauordnung der Landeshauptstadt München

August – Sept. 1994 Praktikum beim Deutschen Zentrum für Luft- und Raumfahrt (Deutsches Fernerkundungsdatenzentrum), Oberpfaffenhofen

Jan. 1995 – Dez. 1996 Studentische Hilfskraft am Lehrstuhl für Photogrammetrie und Fernerkundung an der Universität der Bundeswehr München, Neubiberg

**Berufstätigkeit**

| | |
|---|---|
| Februar - Mai 1997 | Angestellte bei der BDO Deutsche Warentreuhand AG – Wirtschaftsprüfungsgesellschaft in München |
| Juni 1997 – Juni 1998 | Wissenschaftlicher Mitarbeiter am Institut für Geographie der Ludwig-Maximilians-Universität München im Rahmen des DFG-Forschungsprojektes "Ermittelung eines Bodenfeuchteindex für das Einzugsgebiet der Weser mit Hilfe von ERS SAR Daten" |
| Juli 1998 – Sept. 2000 | Wissenschaftlicher Mitarbeiter am Institut für Geographie der Ludwig-Maximilians-Universität München im Rahmen des DFG-Forschungsprojektes "Bestimmung des Stickstoffgehaltes von Vegetation – ein Beitrag zur deutschen BAHC Forschung"; mit Vorbereitung der Promotion |
| seit Oktober 2000 | Wissenschaftlicher Mitarbeiter in Forschung und Lehre am Institut für Geographie der Ludwig-Maximilians-Universität München und Promotion |